Copy 3
RM SL56J10

[redacted]

R.A. A73L113 c.1

# RESEARCH MEMORANDUM

for the

Bureau of Aeronautics, Department of the Navy

STATIC LATERAL AND DIRECTIONAL STABILITY AND CONTROL CHARACTERISTICS OF A 1/15-SCALE MODEL OF THE GRUMMAN F11F-1 AIRPLANE AT MACH NUMBERS OF 1.41, 1.61, AND 2.01

TED NO. NACA ~~AD~~ 3125

By Ross B. Robinson and Cornelius Driver

Langley Aeronautical Laboratory
Langley Field, Va.

CLASSIFICATION CHANGED
UNCLASSIFIED
To
authority of JPW #48 Date 5-9-61

LIBRARY COPY
DEC 6 1956
LANGLEY AERONAUTICAL LABORATOR
LIBRARY NACA
LANGLEY FIELD, VIRGINIA

CLASSIFIED DOCUMENT

This material contains information affecting the National Defense of the United States within the meaning of the espionage laws, Title 18, U.S.C., Secs. 793 and 794, the transmission or revelation of which in any manner to an unauthorized person is prohibited by law.

NATIONAL ADVISORY COMMITTEE FOR AERONAUTICS

WASHINGTON

[redacted]

Grumman F11F-1

NASA Technical Library
3 1176 01438 5059

NACA RM SL56J10

NATIONAL ADVISORY COMMITTEE FOR AERONAUTICS

RESEARCH MEMORANDUM

for the

Bureau of Aeronautics, Department of the Navy

# STATIC LATERAL AND DIRECTIONAL STABILITY AND CONTROL CHARACTERISTICS OF A 1/15-SCALE MODEL OF THE GRUMMAN F11F-1 AIRPLANE AT MACH NUMBERS OF 1.41, 1.61, AND 2.01

TED NO. NACA ~~AD 3125~~ NE 370

By Ross B. Robinson and Cornelius Driver

## SUMMARY

An investigation has been made in the Langley 4- by 4-foot supersonic pressure tunnel to determine the static lateral and directional stability and control characteristics of a 1/15-scale model of the Grumman F11F-1 airplane at Mach numbers of 1.41, 1.61, and 2.01. The complete model and various combinations of component parts were tested as well as various configuration changes including modified bodies and modified vertical tails.

The results indicated that, because of decreases in the vertical-tail effectiveness and because of the magnitude of the unstable wing-body moment, the directional stability of the complete configuration progressively decreased with increasing Mach number and angle of attack until regions of directional instability occurred. Increasing the size of the vertical tail was effective in delaying the instability to higher Mach numbers or higher angles of attack.

The flaperon provided positive lateral control throughout the angle-of-attack and angle-of-sideslip ranges, but, with a maximum deflection angle of 25°, provided a rolling moment equivalent to the induced rolling moments incurred at about 6° of sideslip.

The rudder provided positive directional control throughout the angle-of-attack and angle-of-sideslip ranges but, because of the low level of directional stability and because of the nonlinear variation of yawing moment with sideslip, some deflections of the rudder would result in second trim points.

CONFIDENTIAL

## INTRODUCTION

At the request of the Bureau of Aeronautics, Department of the Navy, the National Advisory Committee for Aeronautics has conducted an investigation of the aerodynamic characteristics of a 1/15-scale model of the Grumman F11F-1 at subsonic, transonic, and supersonic speeds. The designation F11F-1 supersedes the previous model designated Grumman F9F-9. The F11F-1 is a jet-propelled fighter design having a wing with 35° of sweep of the quarter-chord line, an aspect ratio of 4, a taper ratio of 0.5, and NACA 65A-series airfoil sections having a thickness ratio of 6 percent at the root and 4 percent at the tip. The wing was mounted at 0° incidence in a semihigh position on the fuselage and the all-movable horizontal tail was located slightly below the extended chord line of the wing. The fuselage was indented in the vicinity of the wing to reduce drag rise in the transonic speed range.

Tests of a 1/15-scale model of the original F11F-1 airplane have been made at subsonic speeds in the Langley low-turbulence pressure tunnel and at transonic speeds in the Langley 8-foot transonic tunnel (ref. 1). The results of limited tests of this configuration in the Langley 4- by 4-foot supersonic pressure tunnel at a Mach number of 1.41 are presented in reference 2. Static longitudinal stability and control characteristics of the present modified F11F-1 configuration at Mach numbers of 1.41, 1.61, and 2.01 are given in reference 3.

The present report contains the results of an investigation to determine the static lateral and directional stability and control characteristics of the modified F11F-1 configuration at Mach numbers of 1.41, 1.61, and 2.01, at Reynolds numbers, based on the wing mean geometric chord, of $1.63 \times 10^6$, $1.56 \times 10^6$, and $1.35 \times 10^6$, respectively. The investigation was made in the Langley 4- by 4-foot supersonic pressure tunnel.

## COEFFICIENTS AND SYMBOLS

The results are presented as force and moment coefficients referred to the stability-axis system (fig. 1) with the reference center of moments located at a longitudinal position corresponding to 25 percent of the wing mean geometric chord. The coefficients and symbols are defined as follows:

$C_L$ lift coefficient, $\frac{F_L}{qS}$

$C'_D = \frac{F'_D}{qS}$

[redacted]

| | |
|---|---|
| $C_m$ | pitching-moment coefficient, $\frac{M_{Y_s}}{qS\bar{c}}$ |
| $C_l$ | rolling-moment coefficient, $\frac{M_{X_s}}{qSb}$ |
| $C_n$ | yawing-moment coefficient, $\frac{M_{Z_s}}{qSb}$ |
| $C_Y$ | side-force coefficient, $\frac{F_Y}{qS}$ |
| $F_L$ | lift force |
| $F'_D$ | approximate drag force |
| $F_Y$ | lateral force |
| $M_{Y_s}$ | pitching moment about stability axes |
| $M_{X_s}$ | rolling moment about stability axes |
| $M_{Z_s}$ | yawing moment about stability axes |
| $q$ | free-stream dynamic pressure, lb/sq ft |
| $S$ | wing area including fuselage intercept, sq ft |
| $b$ | wing span, in. |
| $\bar{c}$ | wing mean geometric chord, in. |
| $M$ | free-stream Mach number |
| $R$ | Reynolds number based on $\bar{c}$ |
| $\alpha$ | angle of attack of fuselage reference line, deg |
| $\beta$ | angle of sideslip of fuselage reference line, deg |
| $i_t$ | horizontal-tail incidence angle with respect to fuselage reference line, positive with trailing edge down, deg |
| $\delta_f$ | flaperon deflection angle, normal to hinge line, positive with trailing edge up, deg |

[redacted]

$\delta_r$ rudder deflection angle, normal to hinge line, positive with trailing edge left, deg

$\delta_v$ deflection angle of entire vertical tail, with respect to fuselage line, positive with trailing edge left, deg

$C_{n_\beta}$ directional-stability parameter, $\frac{\partial C_n}{\partial \beta}$

$C_{l_\beta}$ effective-dihedral parameter, $\frac{\partial C_l}{\partial \beta}$

$C_{Y_\beta}$ side-force parameter, $\frac{\partial C_Y}{\partial \beta}$

$C_{n_{\delta_f}} = \frac{\partial C_n}{\partial \delta_f}$

$C_{l_{\delta_f}} = \frac{\partial C_l}{\partial \delta_f}$

$C_{n_{\delta_r}} = \frac{\partial C_n}{\partial \delta_r}$

$C_{l_{\delta_r}} = \frac{\partial C_l}{\partial \delta_r}$

$C_{n_{\delta_v}} = \frac{\partial C_n}{\partial \delta_v}$

$C_{l_{\delta_v}} = \frac{\partial C_l}{\partial \delta_v}$

Model components:

W wing

$B^1$ body with production nose

$B^2$ body with photographic nose

$B^3$ body with production nose and afterburner ring

H modified horizontal tail of production configuration

$V^1$ denotes original tail

$V^2$ extended-tip and extended-chord tail

$V^3$ extended-chord tail

## MODEL AND APPARATUS

A three-view drawing of the model is shown in figure 2(a). Sketches of the original (refs. 1 and 2) and production configurations, the production and photographic noses, the dorsal, ventral, and horizontal fins, and the three vertical tails are given in figures 2(b) to 2(f). The afterburner ring of body $B^3$ is shown as a dashed line in figure 2(f). Several photographs of the model are presented in figure 3. The geometric characteristics of the model are presented in table I.

The basic configuration for this investigation was composed of the body with the production nose $B^1$ (fig. 2(c)) and inlets faired closed, the wing, the modified horizontal tail at $i_t = 0^\circ$ (fig. 2(b)) and vertical tail $V^1$ at $0^\circ$ incidence (fig. 2(f)). The wing had $35^\circ$ of sweep of the quarter-chord line, an aspect ratio of 4, a taper ratio of 0.5, and NACA 65A-series airfoils having thickness ratios of 6 percent and 4 percent at the root and tip, respectively. The wing was mounted in a semihigh position on the body and had $2.5^\circ$ of negative dihedral and $0^\circ$ of incidence with respect to the fuselage reference line. An all-movable horizontal tail was mounted 0.069 wing semispan below the wing root chord line extended.

Two additional vertical tails were tested: (a) tail $V^2$, which had both an extended tip and extended chord and (b) tail $V^3$, which had the same span as tail $V^1$ but had an extended chord (fig. 2(f)). A dorsal, a ventral, and a horizontal fin (figs. 2(d) and 2(e)) were also used.

Longitudinal control was obtained by changing the incidence of the horizontal tail, lateral control by deflection of a flap-type spoiler (flaperon) in the upper surface of the left wing only (fig. 2(a)), and directional control by deflection of either the rudder or the entire vertical tail $V^1$ (fig. 2(a)). All control deflections were set manually.

For the tests made with open inlets the faired plugs shown in figure 2(a) were removed.

Forces and moments were measured by a six-component strain-gage balance contained in the sting-mounted model. For the tests at $M = 1.61$

and 2.01, the model was mounted on a remotely controlled rotary sting, while for the tests at $M = 1.41$ a manually adjustable sting was employed. A rake of total- and static-pressure tubes was used at the base of the model to measure the internal flow of the open inlet configuration.

## Tests, Corrections, and Accuracy

Tests.- The test conditions are summarized in the following table:

| Mach number | Stagnation temperature, °F | Stagnation pressure, lb/sq ft | Reynolds number | Dewpoint |
|---|---|---|---|---|
| 1.41 | 100 | 1,440 | $1.63 \times 10^6$ | Less than -25° F |
| 1.61 | 100 | 1,440 | 1.56 | Less than -25° F |
| 2.01 | 100 | 1,440 | 1.35 | Less than -25° F |

At $M = 1.41$ the model was tested through an angle-of-attack range of about -4° to about 15° at $\beta \approx 0°$ and 4.9° and through an angle-of-sideslip range of -4° to about 14° at $\alpha \approx 0°$ and 5.2°. At $M = 1.61$ and $M = 2.01$, the angle-of-sideslip range was from 0° to about 20° at $\alpha = 0°$, and from 0° to about 15° at angles of attack of approximately 4°, 8°, 12°, and 16°.

Corrections and accuracy.- The angles of attack and sideslip have been corrected for the deflections of the balance and sting caused by aerodynamic loads. Since the angularity of the airstream was less than ±0.10° and the Mach number variation less than ±0.01, the data have not been corrected for these variations.

For all the closed-inlet configurations the longitudinal-force coefficients were adjusted by equating the measured base pressure to the free-stream static pressure. For the open-inlet configurations, corrections were made for the base pressure on the rim of the model base, the static pressure in the balance chamber inside the model, and the internal drag as determined by total- and static-pressure measurements of the internal air flow.

For the tests at a Mach number of 1.41, angles of attack and sideslip are estimated to be accurate within ±0.1°; for the tests at Mach numbers of 1.61 and 2.01, the angles are probably within ±0.2°. All control deflections are probably correct within ±0.10°. The maximum errors in the coefficients are estimated to be as follows:

[redacted]

| | |
|---|---|
| $C_L$ | ±0.0070 |
| $C_X$ | ±0.0020 |
| $C_m$ | ±0.0005 |
| $C_l$ | ±0.0001 |
| $C_n$ | ±0.0002 |
| $C_Y$ | ±0.0015 |

## PRESENTATION OF RESULTS

A complete index of the figures is shown as table II.

The basic results presenting the aerodynamic characteristics in sideslip for various configurations are shown in figures 4 to 24. The basic lateral control results are shown in figures 25 to 28 and the basic directional control results are shown in figures 29 and 30.

The sideslip derivatives are summarized in figures 31 to 36. The lateral and directional control effectiveness are summarized in figures 37 and 38, respectively.

A summary of the variation of the sideslip derivatives with Mach number at subsonic, transonic, and supersonic speeds is presented in figure 39.

## DISCUSSION

### Static Lateral and Directional Stability

Directional characteristics.- The directional-stability parameter $C_{n_\beta}$ of the basic configuration $(WB^1HV^1)$ indicated a rather rapid deterioration with increasing angle of attack and with increasing Mach number until regions of undesirably low stability were encountered (fig. 32(a)). The model was directionally unstable at angles of attack above 13° for all Mach numbers tested. With the vertical tail removed (fig. 32(b)), a large unstable $C_{n_\beta}$ occurred that was essentially invariant with angle of attack or Mach number. Hence, the deterioration of $C_{n_\beta}$ for the basic configuration both with angle of attack and Mach number appeared to be a result of a decrease in vertical-tail effectiveness. Estimates of the lift-curve-slope variation with Mach number for the isolated vertical tail obtained through the use of reference 4 indicated that the decrease in tail contribution with Mach number was as might be expected. The loss in tail contribution with increasing angle of attack apparently resulted from

[redacted]

an adverse sidewash flow at the tail (see ref. 5) and possibly some decrease in dynamic pressure at the tail.

Losses in tail contribution due to Mach number became extremely critical inasmuch as a large percentage of the tail contribution was consumed in overcoming the instability of the wing-body and any further losses in tail contribution due to angle of attack only hastened the occurrence of directional instability for the complete configuration. In this regard, it might be pointed out that any additional losses in tail contribution that might occur for a full-scale airplane from such sources as structural elasticity or control deflection would result in still greater losses in directional stability.

Increasing the size of the vertical tail resulted in an increased tail contribution so that the deterioration of $C_{n_\beta}$ for the complete configuration was delayed to higher angles of attack and to higher Mach numbers (figs. 31 and 33). Although the enlarged tails ($V^2$ and $V^3$) had equal areas, the extended-tip tail ($V^2$) with its higher aspect ratio was somewhat more effective than the extended-chord tail ($V^3$). The vertical-tail contributions at $\alpha = 0^\circ$ were found to be in agreement with values estimated on the basis of the isolated-tail lift-curve slopes (ref. 4) assuming that the fuselage forms a perfect end plate. Although the differences were small, the increment of $C_{n_\beta}$ provided by the extended-tip tail $V^2$ decreased less rapidly with increasing angle of attack than did that for the extended-chord tail $V^3$. This was a result, possibly, of the added area for tail $V^2$ being above the sidewash field (figs. 31 and 33).

The effects of the addition of a dorsal fin, a ventral fin, and a horizontal fin to the basic model (tail $V^1$) at $M = 1.61$ are compared in figure 34. The addition of the dorsal fin or the horizontal fin had little effect on the directional characteristics and did, in fact, result in some slight decreases in $C_{n_\beta}$ in the low angle-of-attack range. The ineffectiveness of the dorsal fin may be a result of adverse sidewash in the region occupied by the dorsal. In addition, the dorsal may cause an effective forward movement of the center of pressure for the entire tail.

In contrast, the addition of the ventral fin, although smaller in area than the dorsal fin, resulted in a small increase in directional stability throughout the angle-of-attack and sideslip range (figs. 14 and 34). This result may be an indication of a favorable sidewash region below the body and, to some extent, may be influenced by the longer moment arm attainable with the ventral fin than with the dorsal fin.

The effects of the addition of the afterbody extension ($B^3$) at $M = 1.41$ and $\alpha = 5.2^\circ$ (fig. 9) were to increase the instability of the

wing-body combination slightly at high sideslip angles but, at the same time, to increase slightly the tail contribution for tail $V^3$. The greater tail contribution with the afterbody extension installed probably results from an increased end-plate effect of the body on the tail and from an increase in the carry-over forces from the tail to the body.

The effect of the extended, photographic-type nose $(B^2)$ was to reduce the directional stability parameter $C_{n_\beta}$ throughout the angle-of-attack range for both the tail-on and tail-off configurations at $M = 1.41$ and 1.61 (fig. 35).

The effects of various combinations of component parts on the directional characteristics (fig. 36) reveal nothing unusual at low angles of attack. At the higher angles of attack, however, a rather rapid decrease in the instability (negative $C_{n_\beta}$) of the body alone and body—horizontal-tail combination is indicated. This variation of $C_{n_\beta}$ with $\alpha$ is not apparent when either the wing or vertical tail, or both, are added. These results are indicative of important interference effects between the various components. Pressure measurements over the afterbody and vertical tail would be required in order to obtain a better understanding of these effects.

Negative deflections of the horizontal tail caused an increase in the directional stability (figs. 16 to 18) similar to that observed for other low tail arrangements (ref. 6). This effect apparently results from the superposition of positive pressures from the upper surface of the deflected horizontal tail to the high pressure side of the vertical tail in sideslip. The effect is considerably reduced at $M = 2.01$ (fig. 18) since the portion of the vertical tail that is influenced by the flow field of the horizontal tail decreases with increasing Mach number.

The wing fence (fig. 19) and the air inlets (fig. 20) had little significant effect on the directional characteristics at $M = 1.61$.

Effective dihedral.- The basic complete-model configuration exhibits a positive dihedral effect (negative $C_{l_\beta}$) throughout the angle-of-attack and Mach number ranges investigated (fig. 32(a)) although the variations with angle of attack were quite nonlinear. These nonlinearities are evident for the tail-off configurations as well (fig. 32(b)). The addition of the vertical tail, of course, provides a negative increment of $C_{l_\beta}$ that increases as the tail size increases (fig. 33). The negative increment in $C_{l_\beta}$ provided by the vertical tail decreases with increasing angle of attack (fig. 31).

For $M = 1.61$ the addition of the wing at $\alpha \approx 0^\circ$ provided a slight positive increment of $C_{l_\beta}$ (negative effective dihedral) probably because

of the negative geometric dihedral angle of the wing (see fig. 36). With increasing angle of attack, however, the wing provided an increasingly negative increment of $C_{l_\beta}$ (positive dihedral effect) similar to that generally provided by swept wings at subsonic speeds.

The addition of the horizontal tail, particularly in the presence of the wing, provided a negative dihedral effect (figs. 36(a) and (b)).

The resultant variation of $C_{l_\beta}$ with angle of attack for the complete model was apparently influenced by the vertical tail at the lower angles of attack and by the wing at high angles of attack (figs. 31 and 36).

The ventral, dorsal, and horizontal fins had essentially no effect on $C_{l_\beta}$ (fig. 34).

Effects of sideslip on longitudinal characteristics.- The variations of lift and pitching moment with angle of sideslip indicate rather large changes with increasing angle of attack for the complete configuration (figs. 21 to 23) that may lead to cross coupling of the pitching and yawing motions. This cross-coupling tendency, combined with a low level of directional stability, might contribute to undesirable flight characteristics at high angles of attack.

## Lateral and Directional Control

Lateral control.- The flaperon was effective in producing rolling moment throughout the angle-of-attack and angle-of-sideslip ranges investigated (figs. 25 to 27). The rolling effectiveness $C_{l_{\delta_f}}$ and the yawing-moment variation $C_{n_{\delta_f}}$ decreased with increasing angle of attack (fig. 37).

The maximum flaperon deflection investigated (25°) at $M = 1.61$ provided a rolling-moment increment equivalent to the induced rolling moment incurred at an angle of sideslip of only about 6° at $\alpha = 0°$ (fig. 27).

Directional control.- Deflection of either the rudder or the entire vertical tail was effective in producing yawing moments throughout the angle-of-attack and angle-of-sideslip ranges investigated at $M = 1.61$ (figs. 29 and 30). However, because of the initial low level of directional stability and because of the nonlinear variation of $C_n$ with $\beta$, a sensitive directional control problem would result since some deflections of the rudder or tail would produce second trim points. In fact, the 5° deflection of the entire tail resulted in negative yawing moments throughout the angle-of-attack and angle-of-sideslip ranges. A rudder deflection of 5° provides a trimmed angle of sideslip of about 2° at $\alpha = 0°$ (fig. 29).

[redacted]

### Variation of Sideslip Derivatives with Mach Number

A summary showing the variation of the sideslip derivatives at $\alpha = 0^\circ$ with Mach number as obtained from various sources is presented in figure 39. The low-speed results (M = 0.13) were obtained from reference 7. The transonic results (M = 0.6 to 1.13) were obtained from reference 1, while the supersonic results (M = 1.41 to 2.01) are from the present investigation. The model used in the present investigation differed slightly in nose shape and in the horizontal tail plan form and position from the model used in references 1 and 7. This difference may be seen in figure 2.

Of primary concern, for configurations of the type considered, is the rapid decrease in vertical tail lift-curve slope with increasing supersonic Mach number and the resultant decrease in tail contribution to the directional stability. This decrease in tail contribution, together with the initially large instability of the wing-body combination, leads rapidly to a condition of undesirably low directional stability.

## CONCLUSIONS

An investigation conducted in the Langley 4- by 4-foot supersonic pressure tunnel to determine the static lateral and directional stability and control characteristics of a 1/15-scale model of the Grumman F11F-1 airplane at Mach numbers of 1.41, 1.61, and 2.01 indicated the following conclusions:

1. Because of decreases in the vertical-tail effectiveness and because of the magnitude of the unstable wing-body moment, the directional stability of the complete configuration progressively decreased with increasing Mach number and increasing angle of attack until regions of directional instability occurred.

2. Increasing the size of the vertical tail was effective in delaying the regions of directional instability to higher Mach numbers or higher angles of attack.

3. The flaperon provided positive lateral control throughout the angle-of-attack and angle-of-sideslip ranges with the maximum deflection of 25° providing rolling moment equivalent to the induced rolling moment incurred at about 6° of sideslip.

4. Deflection of the rudder or of the vertical tail was effective in producing yawing moments throughout the angle-of-attack and angle-of-sideslip ranges but, because of the initially low level of directional

[redacted]

stability and because of the nonlinear variation of yawing moments with sideslip, some deflections of the rudder or tail would result in second trim points.

5. The variations of lift and pitching moment with angle of sideslip indicate rather large changes with increasing angle of attack for the complete configuration that may lead to cross coupling of the pitching and yawing motions at high angles of attack.

Langley Aeronautical Laboratory,
National Advisory Committee for Aeronautics,
Langley Field, Va., September 25, 1956.

Ross B. Robinson
Aeronautical Research Engineer

Cornelius Driver
Aeronautical Research Engineer

Approved:

John V. Becker
Chief of Compressibility Research Division

mhg

[redacted]

## REFERENCES

1. Bielat, Ralph P.: A Transonic Wind-Tunnel Investigation of the Performance and of the Static Stability and Control Characteristics of a 1/15-Scale Model of the Grumman F9F-9 Airplane - TED No. NACA DE 390, NACA RM SL54J15, Bur. Aero., 1954.

2. Palazzo, Edward B., and Spearman, M. Leroy: Static Longitudinal and Lateral Stability and Control Characteristics of a Model of a 35° Swept-Wing Airplane at a Mach Number of 1.41. NACA RM L54G08, 1955.

3. Driver, Cornelius: The Aerodynamic Characteristics in Pitch of a 1/15-Scale Model of the Grumman F11F-1 Airplane at Mach Numbers of 1.41, 1.61, and 2.01 - TED No. NACA AD 3125. NACA RM SL56E24, Bur. Aero., 1956.

4. Harmon, Sydney M., and Jeffreys, Isabella: Theoretical Lift and Damping in Roll of Thin Wings With Arbitrary Sweep and Taper at Supersonic Speeds - Supersonic Leading and Trailing Edges. NACA TN 2114, 1950.

5. Spearman, M. Leroy: Static Lateral and Directional Stability and Effective Sidewash Characteristics of a Model of a 35° Swept-Wing Airplane at a Mach Number of 1.61. NACA RM L56E23, 1956.

6. Spearman, M. Leroy, and Robinson, Ross B.: Static Lateral Stability and Control Characteristics of a Model of a 45° Swept-Wing Fighter Airplane With Various Vertical Tails at Mach Numbers of 1.41, 1.61, and 2.01. NACA RM L56D05, 1956.

7. Wolhart, Walter D., and Thomas, David F., Jr.: Wind-Tunnel Investigation at Low Speed of the Yawing, Pitching, and Static Stability Characteristics of a 1/10-Scale Model of the Grumman F9F-9 Airplane - TED No. NACA AD 3109. NACA RM SL55D25, Bur. Aero., 1955.

[redacted]

TABLE I.- GEOMETRIC CHARACTERISTICS OF MODEL

| | |
|---|---|
| **Wing:** | |
| Area, sq ft | 1.11 |
| Aspect ratio | 4.00 |
| Sweepback of quarter-chord line, deg | 35 |
| Taper ratio | 0.500 |
| Mean geometric chord, ft | 0.5453 |
| Airfoil section, root | NACA 65A006 (modified) |
| Airfoil section, tip | NACA 65A004 (modified) |
| Twist, deg | 0 |
| Dihedral, deg | -2.5 |
| Span, ft | 2.109 |
| Incidence, deg | 0 |
| **Horizontal tail:** | |
| Area, sq ft | 0.291 |
| Aspect ratio | 3.50 |
| Sweepback of quarter-chord line, deg | 35 |
| Taper ratio | 0.400 |
| Airfoil section, root | NACA 65A006 |
| Airfoil section, tip | NACA 65A004 |
| Span, ft | 1.01 |

| **Vertical tail:** | $V^1$ | $V^2$ | $V^3$ |
|---|---|---|---|
| Area (exposed), sq ft | 0.177 | 0.222 | 0.222 |
| Aspect ratio (based on exposed area and span) | 1.51 | 1.51 | 1.20 |
| Sweepback of leading edge, deg | 44.5 | 44.5 | 44 |
| Taper ratio | 0.177 | 0.177 | 0.25 |
| Airfoil section, root | NACA 65A006 | 65A006 | 65A006 |
| Airfoil section, tip | NACA 65A004 | 65A004 | 65A004 |

| | |
|---|---|
| **Fuselage:** | |
| Length, $B^1$, in. | 32.31 |
| Length, $B^2$, in. | 33.66 |
| Length, $B^3$, in. | 33.10 |

[redacted]

TABLE II.- INDEX OF DATA FIGURES

[Unless otherwise noted, $i_t = 0^\circ$, $\delta_v = 0^\circ$, $\delta_r = 0^\circ$, and $\delta_f = 0^\circ$]

| Figure | M | Model | α, deg | β, deg | Type of data | Remarks |
|---|---|---|---|---|---|---|
| 4 | 1.41 | $WB^1V^1H$<br>$WB^1V^3H$<br>$WB^1$ | 0 and 5.2 | Range | Basic $(C_n, C_l, C_Y)$ | |
| 5 | 1.61 | $WB^1V^1H$<br>$WB^1V^2H$<br>$WB^1V^3H$<br>$WB^1H$<br>$WB^1$ | 0, 4.2, 8.5, 12.7, and 16 | Range | Basic $(C_n, C_l, C_Y)$ | |
| 6 | 2.01 | $WB^1V^1H$<br>$WB^1V^2H$<br>$WB^1V^3H$<br>$WB^1H$<br>$WB^1$ | 0, 4, 8, 12.3, and 15.5 | Range | Basic $(C_n, C_l, C_Y)$ | |
| 7 | 1.41 | $WB^1H$<br>$WB^1$<br>$WB^1$ | Range | 4.9<br>4.9<br>0 | Basic $(C_n, C_l, C_Y)$ | |
| 8 | 1.41 | $WB^1V^1H$<br>$WB^1V^1H$<br>$WB^1$<br>$WB^1$ | Range | 4.9<br>0<br>4.9<br>0 | Basic $(C_n, C_l, C_Y)$ | |
| 9 | 1.41 | $WB^1V^3H$<br>$WB^3V^3H$<br>$WB^1$<br>$WB^3$ | 5.2 | Range | Basic $(C_n, C_l, C_Y)$ | |
| 10 | 1.41 | $WB^3V^3H$<br>$WB^3V^3H$<br>$WB^1V^3H$ | Range | 0<br>4.9<br>4.9 | Basic $(C_n, C_l, C_Y)$ | |
| 11 | 1.41 | $WB^1V^1H$<br>$WB^2V^1H$ | 0 | Range | Basic $(C_n, C_l, C_Y)$ | |
| 12 | 1.41 | $WB^2V^1H$<br>$WB^2V^1H$<br>$WB^2$<br>$WB^2$ | Range | 4.9<br>0<br>4.9<br>0 | Basic $(C_n, C_l, C_Y)$ | |
| 13 | 1.61 | $WB^1V^1H$<br>$WB^2V^1H$<br>$WB^1$<br>$WB^2$ | 0, 4.2, 8.5, 12.7, and 16 | Range | Basic $(C_n, C_l, C_Y)$ | |
| 14 | 1.61 | $WB^1V^1H$ | 0, 4.2, 8.5, 12.7, and 16 | Range | Basic $(C_n, C_l, C_Y)$ | Ventral, dorsal, and horizontal fins added |

TABLE II.- INDEX OF DATA FIGURES - Continued

[Unless otherwise noted, $i_t = 0^\circ$, $\delta_v = 0^\circ$, $\delta_r = 0^\circ$, and $\delta_f = 0^\circ$]

| Figure | M | Model | α, deg | β, deg | Type of data | Remarks |
|---|---|---|---|---|---|---|
| 15 | 1.61 | $WB^1V^1H$<br>$WB^1V^1$<br>$WB^1H$<br>$WB^1$<br>$B^1V^1H$<br>$B^1V^1$<br>$B^1H$<br>$B^1$ | 0, 4.2, 8.5, 12.7, and 16 | Range | Basic ($C_n$,$C_l$,$C_Y$) | |
| 16 | 1.41 | $WB^1V^1H$ | 5.2 | Range | Basic ($C_n$,$C_l$,$C_Y$) | Horizontal tail deflected 0° and -10° |
| 17 | 1.61 | $WB^1V^1H$<br>$WB^1V^2H$<br>$WB^1V^3H$ | 0, 4.2, 8.5, 12.7, and 16 | Range | Basic ($C_n$,$C_l$,$C_Y$) | Horizontal tail deflected 0°, -10°, and -16.4° |
| 18 | 2.01 | $WB^1V^1H$<br>$WB^1V^1H$<br>$WB^1V^1$ | 0, 4.1, 8.2, 12.3, and 15.7 | Range | Basic ($C_n$,$C_l$,$C_Y$) | Horizontal tail deflected 0° and -10° |
| 19 | 1.61 | $WB^1V^1H$ | 0 and 16 | Range | Basic ($C_n$,$C_l$,$C_Y$) | Fence off and on |
| 20 | 1.61 | $WB^1V^1H$ | 0, 4.2, 8.5, 12.7, and 16 | Range | Basic ($C_n$,$C_l$,$C_Y$) | Inlet open and closed |
| 21 | 1.41 | $WB^1V^1H$<br>$WB^1V^3H$<br>$WB^2V^1H$<br>$WB^1$ | 0, 4.2, 8.5, 12.7, and 16 | Range | Basic ($C_m$,$C'_D$,$C_L$) | |
| 22 | 1.61 | $WB^1V^1H$<br>$WB^1V^2H$<br>$WB^1V^3H$<br>$WB^1H$<br>$WB^1$<br>$WB^1V^1$ | 0, 4.2, 8.5, 12.7, and 16 | Range | Basic ($C_m$,$C'_D$,$C_L$) | |
| 23 | 2.01 | $WB^1V^1H$<br>$WB^1V^2H$<br>$WB^1V^3H$<br>$WB^1H$<br>$WB^1$ | 0, 4.1, 8.2, 12.4, and 15.7 | Range | Basic ($C_m$,$C'_D$,$C_L$) | |
| 24 | 1.61 | $WB^1V^1H$<br>$WB^1V^1$<br>$WB^1H$<br>$WB^1$<br>$B^1V^1H$<br>$B^1V^1$<br>$B^1H$<br>$B^1$ | 0, 4.2, 8.5, 12.7, and 16 | Range | Basic ($C_m$,$C'_D$,$C_L$) | |
| 25 | 1.41 | $WB^1V^1H$ | Range | 0 | Basic ($C_m$,$C'_D$, $C_L$,$C_n$,$C_l$,$C_Y$) | Flaperon deflected 0° and 25° |

[redacted]

TABLE II.- INDEX OF DATA FIGURES - Concluded

[Unless otherwise noted, $i_t = 0°$, $\delta_v = 0°$, $\delta_r = 0°$, and $\delta_f = 0°$]

| Figure | M | Model | α, deg | β, deg | Type of data | Remarks |
|---|---|---|---|---|---|---|
| 26 | 1.61 | $WB^1V^1H$ | Range | 0 | Basic $(C_m, C'_D, C_L, C_n, C_l, C_Y)$ | Flaperon deflected 0°, 5°, and 25° |
| 27 | 1.61 | $WB^1V^1H$ | 0, 4.2, 8.5, and 12.7 | Range | Basic $(C_n, C_l, C_Y)$ | Flaperon deflected 0°, 5°, and 25° |
| 28 | 1.61 | $WB^1V^1H$ | 0, 4.2, 8.5, and 12.7 | Range | Basic $(C_m, C'_D, C_L)$ | Flaperon deflected 0°, 5°, and 25° |
| 29 | 1.61 | $WB^1V^1H$ | 0, 4.2, 8.5, and 12.7 | Range | Basic $(C_m, C_l, C_Y)$ | Rudder and vertical tail deflected 0° and 5° |
| 30 | 1.61 | $WB^1V^1H$ | Range | 0 | Basic $(C_n, C_l, C_Y)$ | Rudder and vertical tail deflected 0° and 5° |
| 31 | 1.41<br>1.41<br>1.41<br>1.61<br>1.61<br>1.61<br>1.61<br>2.01<br>2.01<br>2.01<br>2.01 | $WB^1V^1H$<br>$WB^1V^3H$<br>$WB^1$<br>$WB^1V^1H$<br>$WB^1V^2H$<br>$WB^1V^3H$<br>$WB^1$<br>$WB^1V^1H$<br>$WB^1V^2H$<br>$WB^1V^3H$<br>$WB^1$ | Range | ------ | Summary $(C_{n_\beta}, C_{l_\beta}, C_{Y_\beta})$ | |
| 32 | 1.41<br>1.61<br>2.01<br>1.41<br>1.61<br>2.01 | $WB^1V^1H$<br>$WB^1V^1H$<br>$WB^1V^1H$<br>$WB^1$<br>$WB^1$<br>$WB^1$ | Range | ------ | Summary $(C_{n_\beta}, C_{l_\beta}, C_{Y_\beta})$ | |
| 33 | 1.41 to 2.01 | $WB^1V^1H$<br>$WB^1V^2H$<br>$WB^1V^3H$<br>$WB^1$ | 0 | ------ | Summary $(C_{n_\beta}, C_{l_\beta}, C_{Y_\beta})$ | |
| 34 | 1.61 | $WB^1V^1H$ | Range | ------ | Summary $(C_{n_\beta}, C_{l_\beta}, C_{Y_\beta})$ | Ventral, dorsal, and horizontal fins added |
| 35 | 1.41 and 1.61 | $WB^1V^1H$<br>$WB^1$ | Range | ------ | Summary $(C_{n_\beta}, C_{l_\beta}, C_{Y_\beta})$ | Production and photographic noses |
| 36 | 1.61 | $WB^1V^1H$<br>$B^1V^1H$<br>$WB^1H$<br>$B^1H$<br>$WB^1V^1$<br>$B^1V^1$<br>$WB^1$<br>$B^1$ | Range | ------ | Summary $(C_{n_\beta}, C_{l_\beta}, C_{Y_\beta})$ | Effects of component parts |
| 37 | 1.41 and 1.61 | $WB^1V^1H$ | Range | 0 | Summary $(C_{n_{\delta_f}}, C_{l_{\delta_f}})$ | Flaperon effectiveness |
| 38 | 1.61 | $WB^1V^1H$ | Range | 0 | Summary $(C_{n_\delta}, C_{l_\delta}, C_{Y_\delta})$ | Rudder and vertical-tail effectiveness |
| 39 | 0 to 2.01 | $WB^1V^1H$<br>$WB^1$ | 0 | ------ | Summary $(C_{n_\beta}, C_{l_\beta}, C_{Y_\beta})$ | |

[redacted]

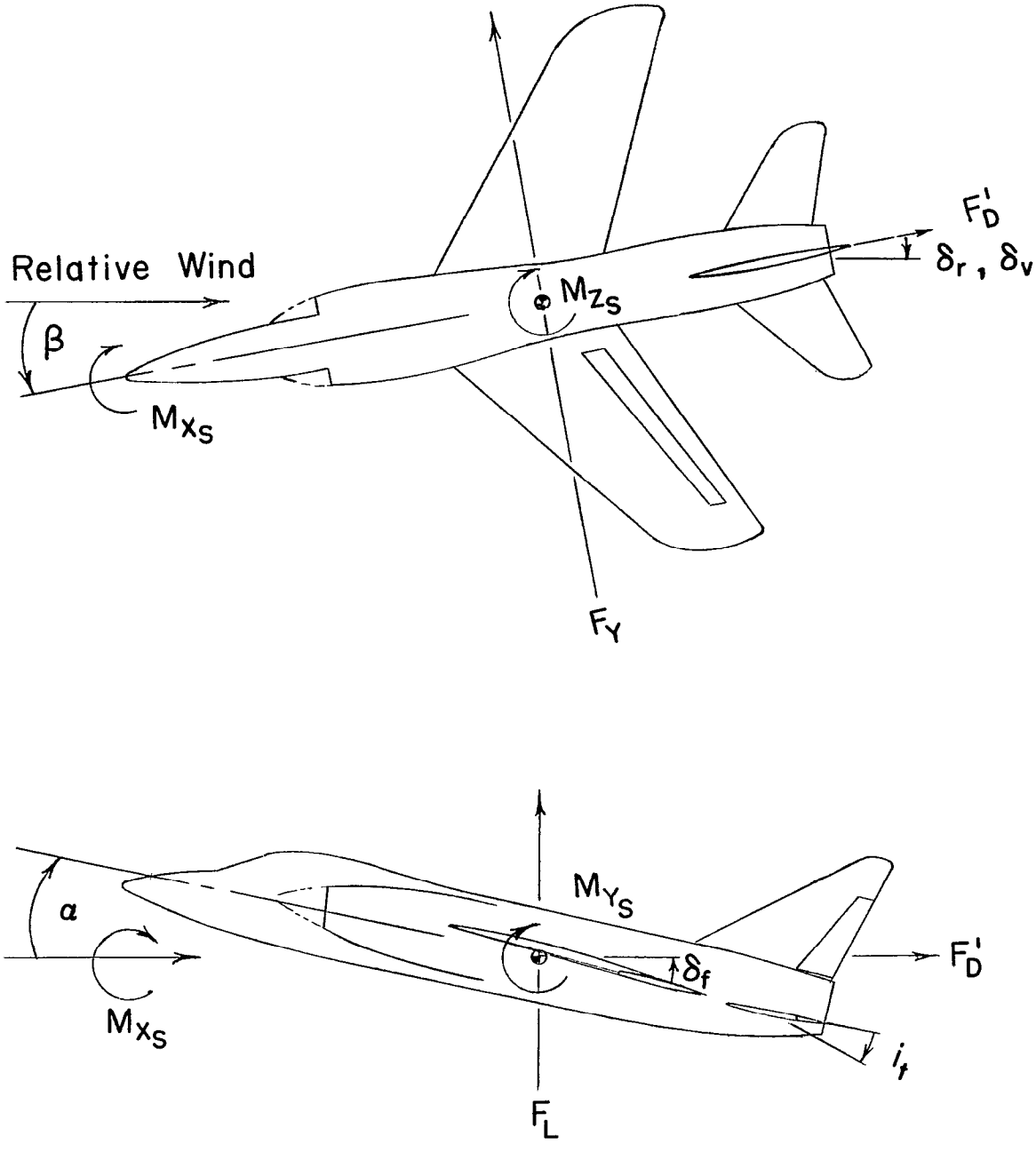


Figure 1.- Stability axis system. Arrows indicate positive directions.

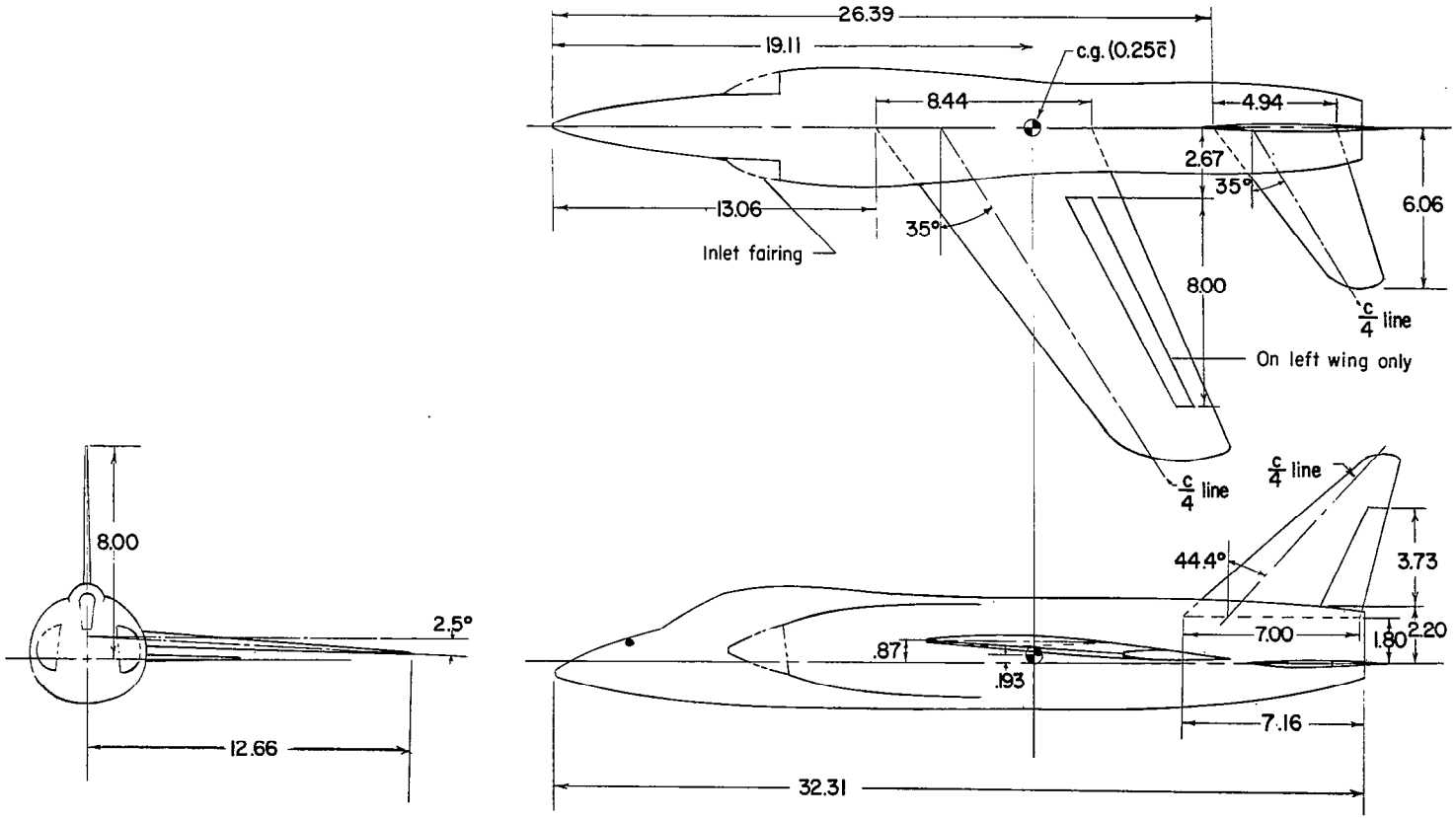


(a) Three-view drawing of basic model.

Figure 2.- Details of models. All dimensions in inches except as noted.

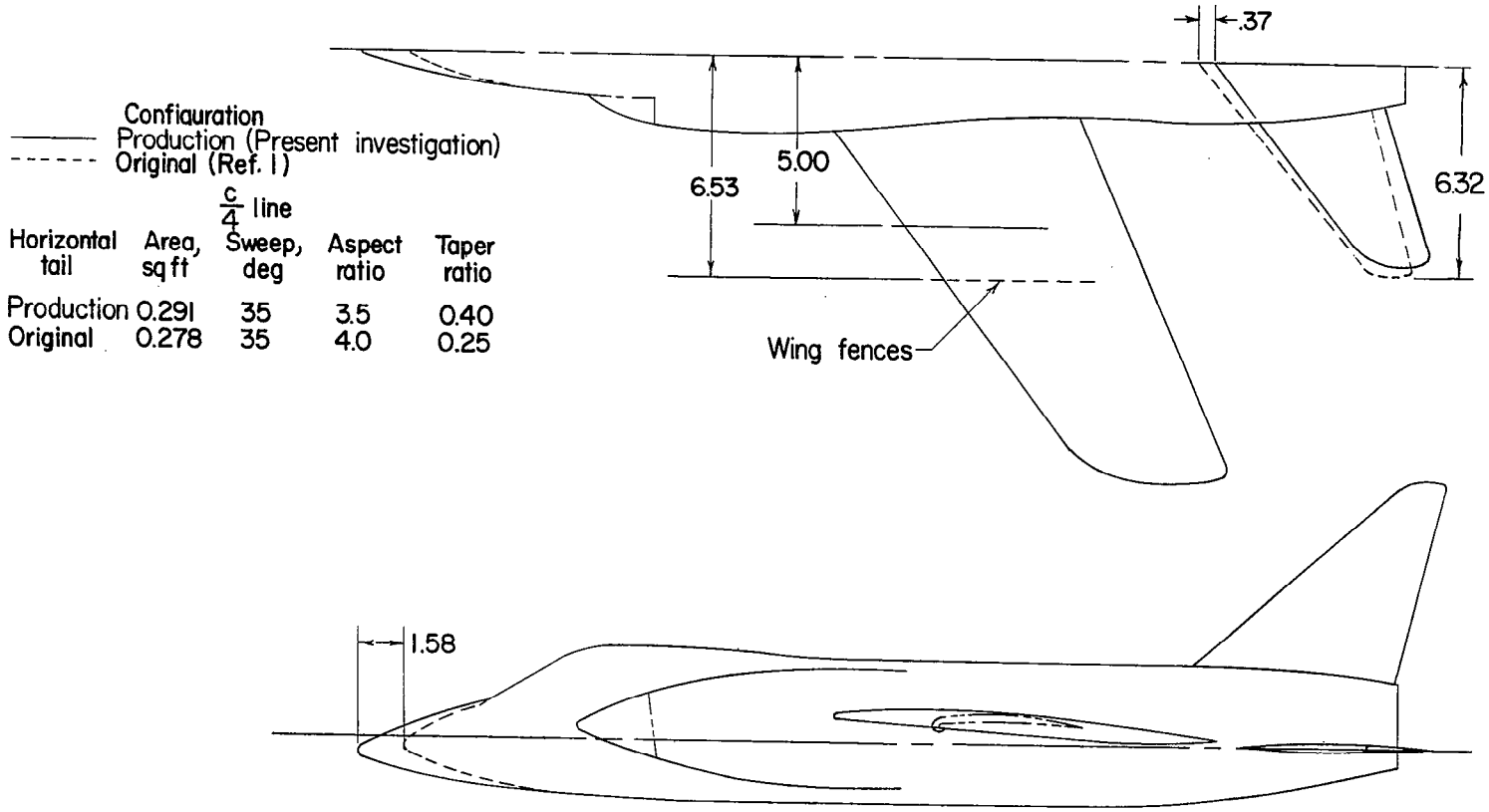


(b) Original and production models.

Figure 2.- Continued.

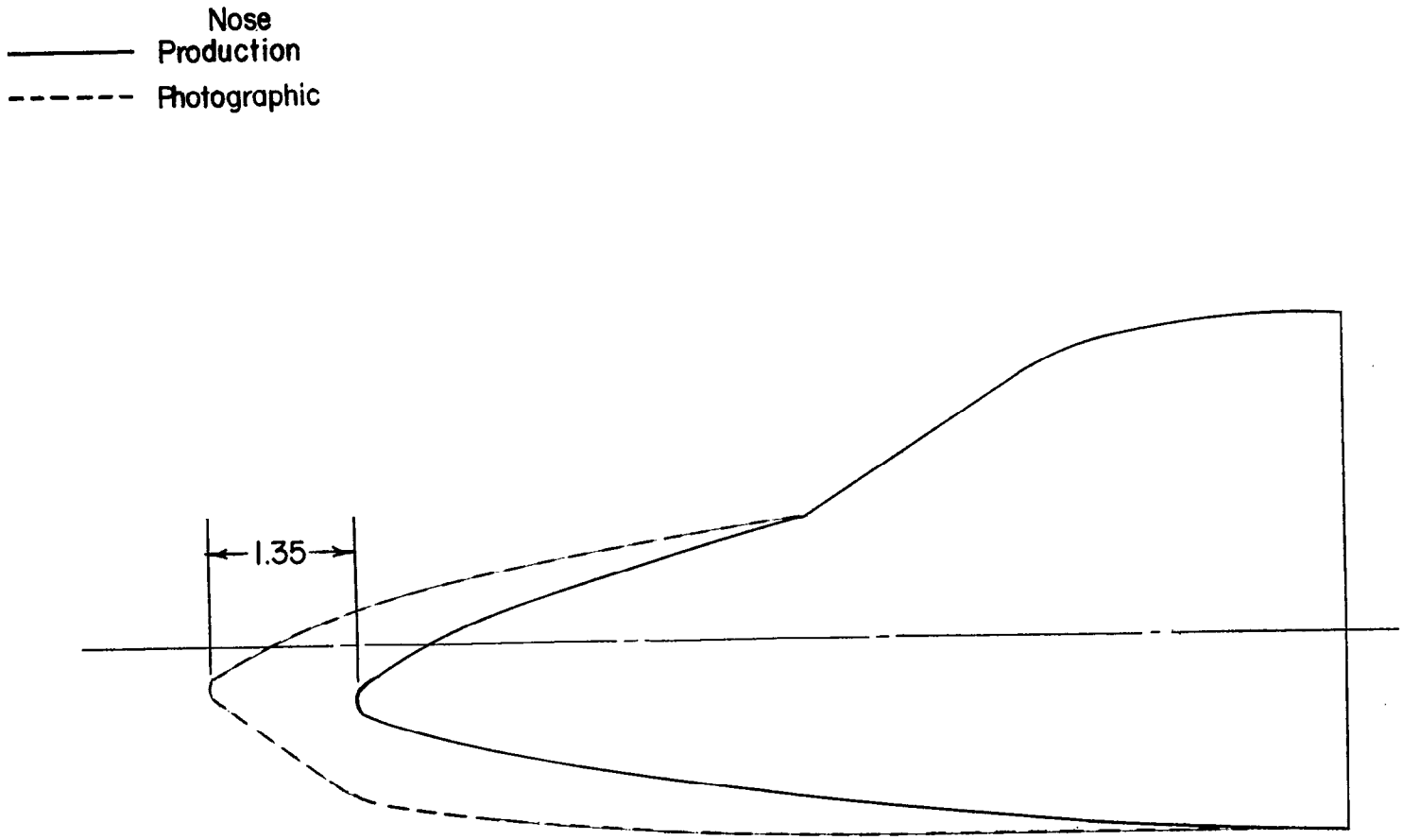


(c) Production and photographic noses.

Figure 2.- Continued.

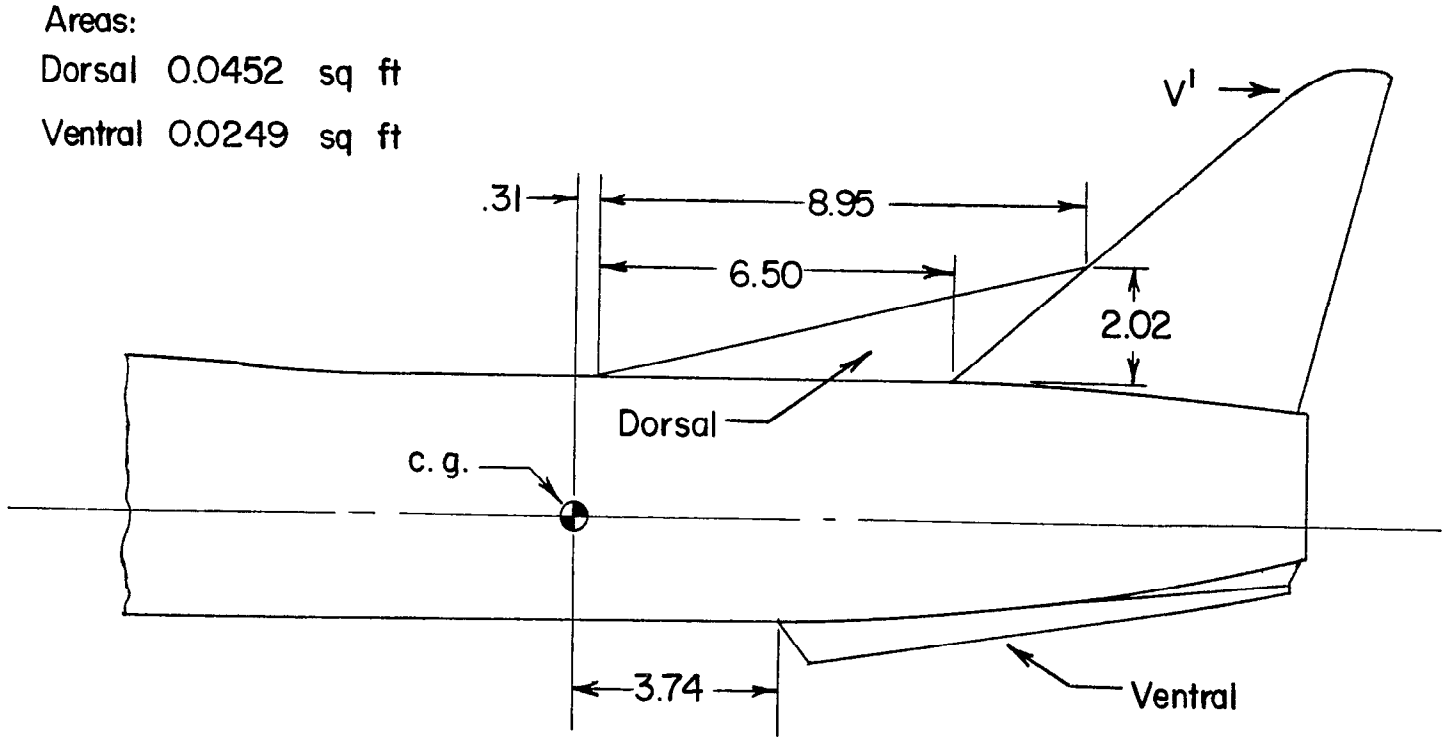


(d) Dorsal and ventral fins.

Figure 2.- Continued.

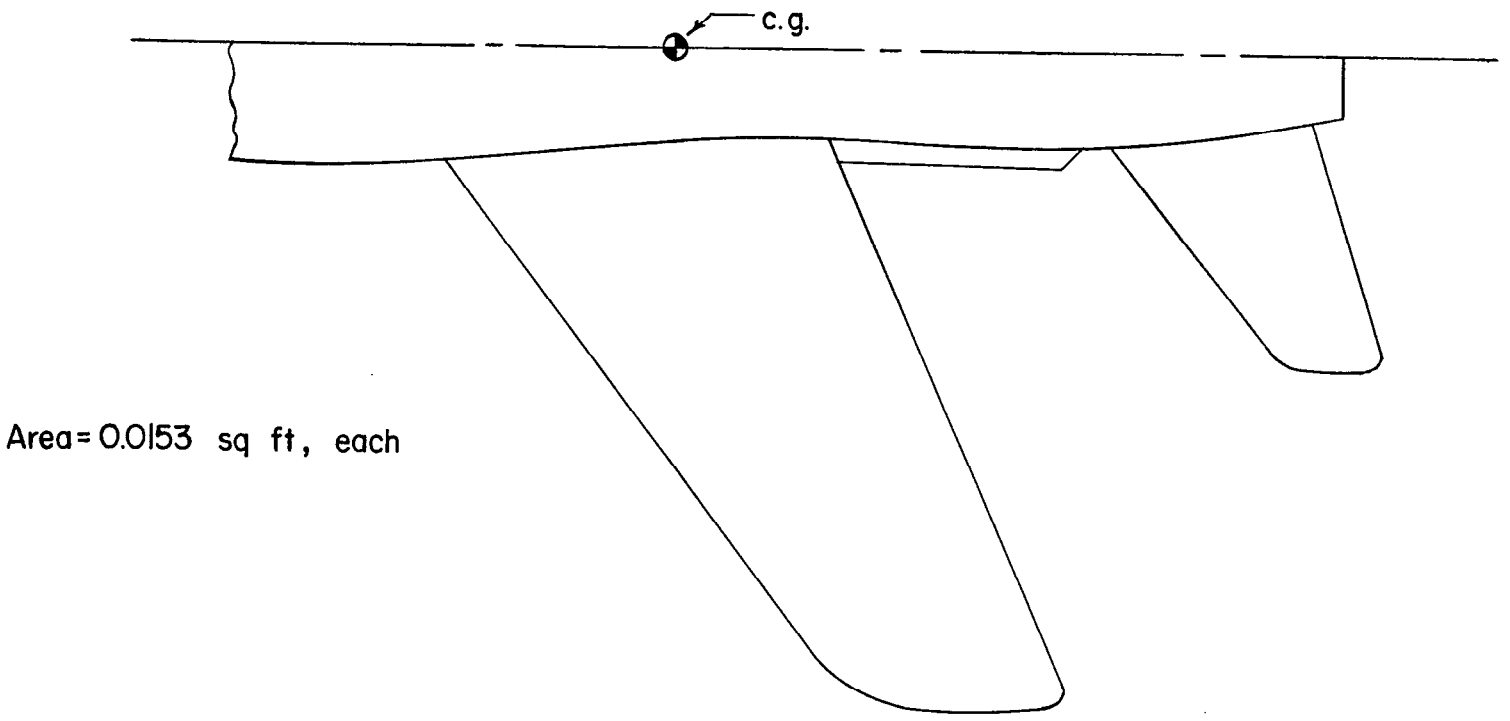


(e) Horizontal fin.

Figure 2.- Continued.

| | | h, in. | $C_r$, in. | $C_t$, in. | $\Lambda$, deg | Area, sq ft | Aspect ratio | Taper ratio |
|---|---|---|---|---|---|---|---|---|
| ——— | $V^1$ | 8.00 | 7.00 | 1.24 | 44.5 | .177 | 1.51 | 0.177 |
| — — — | $V^2$ | 8.73 | 7.83 | 1.39 | 44.5 | .222 | 1.51 | 0.177 |
| - - - - | $V^3$ | 8.00 | 8.23 | 2.07 | 44.0 | .222 | 1.20 | 0.250 |

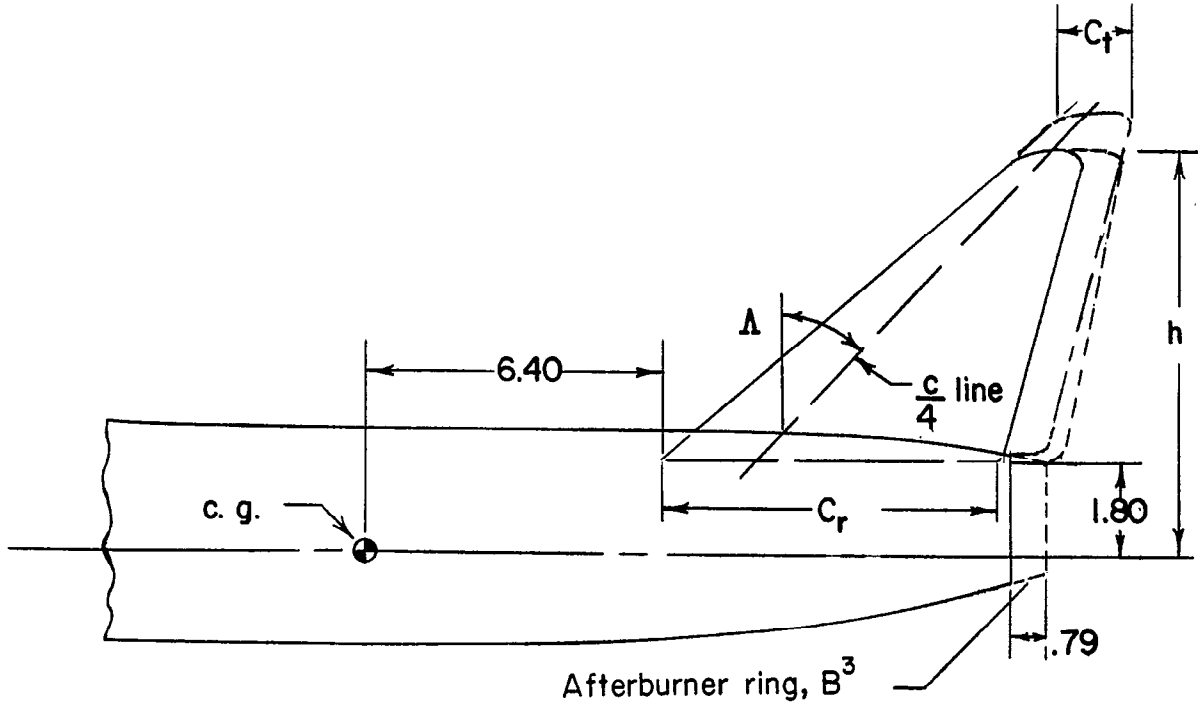


(f) Vertical tails.

Figure 2.- Concluded.

(a) Three-quarter front view. L-88318

Figure 3.- Photographs of model.

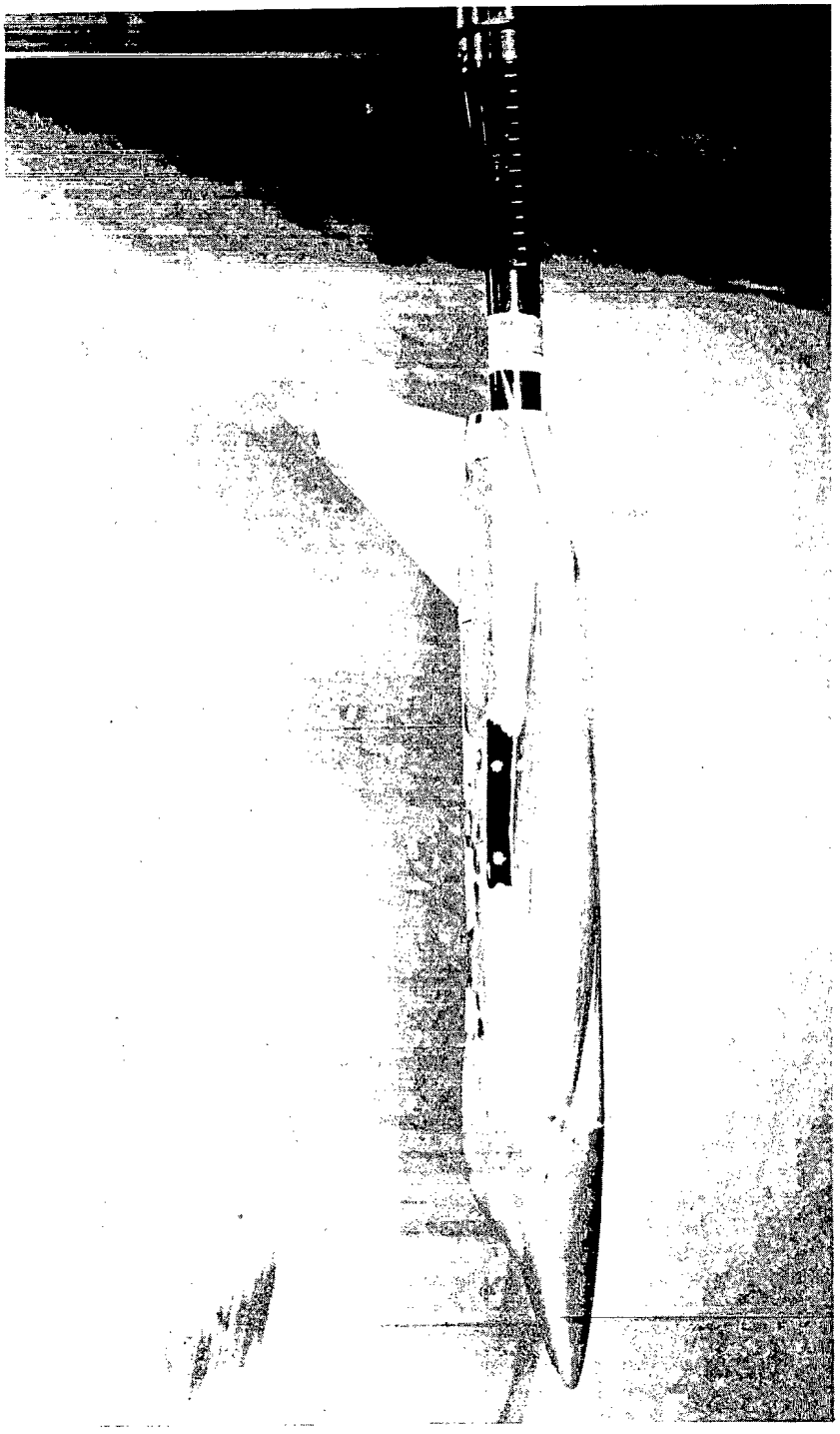

L-88321

(b) Side view.

Figure 3.- Continued..

[redacted]

(c) Top view. L-88322

Figure 3.- Continued.

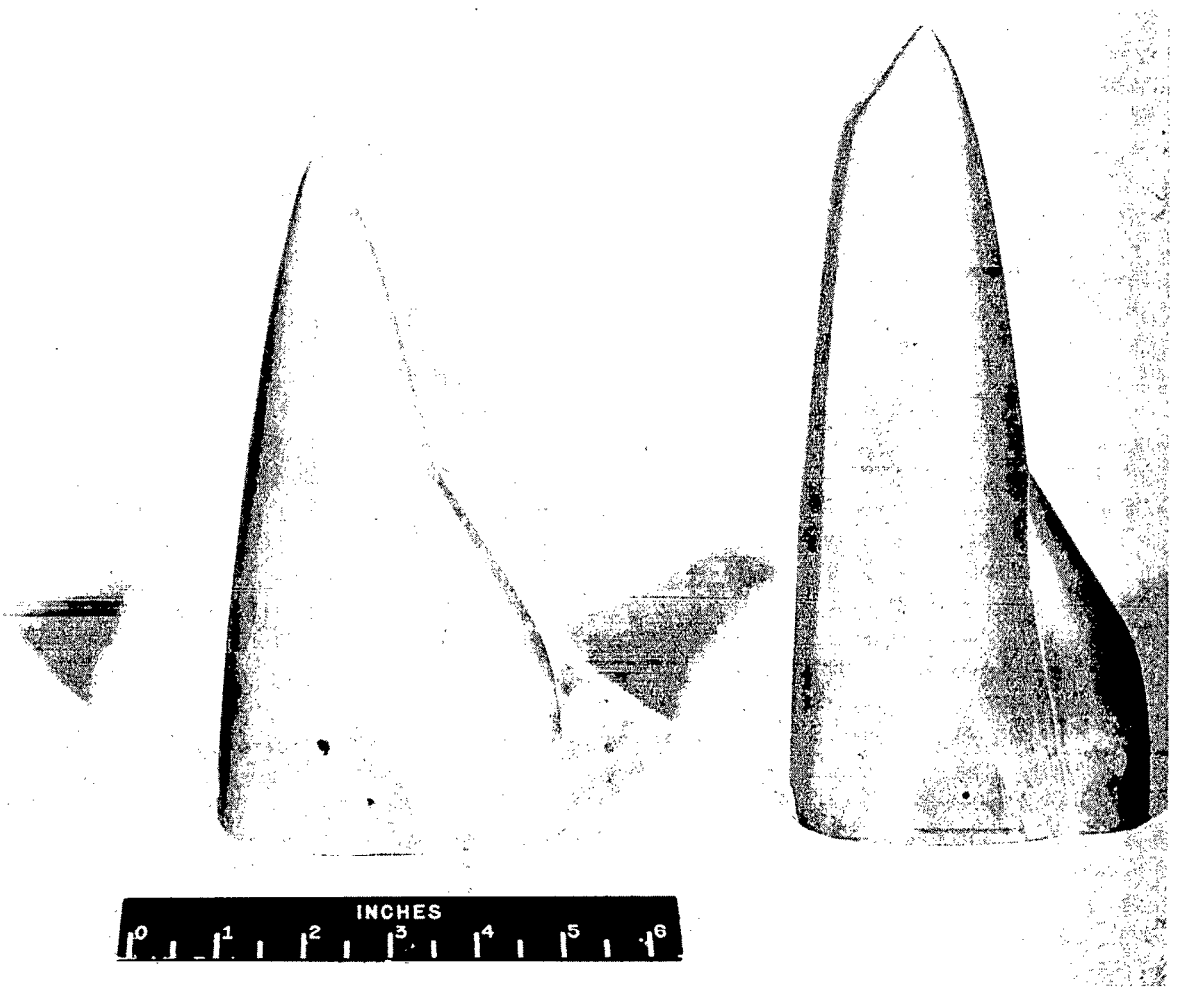


(d) Noses, production and photograph. L-88319.1

Figure 3.- Concluded.

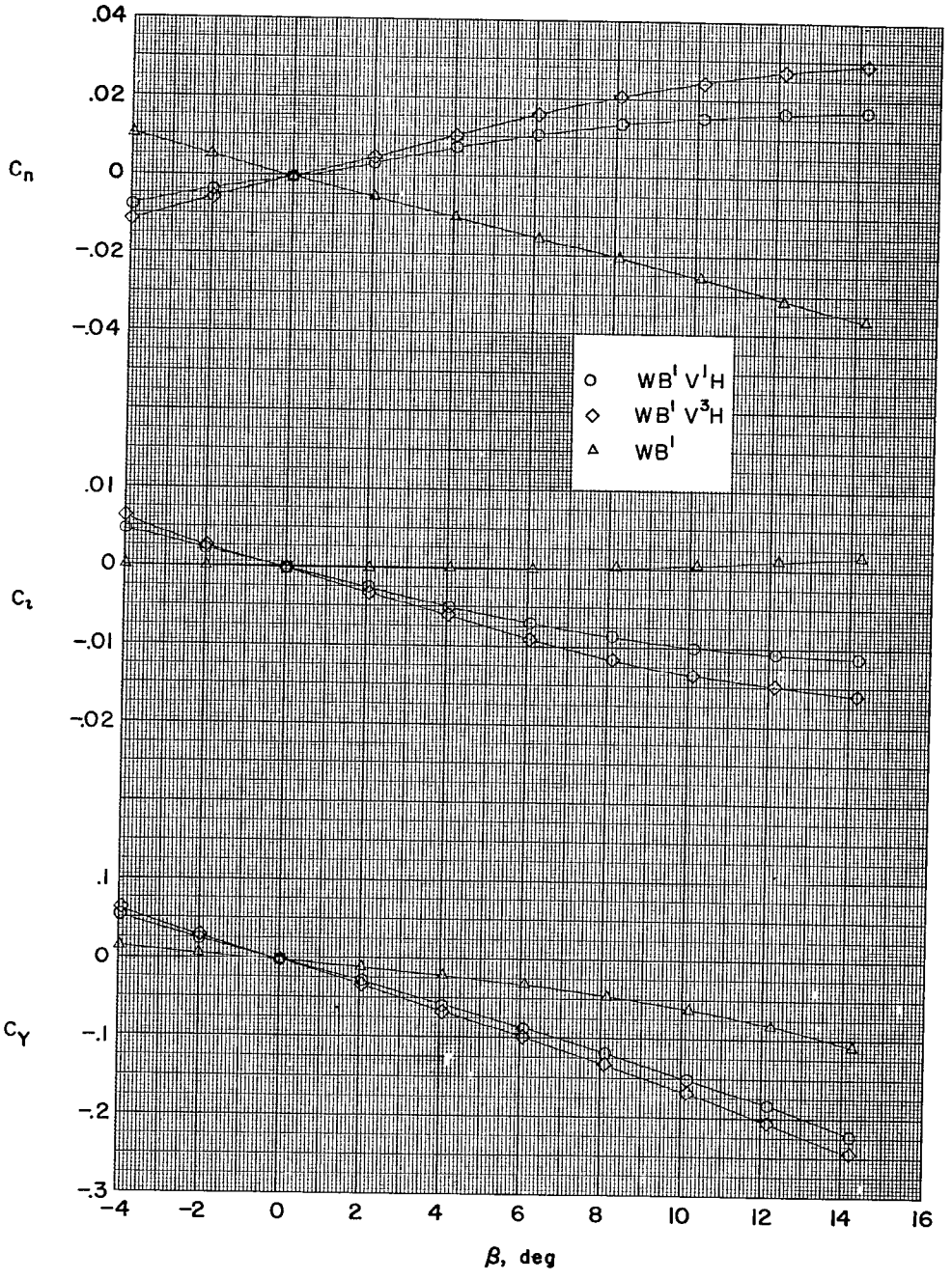


(a) $\alpha = 0^{\circ}$.

Figure 4.- Effects of various vertical tails on sideslip characteristics. Production model; M = 1.41.

[redacted]

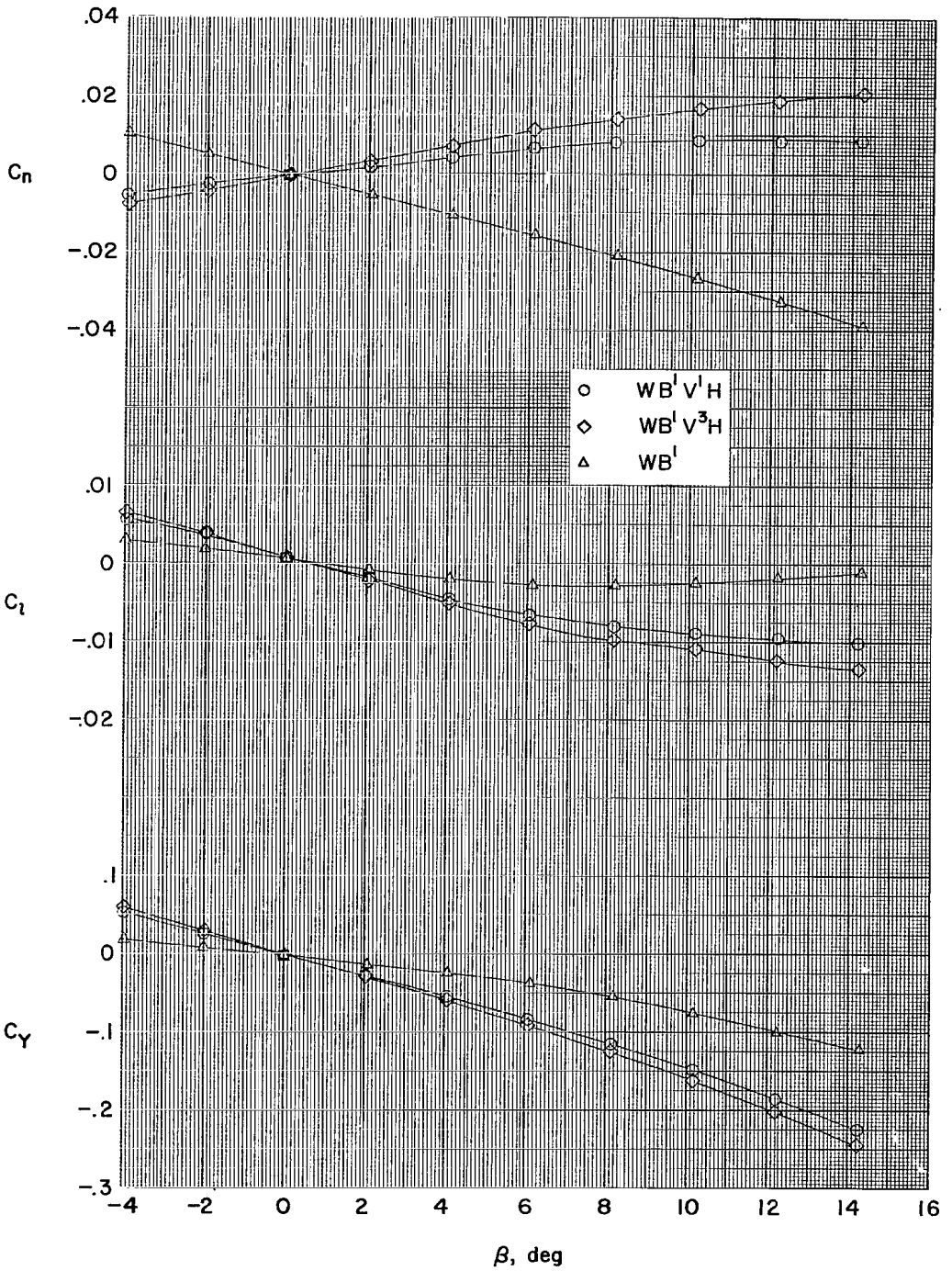


(b) $\alpha \approx 5.2^{\circ}$.

Figure 4.- Concluded.

[redacted]

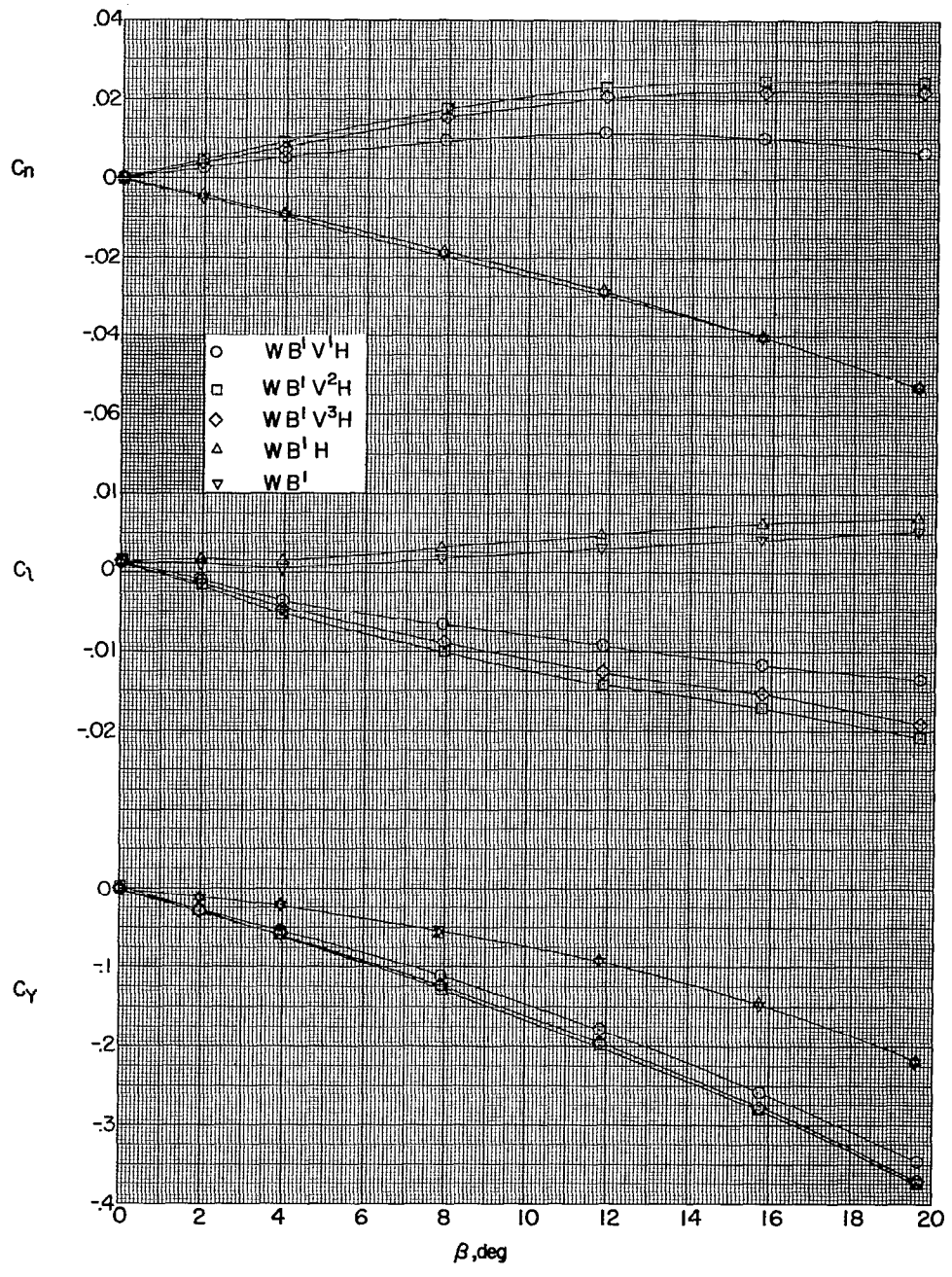


(a) $\alpha = 0^{\circ}$.

Figure 5.- Effect of various vertical tails on the sideslip characteristics. Production model; M = 1.61.

[redacted]

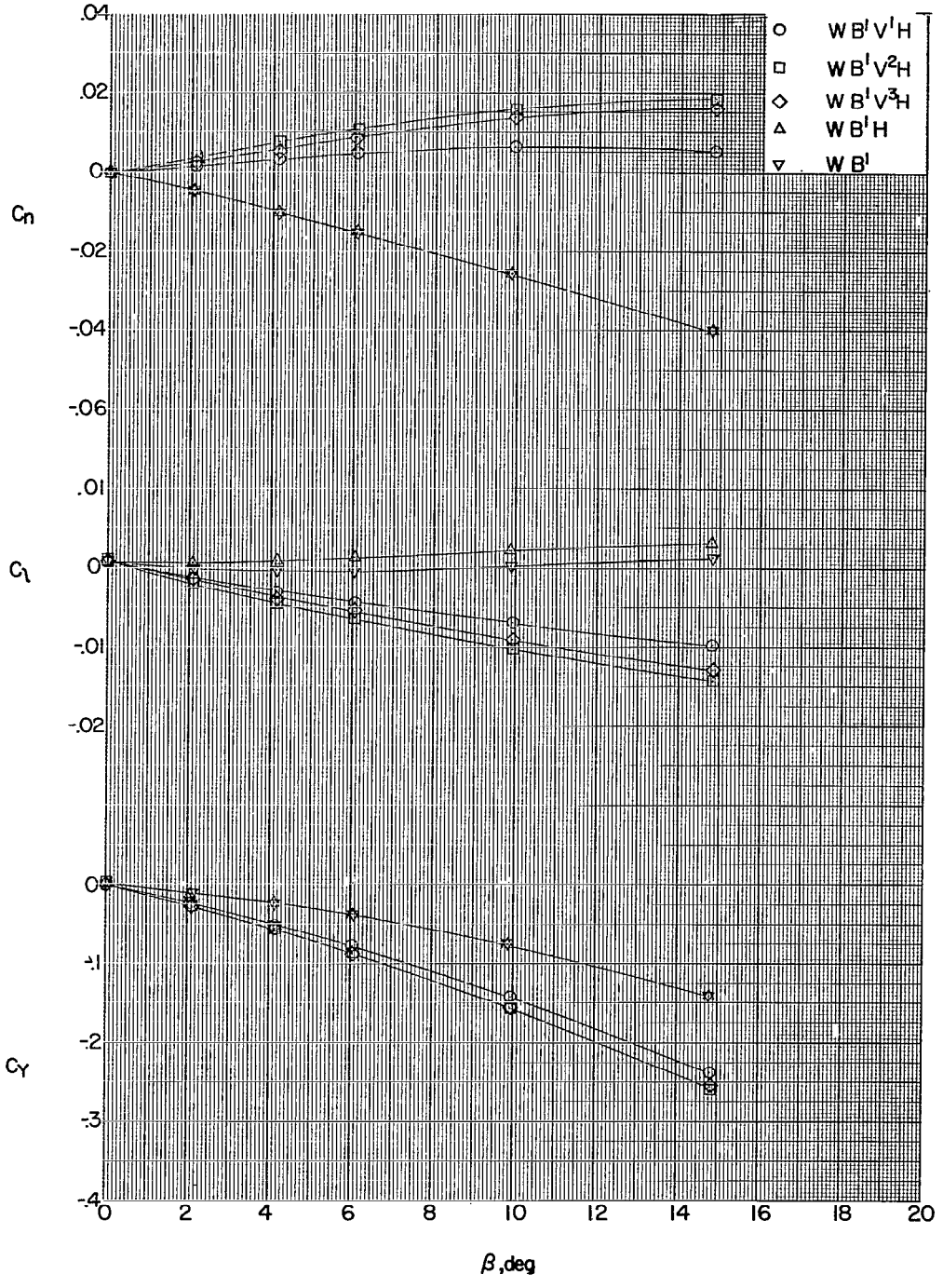


(b) $\alpha \approx 4.2^\circ$.

Figure 5.- Continued.

[redacted]

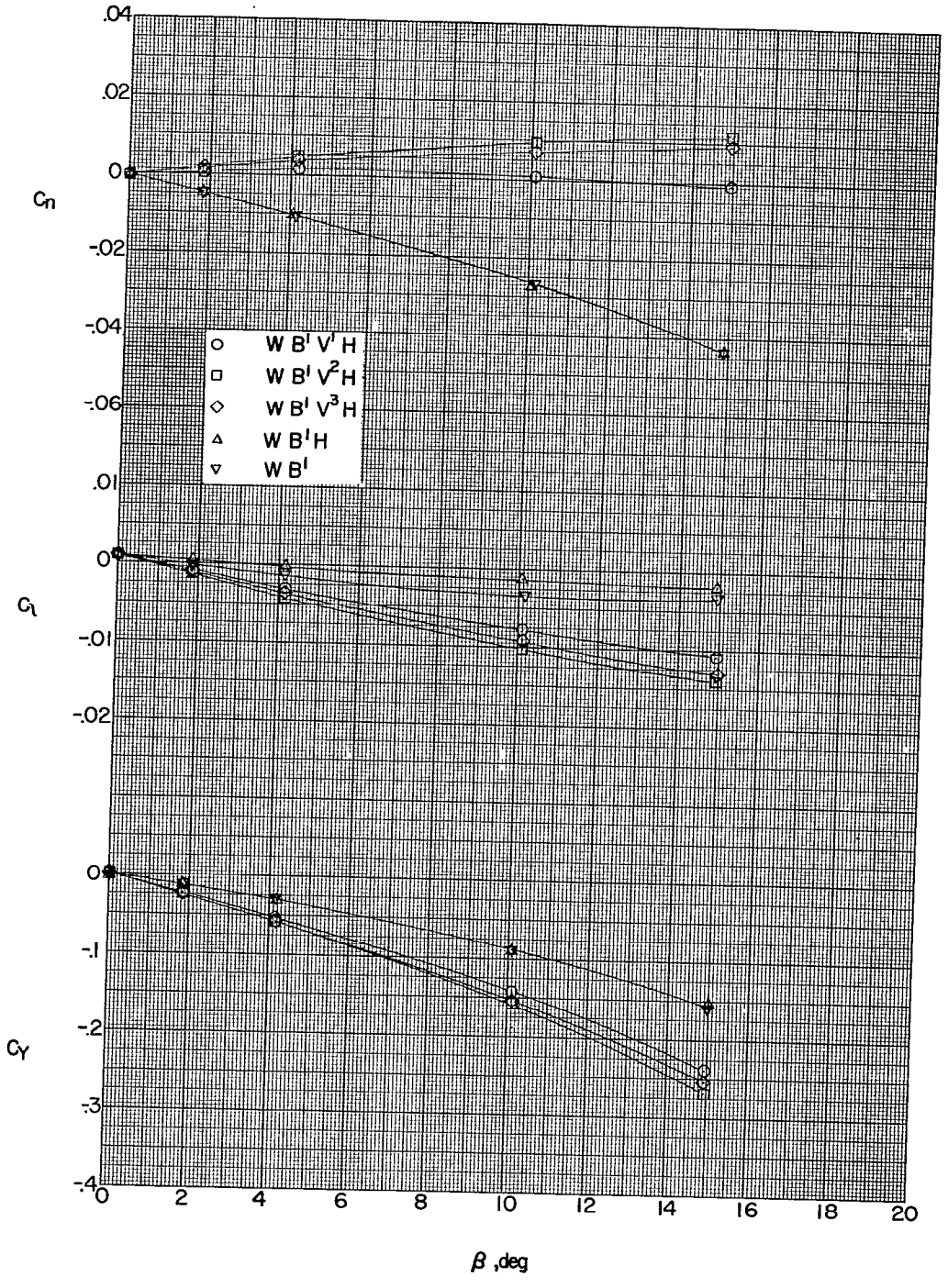


(c) $\alpha \approx 8.5°$.

Figure 5.- Continued.

[redacted]

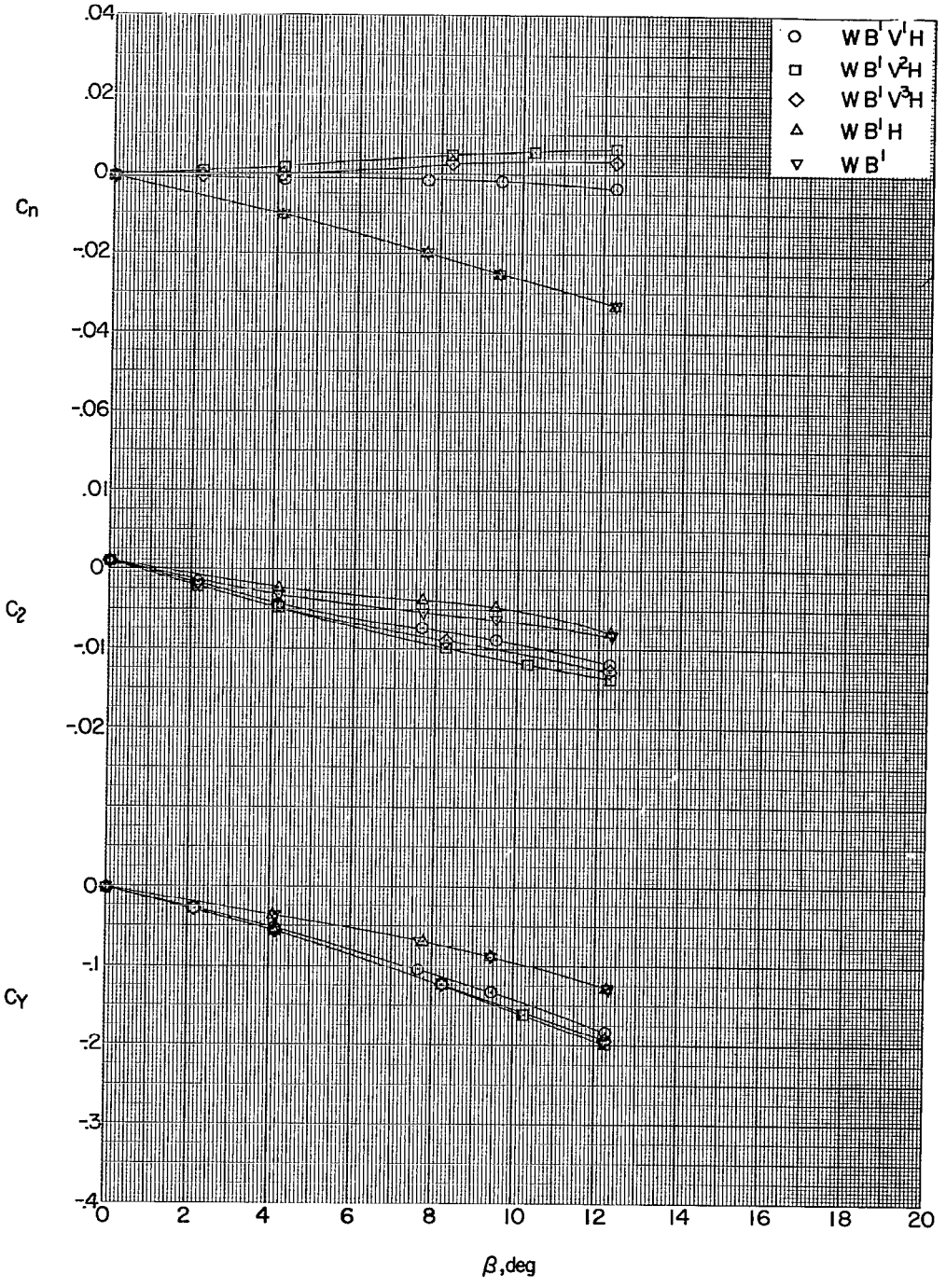


(d) $\alpha \approx 12.7^{\circ}$.

Figure 5.- Continued.

[redacted]

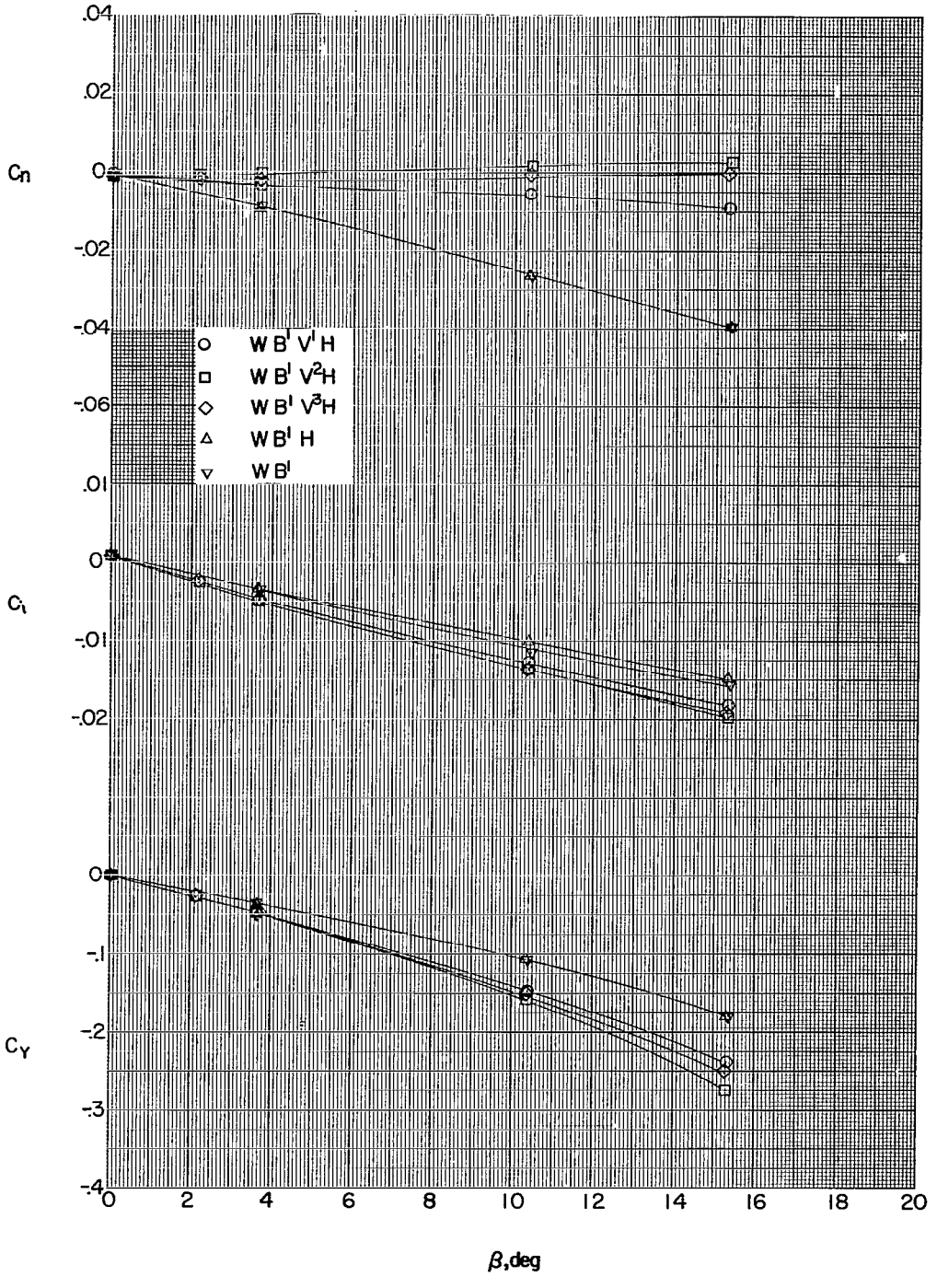


(e) $\alpha \approx 16^{\circ}$.

Figure 5.- Concluded.

[redacted]

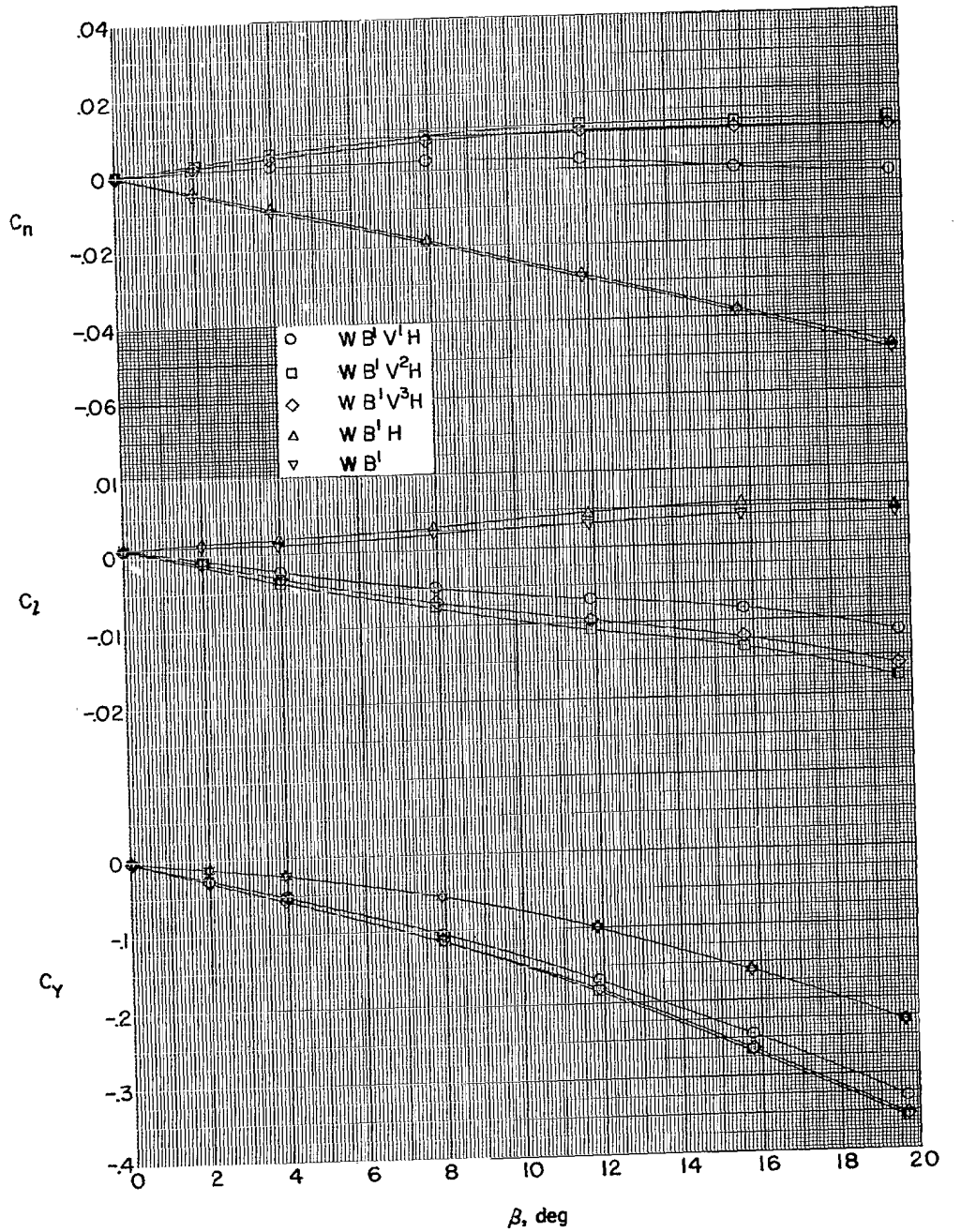


(a) $\alpha = 0$.

Figure 6.- Effect of vertical tails on the sideslip characteristics. Production model; M = 2.01.

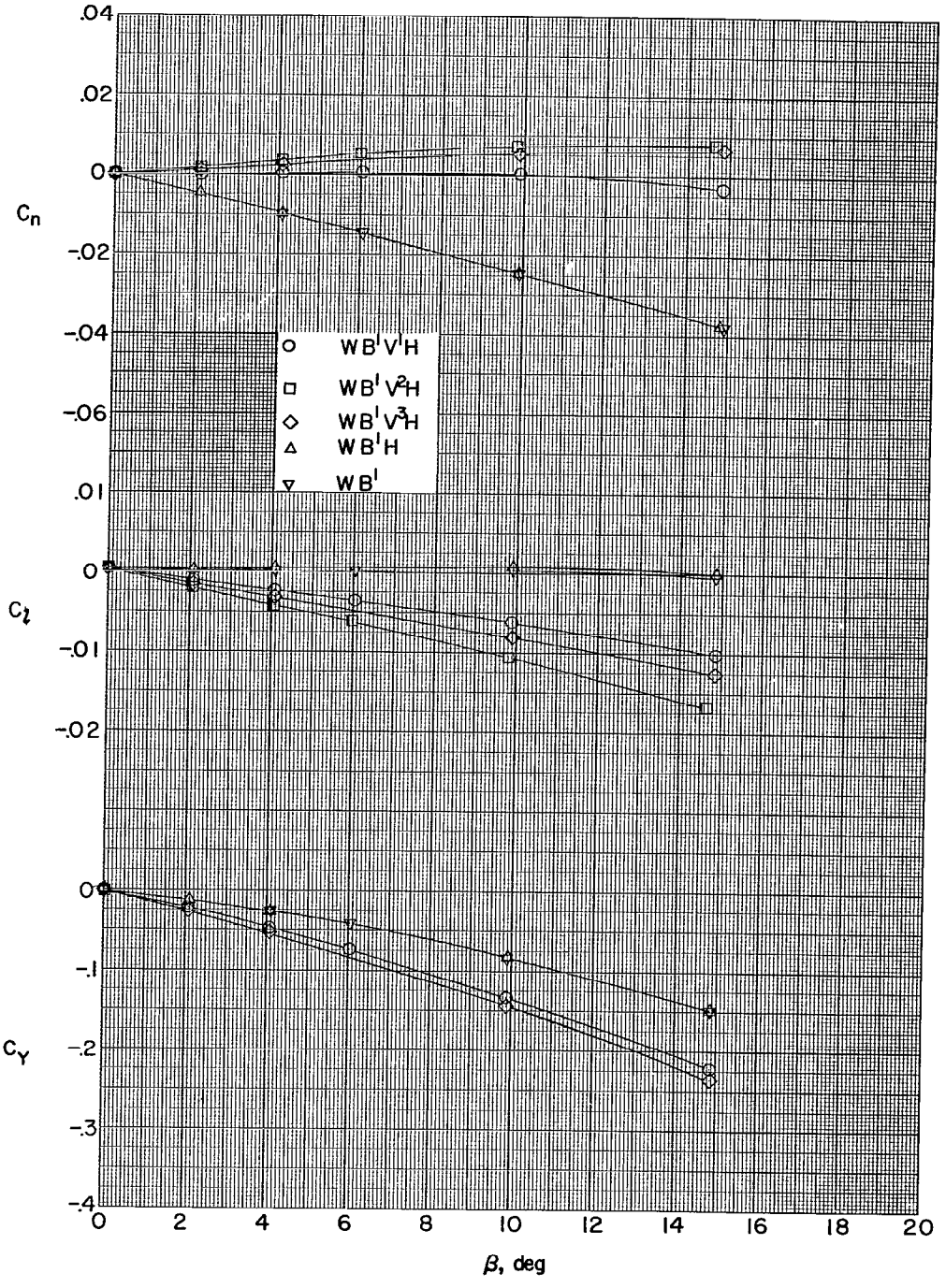


(b) $\alpha \approx 4.1^{\circ}$.

Figure 6.- Continued.

[redacted]

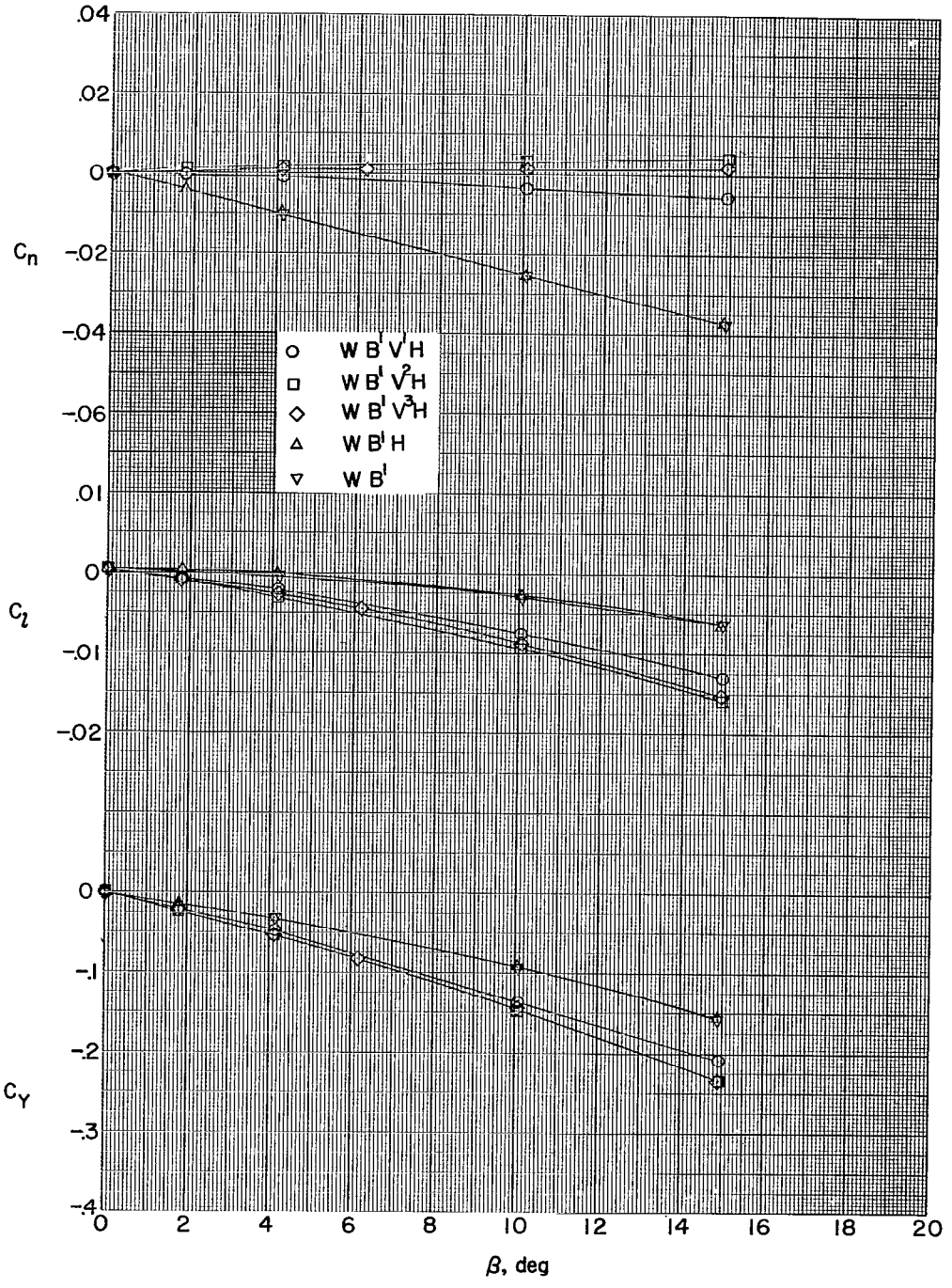


(c) $\alpha \approx 8.2^{\circ}$.

Figure 6.- Continued.

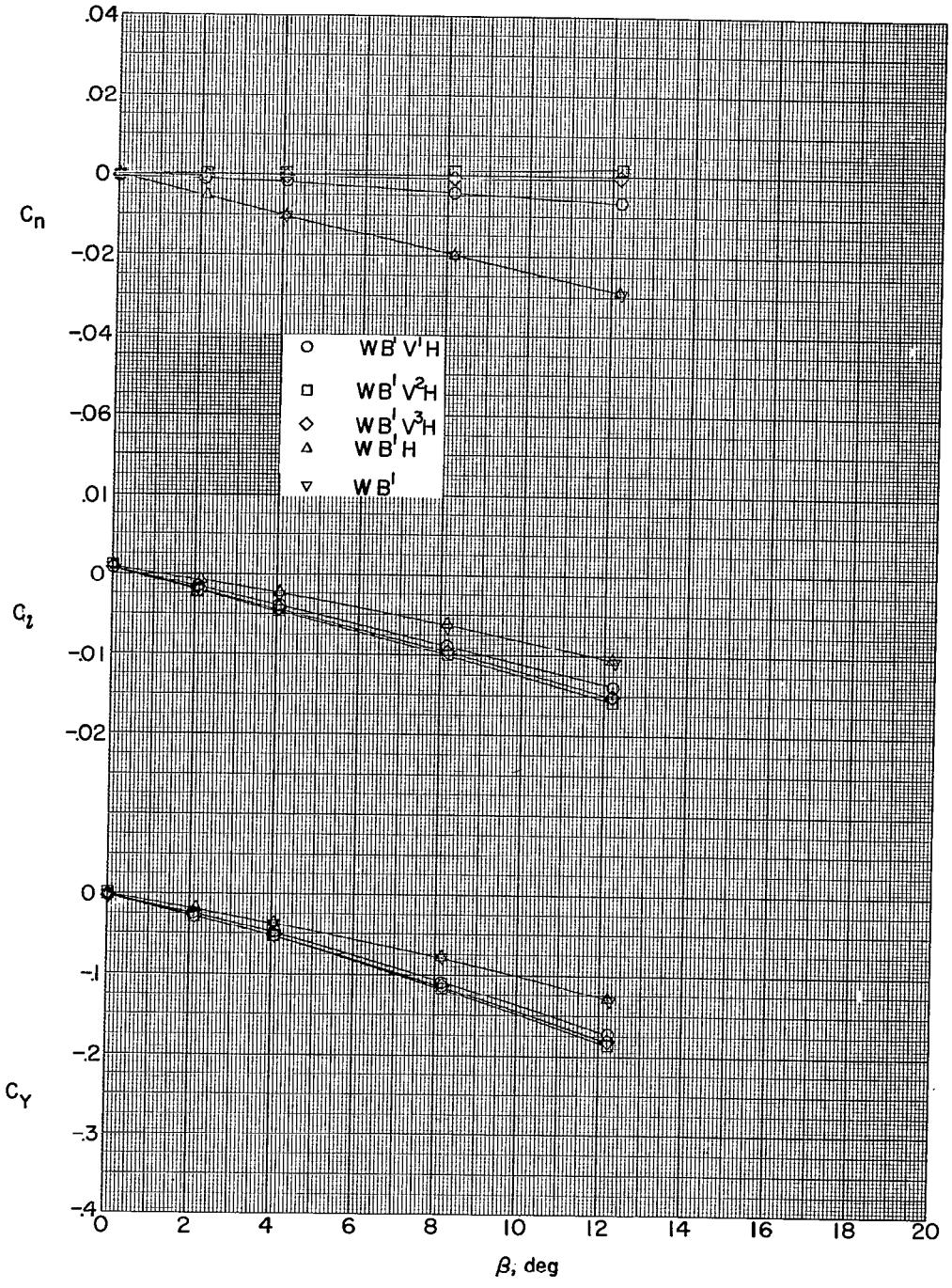


(d) $\alpha \approx 12.3^{\circ}$.

Figure 6.- Continued.

[redacted]

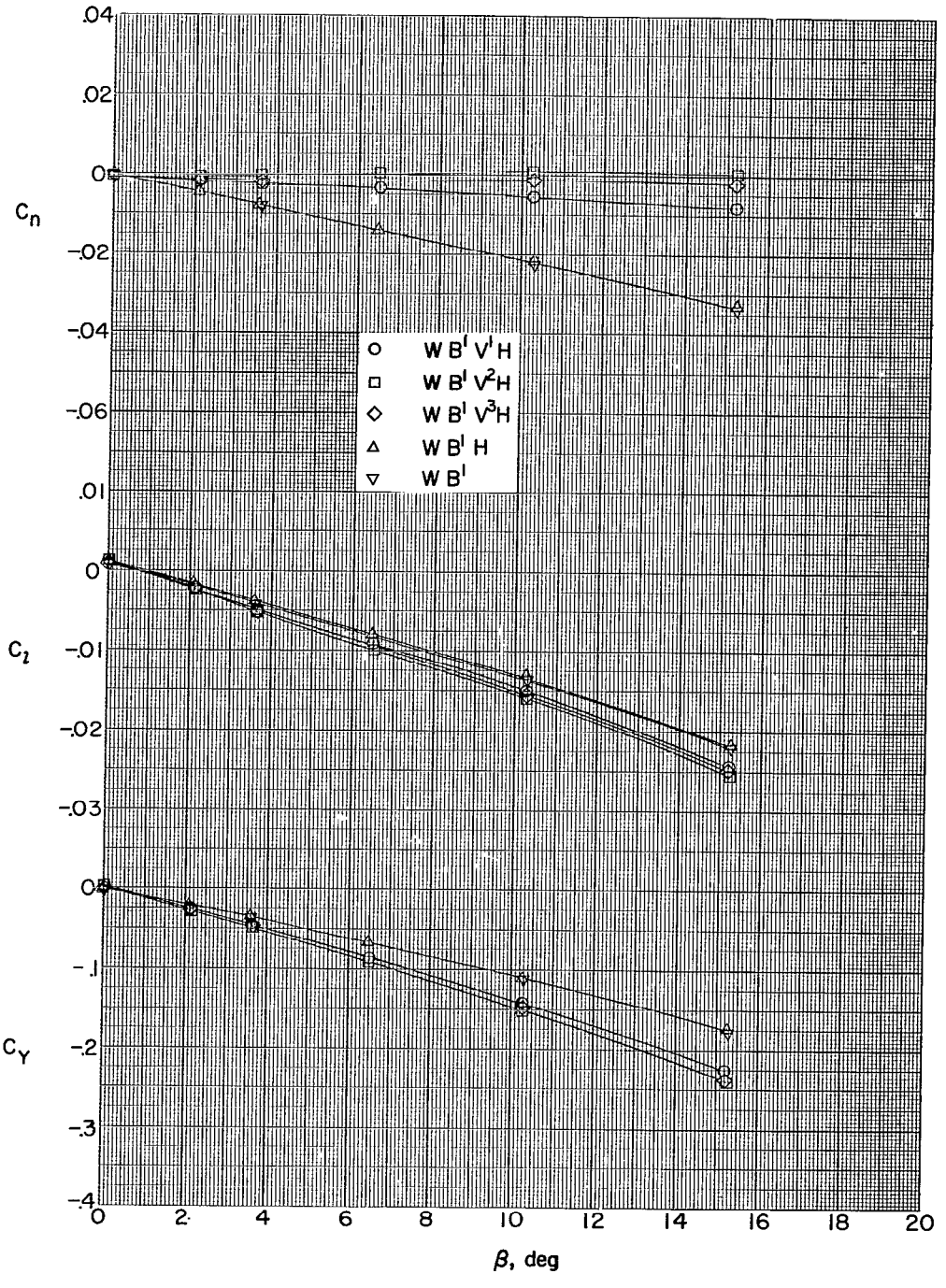


(e) $\alpha \approx 15.5^{\circ}$.

Figure 6.- Concluded.

[redacted]

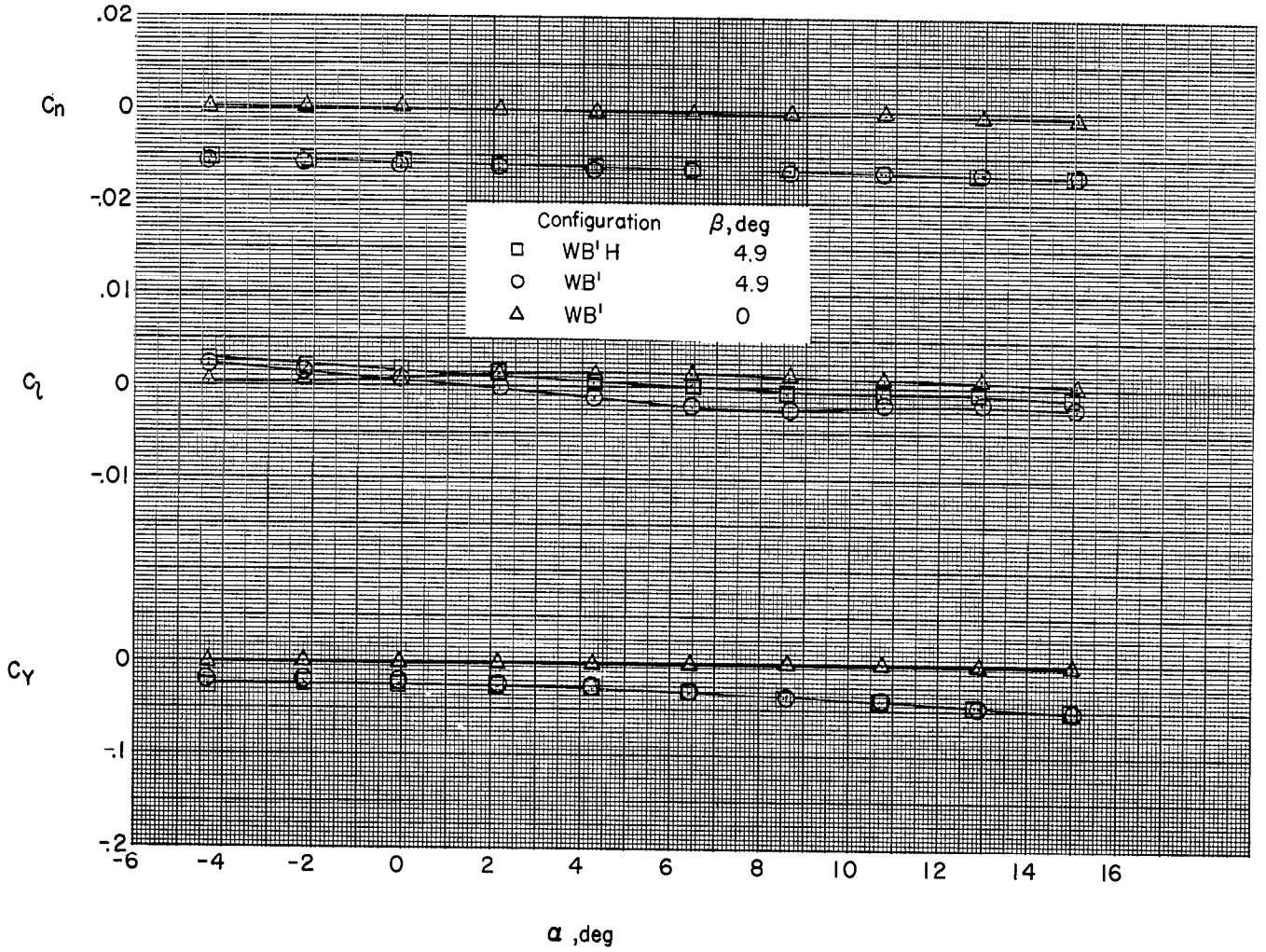


Figure 7.- Effect of horizontal tail on the variation of $C_n$, $C_l$, and $C_Y$ with $\alpha$ for the wing-body combination. Production nose; M = 1.41.

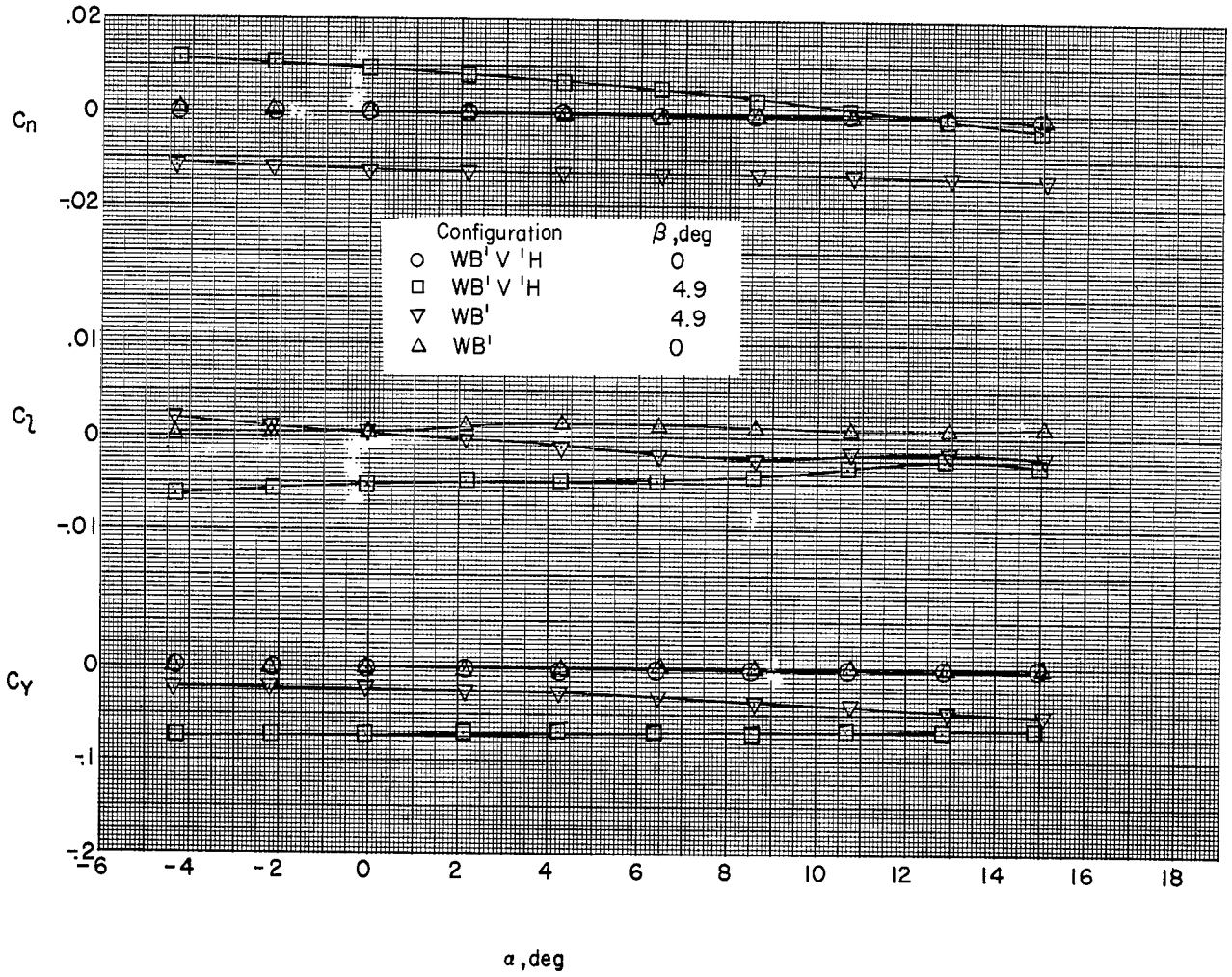


Figure 8.- Effect of vertical and horizontal tails on the variation of $C_n$, $C_l$, and $C_Y$ with $\alpha$ for the wing-body combination. Production model; M = 1.41.

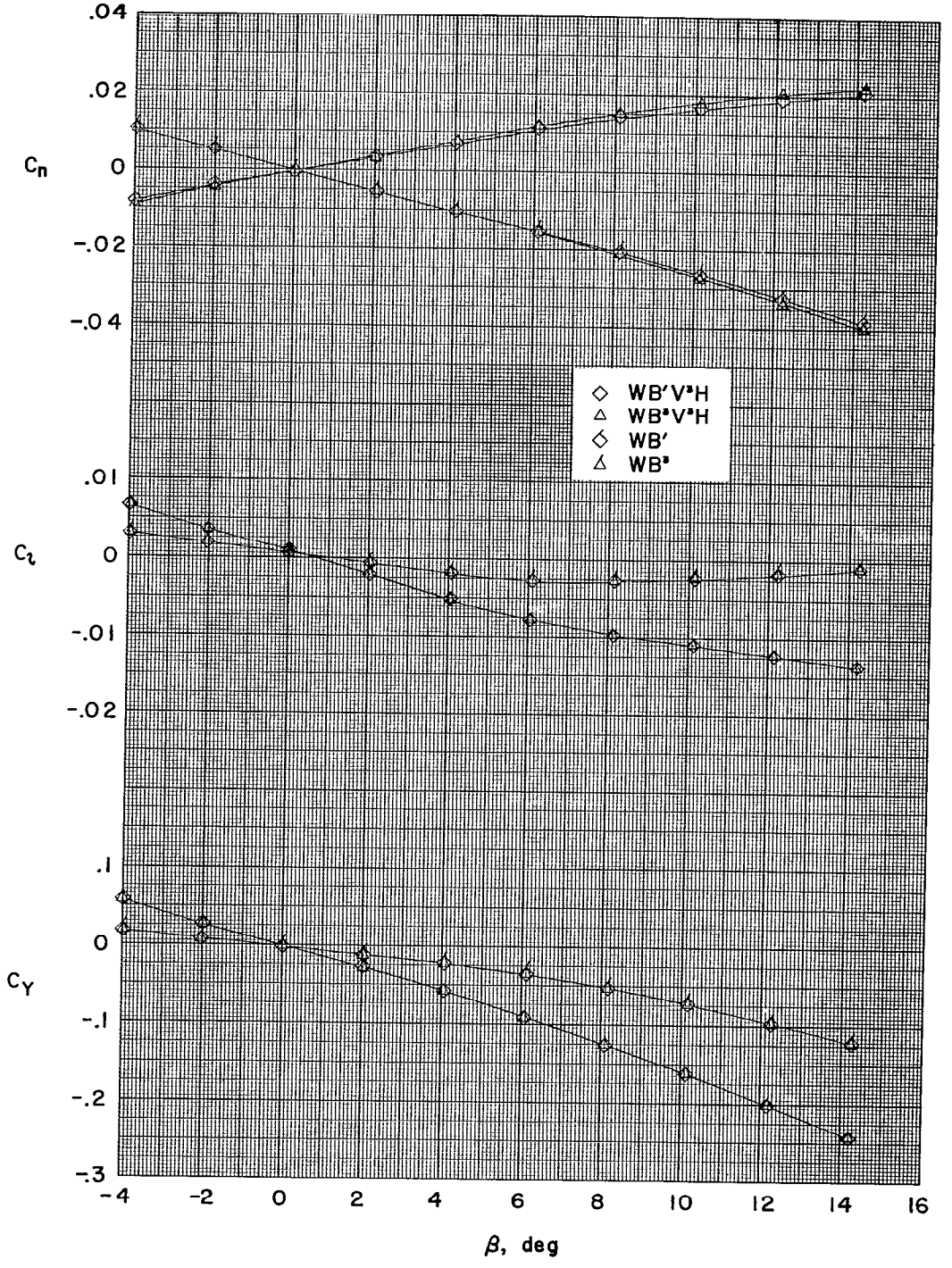


Figure 9.- Effect of afterbody modification, complete model, and wing-body combination on sideslip characteristics. $\alpha = 5.2^{\circ}$.

[redacted]

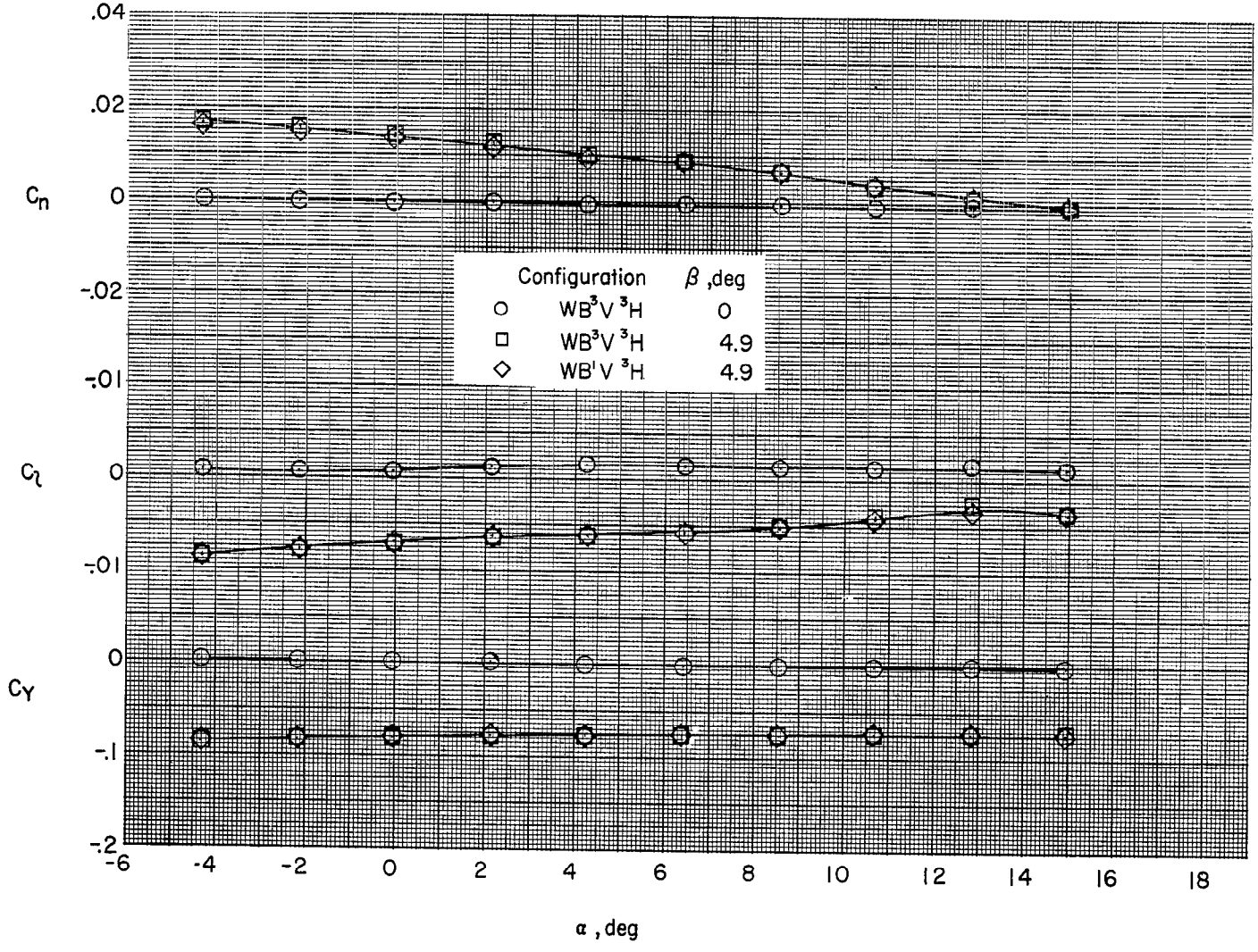


Figure 10.- Effect of afterbody modification with tail $V^3$ on the variation of $C_n$, $C_l$, and $C_Y$ with $\alpha$ for the complete model. M = 1.41.

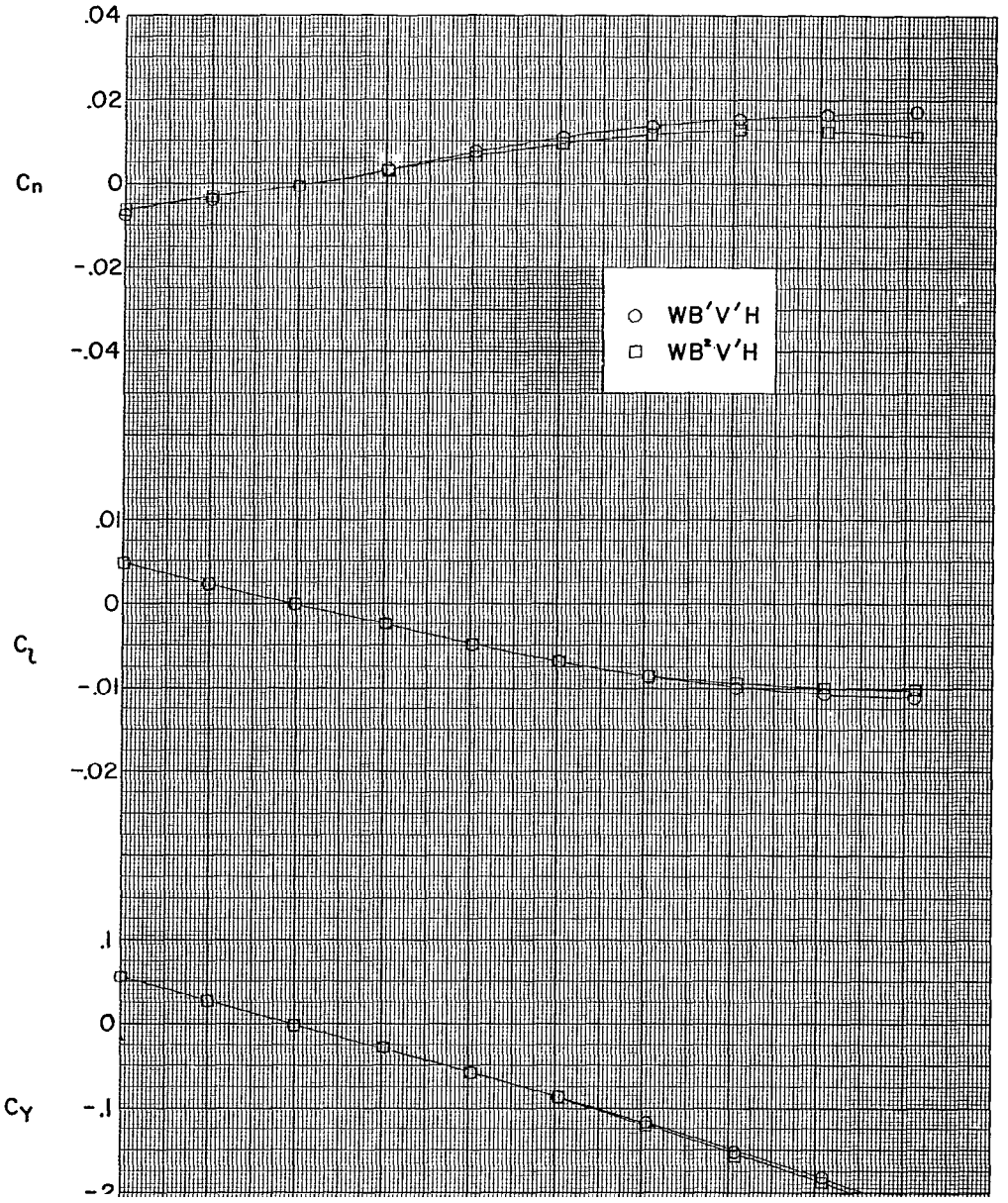
.04
.02
$C_n$
0
-.02
-.04
○ WB'V'H
□ WB²V'H
.01
0
$C_l$
-.01
-.02
.1
0
$C_Y$
-.1

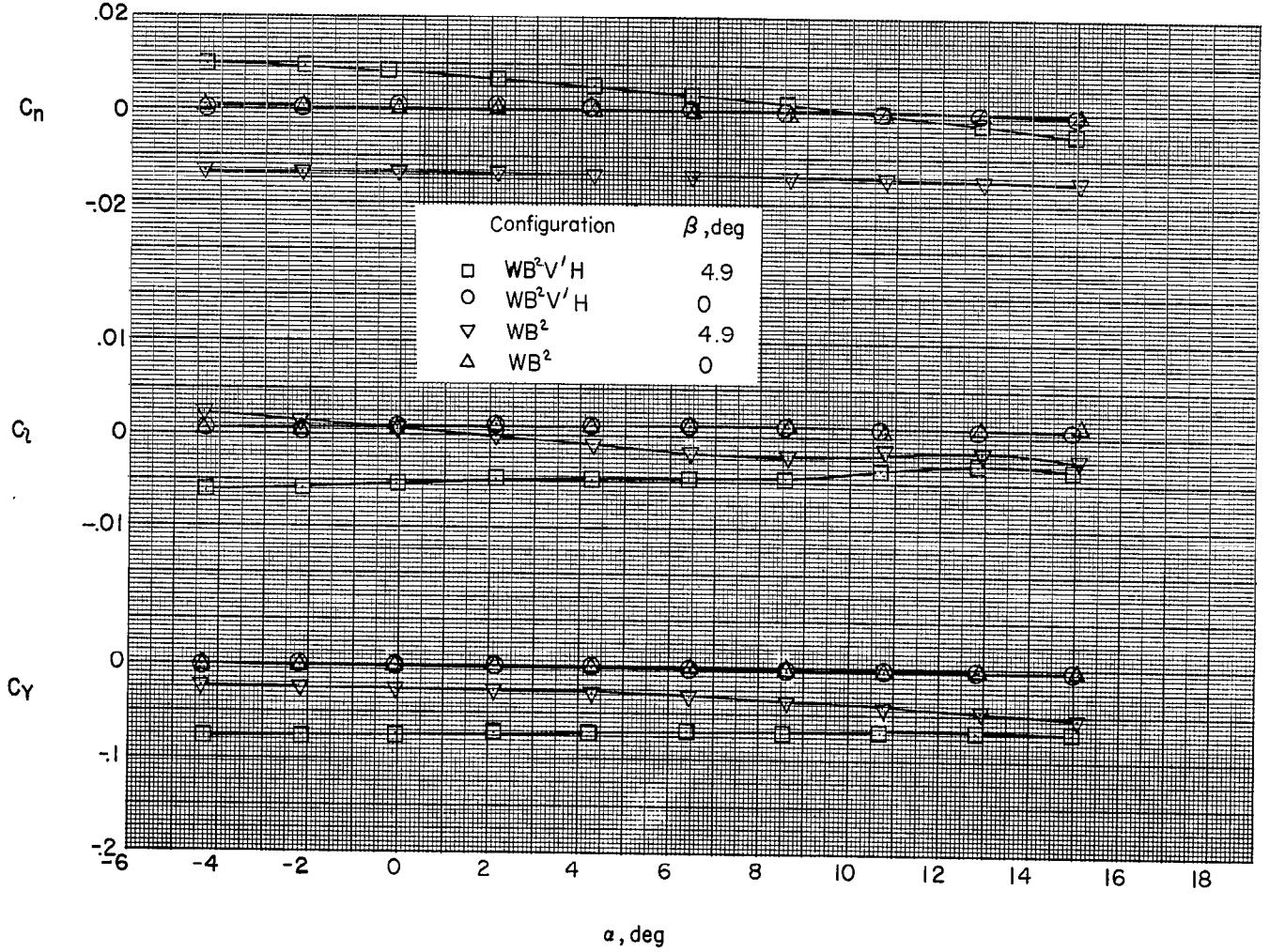


Figure 12.- Effect of vertical and horizontal tails on the variation of $C_n$, $C_l$, and $C_Y$ with $\alpha$ for the complete model and wing-body combination with photographic nose $(B^2)$. $M = 1.41$.

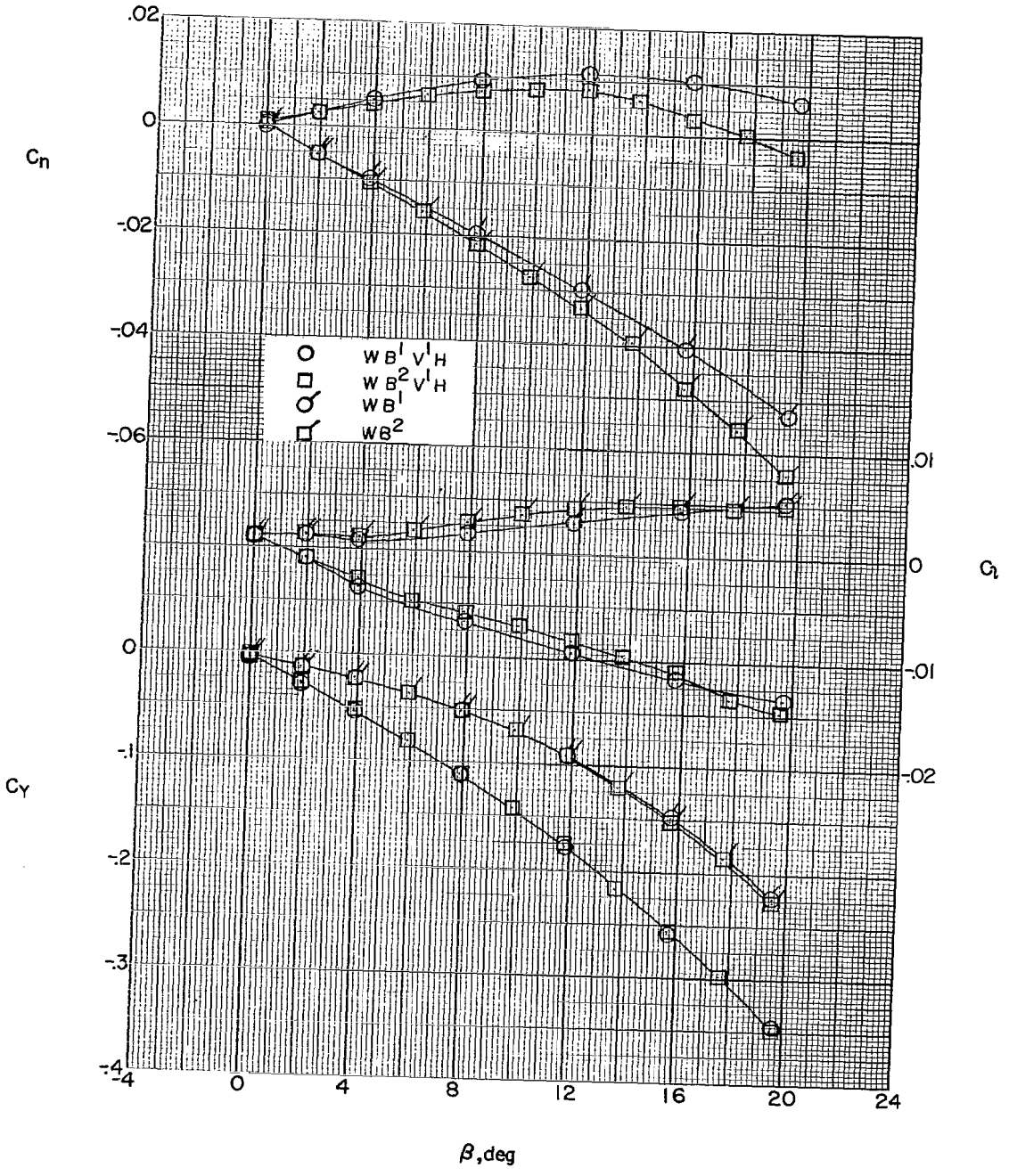


(a) $\alpha \approx 0^\circ$.

Figure 13.- Effect of photographic nose on the sideslip characteristics of the complete production model and wing-body combination. M = 1.61.

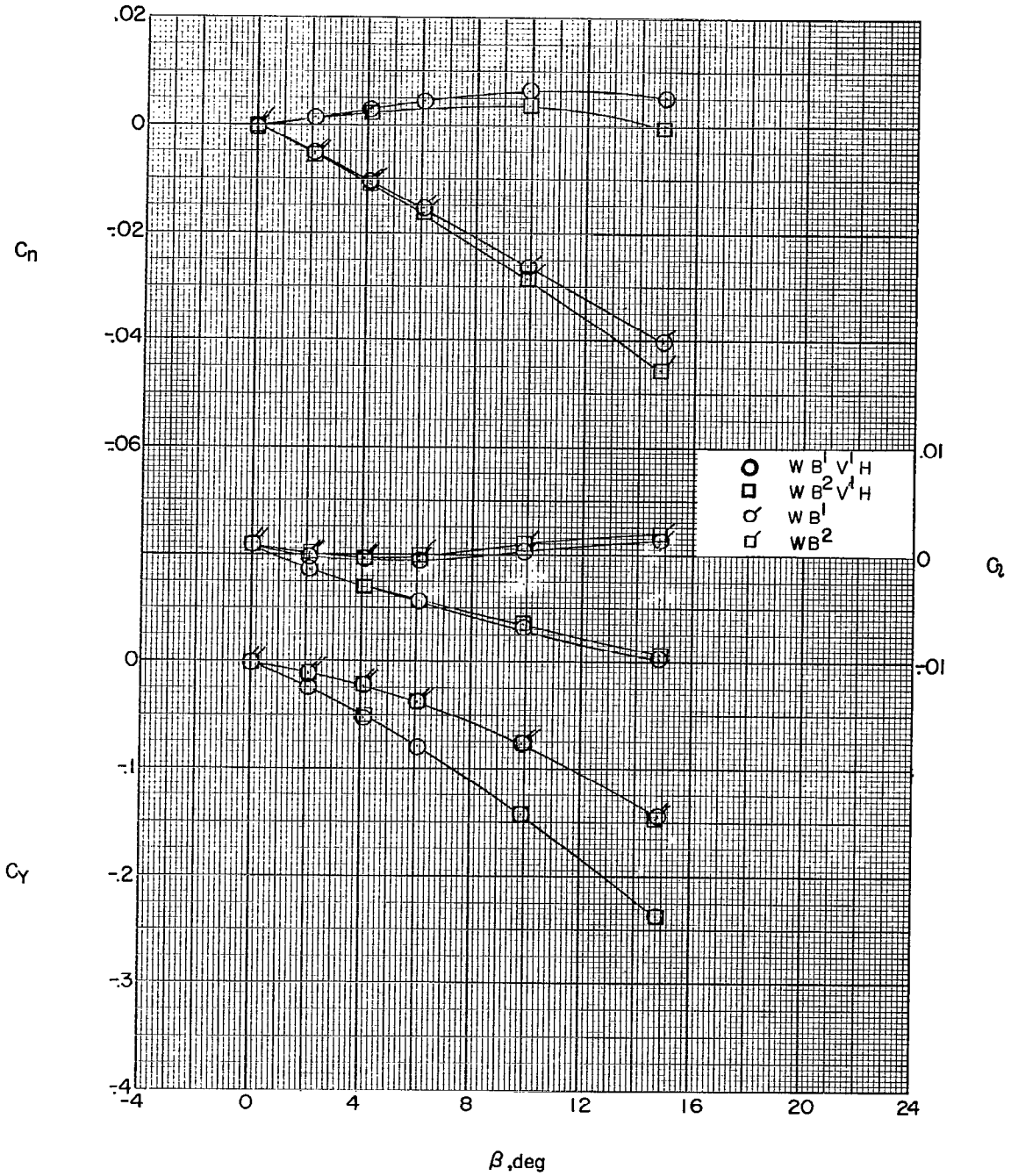


(b) $\alpha \approx 4.2^\circ$.

Figure 13.- Continued.

[redacted]

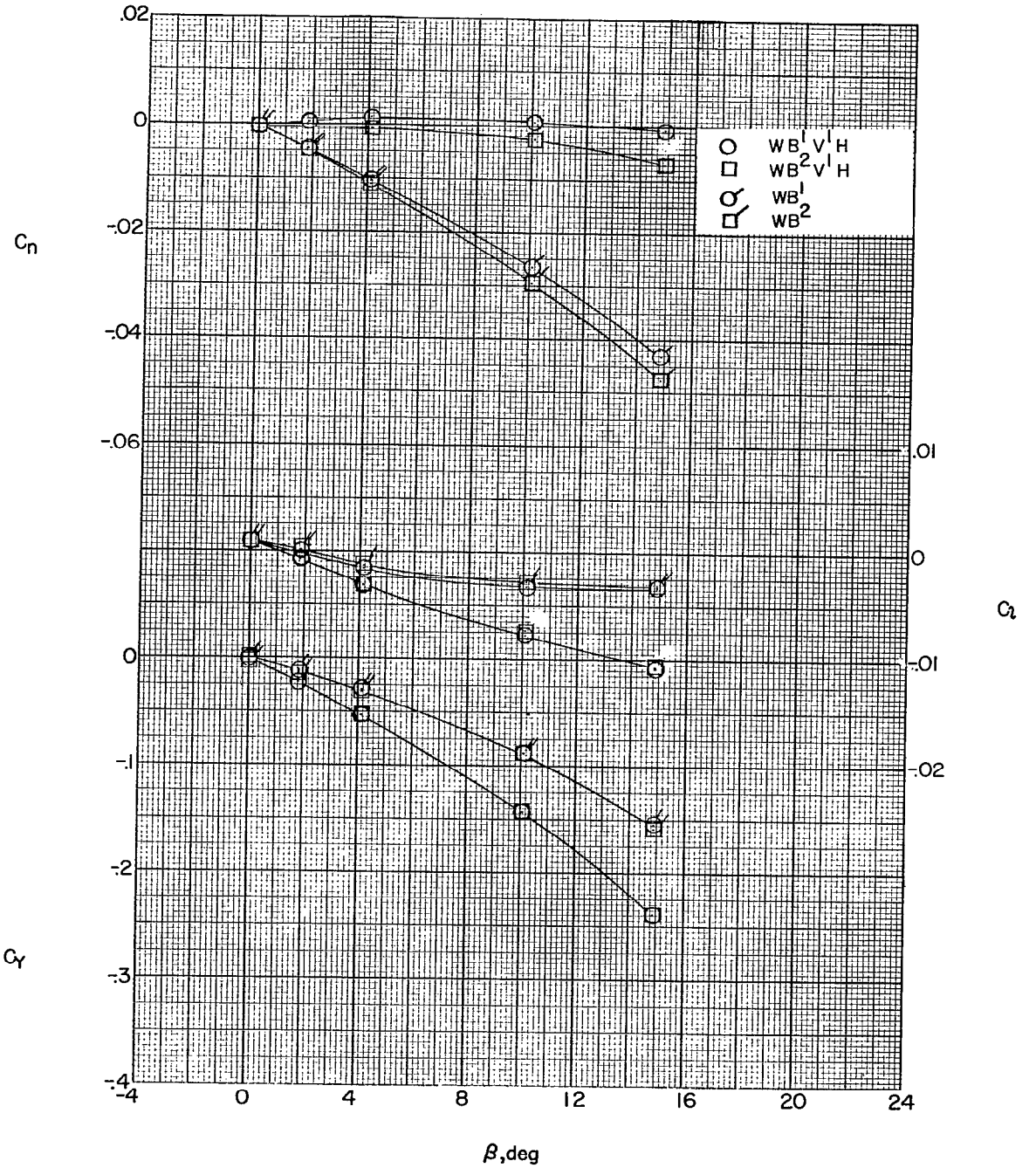


(c) $\alpha \approx 8.5^{\circ}$.

Figure 13.- Continued.

[redacted]

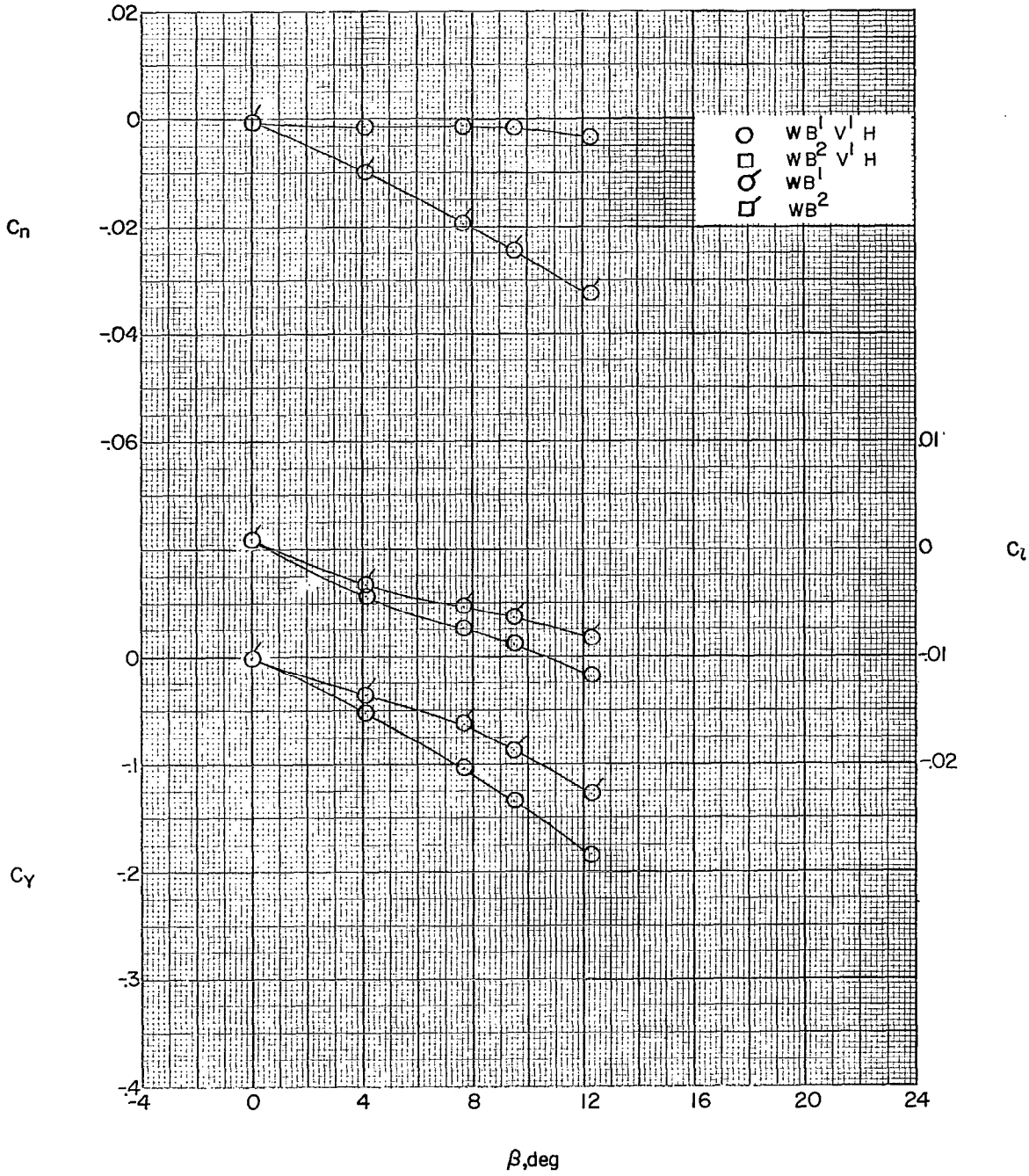


(d) $\alpha \approx 12.7^{\circ}$.

Figure 13.- Continued.

[redacted]

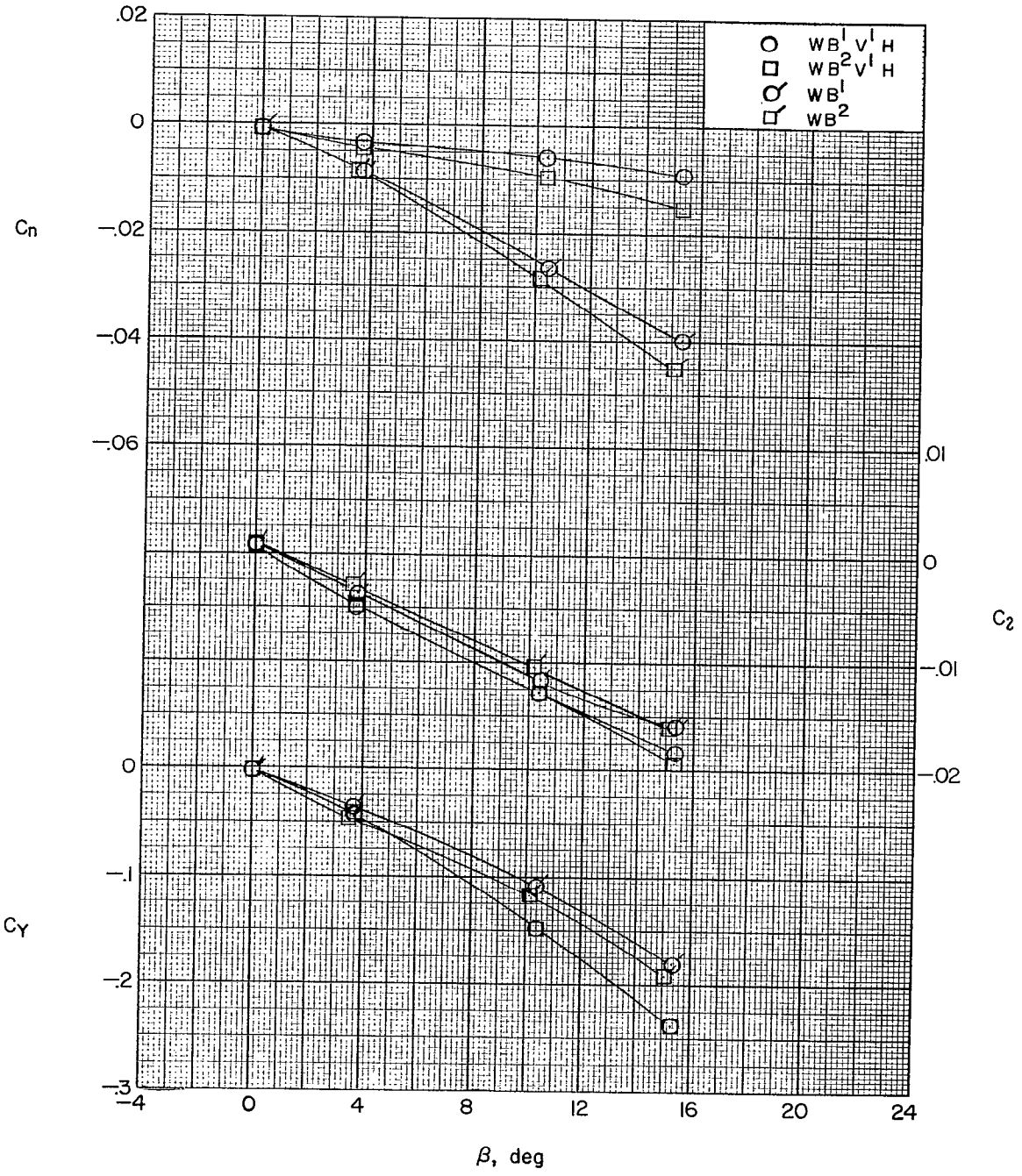


(e) $\alpha \approx 16^{\circ}$.

Figure 13.- Concluded.

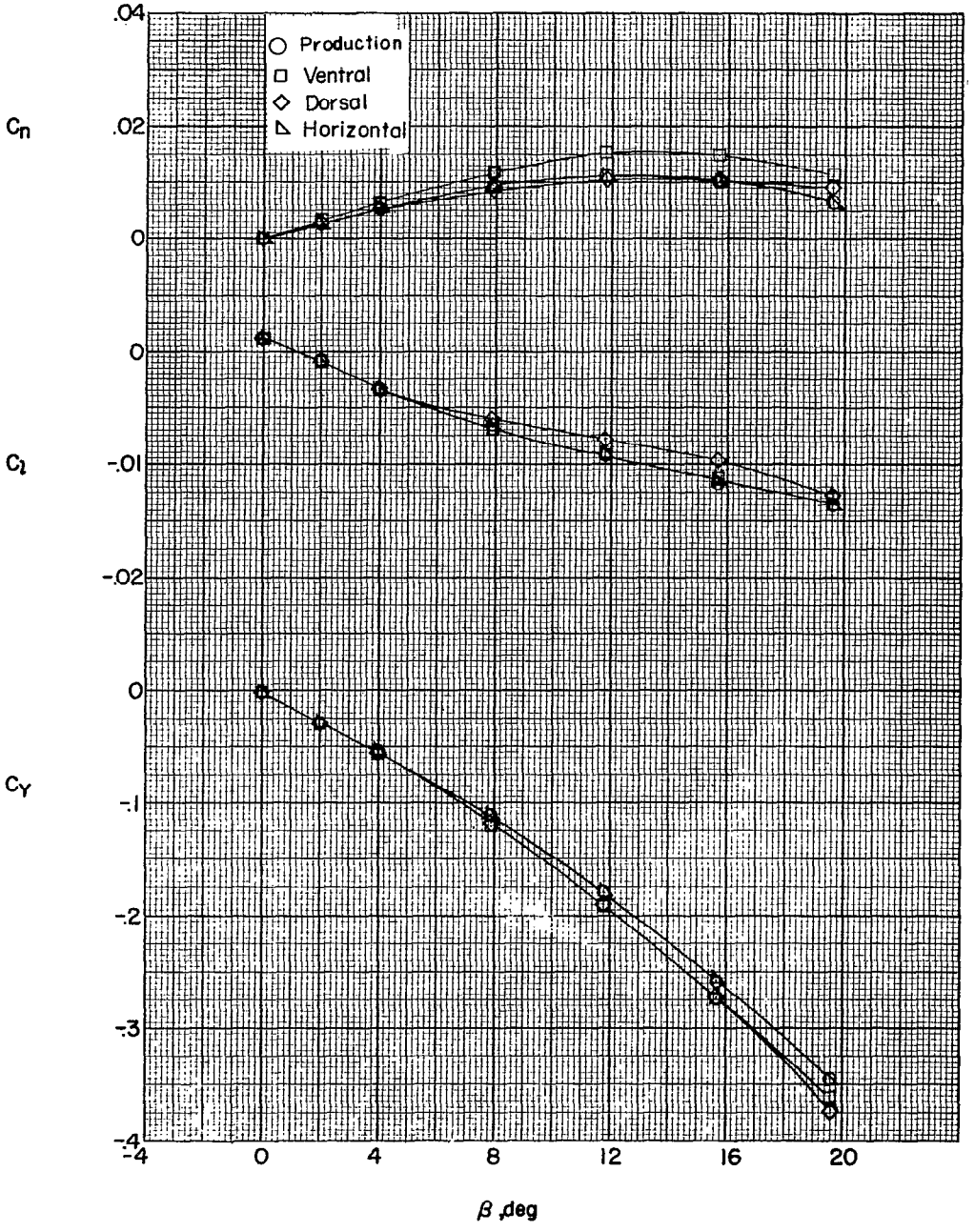


(a) $\alpha \approx 0°$.

Figure 14.- Effect of ventral, dorsal, and horizontal fins on the sideslip characteristics of the complete production model. M = 1.61.

[redacted]

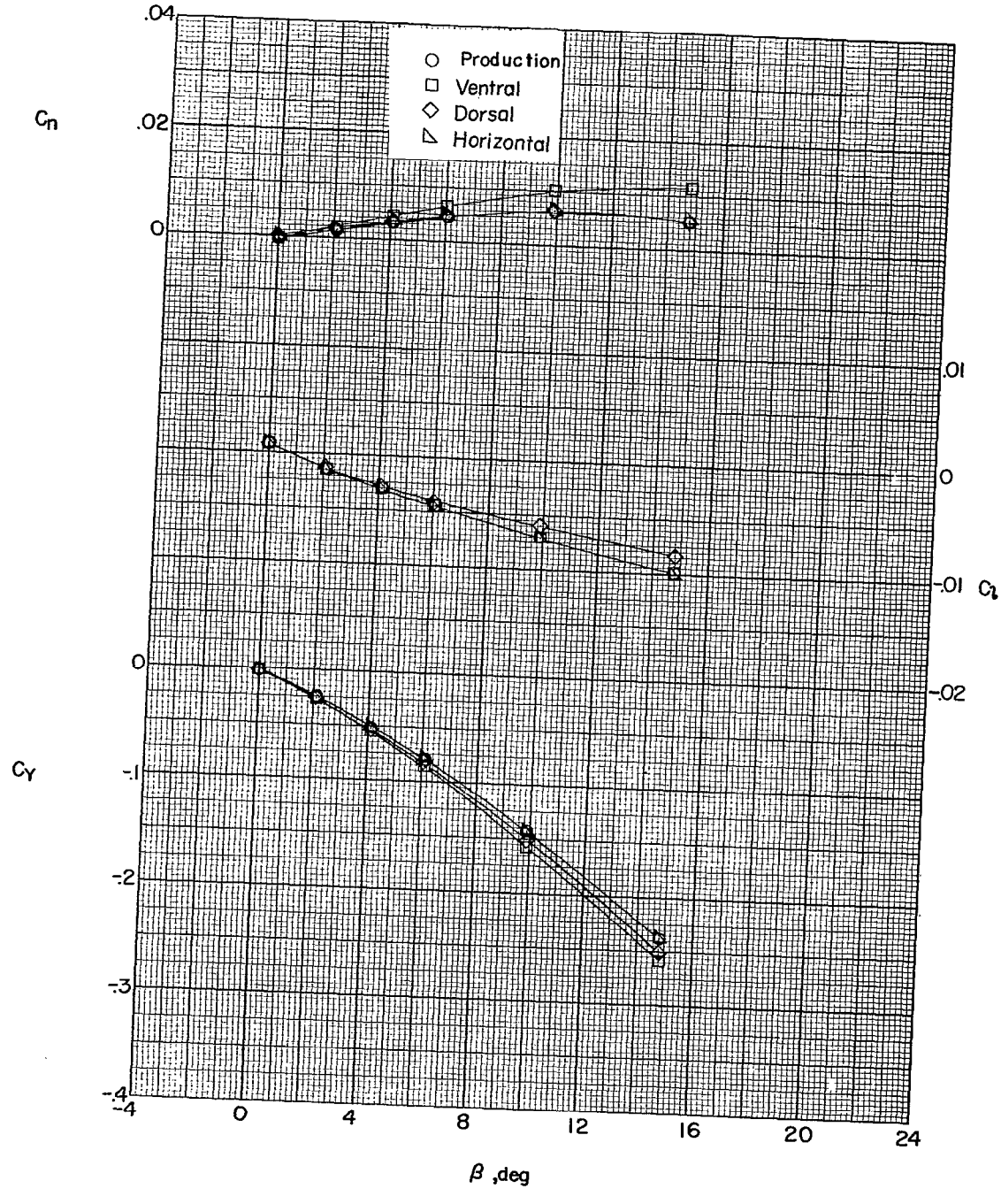


(b) $\alpha \approx 4.2^{\circ}$.

Figure 14.- Continued.

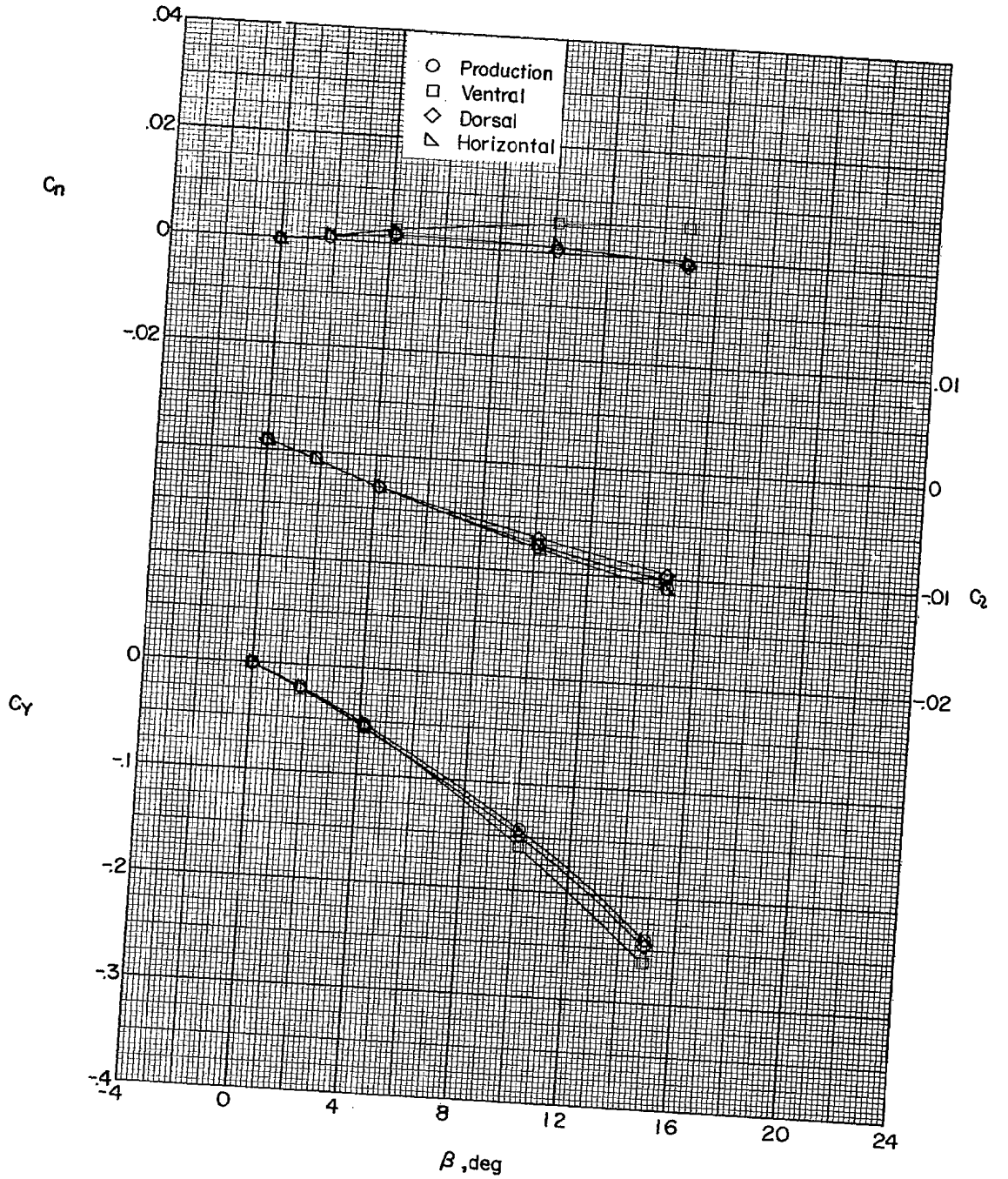


(c) $\alpha \approx 8.5°$.

Figure 14.- Continued.

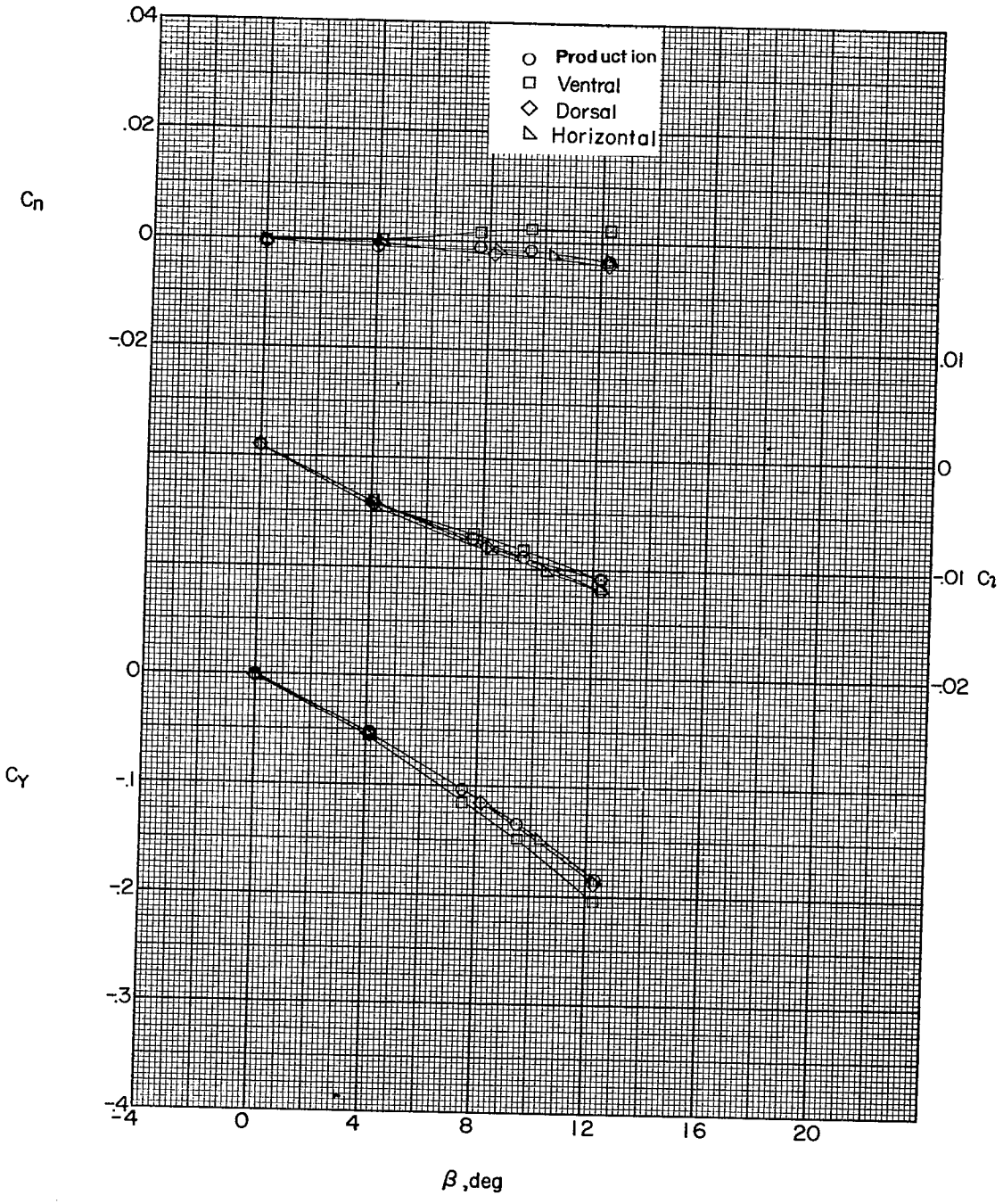


(d) $\alpha \approx 12.7^{\circ}$.

Figure 14.- Continued.

[redacted]

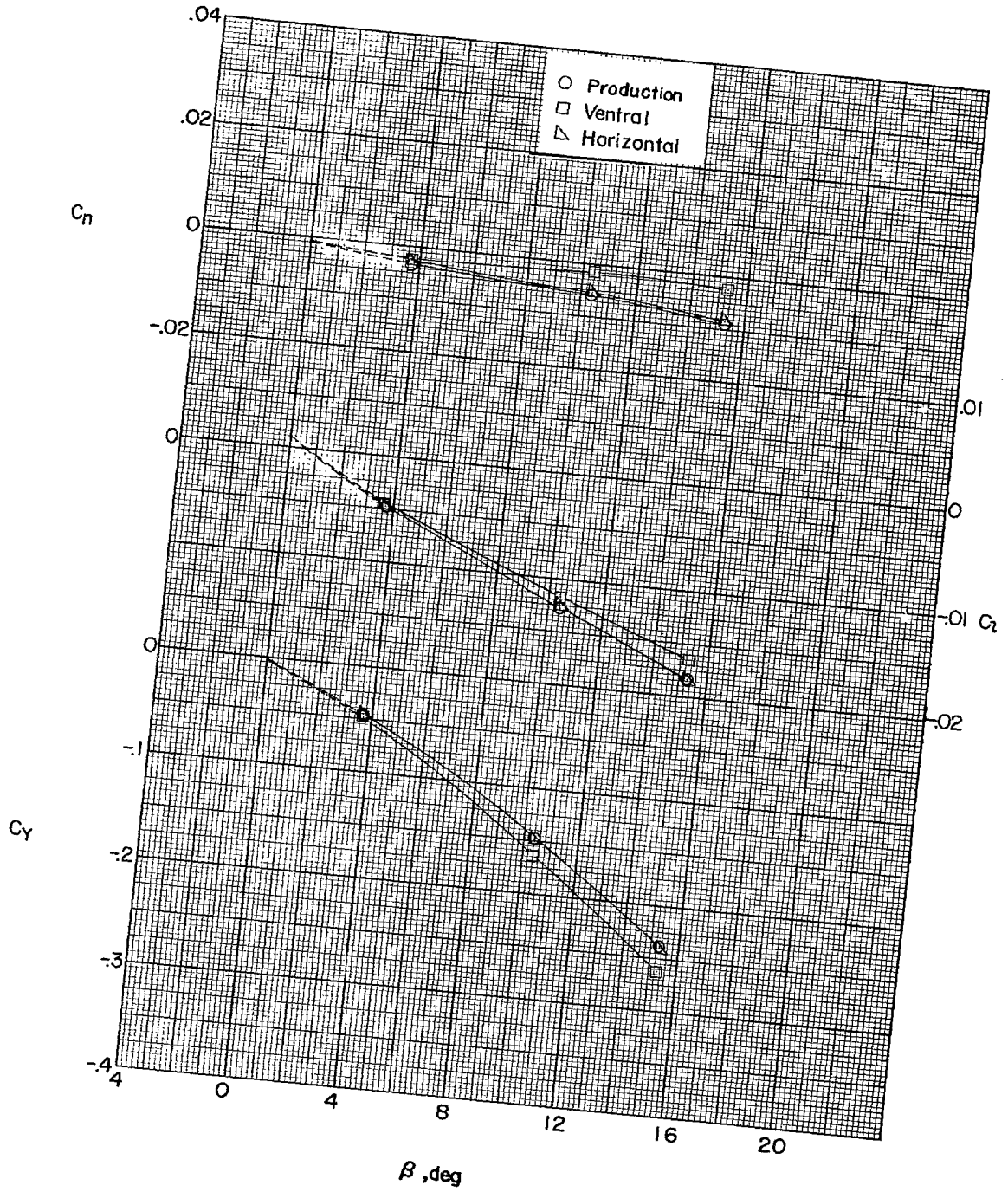


(e) $\alpha = 16^{\circ}$.

Figure 14.- Concluded.

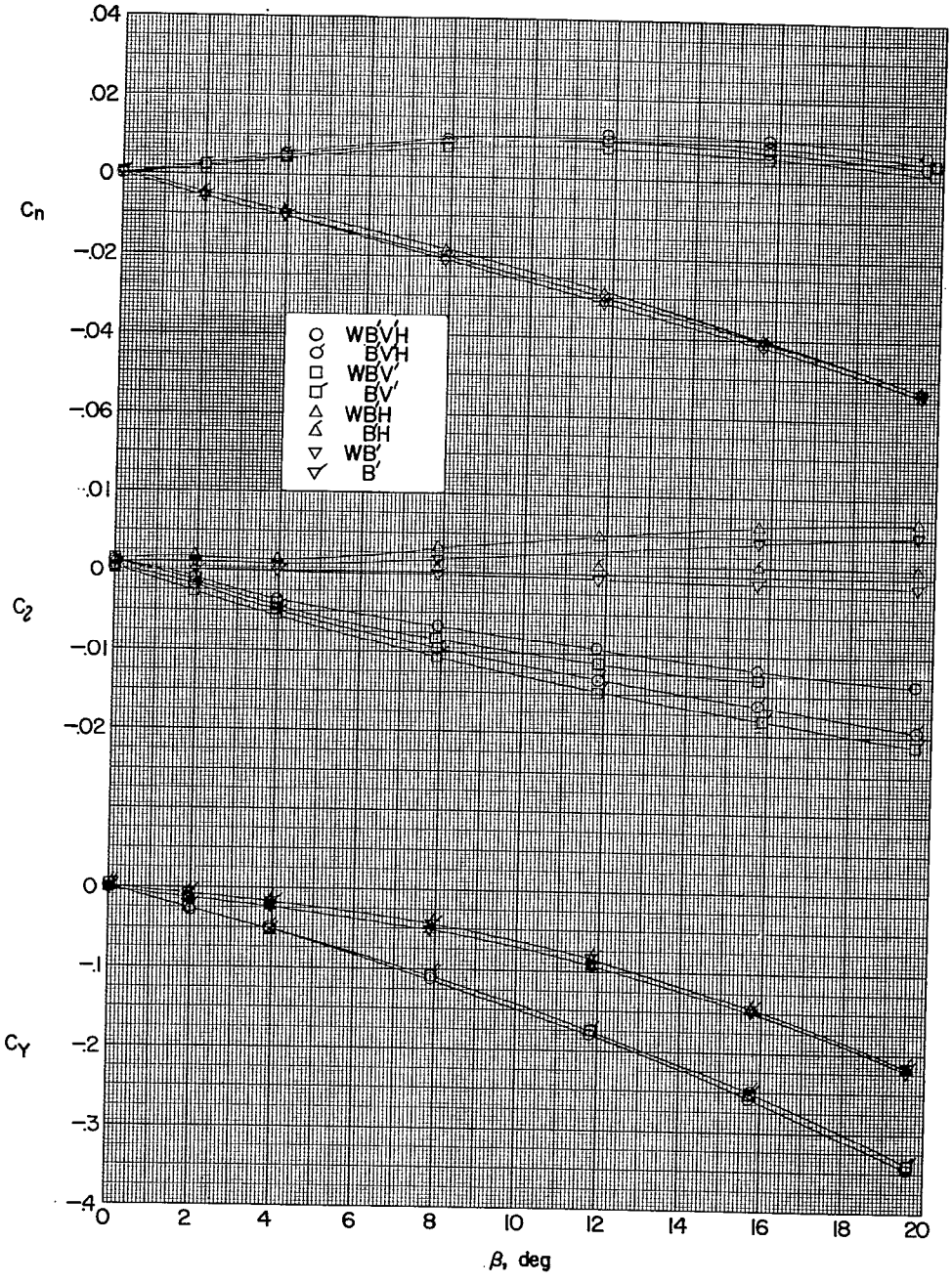


(a) $\alpha \approx 0^{\circ}$.

Figure 15.- Effects of various combinations of components on the sideslip characteristics. Production model; tail $V_1$; M = 1.61.

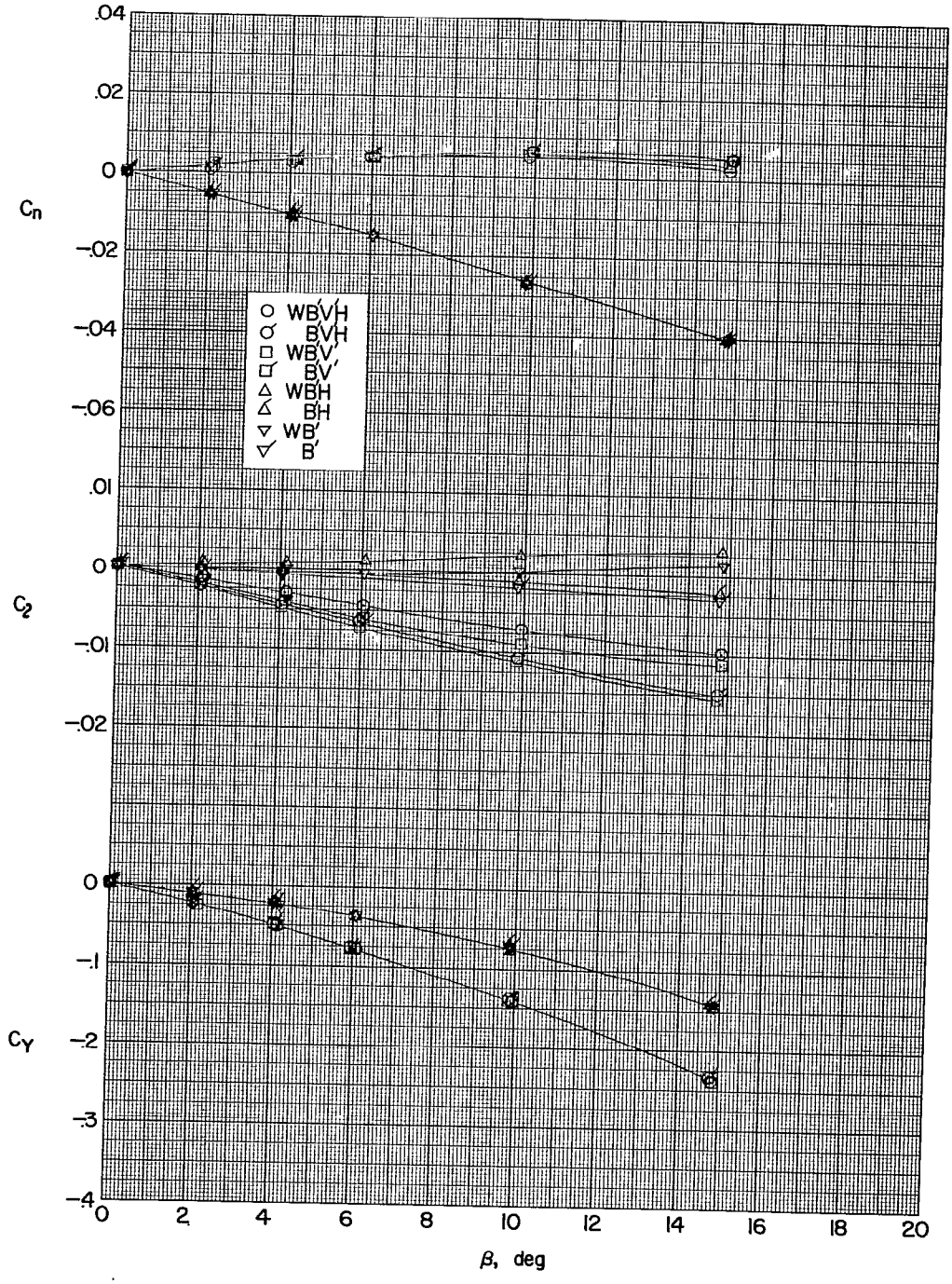


(b) $\alpha \approx 4.2^{\circ}$.

Figure 15.- Continued.

[redacted]

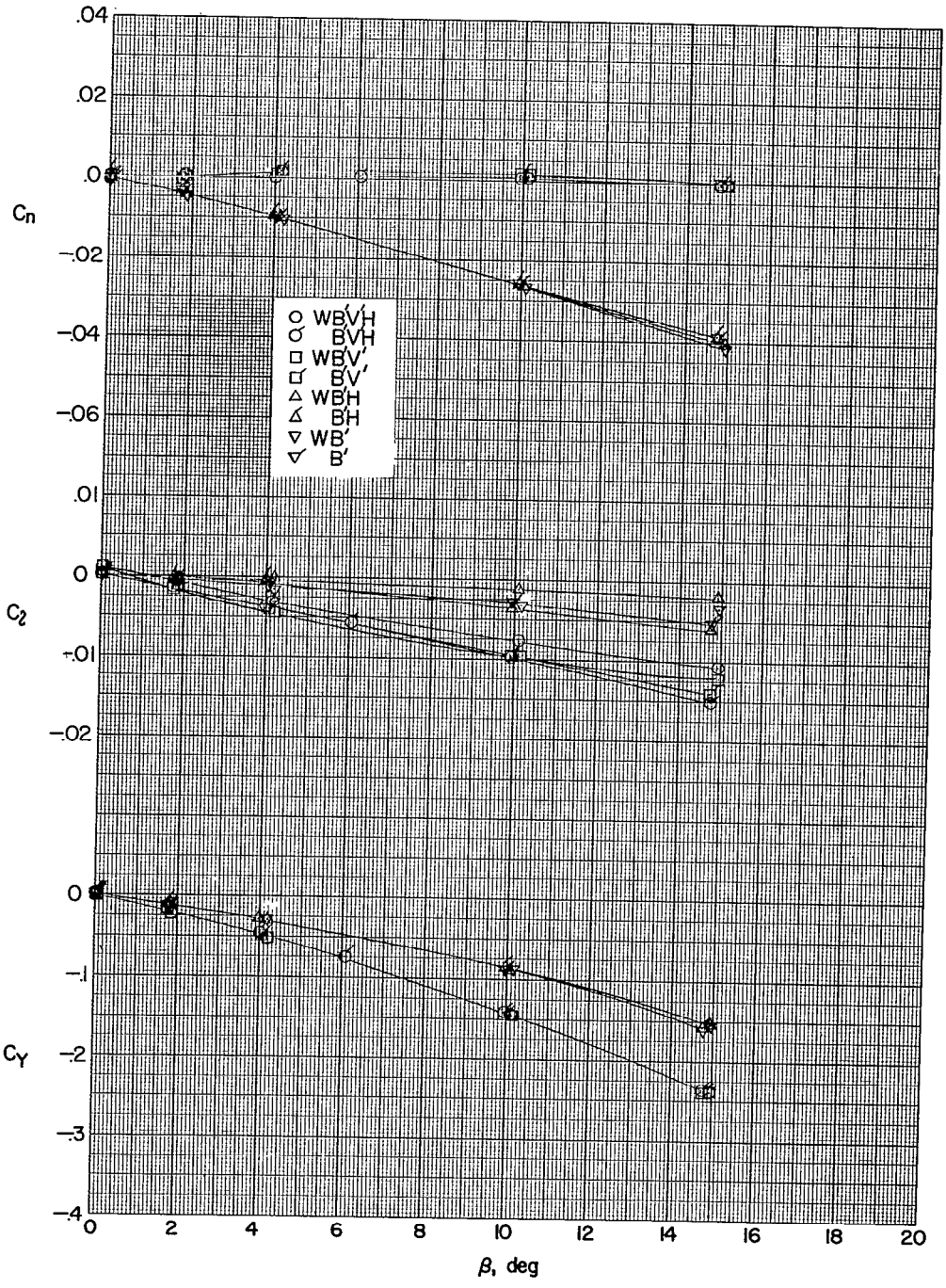


(c) $\alpha \approx 8.5^\circ$.

Figure 15.- Continued.

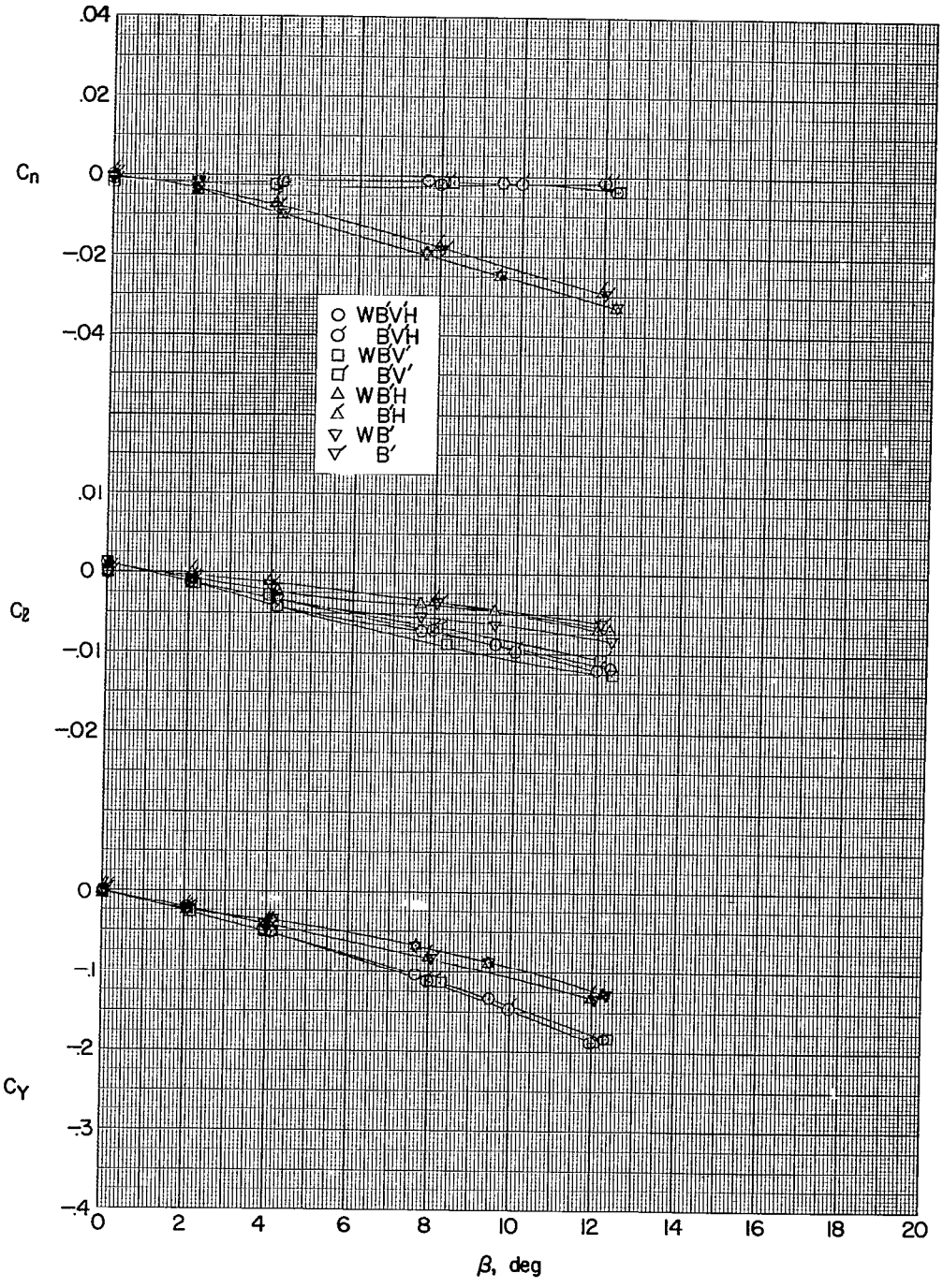


(d) $\alpha \approx 12.7^{\circ}$.

Figure 15.- Continued.

[redacted]

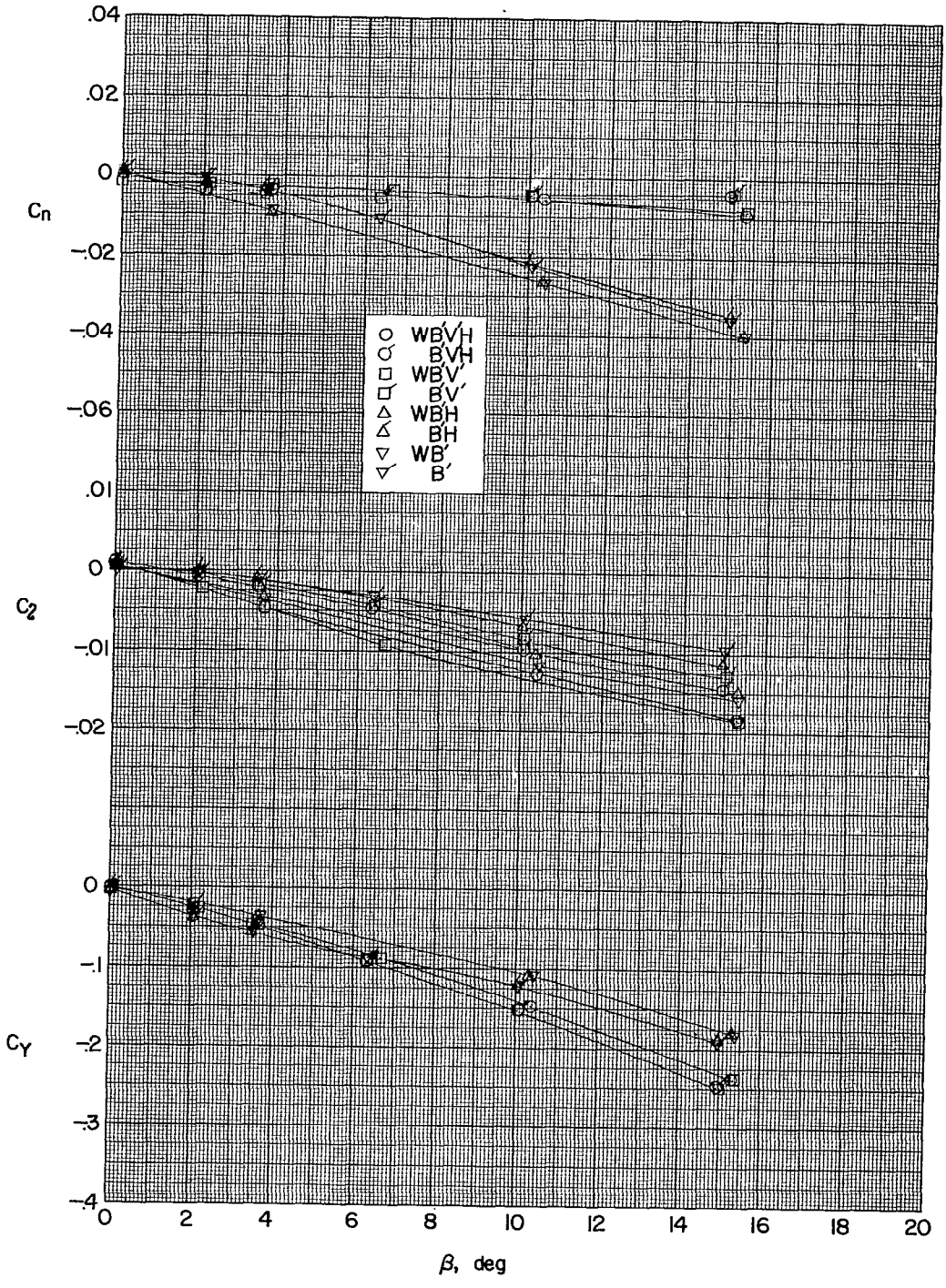


(e) $\alpha \approx 16^{\circ}$.

Figure 15.- Concluded.

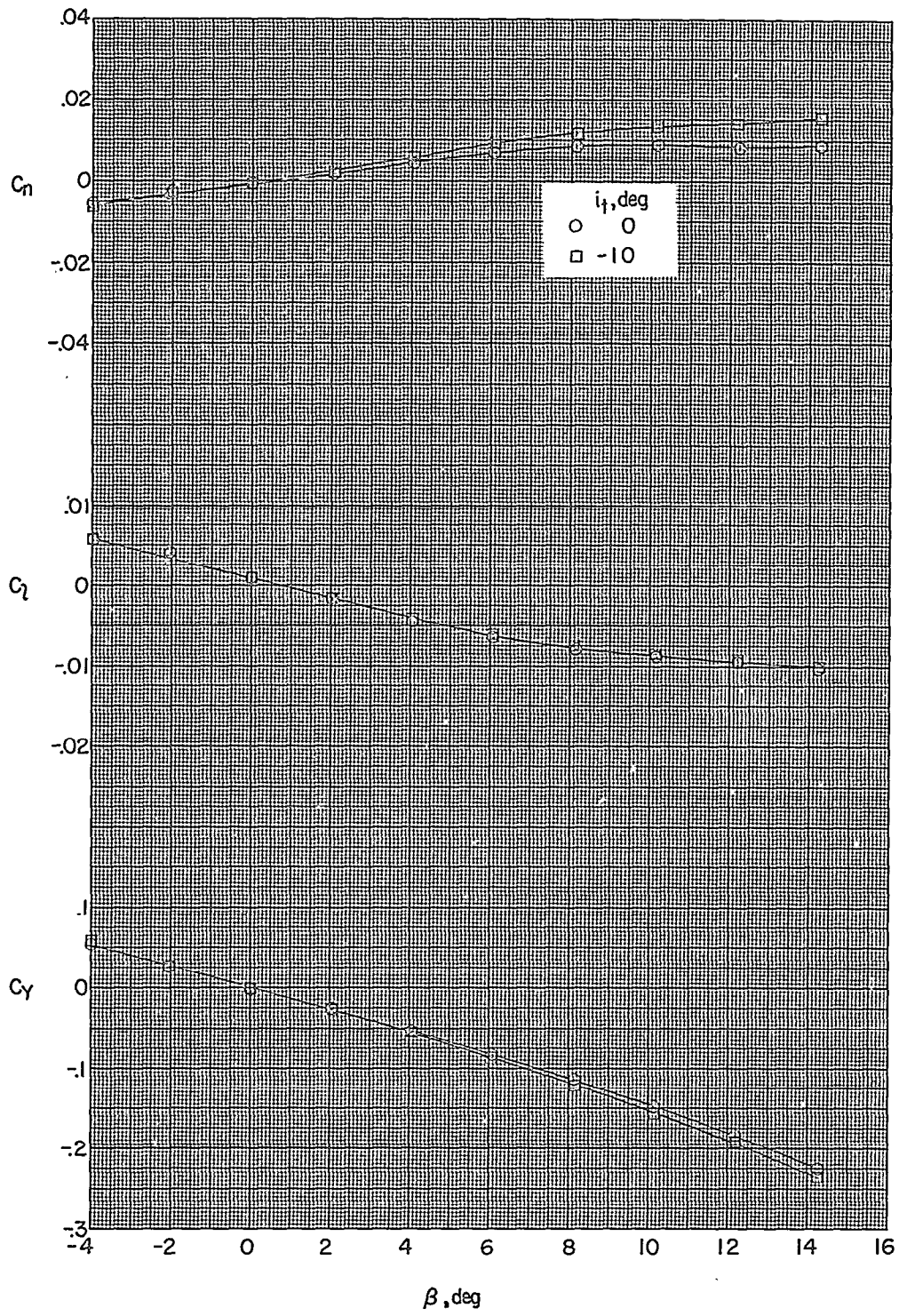


Figure 16.- Effect of horizontal-tail deflection on the sideslip characteristics of the complete production model. $\alpha \approx 5.2^{\circ}$; M = 1.41.

[redacted]

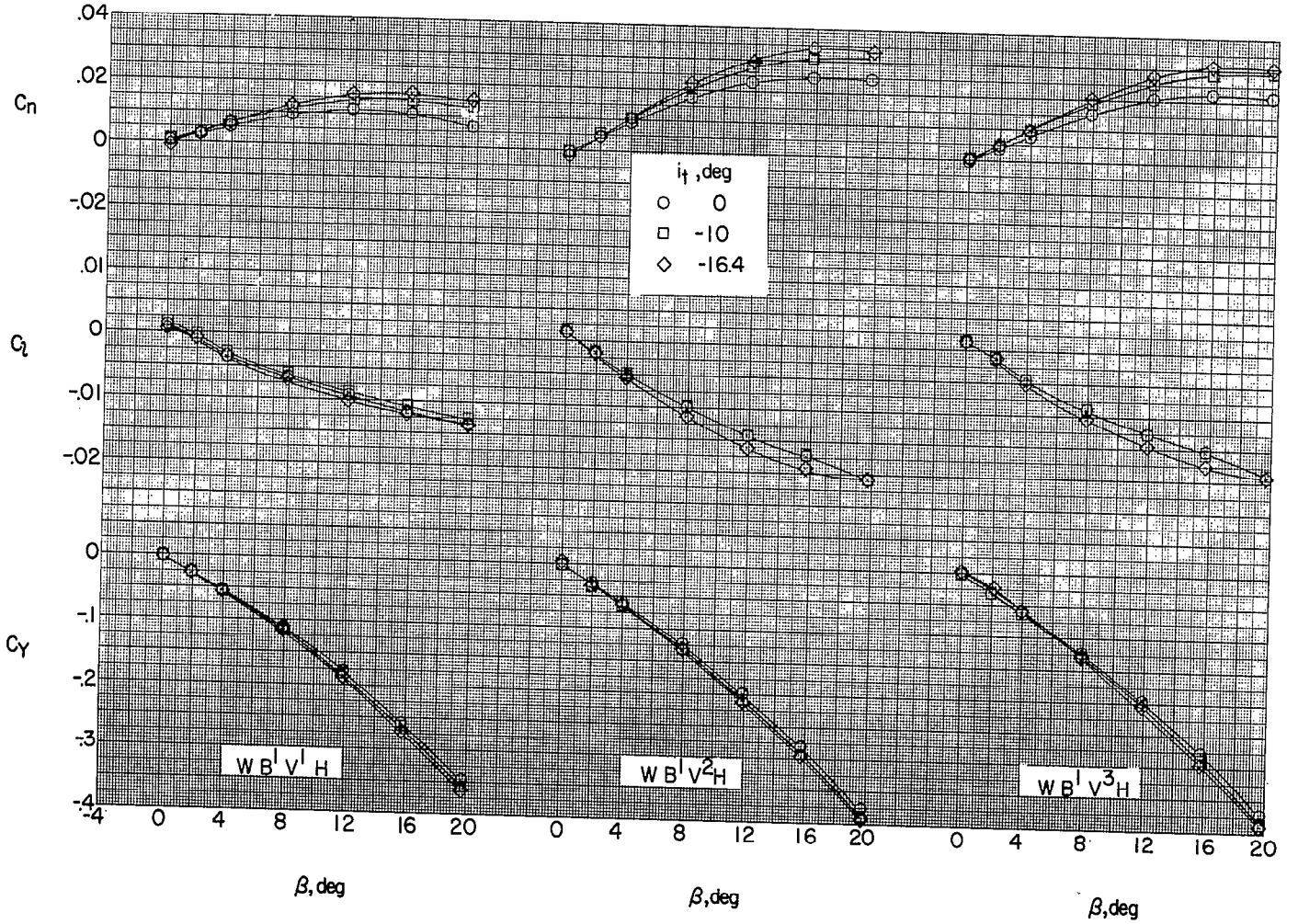


(a) $\alpha \approx 0^\circ$.

Figure 17.- Effects of horizontal-tail deflection on the sideslip characteristics of the complete production model with various vertical tails. M = 1.61.

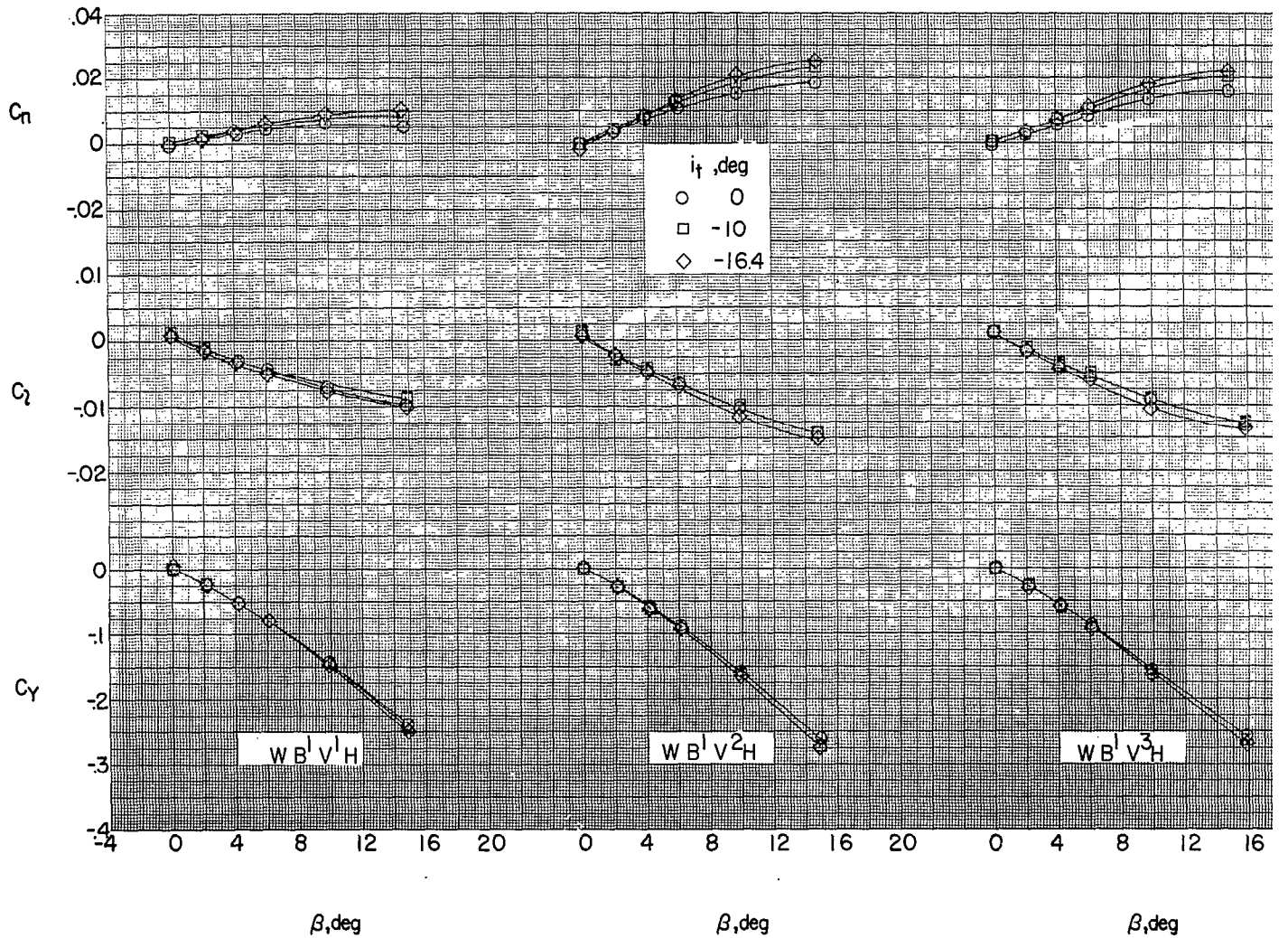


(b) $\alpha \approx 4.2^{\circ}$.

Figure 17.- Continued.

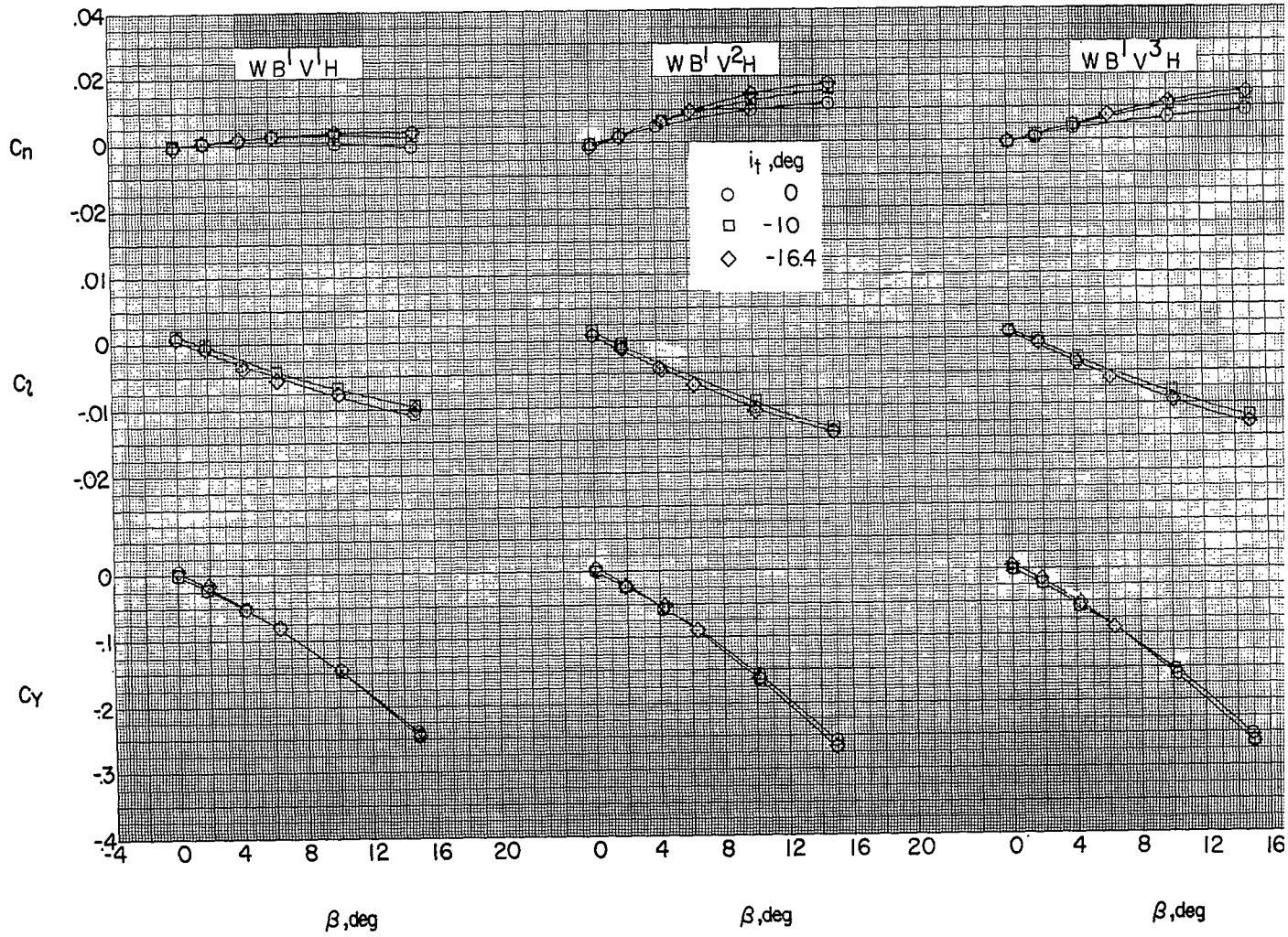


(c) $\alpha \approx 8.5^{\circ}$.

Figure 17.- Continued.

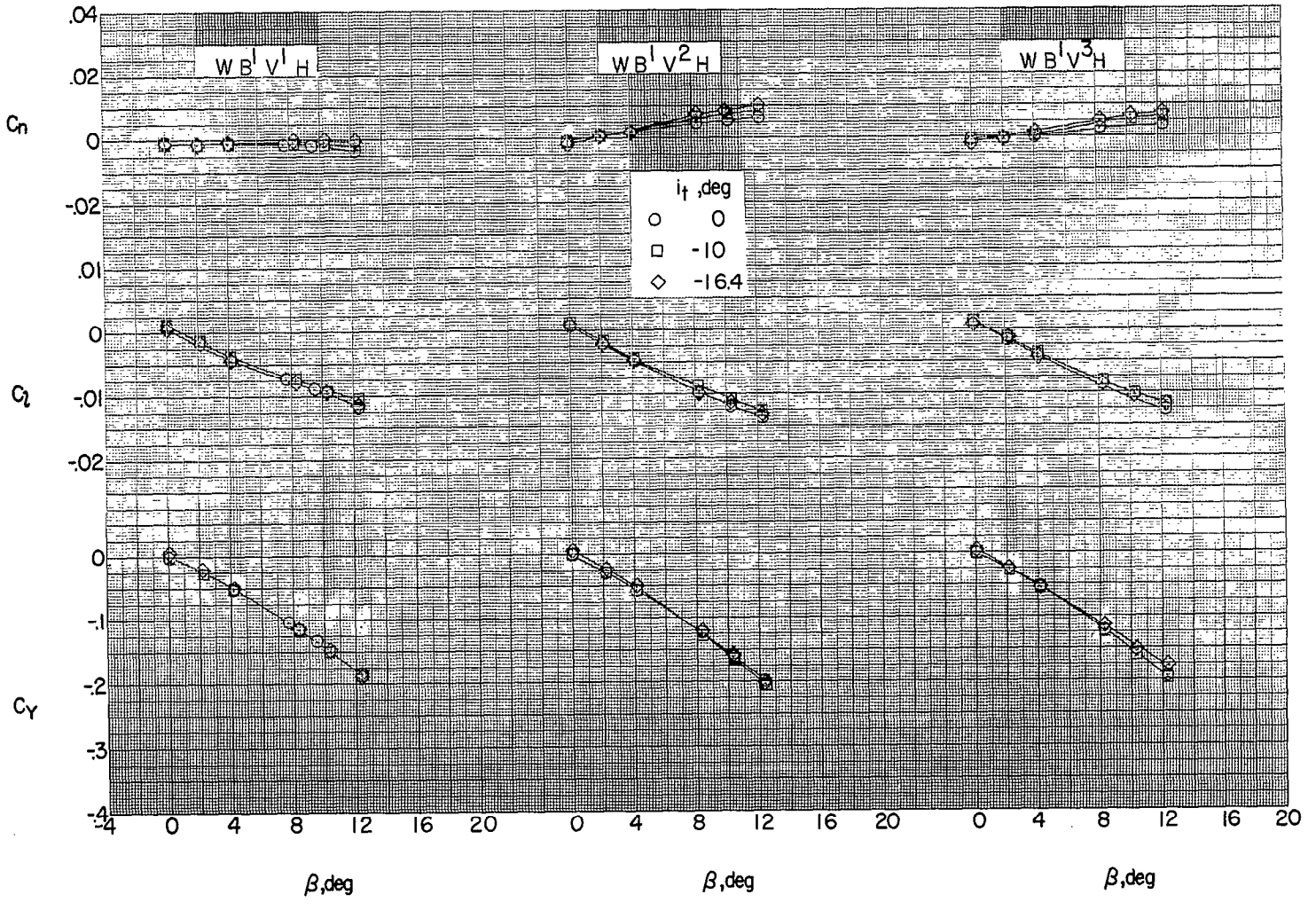


(d) $\alpha \approx 12.7^{\circ}$.

Figure 17.- Continued.

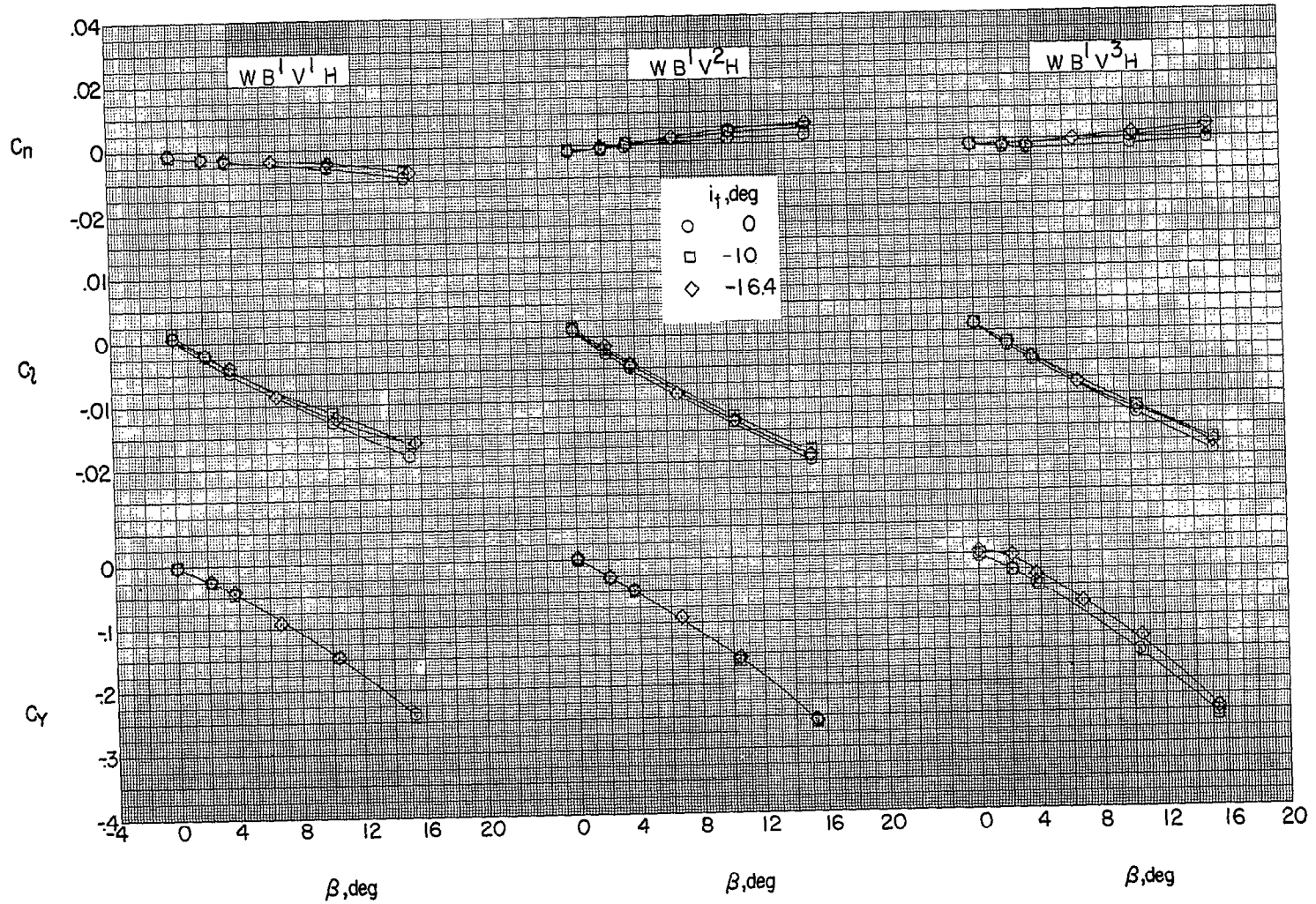


(e) $\alpha \approx 16^{\circ}$.

Figure 17.- Concluded.

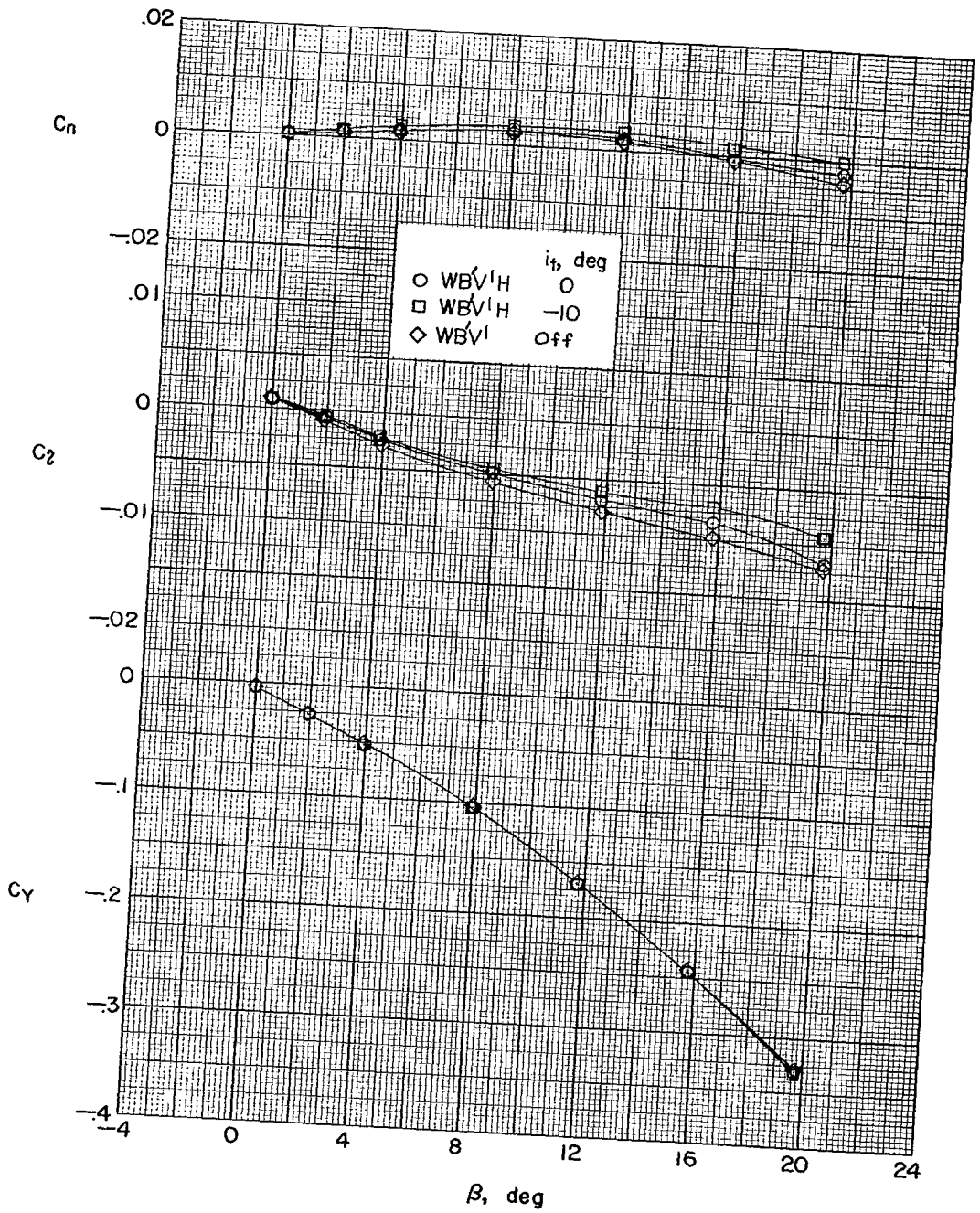


(a) $\alpha \approx 0^\circ$.

Figure 18.- Effect of horizontal tail and horizontal-tail incidence on the sideslip characteristics for the production model. M = 2.01.

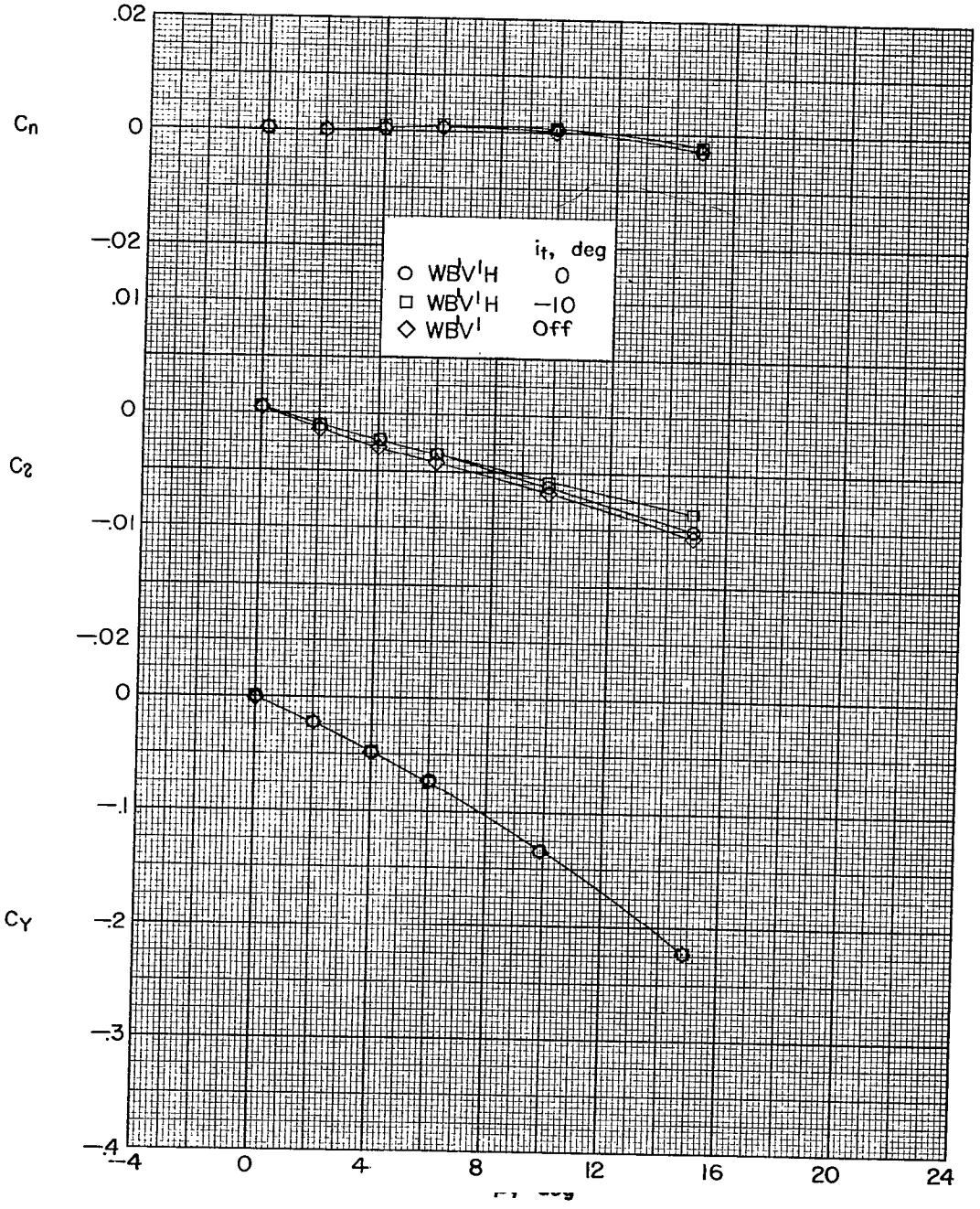
.02
0
−.02
.01
0
−.01
−.02
0
−.1
−.2
−.3
−.4
$C_n$
$C_l$
$C_Y$
$i_t$, deg
○ WBV'H 0
□ WBV'H −10
◇ WBV' Off
−4
0
4
8
12
16
20
24

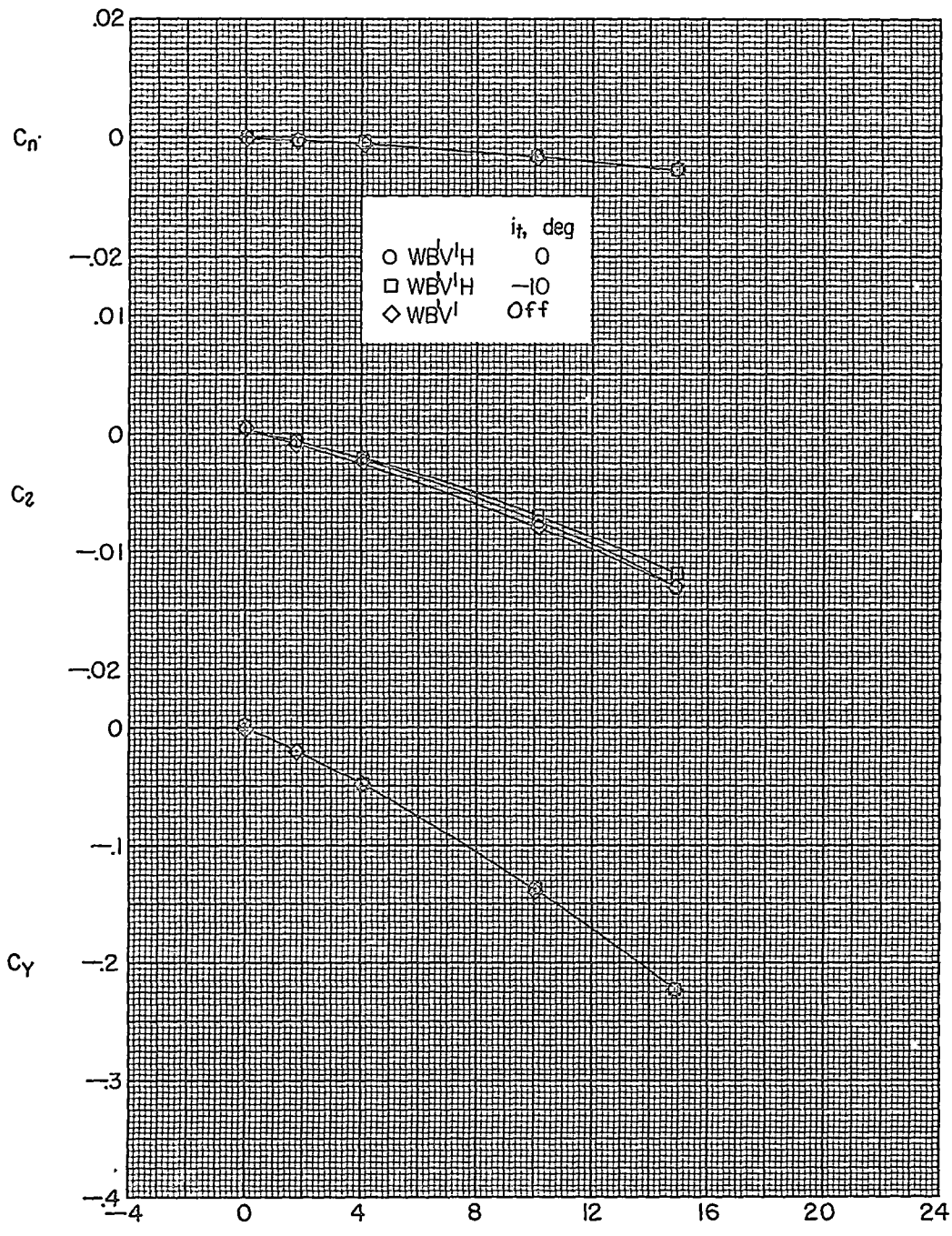
.02
0
−.02
.01
0
−.01
−.02
0
−.1
−.2
−.3
−.4
$C_n$
$C_l$
$C_Y$
−4
0
4
8
12
16
20
24
$i_t$, deg
○ WBV'H 0
□ WBV'H −10
◇ WBV' Off

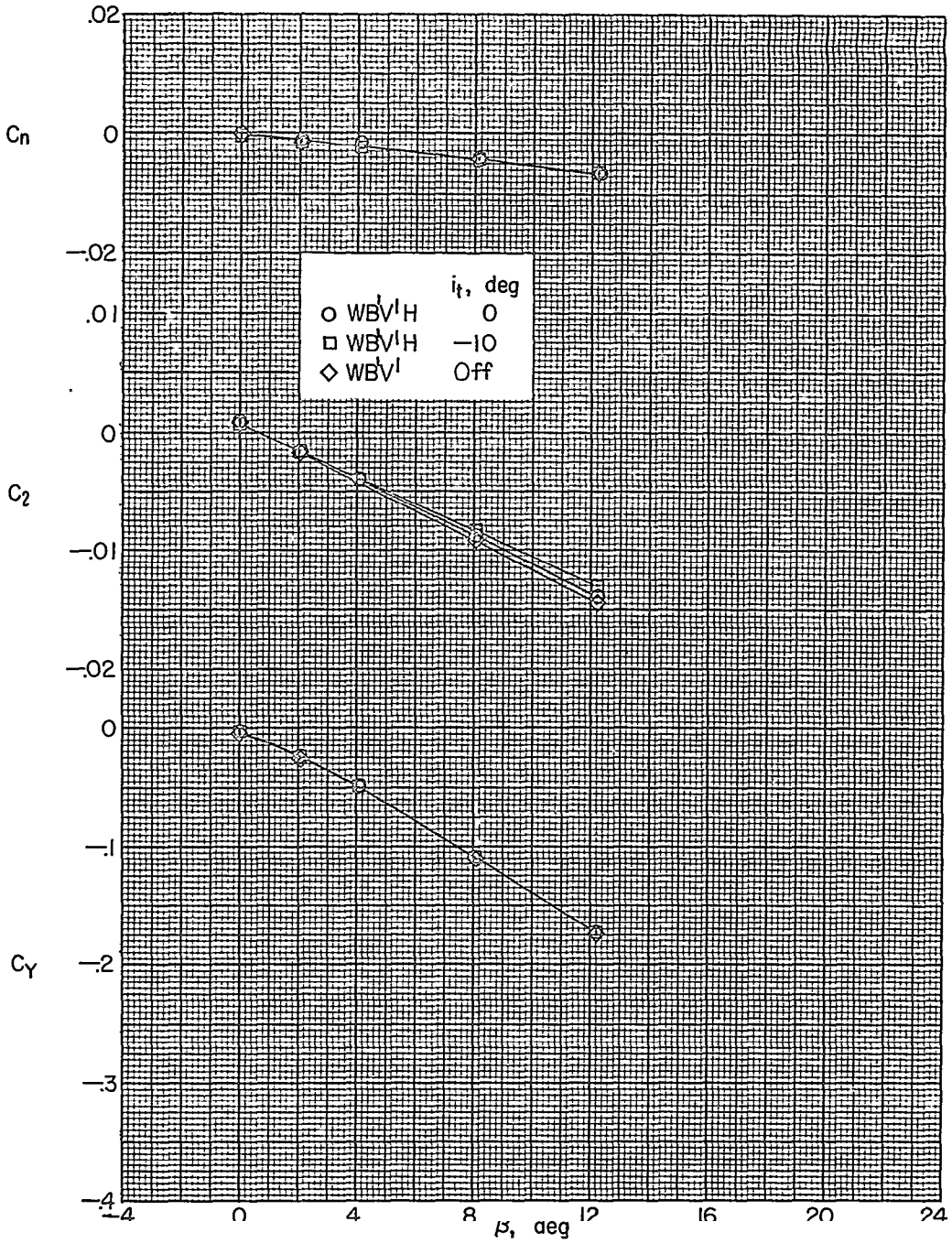
.02
0
−.02
.01
0
−.01
−.02
0
−.1
−.2
−.3
−.4
$C_n$
$C_l$
$C_Y$
−4
0
4
8
12
16
20
24
β, deg
$i_t$, deg
○ WBV'H 0
□ WBV'H −10
◇ WBV' Off

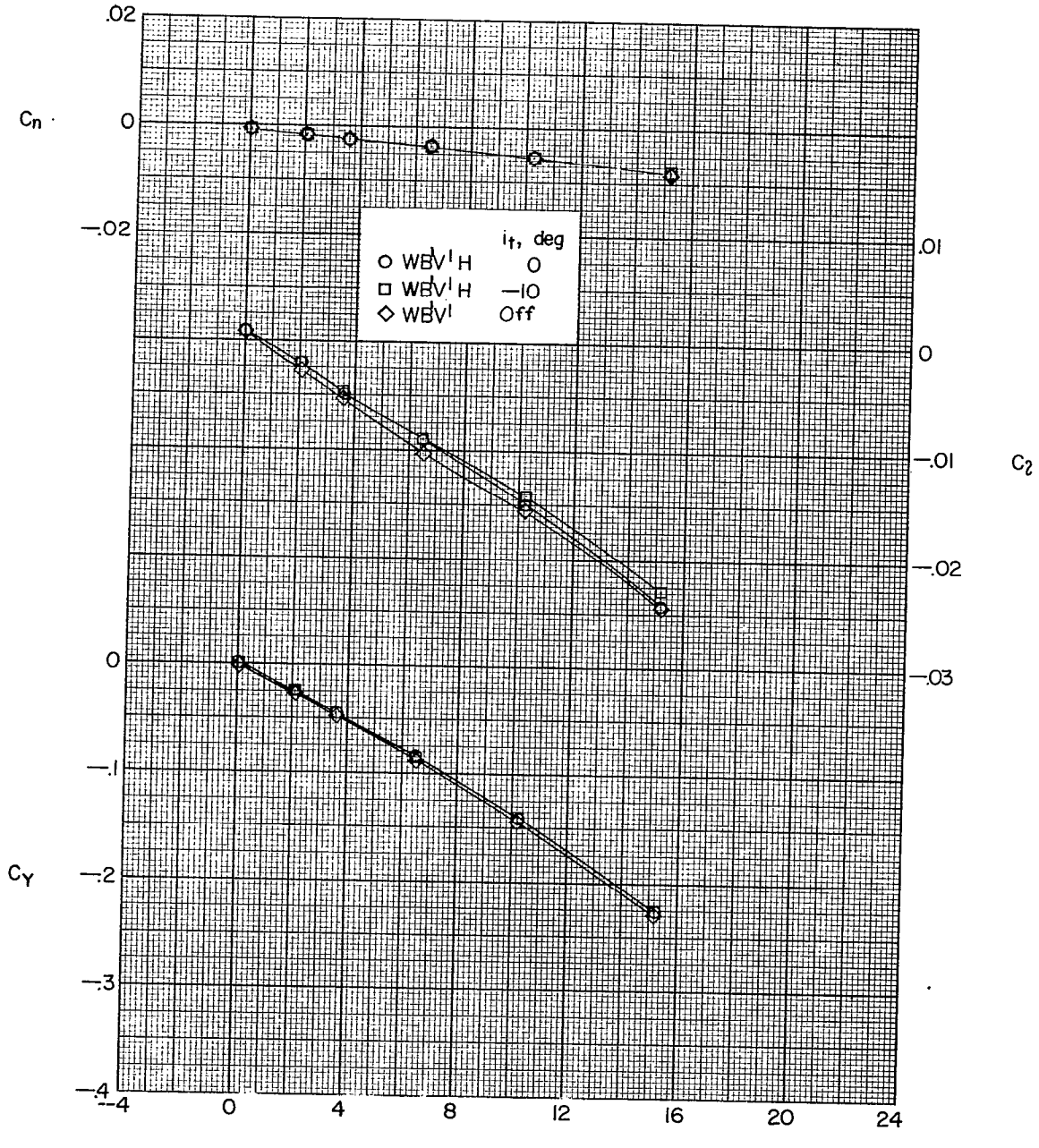
$C_n$
$C_Y$
$C_l$
.02
0
−.02
0
−.1
−.2
−.3
−.4
.01
0
−.01
−.02
−.03
−4
0
4
8
12
16
20
24
$i_t$, deg
○ WBV' H 0
□ WBV' H −10
◇ WBV' Off

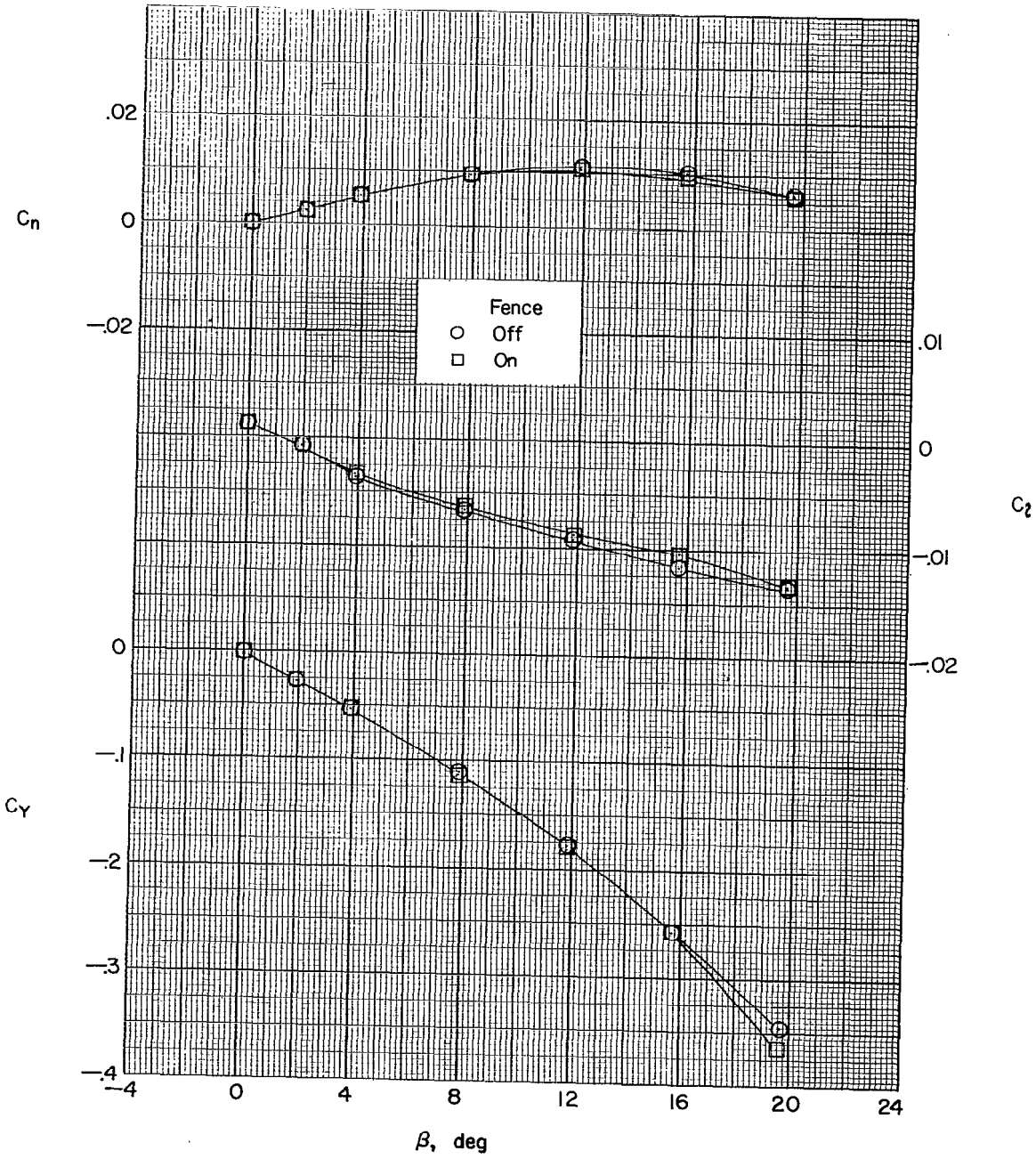
.02
0
−.02
$C_n$
Fence
Off
On
.01
0
−.01
−.02
$C_l$
0
−.1
−.2
−.3
−.4
$C_Y$
−4
0
4
8
12
16
20
24
β, deg

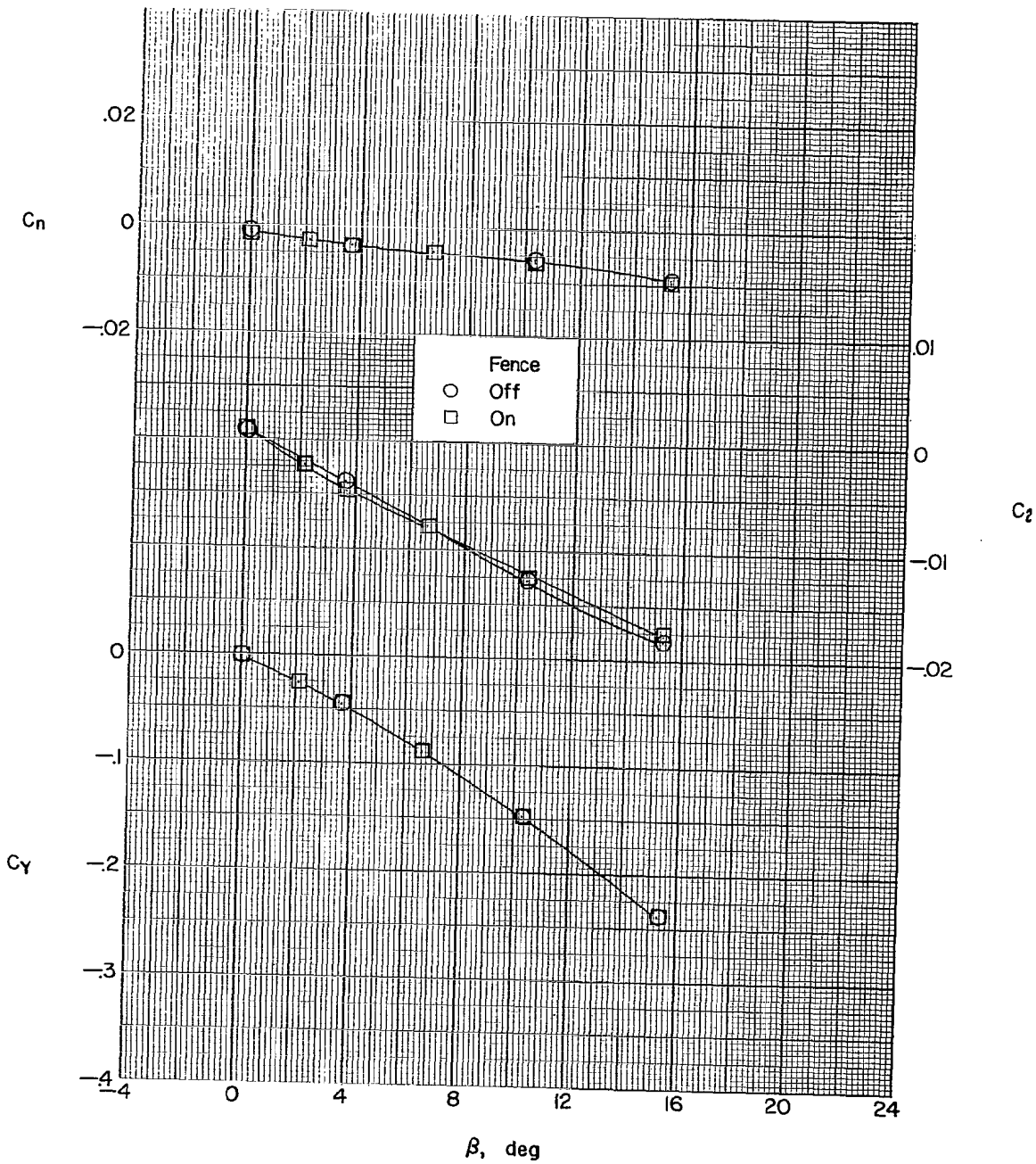


(b) $\alpha \approx 16.0°$.

Figure 19.- Concluded.

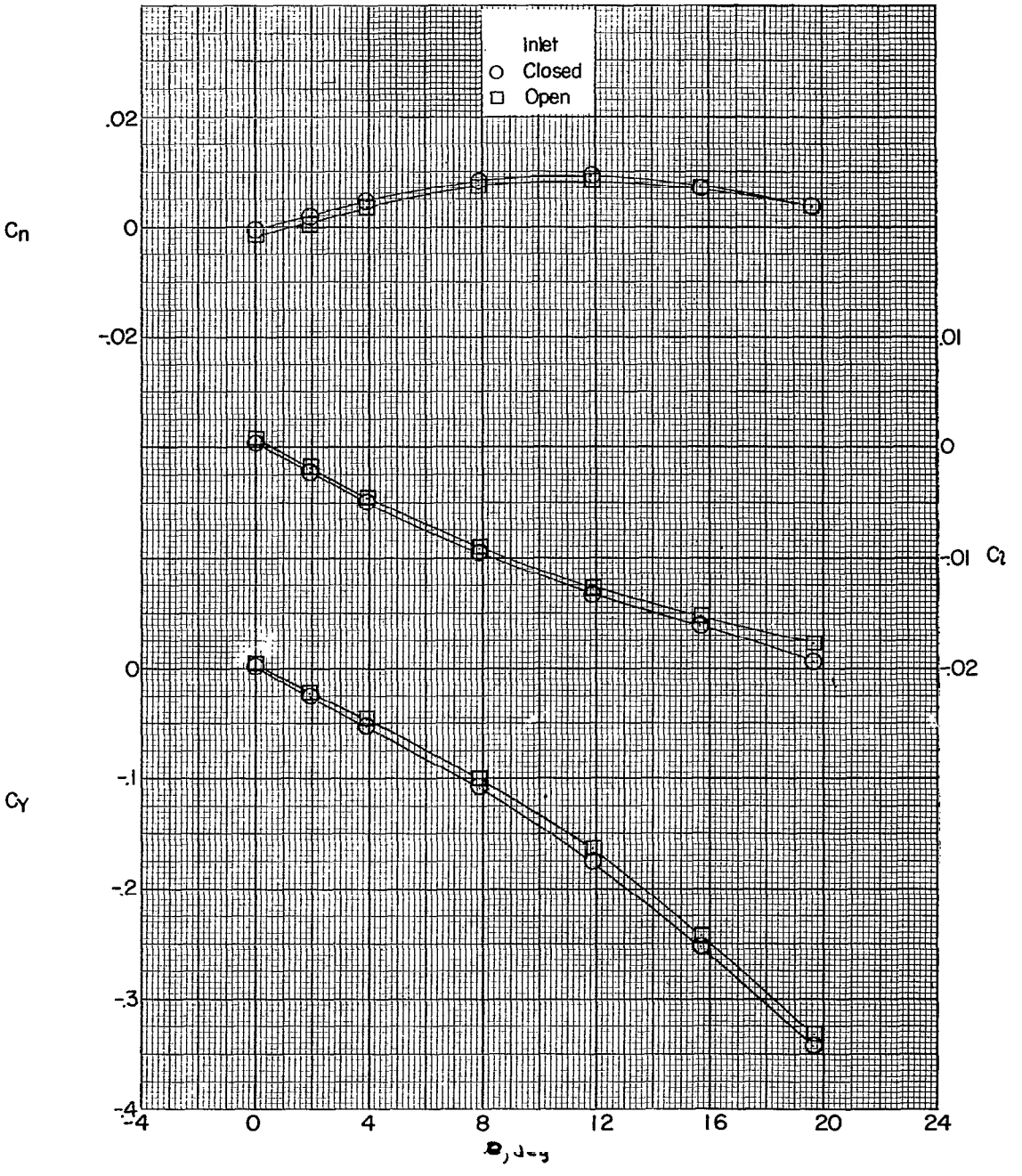
Inlet
Closed
Open
.02
0
-.02
$C_n$
.01
0
-.01
$C_l$
-.02
0
-.1
$C_Y$
-.2
-.3
-.4
-4
0
4
8
12
16
20
24

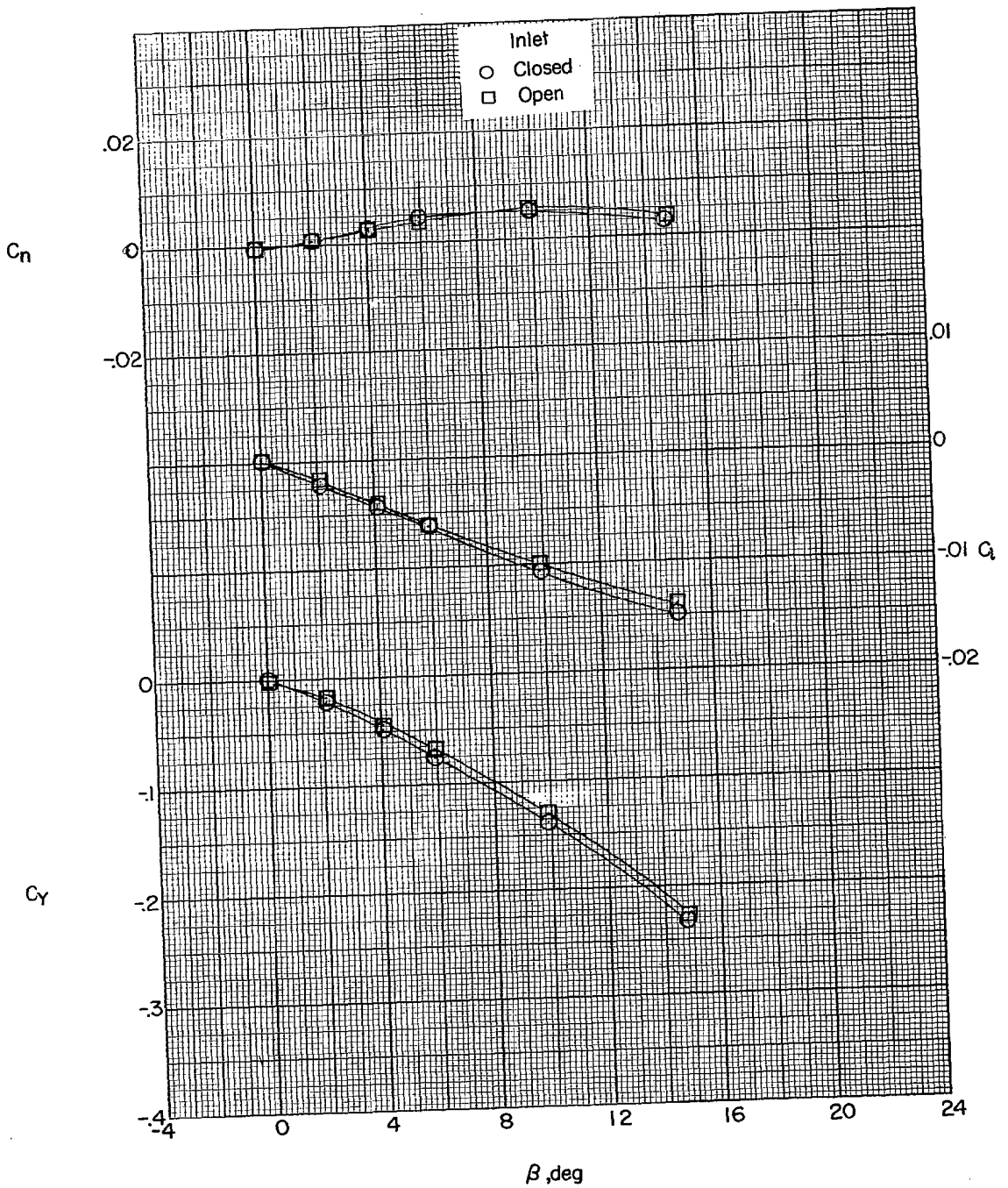


(b) $\alpha \approx 4.2^{\circ}$.

Figure 20.- Continued.

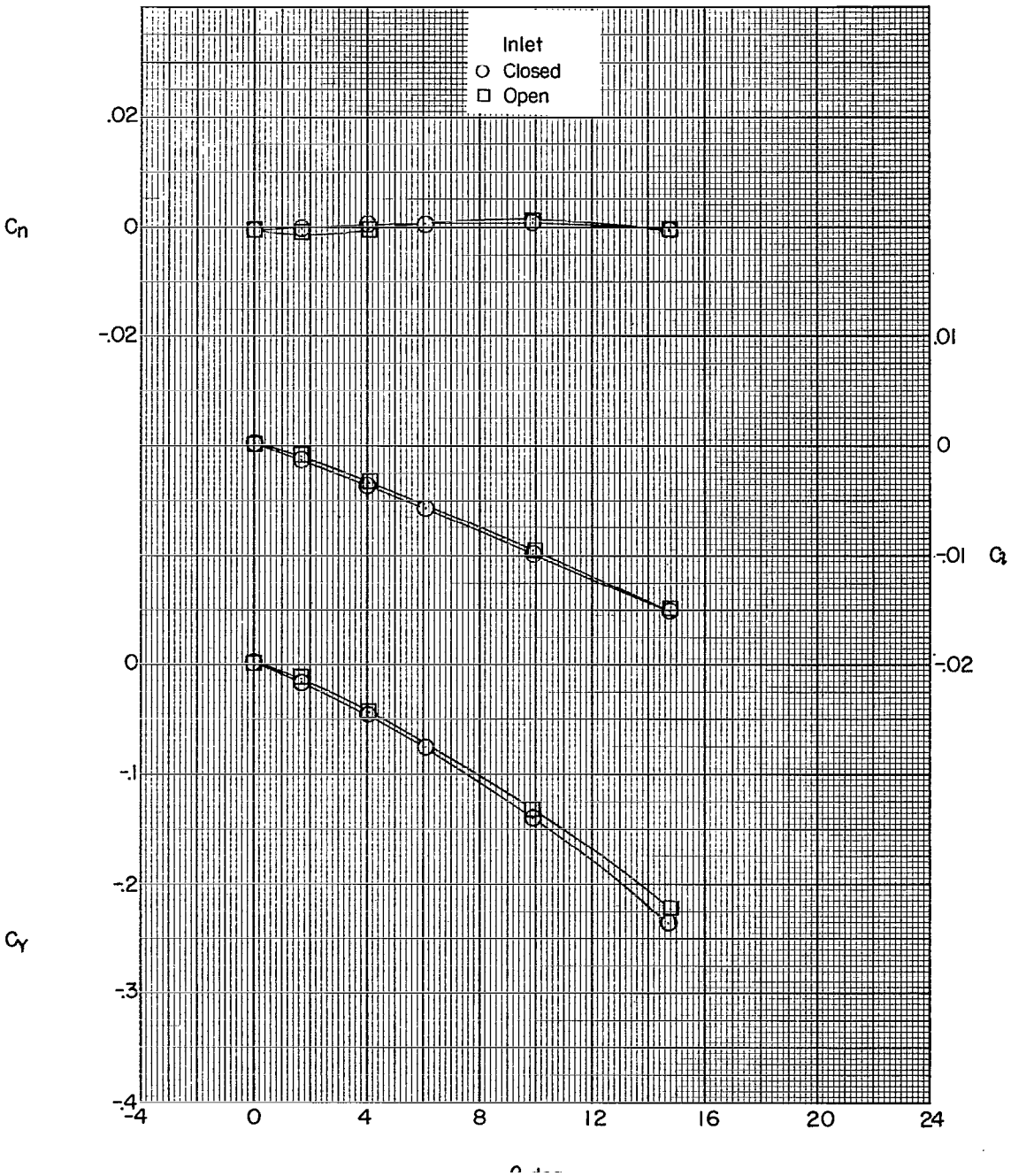
Inlet
O Closed
□ Open
$C_n$
$C_Y$
$C_l$
.02
0
-.02
-.1
-.2
-.3
-.4
.01
-.01
-4
0
4
8
12
16
20
24

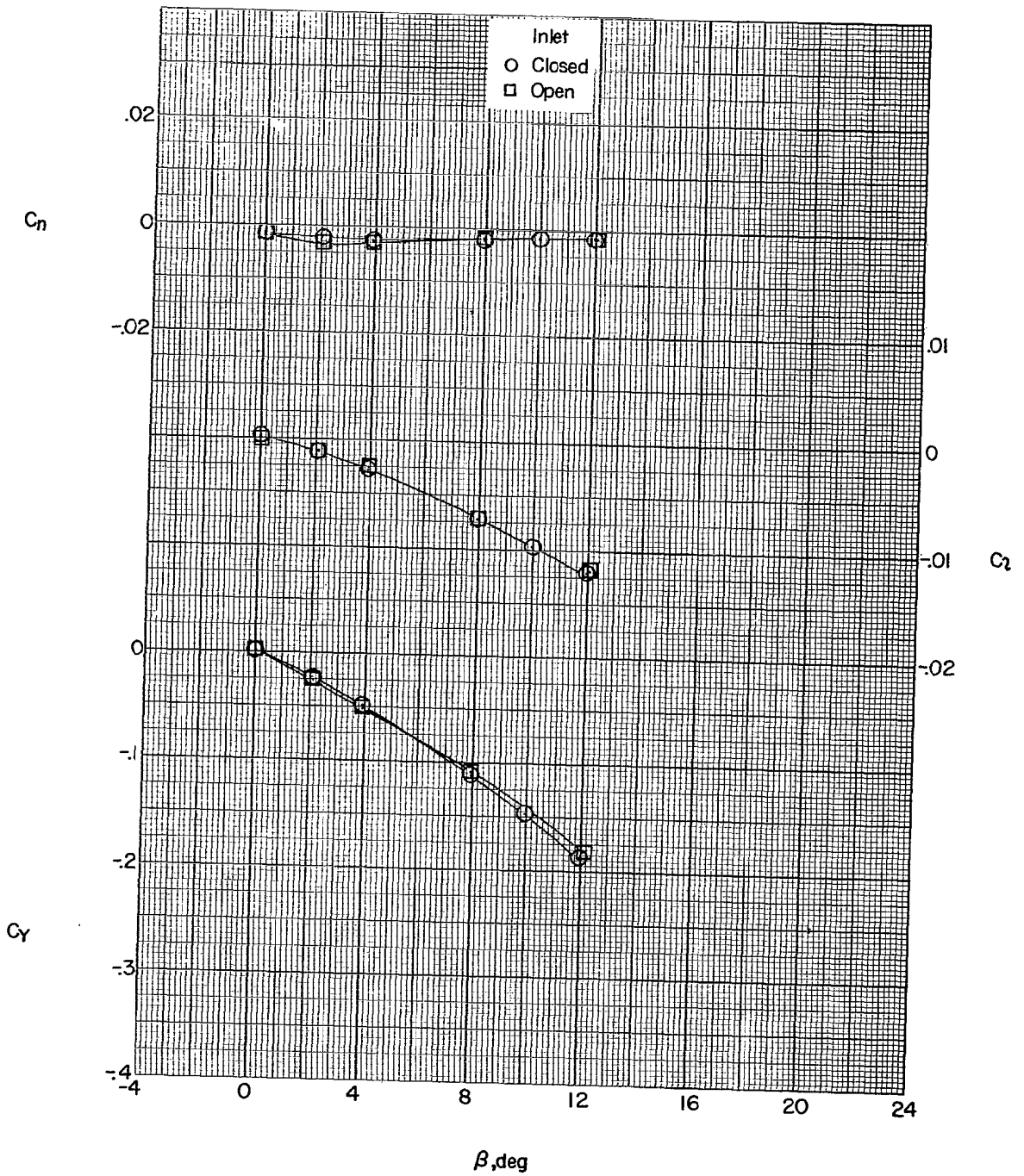


(d) $\alpha \approx 12.7°$.

Figure 20.- Continued.

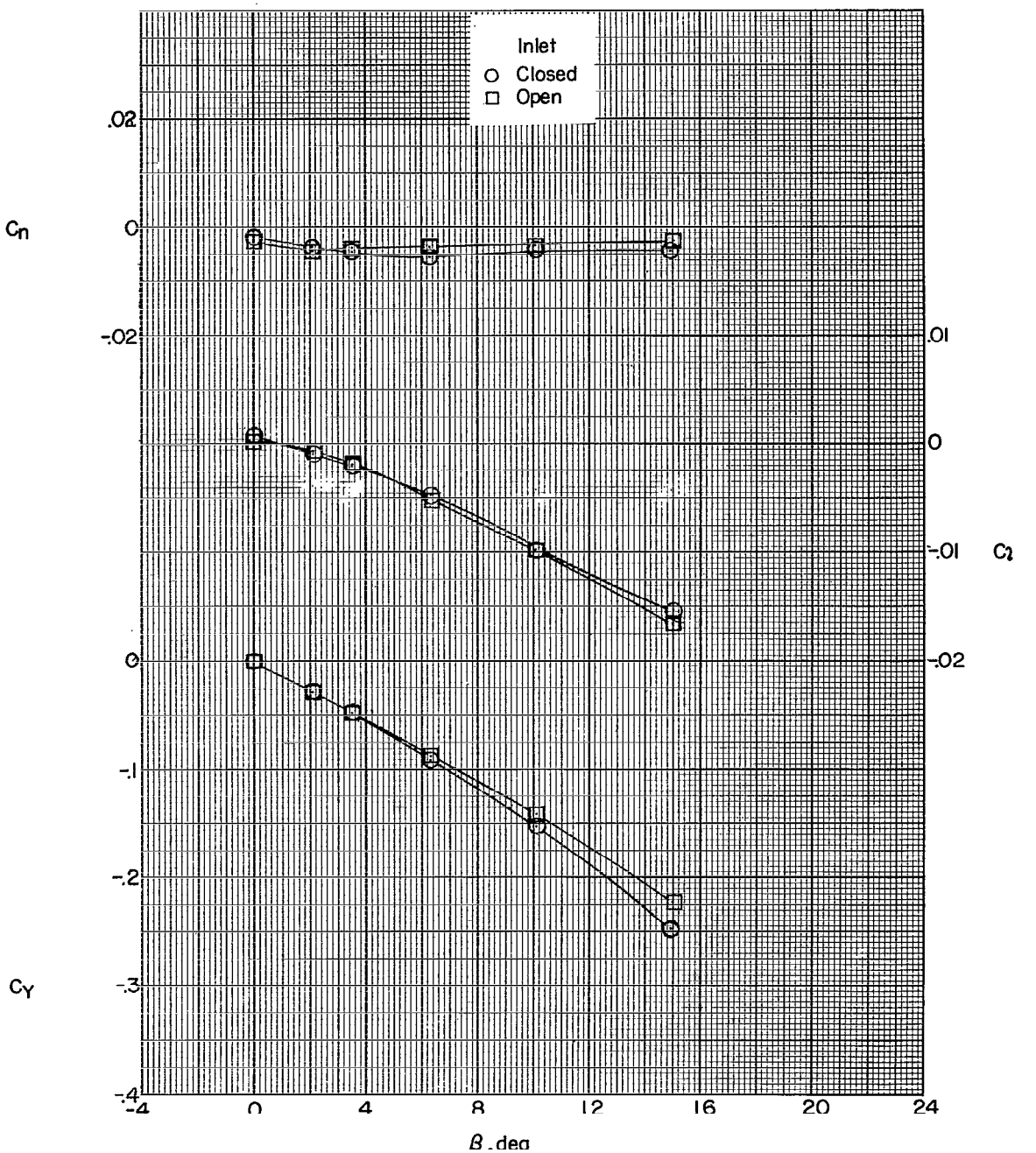
Inlet
Closed
Open
.02
0
-.02
$C_n$
.01
0
-.01
$C_l$
0
-.02
-.1
-.2
$C_Y$
-.3
-.4
-4
0
4
8
12
16
20
24
β, deg

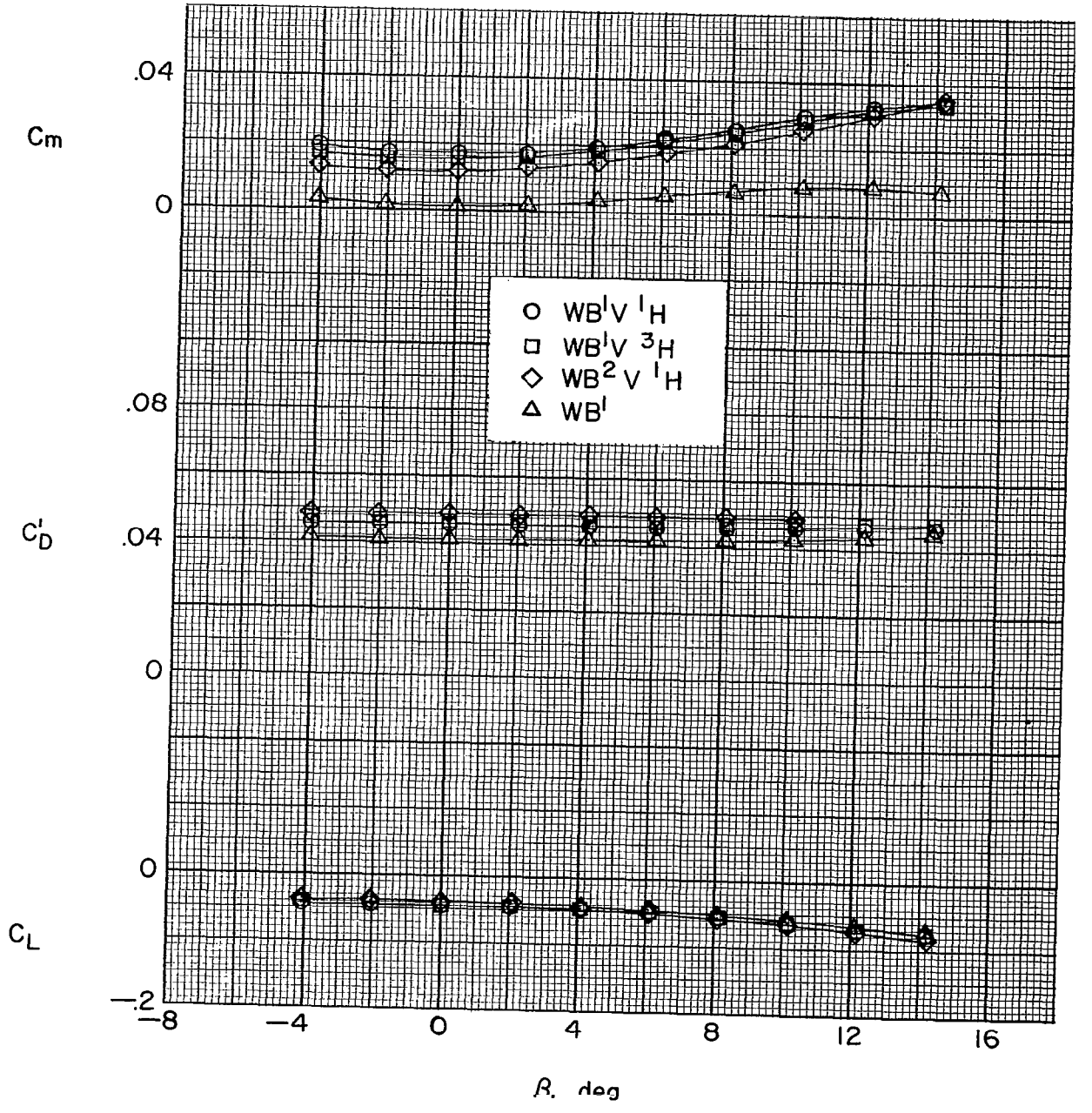
Cm
.04
0
.08
C'D
.04
0
0
CL
-.2
-8
-4
0
4
8
12
16
α, deg
WB¹V ¹H
WB¹V ³H
WB²V ¹H
WB¹

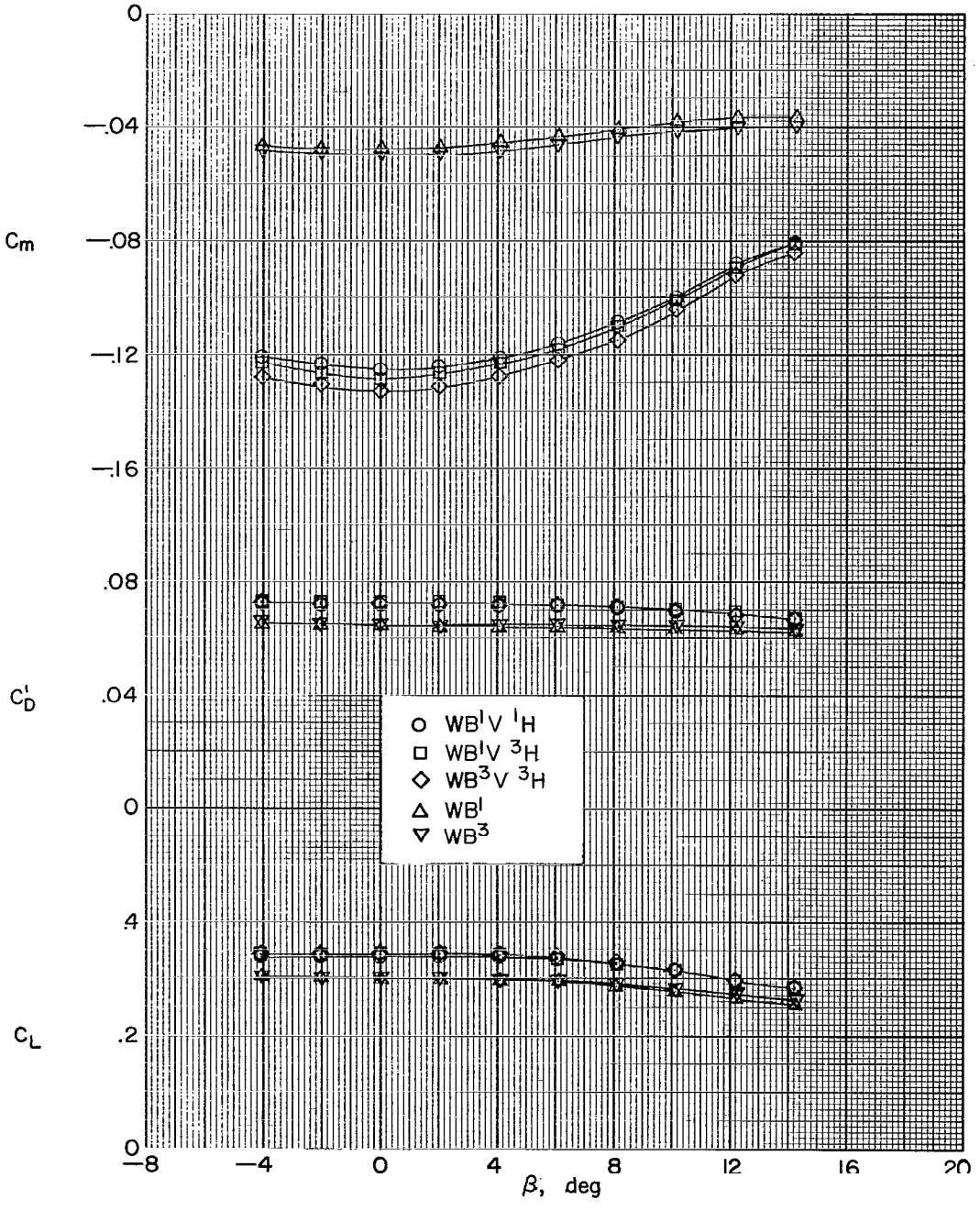
0
−.04
−.08
−.12
−.16
$C_m$
.08
.04
0
$C'_D$
.4
.2
0
$C_L$
−8
−4
0
4
8
12
16
20
β, deg
WB¹V ¹H
WB¹V ³H
WB³V ³H
WB¹
WB³

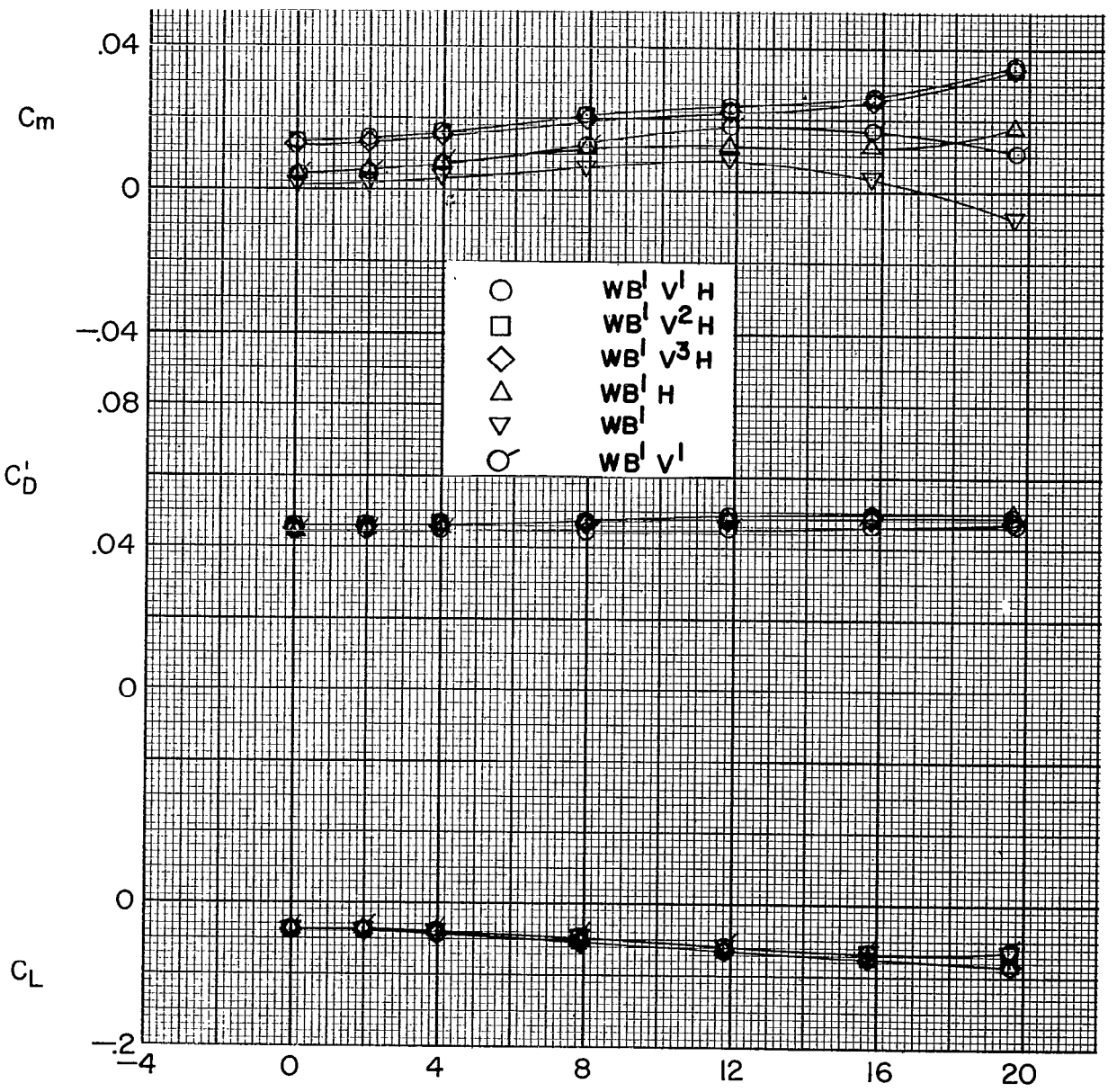


(a) $\alpha \approx 0^{\circ}$.

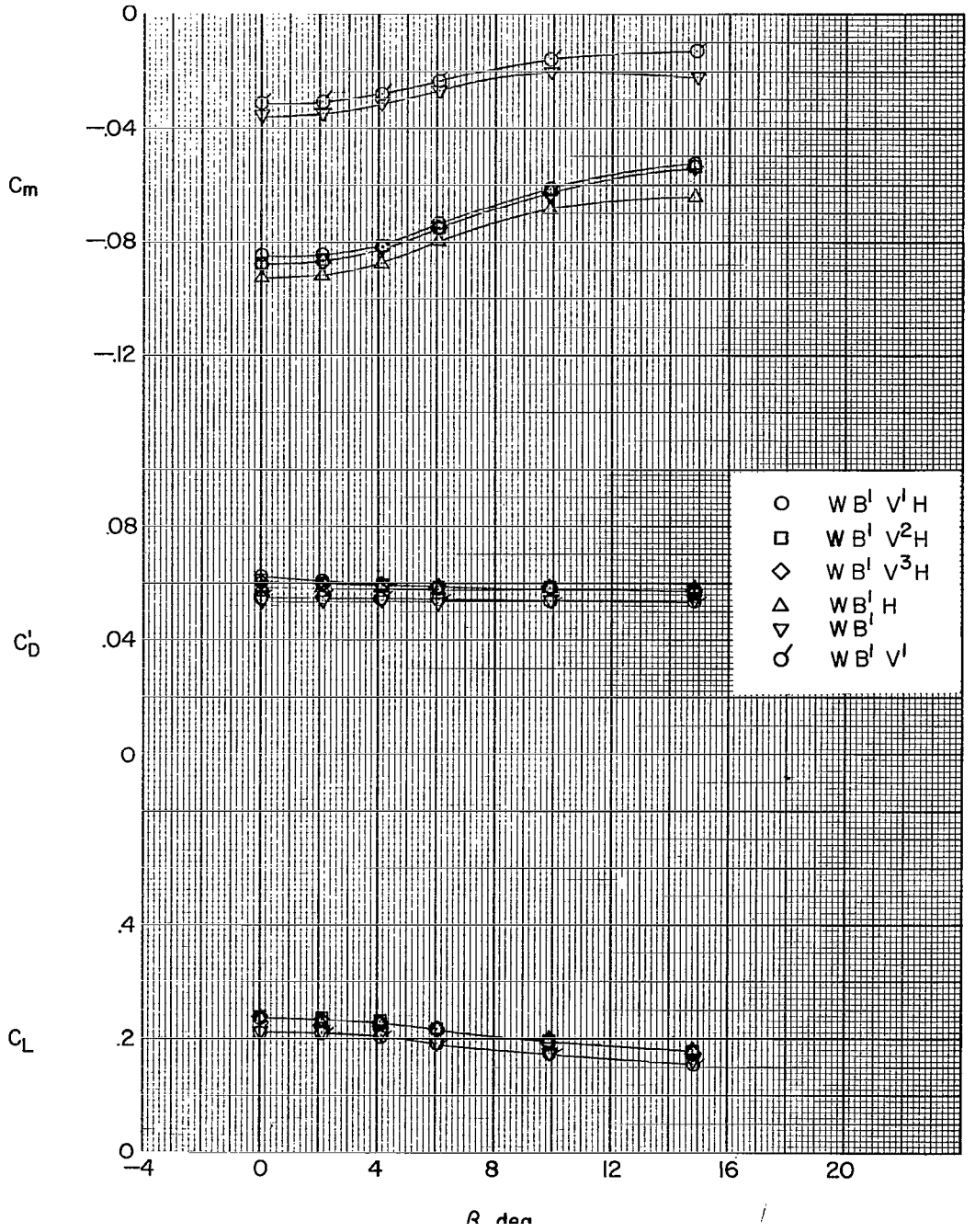
0
−.04
−.08
−.12
$C_m$
.08
.04
0
$C'_D$
.4
.2
0
$C_L$
−4
0
4
8
12
16
20
α, deg
WB' V'H
WB' V²H
WB' V³H
WB' H
WB'
WB' V'

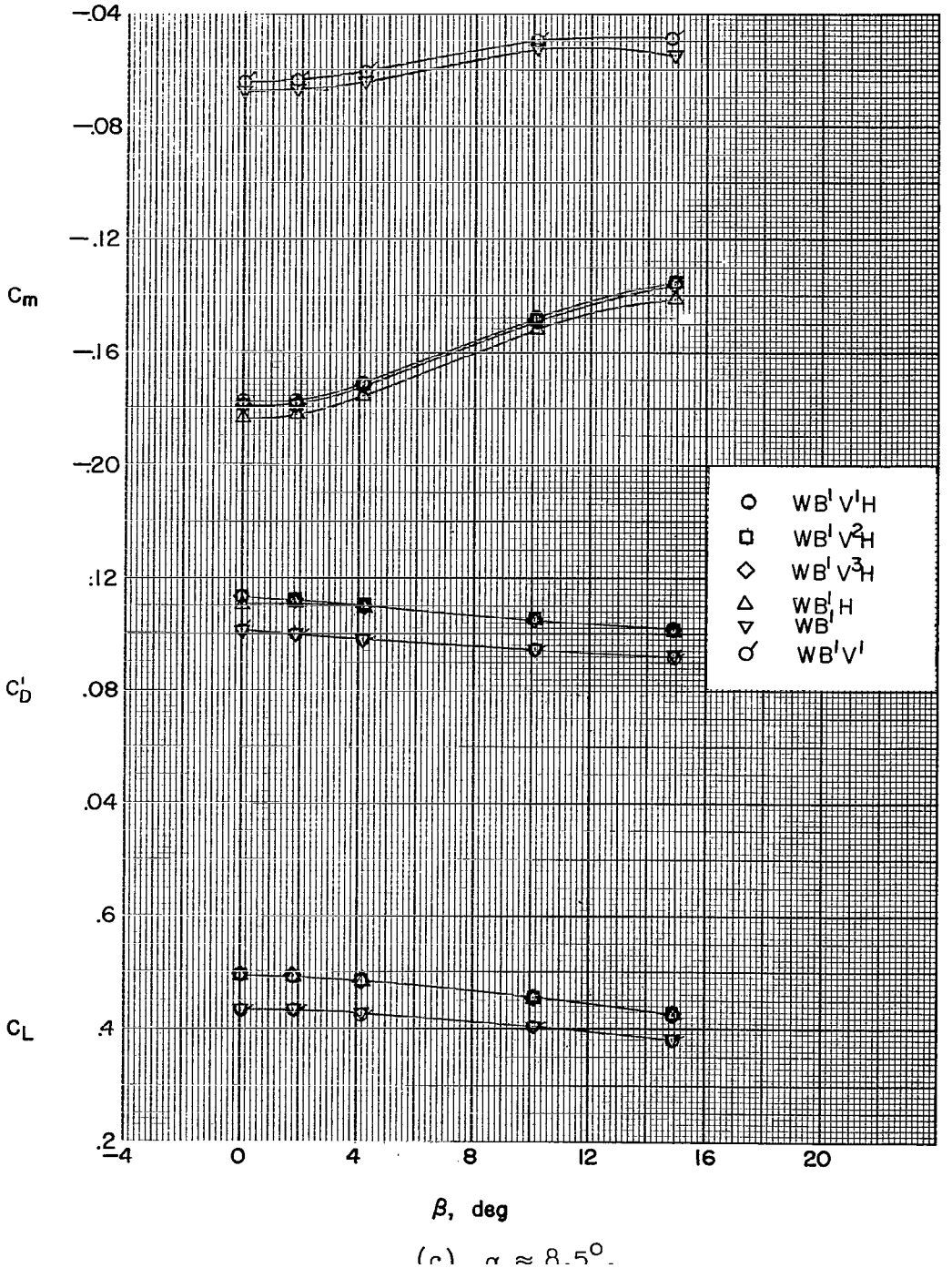


(c) $\alpha \approx 8.5^\circ$.

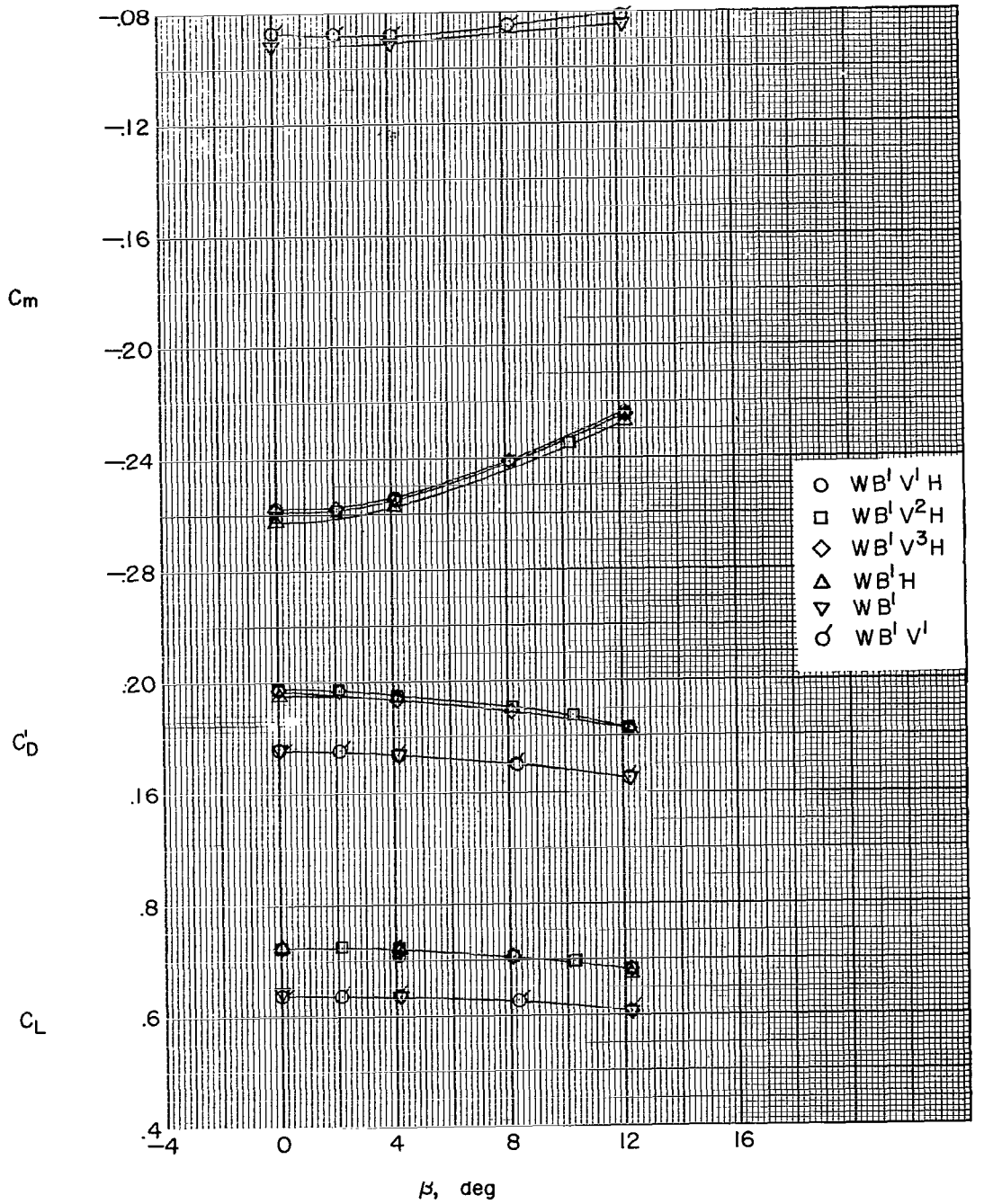
-.08
-.12
-.16
-.20
-.24
-.28
$C_m$
.20
$C'_D$
.16
.8
.6
$C_L$
.4
-4
0
4
8
12
16
β, deg
WB' V' H
WB' V² H
WB' V³ H
WB' H
WB'
WB' V'

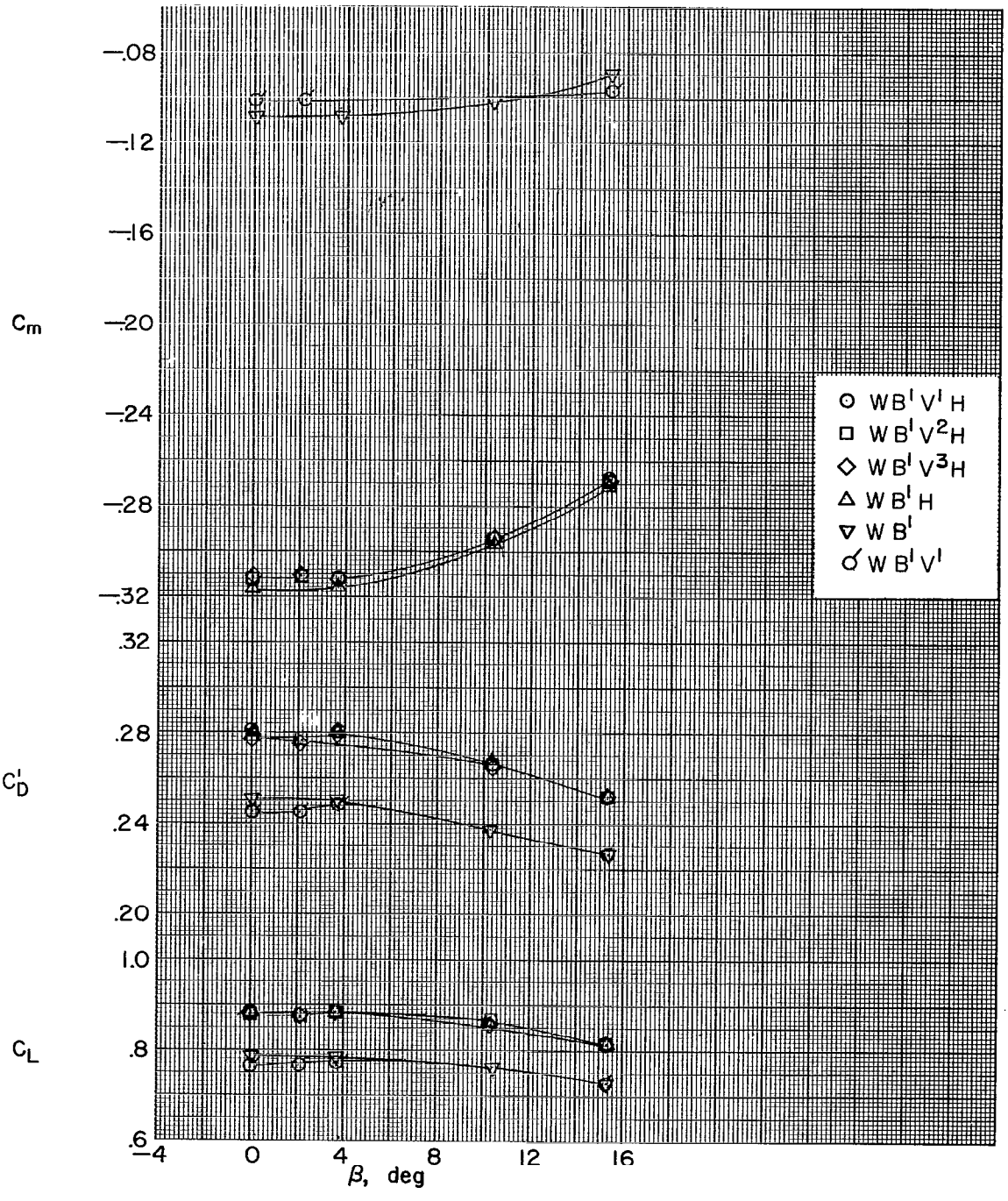
$C_m$
$C_D'$
$C_L$
−.08
−.12
−.16
−.20
−.24
−.28
−.32
.32
.28
.24
.20
1.0
.8
.6
−4
0
4
8
12
16
β, deg
WB' V' H
WB' V² H
WB' V³ H
WB' H
WB'
WB' V'

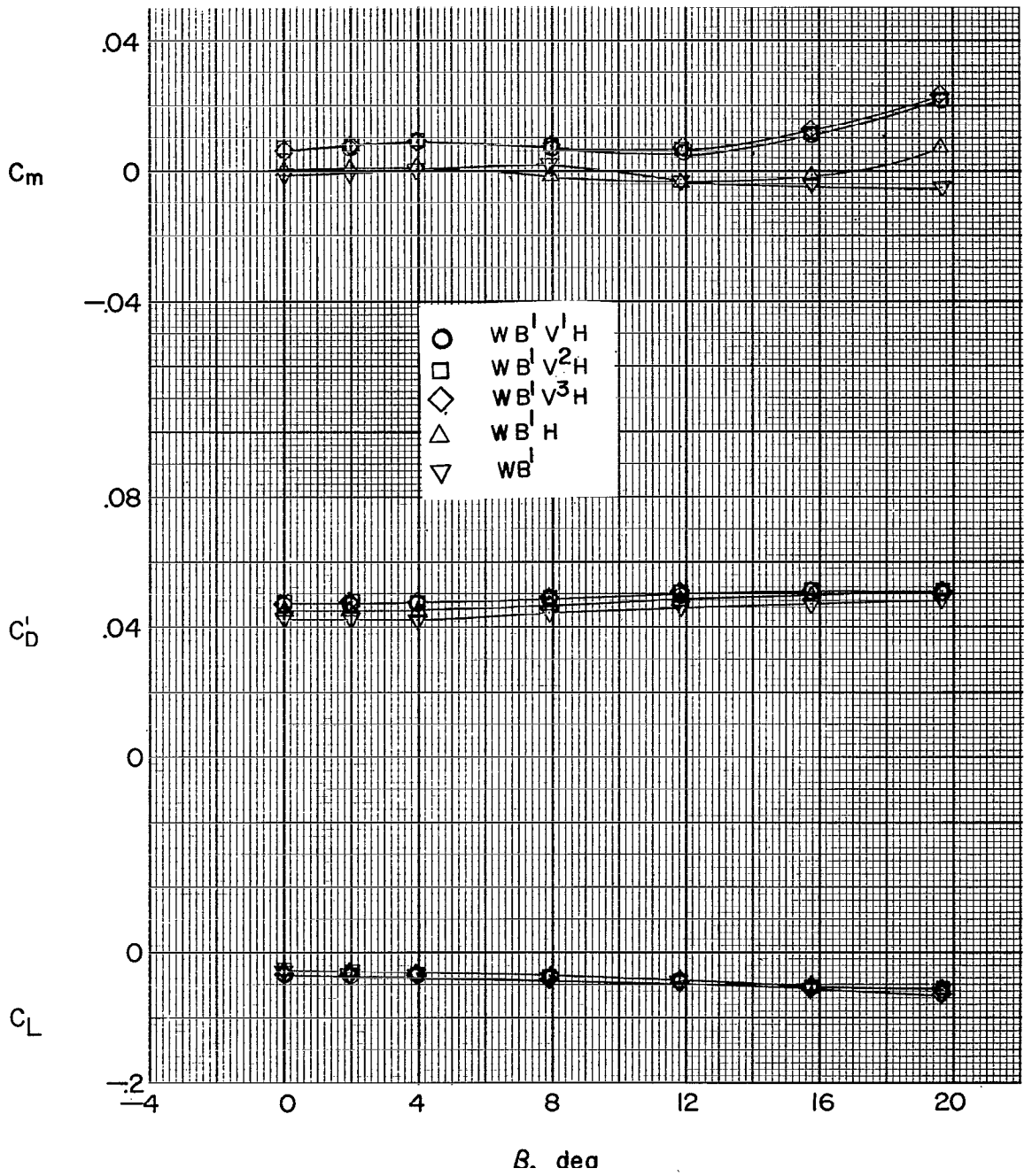
.04
0
−.04
.08
.04
0
0
−.2
$C_m$
$C'_D$
$C_L$
−4
0
4
8
12
16
20
α, deg
WB' V' H
WB' V² H
WB' V³ H
WB' H
WB'

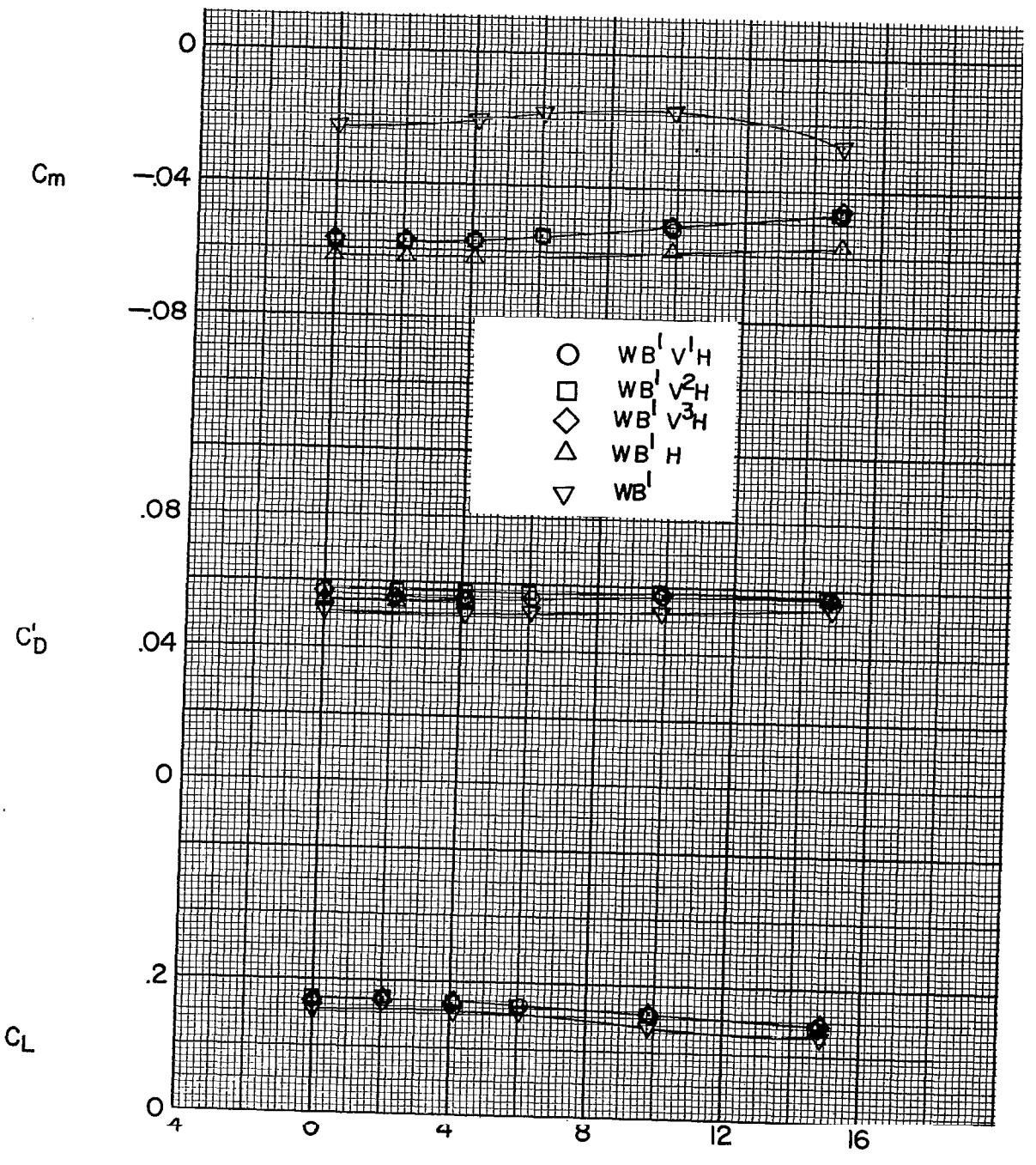
0
$C_m$
−.04
−.08
.08
$C'_D$
.04
0
.2
$C_L$
0
4
0
4
8
12
16
$WB^I V^I H$
$WB^I V^2 H$
$WB^I V^3 H$
$WB^I H$
$WB^I$

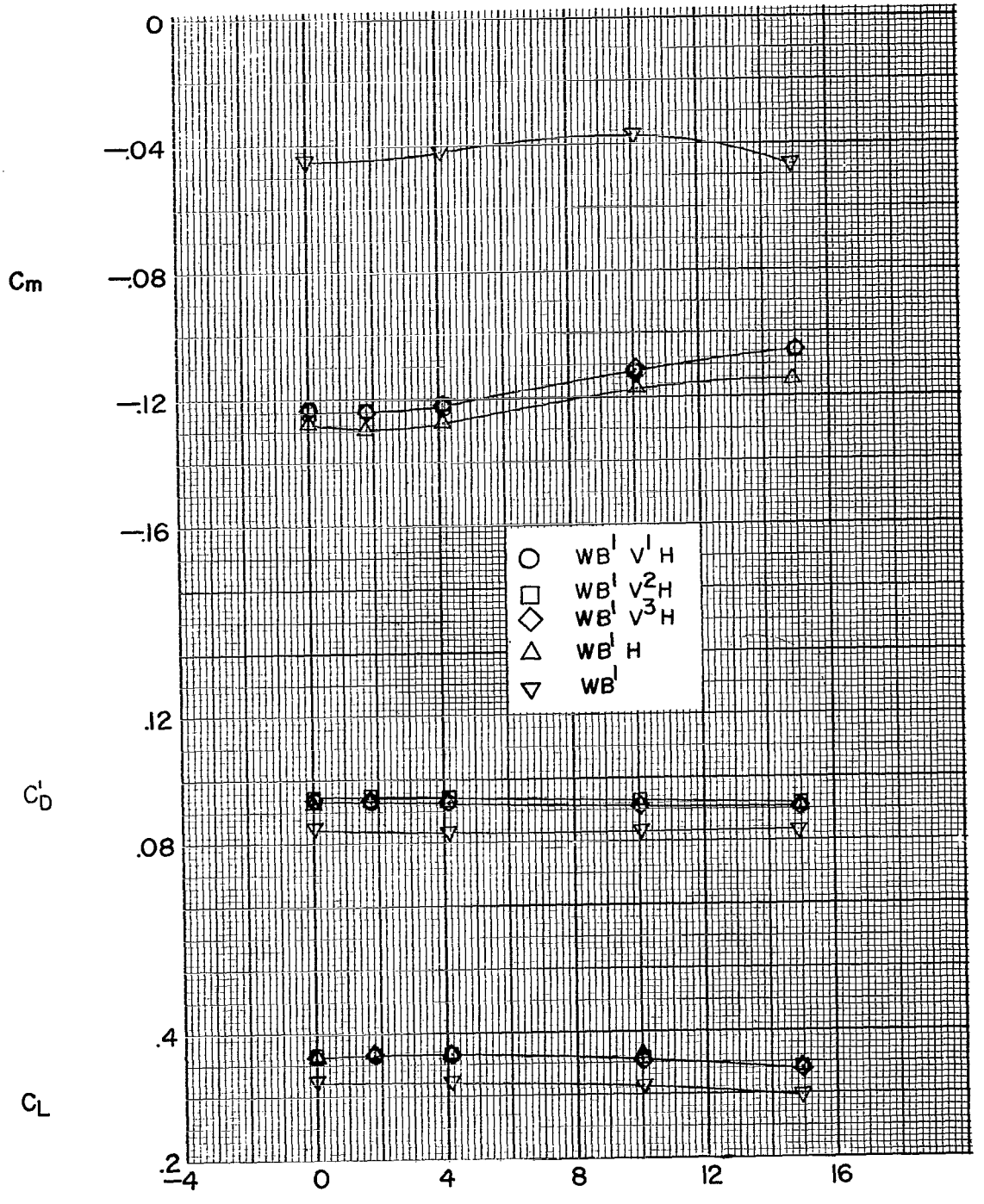
0
-.04
-.08
-.12
-.16
Cm
.12
C'D
.08
.4
CL
.2
-4
0
4
8
12
16
WB' V' H
WB' V2H
WB' V3H
WB' H
WB'

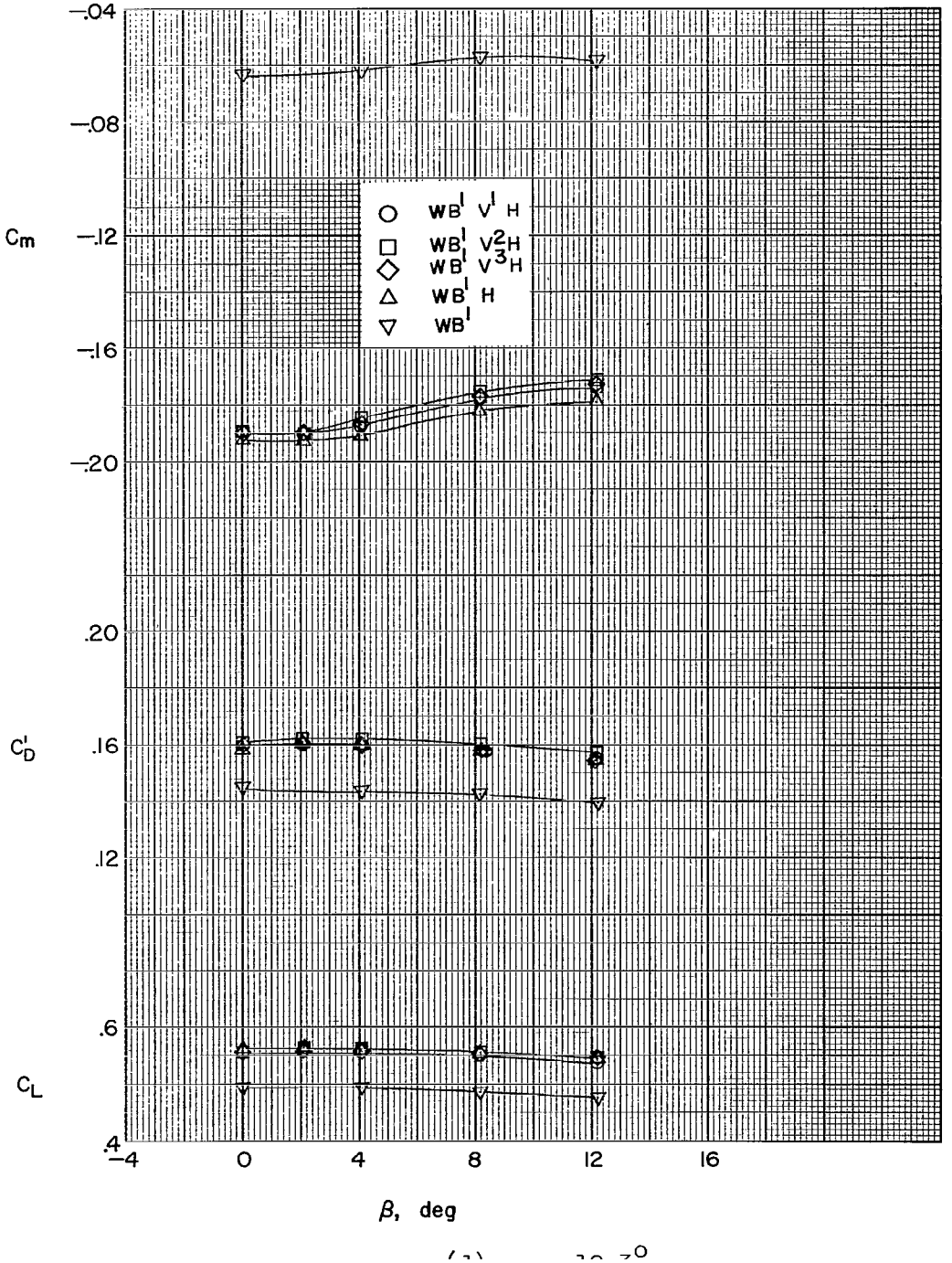
−.04
−.08
−.12
−.16
−.20
.20
.16
.12
.6
.4
$C_m$
$C_D'$
$C_L$
$WB^1$ $V^1$ H
$WB^1$ $V^2H$
$WB^1$ $V^3H$
$WB^1$ H
$WB^1$
−4
0
4
8
12
16
β, deg

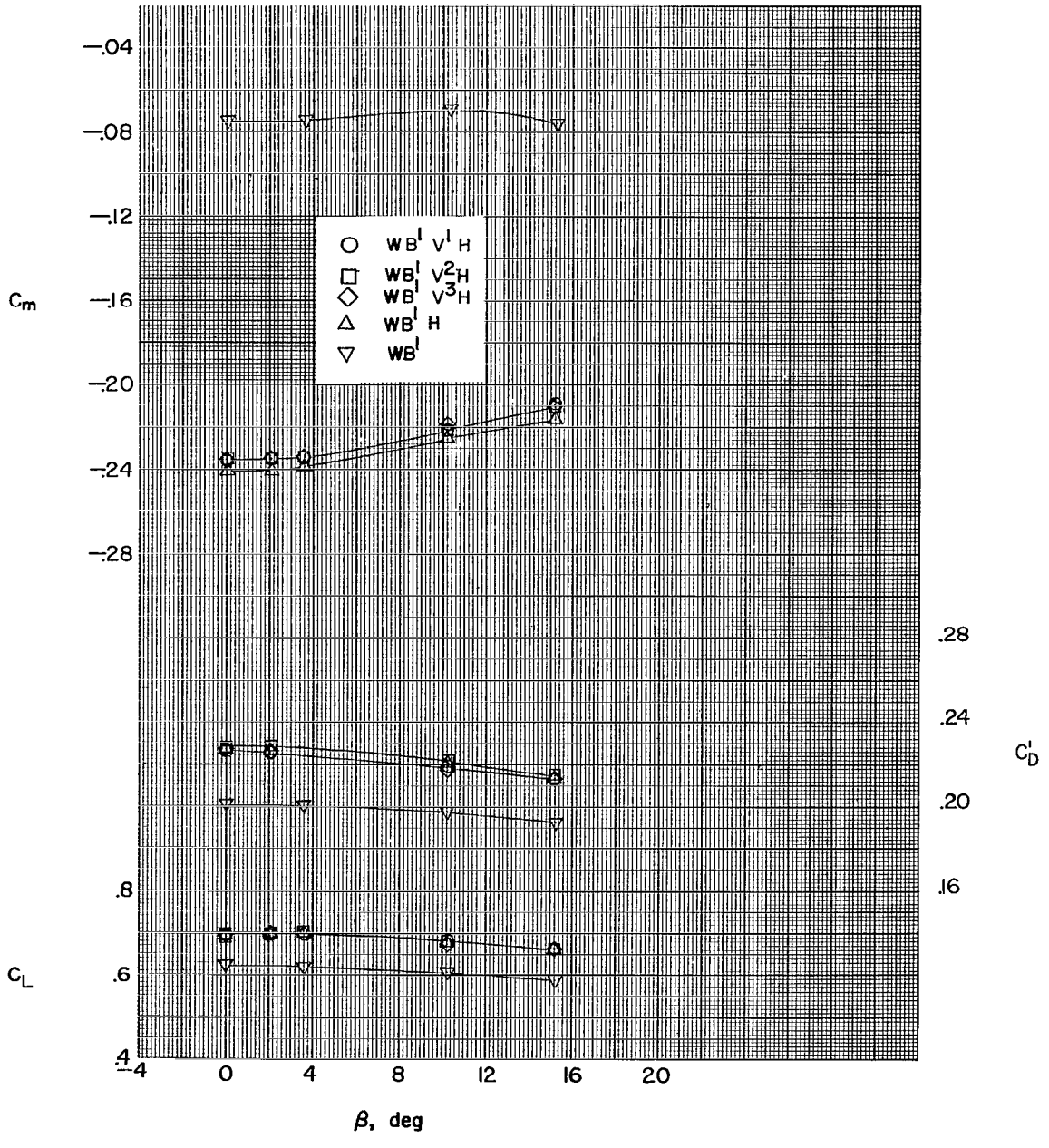
$C_m$
-.04
-.08
-.12
-.16
-.20
-.24
-.28
$C_L$
.8
.6
.4
$C'_D$
.28
.24
.20
.16
-4
0
4
8
12
16
20
$\beta$, deg
$WB^1V^1H$
$WB^1V^2H$
$WB^1V^3H$
$WB^1H$
$WB^1$

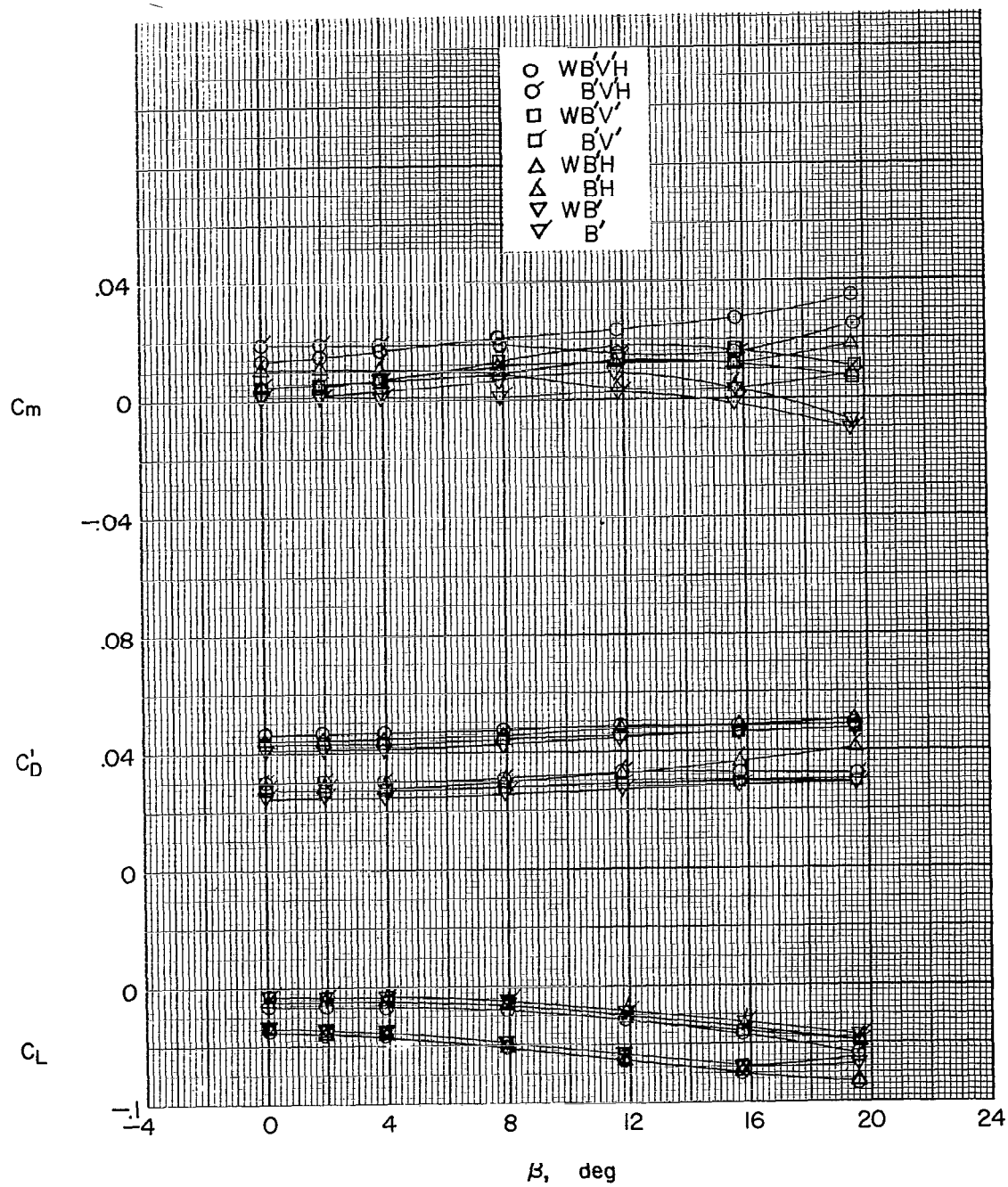
WB′V′H
B′V′H
WB′V′
B′V′
WB′H
B′H
WB′
B′
.04
0
−.04
.08
.04
0
0
−.1
Cm
C′D
CL
−4
0
4
8
12
16
20
24
β, deg

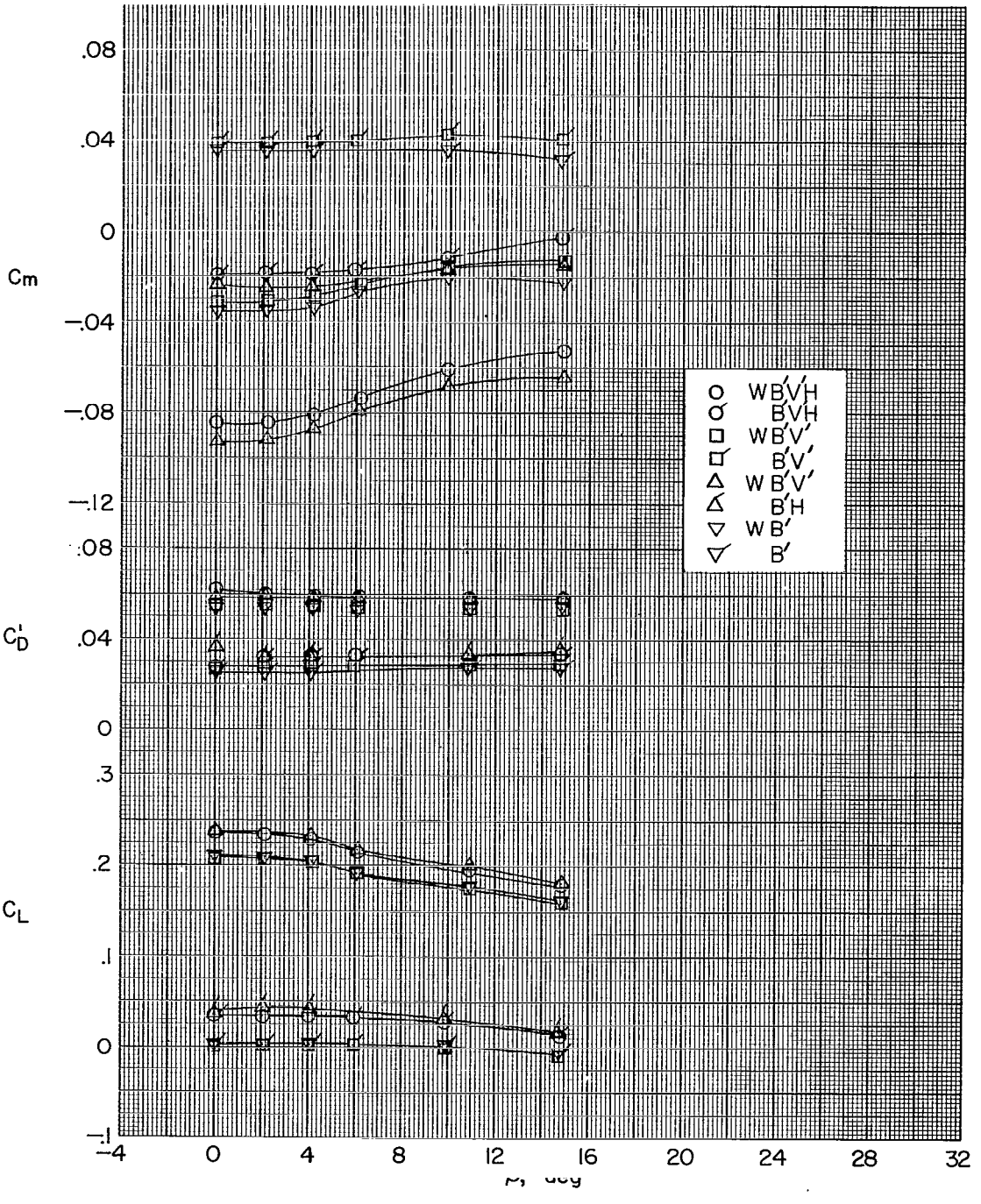
.08
.04
0
Cm
−.04
−.08
−.12
.08
C'D
.04
0
.3
.2
CL
.1
0
−.1
−4
0
4
8
12
16
20
24
28
32
α, deg
WB'V'H
B'V'H
WB'V'
B'V'
WB'V'
B'H
WB'
B'

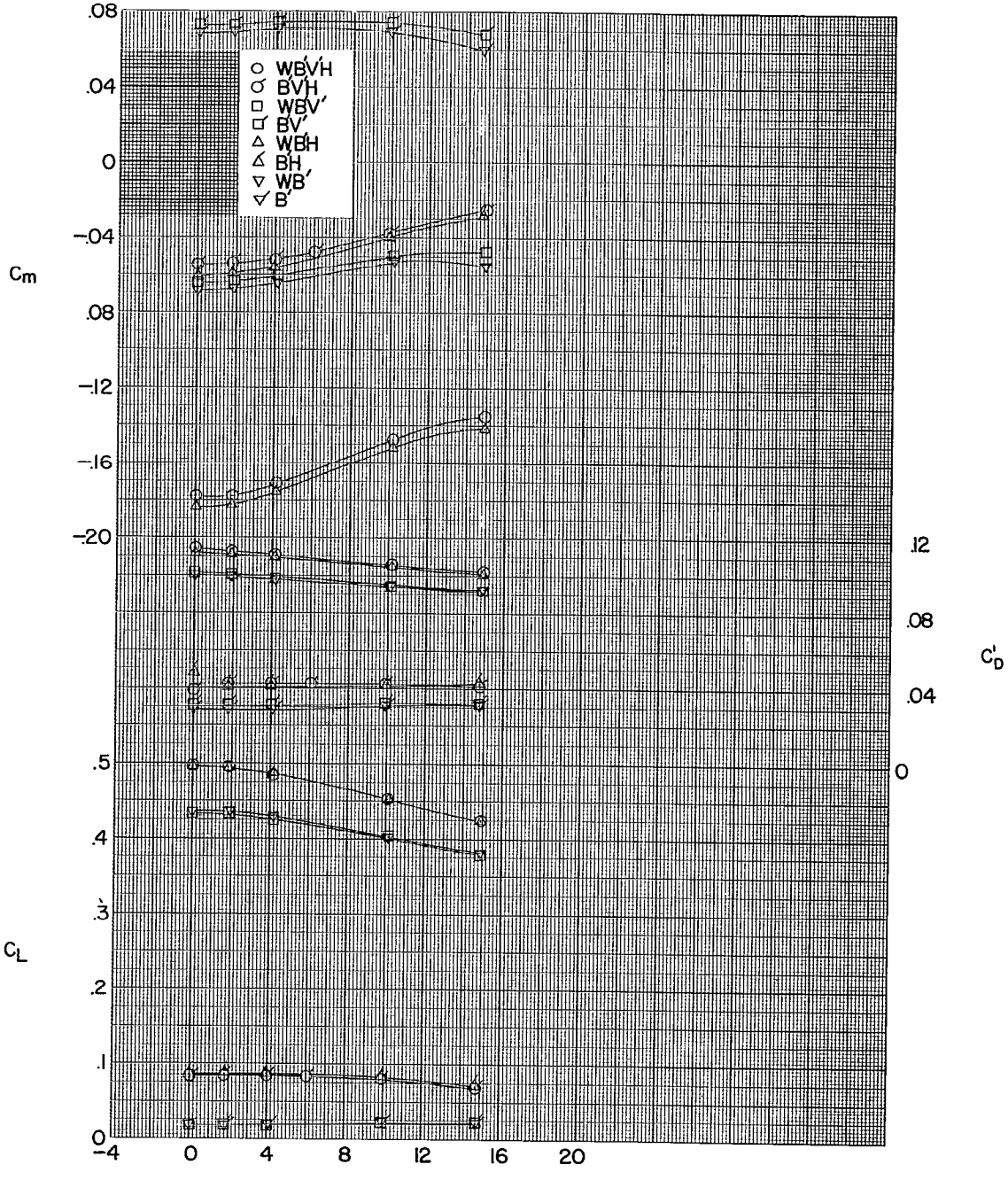
WBV'H
BV'H
WBV'
BV'
WBH
BH
WB'
B'
$C_m$
$C_L$
$C'_D$
.08
.04
0
-.04
-.08
-.12
-.16
-.20
.5
.4
.3
.2
.1
0
.12
.08
.04
0
-4
0
4
8
12
16
20

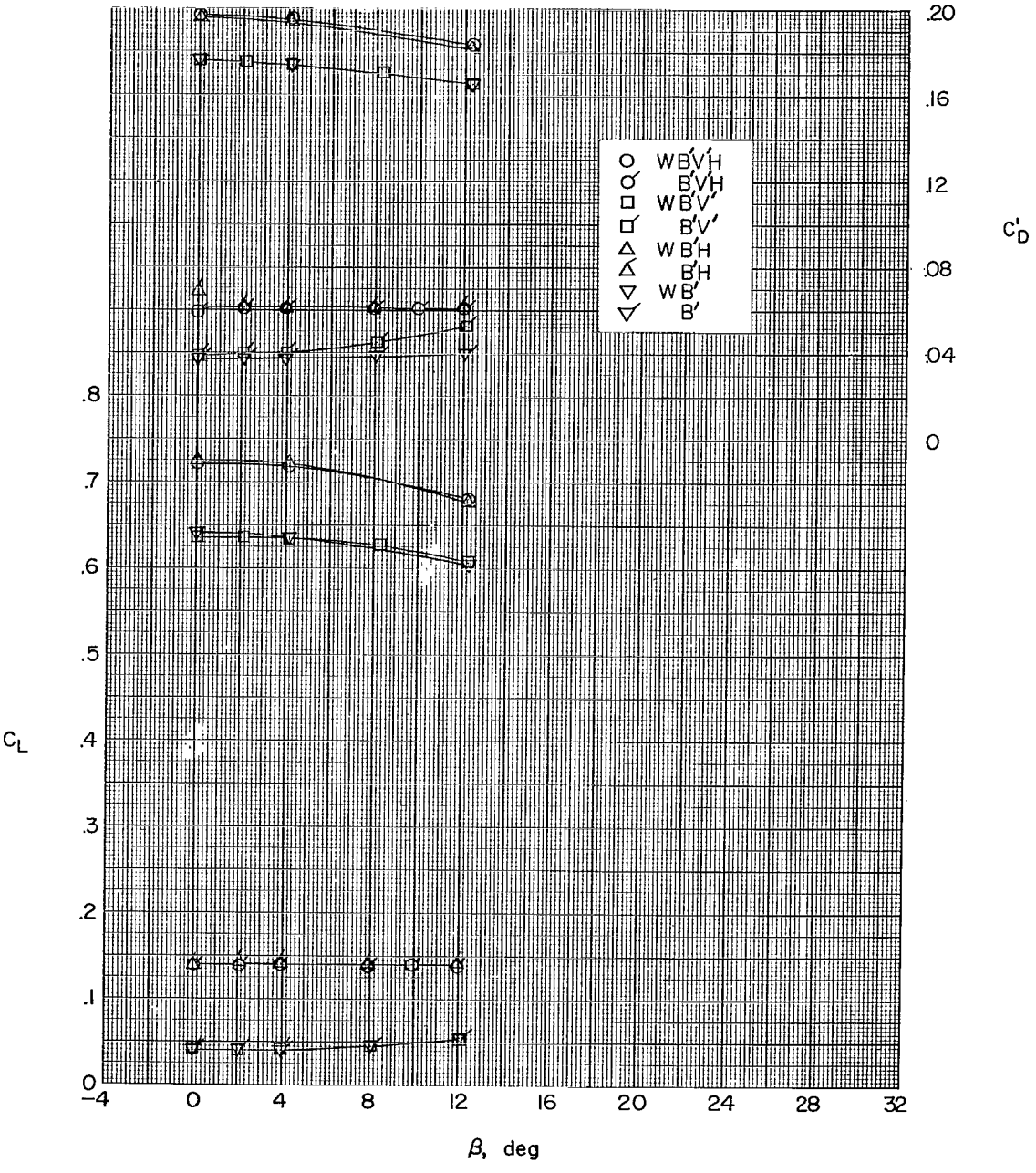


(d) $\alpha \approx 12.7^{\circ}$.

Figure 24.- Continued.

[redacted]

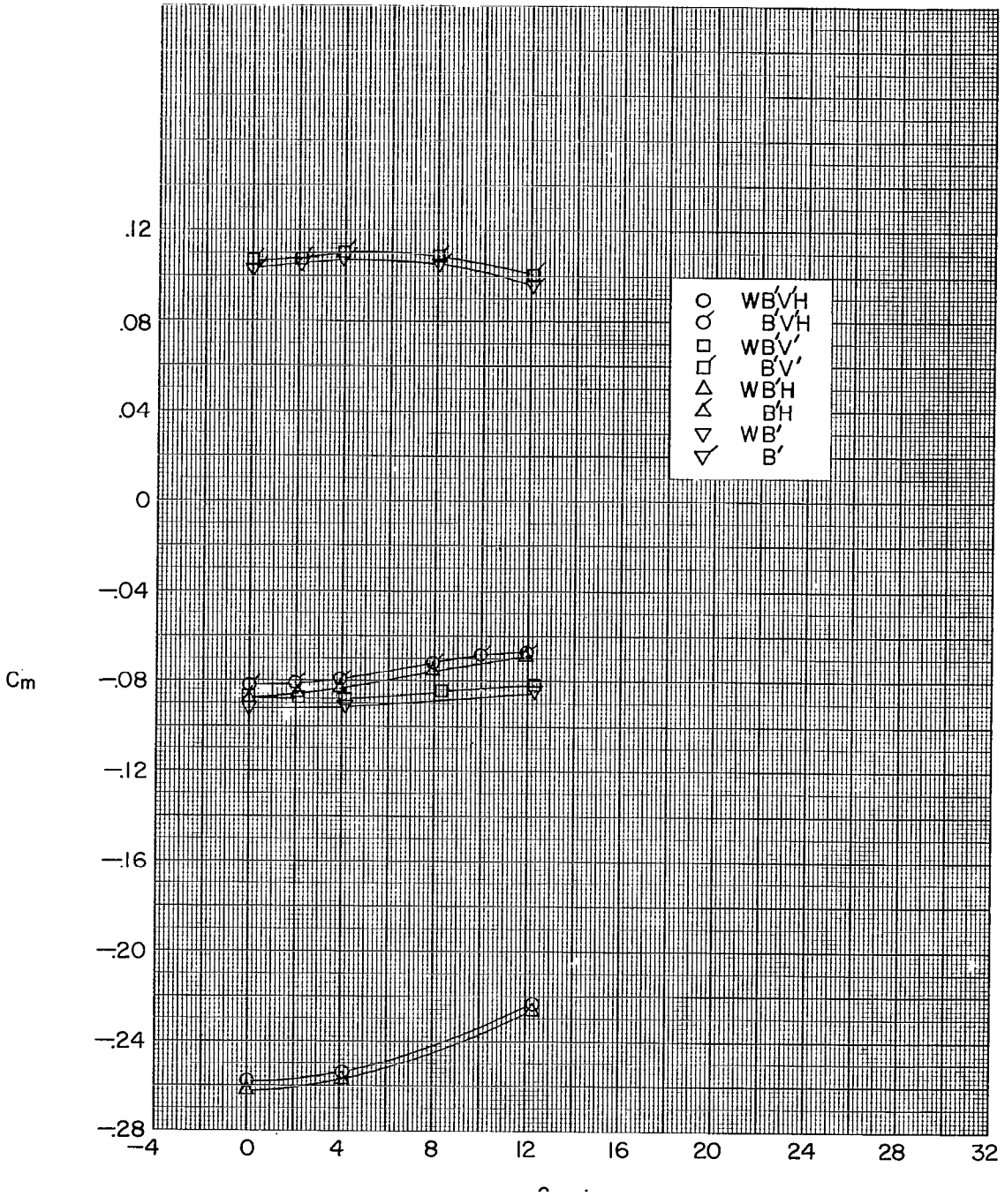
WB′V′H
B′V′H
WB′V′
B′V′
WB′H
B′H
WB′
B′
.12
.08
.04
0
−.04
−.08
−.12
−.16
−.20
−.24
−.28
Cm
−4
0
4
8
12
16
20
24
28
32

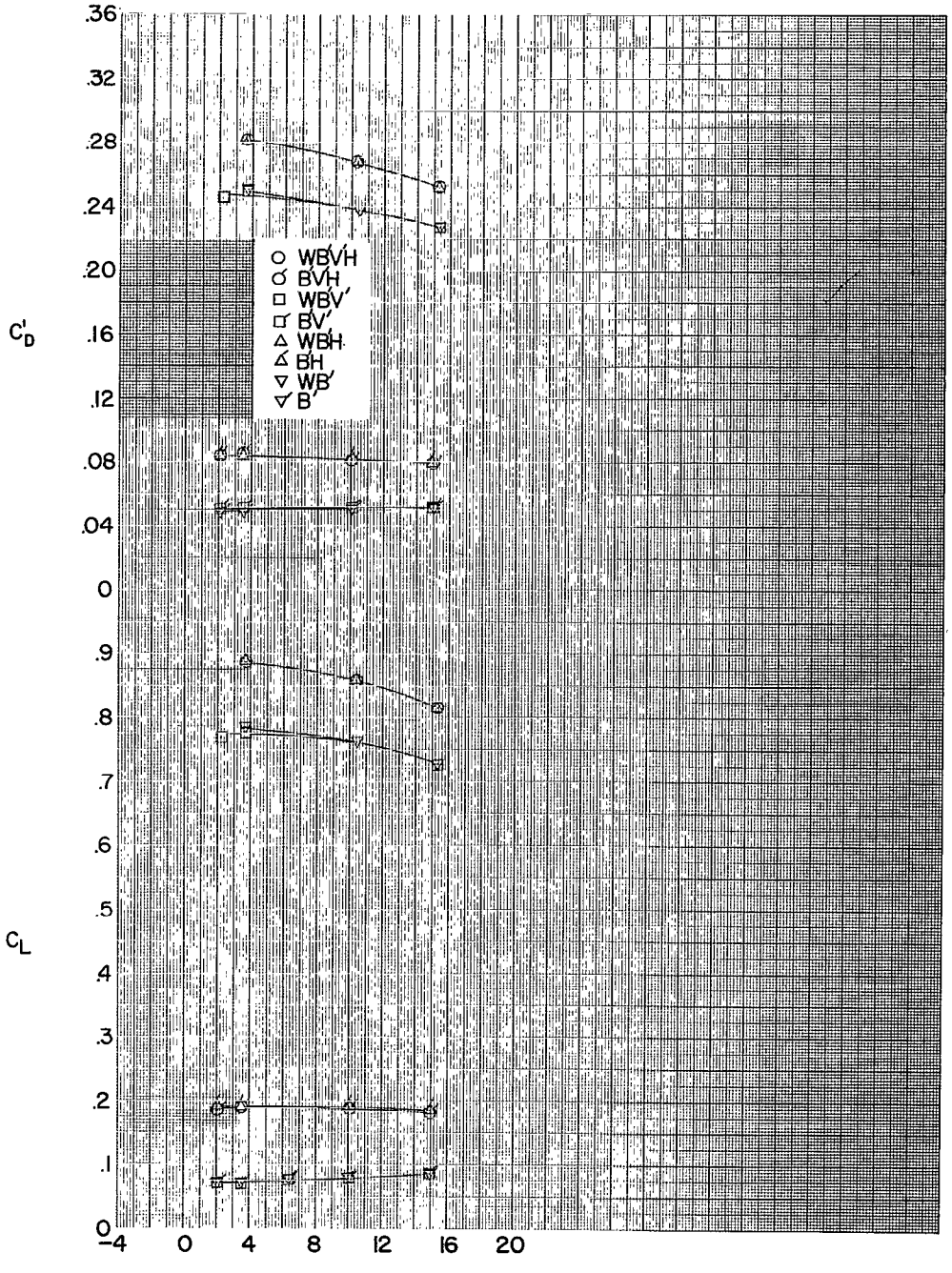
$C'_D$
$C_L$
.36
.32
.28
.24
.20
.16
.12
.08
.04
0
.9
.8
.7
.6
.5
.4
.3
.2
.1
0
−4
0
4
8
12
16
20
WBV'H
BV'H
WBV'
BV'
WBH
BH
WB'
B'

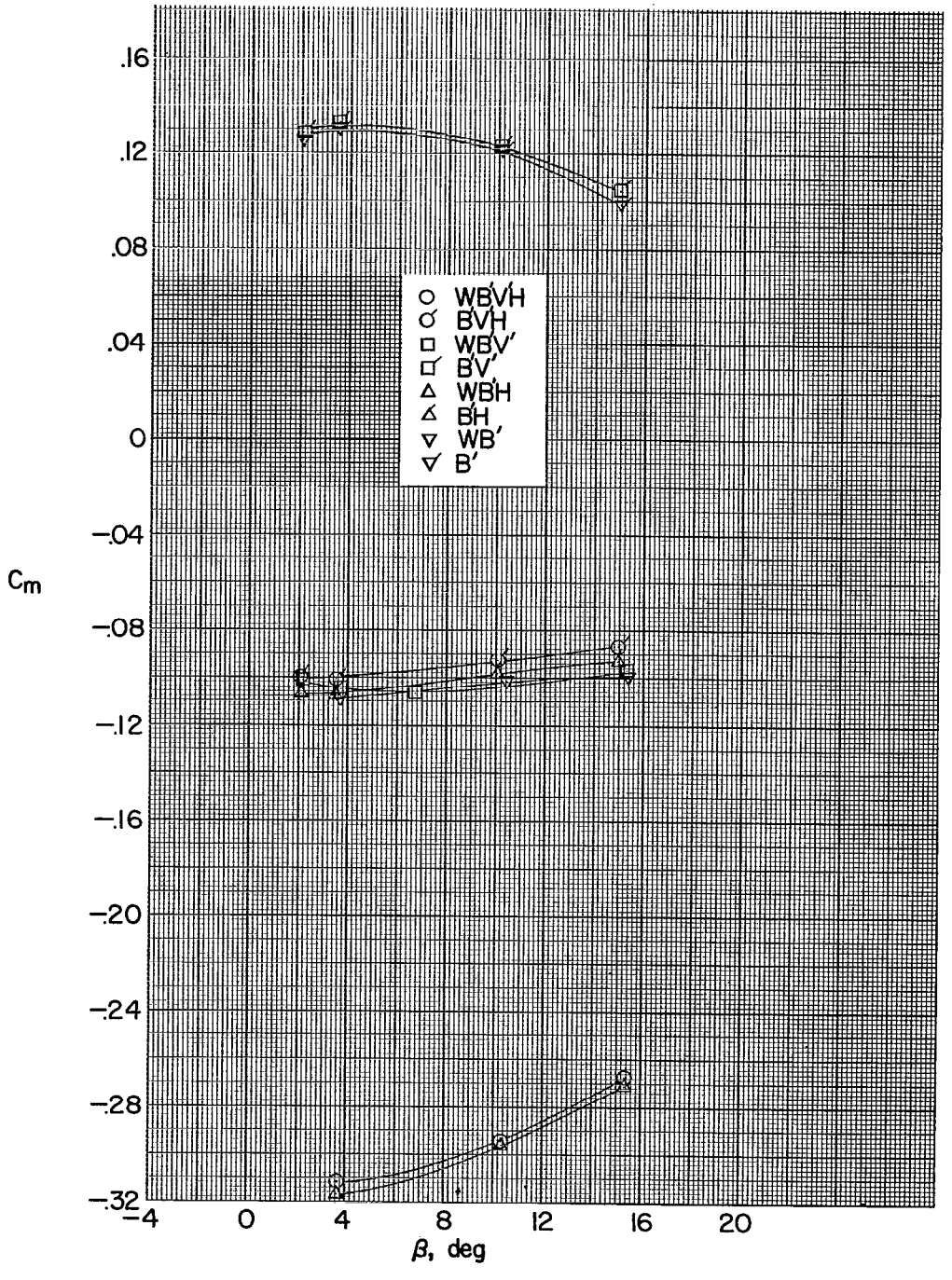
.16
.12
.08
.04
0
−.04
−.08
−.12
−.16
−.20
−.24
−.28
−.32
$C_m$
−4
0
4
8
12
16
20
β, deg
WB'VH
B'VH
WB'V'
B'V'
WBH
B'H
WB'
B'

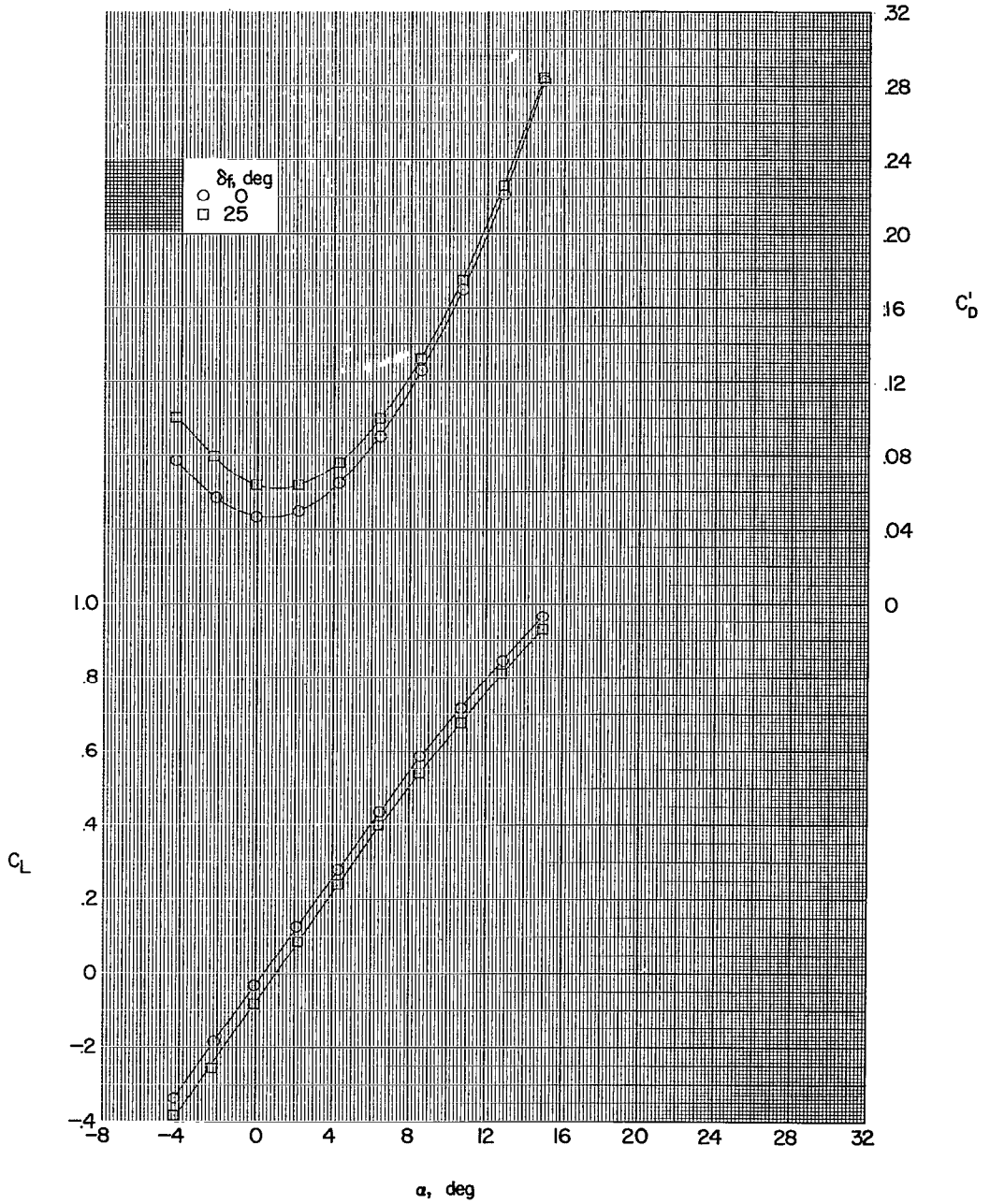


(a) Variation of $C'_D$ and $C_L$ with $\alpha$.

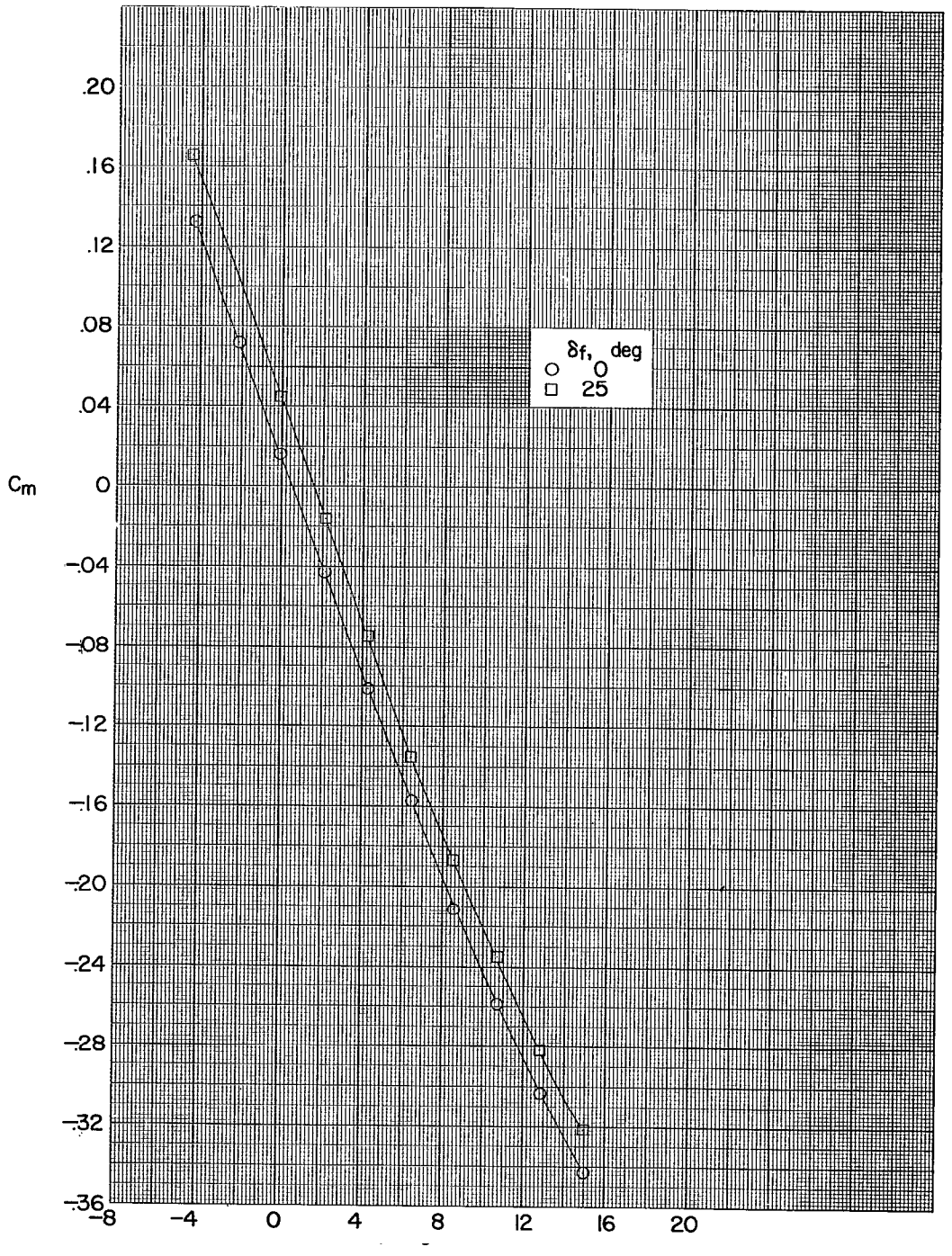
.20
.16
.12
.08
.04
0
-.04
-.08
-.12
-.16
-.20
-.24
-.28
-.32
-.36
$C_m$
-8
-4
0
4
8
12
16
20
$\delta_f$, deg
○ 0
□ 25

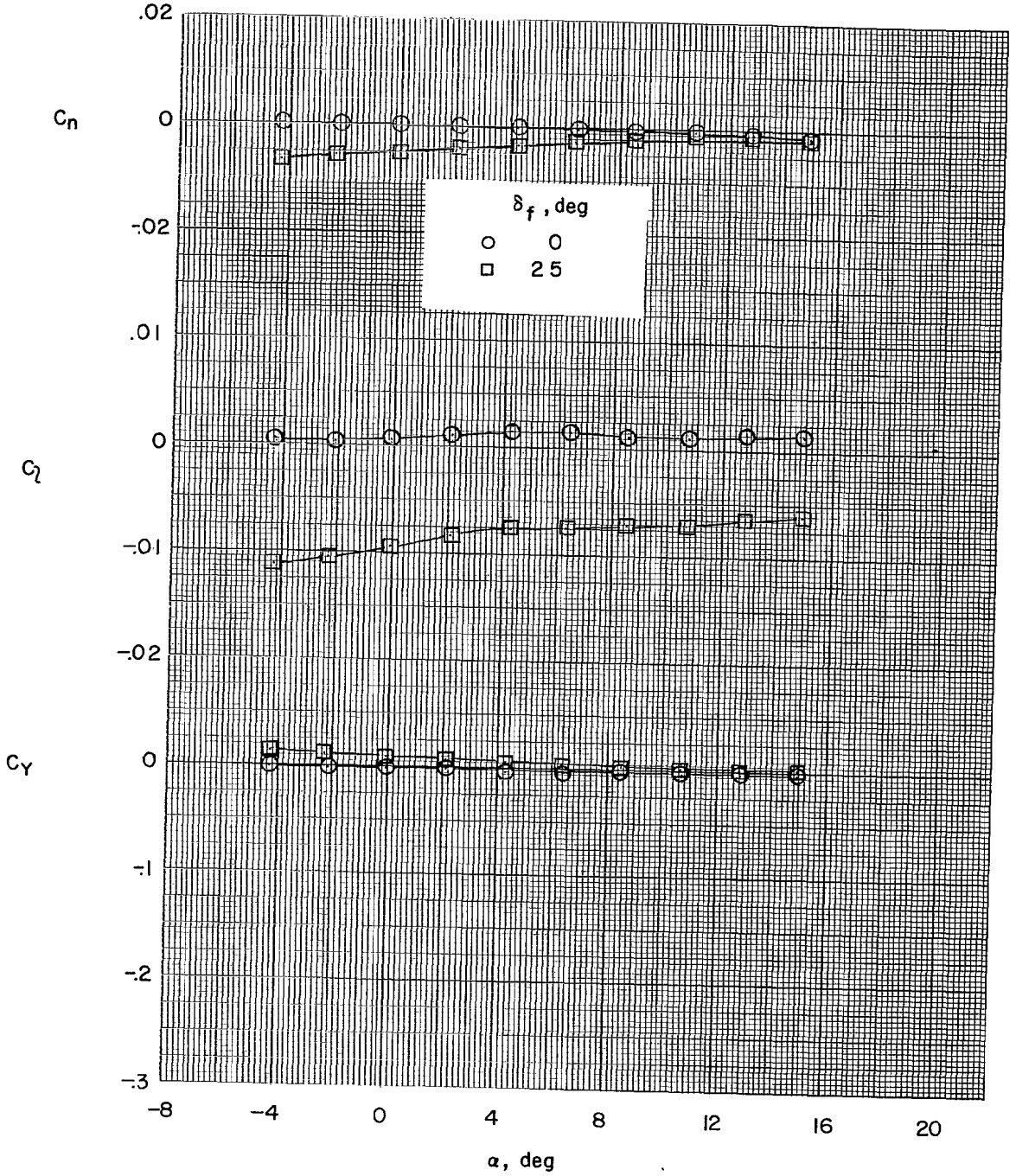


(c) Variation of $C_n$, $C_l$, and $C_Y$ with $\alpha$.

Figure 25.- Concluded.

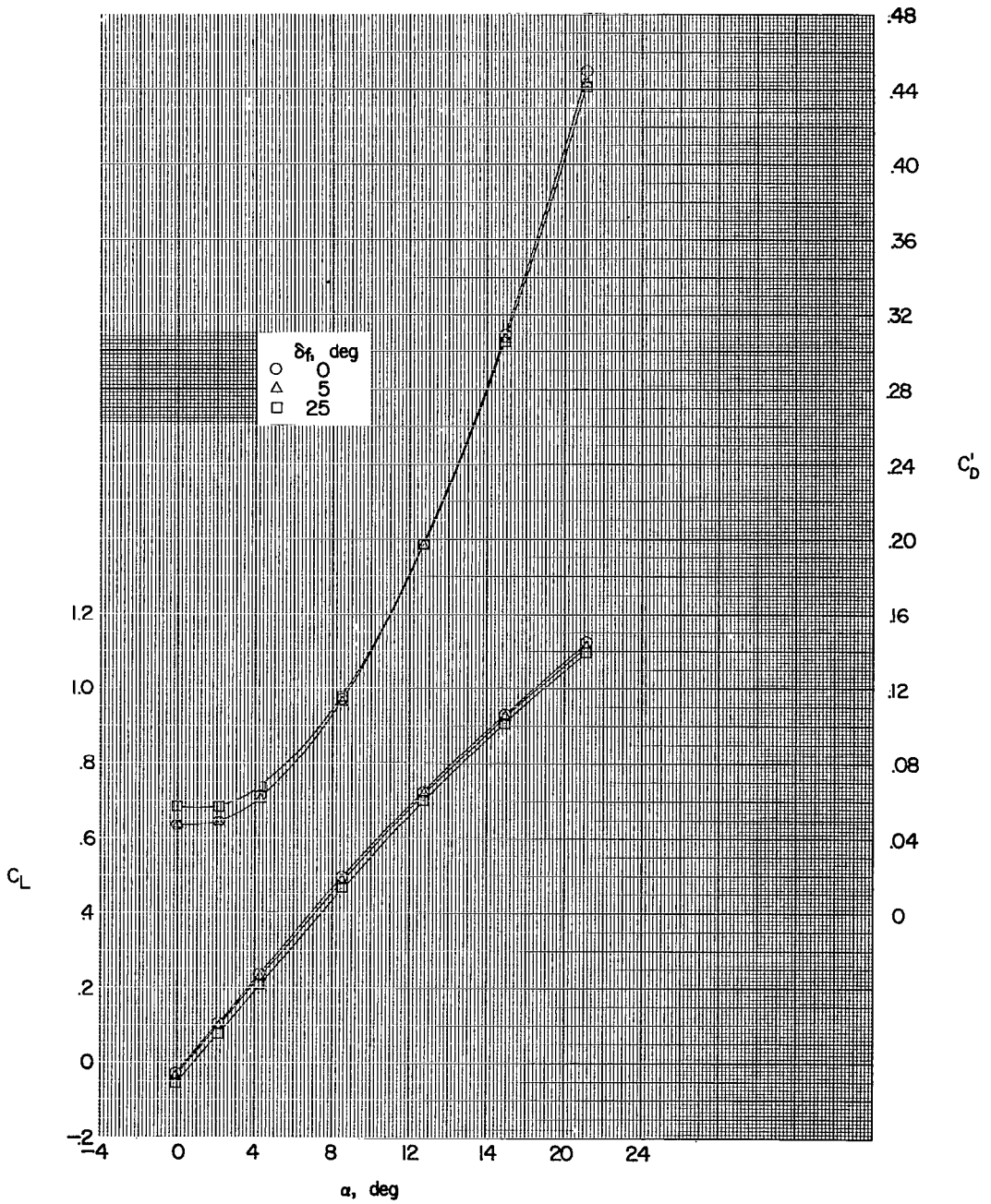


(a) Variation of $C'_D$ and $C_L$ with $\alpha$.

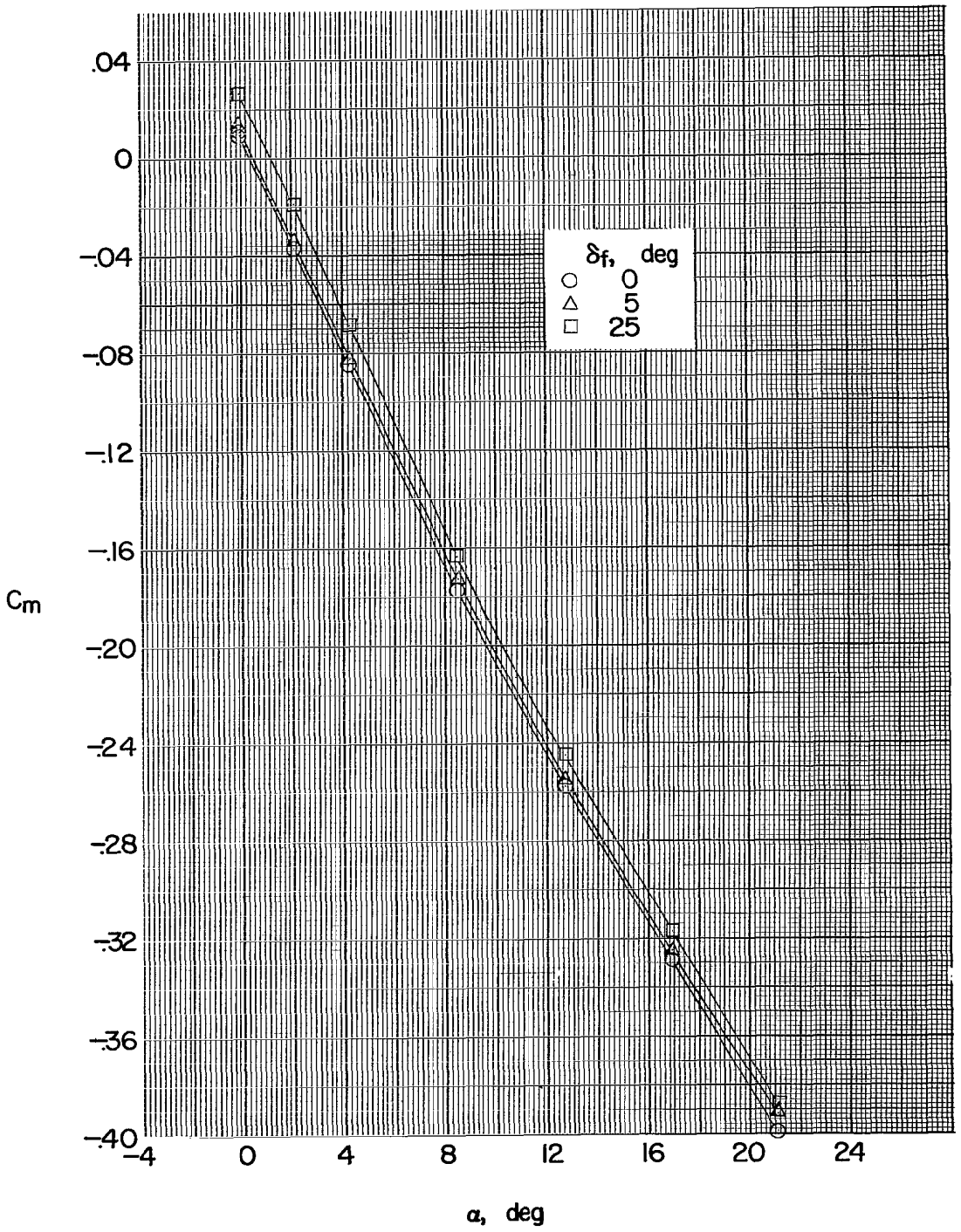


(b) Variation of $C_m$ with $\alpha$.

Figure 26.- Continued.

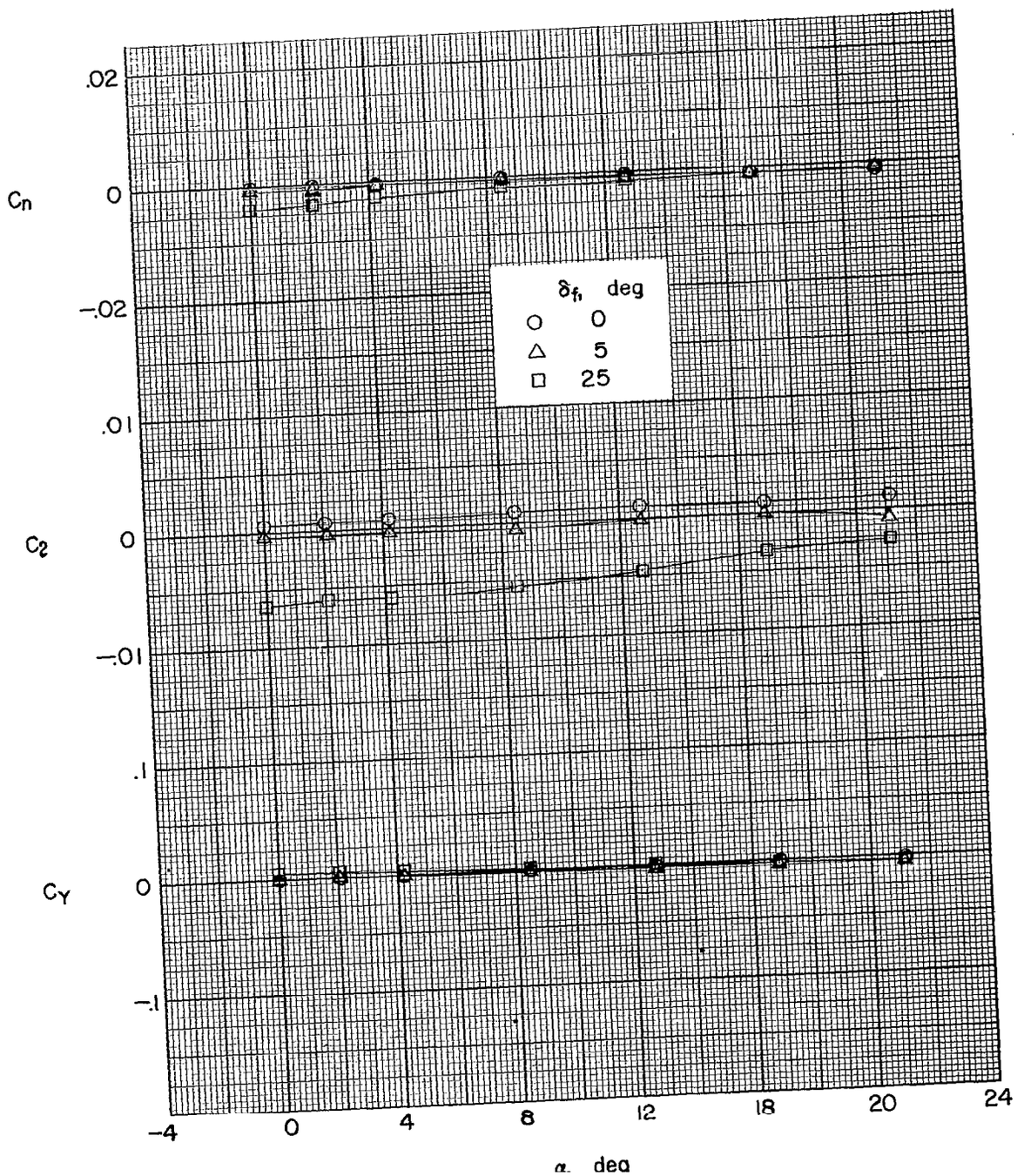
.02
0
−.02
.01
0
−.01
.1
0
−.1
$C_n$
$C_l$
$C_Y$
$\delta_f$, deg
○ 0
△ 5
□ 25
−4
0
4
8
12
18
20
24
α, deg

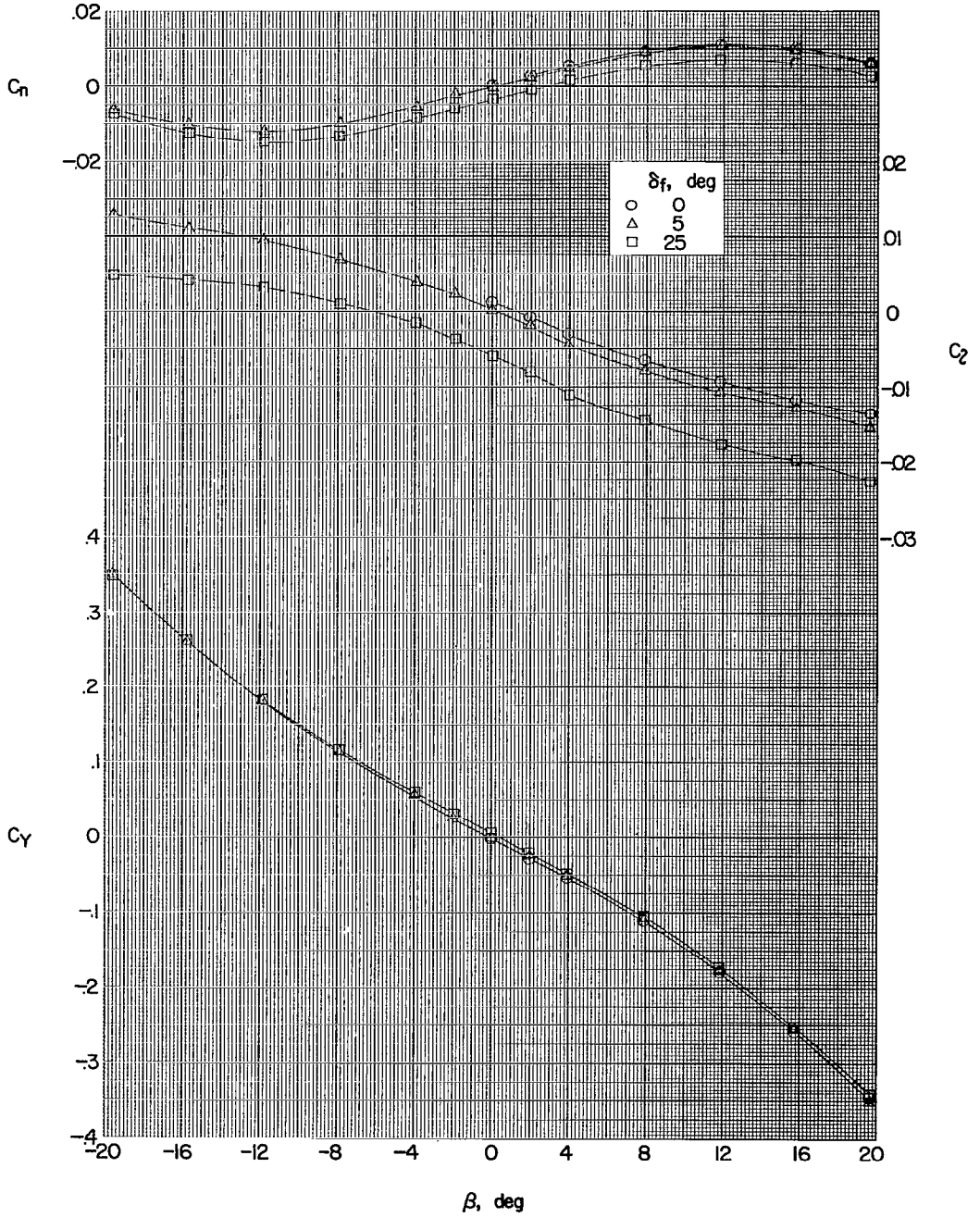


(a) $\alpha \approx 0^\circ$.

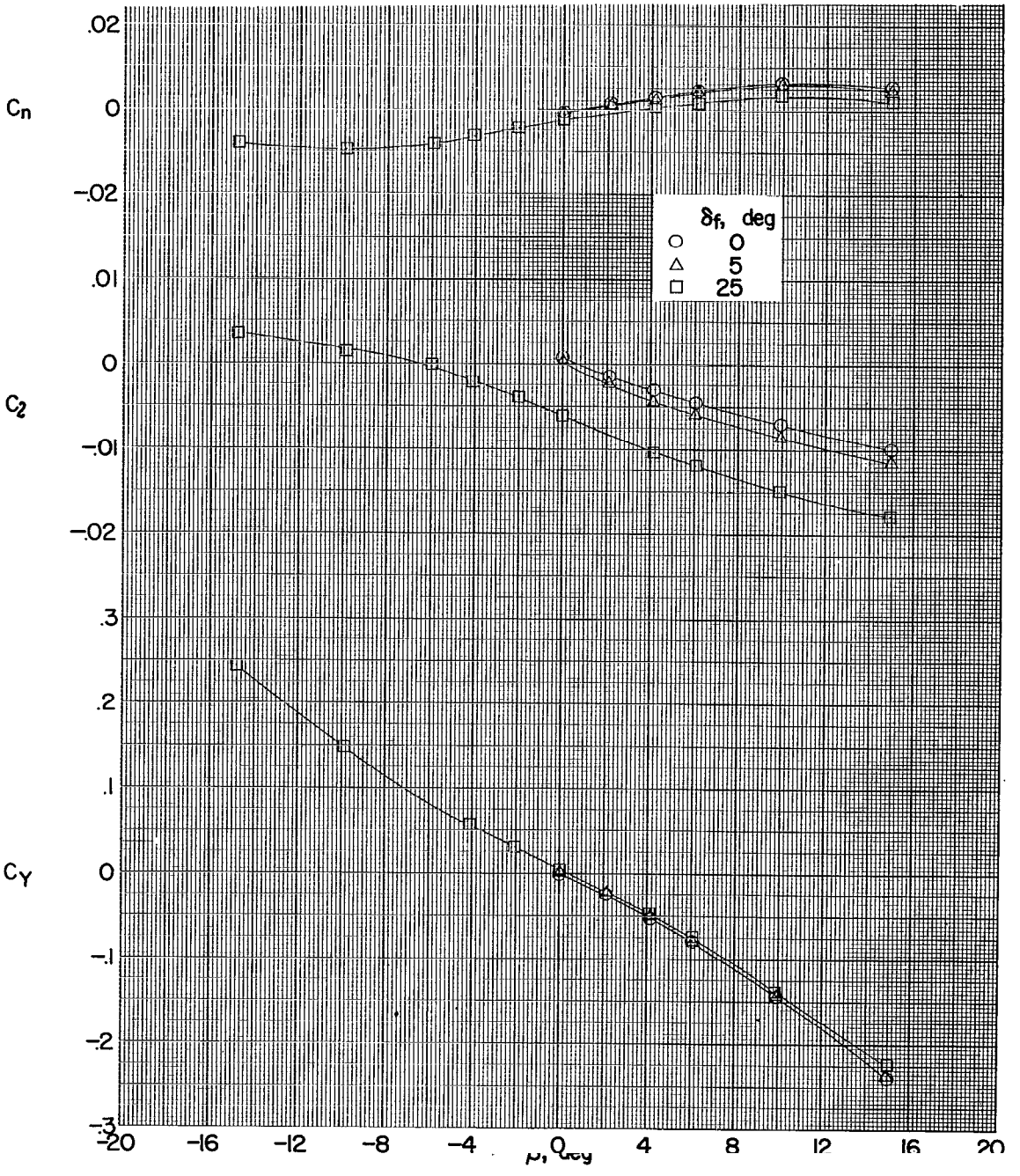
$C_n$
$C_l$
$C_Y$
.02
0
-.02
.01
0
-.01
-.02
.3
.2
.1
0
-.1
-.2
-.3
-20
-16
-12
-8
-4
0
4
8
12
16
20
$\beta, \alpha_{deg}$
$\delta_f$, deg
○ 0
△ 5
□ 25

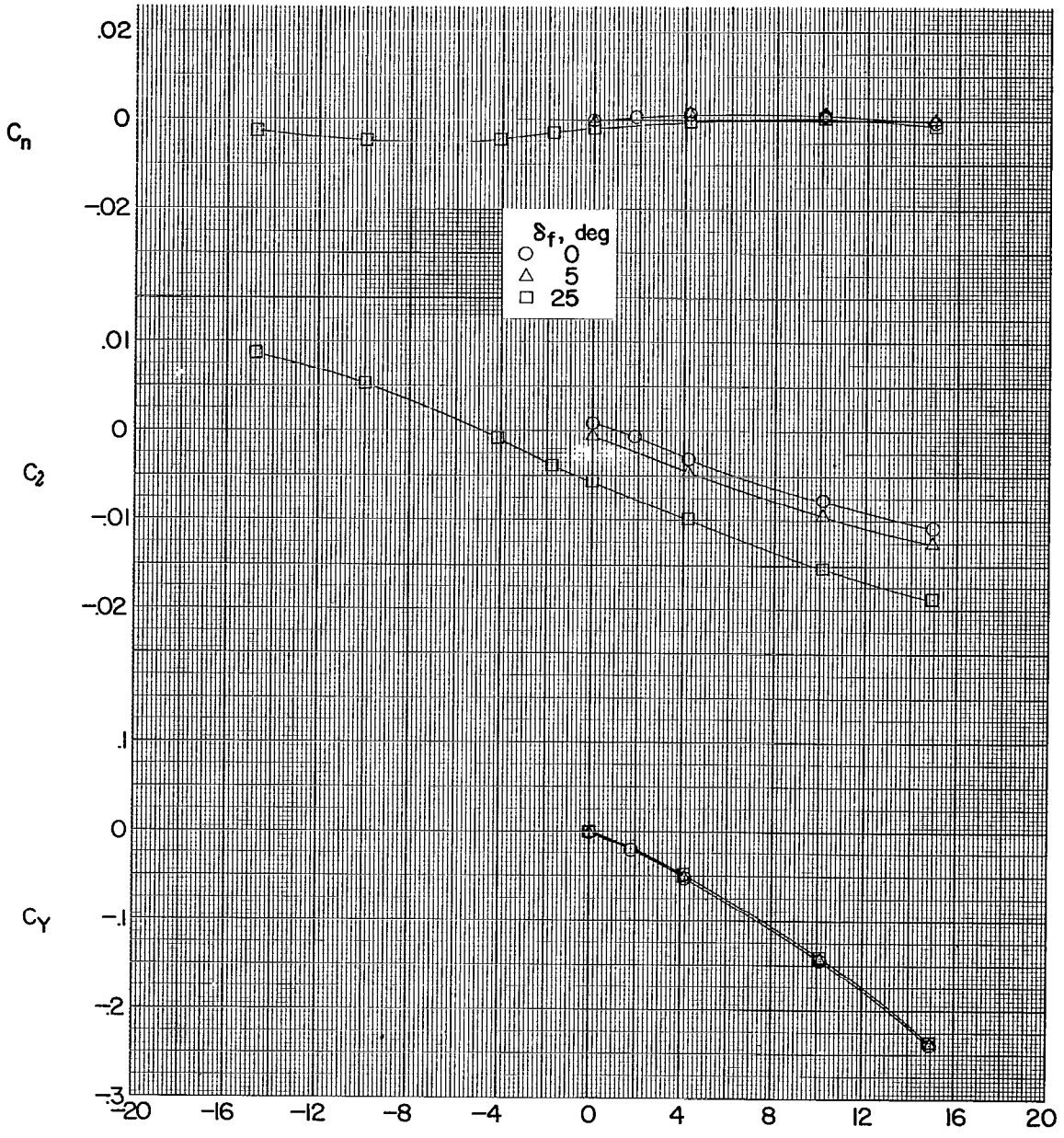


(a) $\alpha \approx 8.5^\circ$

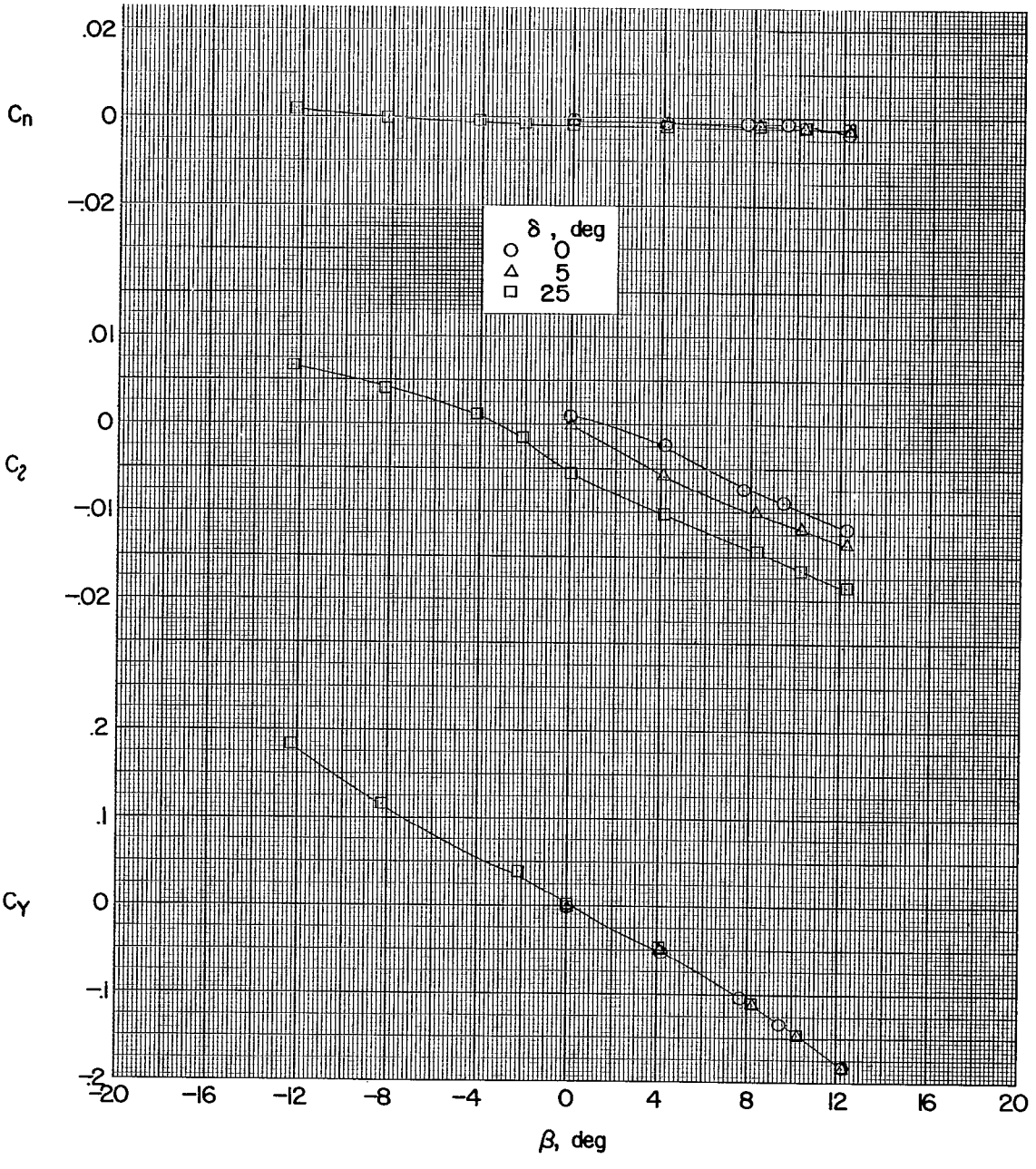


(d) $\alpha \approx 12.7^{\circ}$.

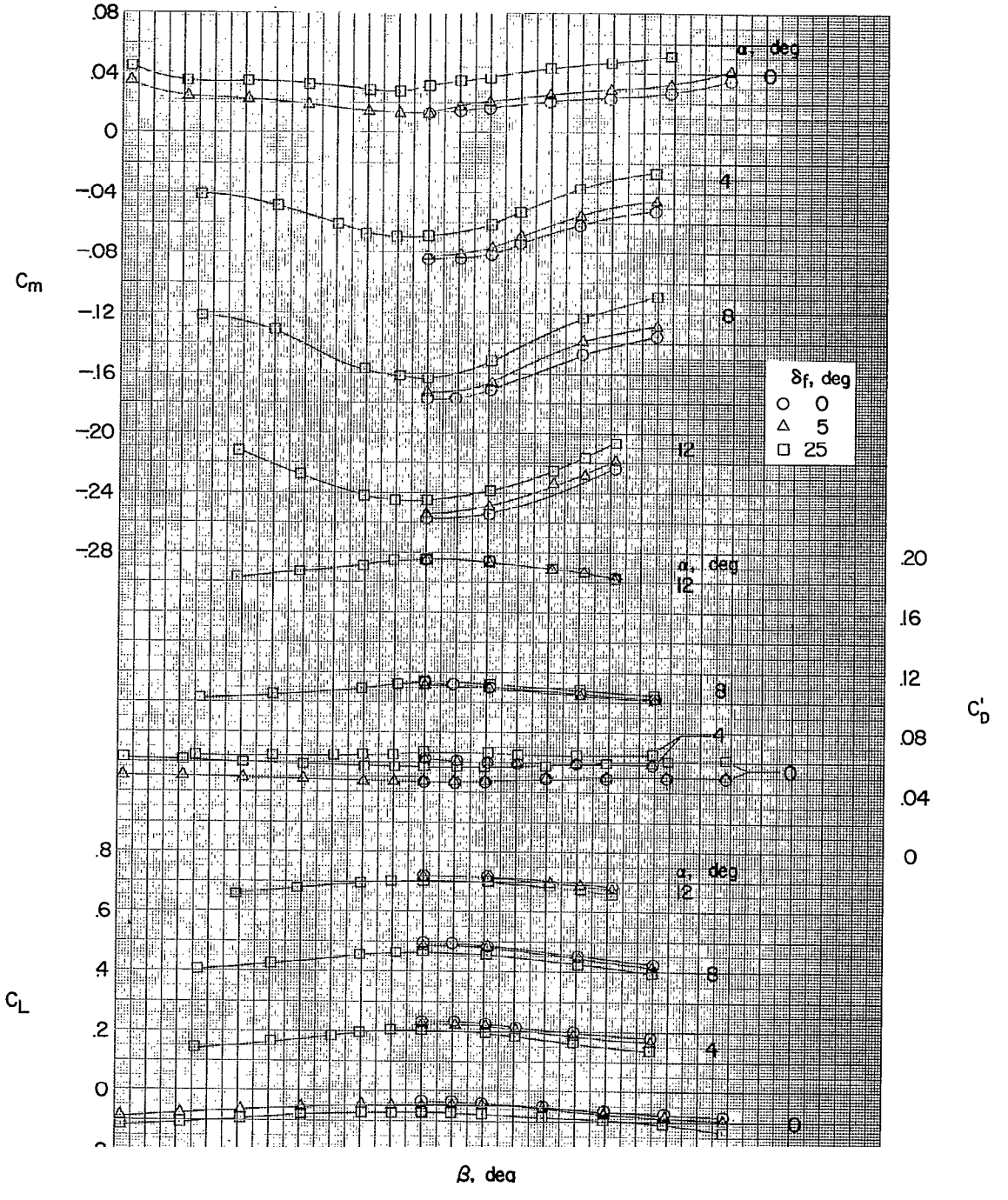
.08
.04
0
-.04
-.08
-.12
-.16
-.20
-.24
-.28
$C_m$
$\alpha$, deg
0
4
8
12
$\delta_f$, deg
○ 0
△ 5
□ 25
.20
.16
.12
.08
.04
0
$C'_D$
.8
.6
.4
.2
0
$C_L$
$\beta$, deg

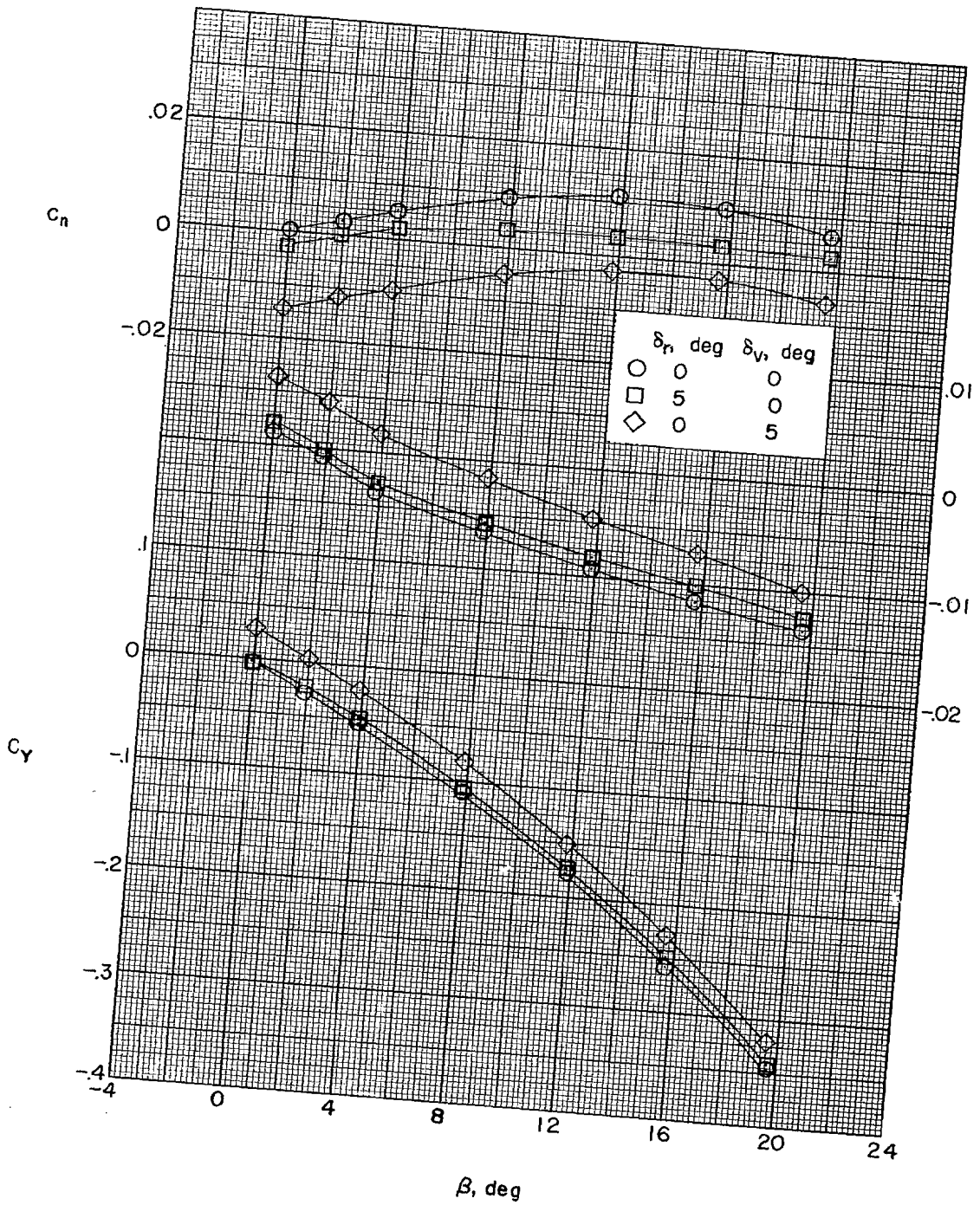


(a) $\alpha \approx 0^\circ$.

Figure 29.- Effects of rudder and vertical-tail deflections. Complete production model; M = 1.61.

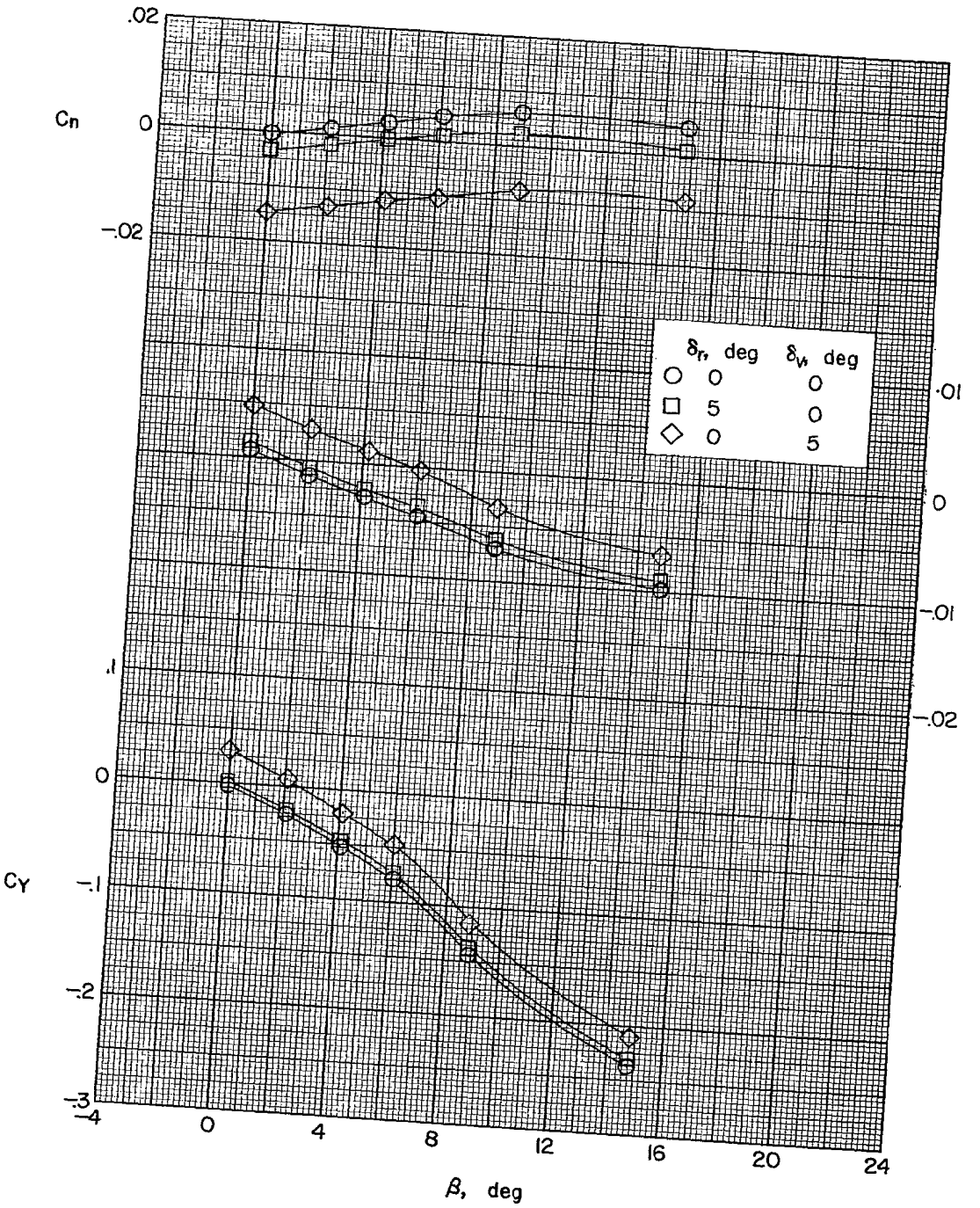


(b) $\alpha \approx 4.2^{\circ}$.

Figure 29.- Continued.

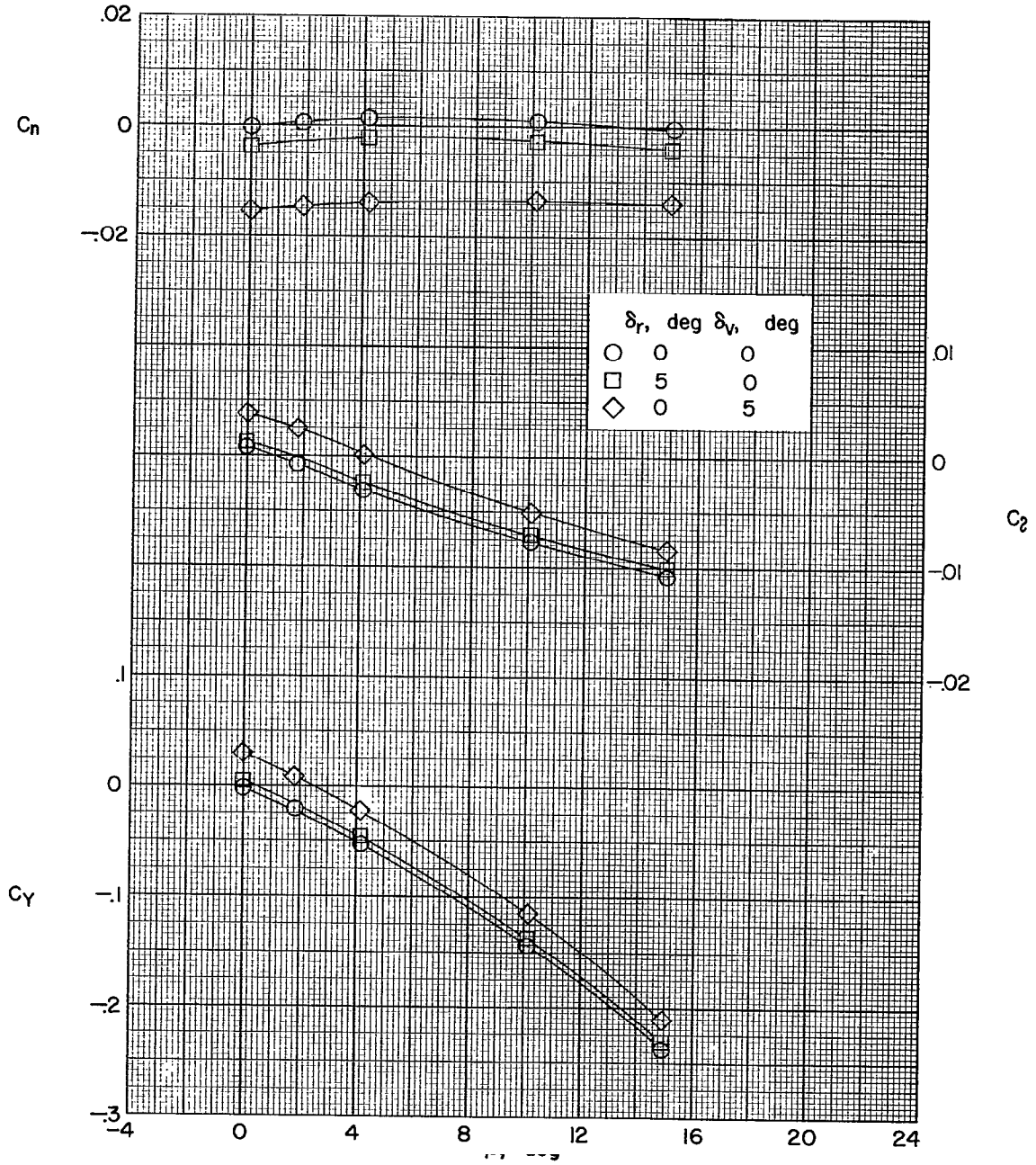
$C_n$
$C_Y$
$C_\ell$
$\delta_r$, deg $\delta_v$, deg
0 0
5 0
0 5
.02
0
-.02
.1
0
-.1
-.2
-.3
.01
0
-.01
-.02
-4
0
4
8
12
16
20
24

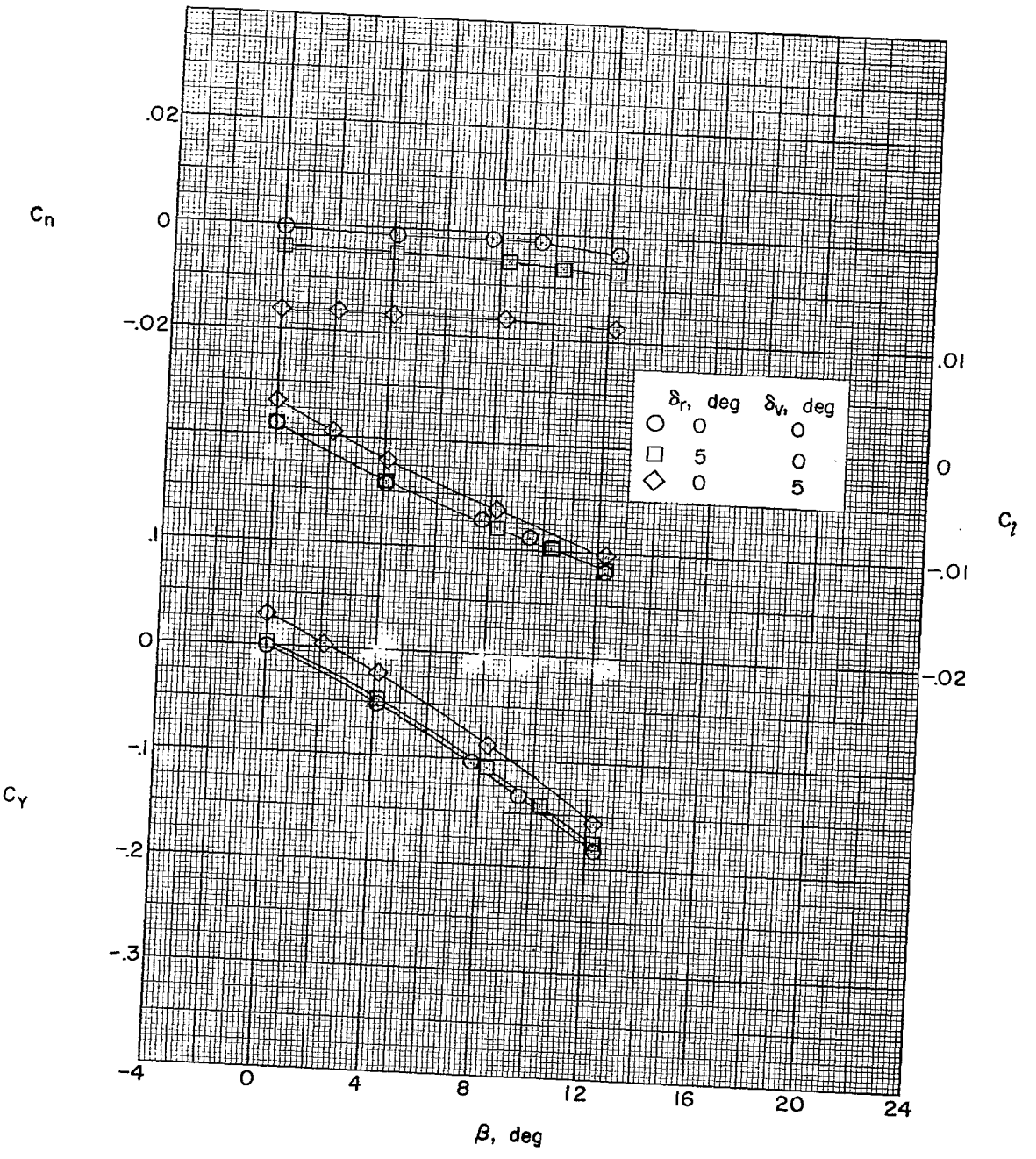


(d) $\alpha \approx 12.7^{\circ}$.

Figure 29.- Concluded.

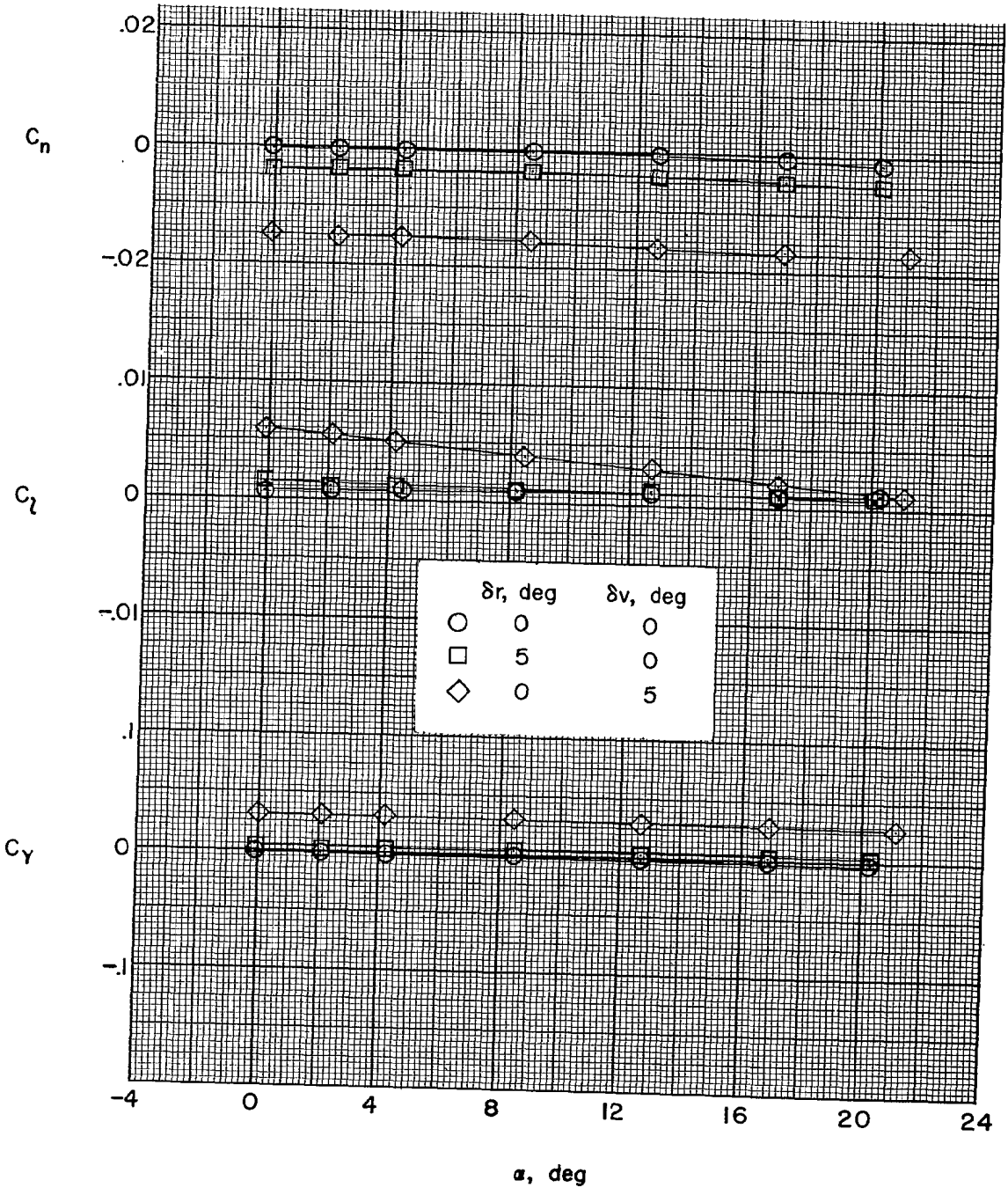


Figure 30.- Effects of rudder and vertical-tail deflections on the variation of $C_l$, $C_n$, and $C_Y$ with $\alpha$. Complete production model; $\beta = 0^\circ$; M = 1.61.

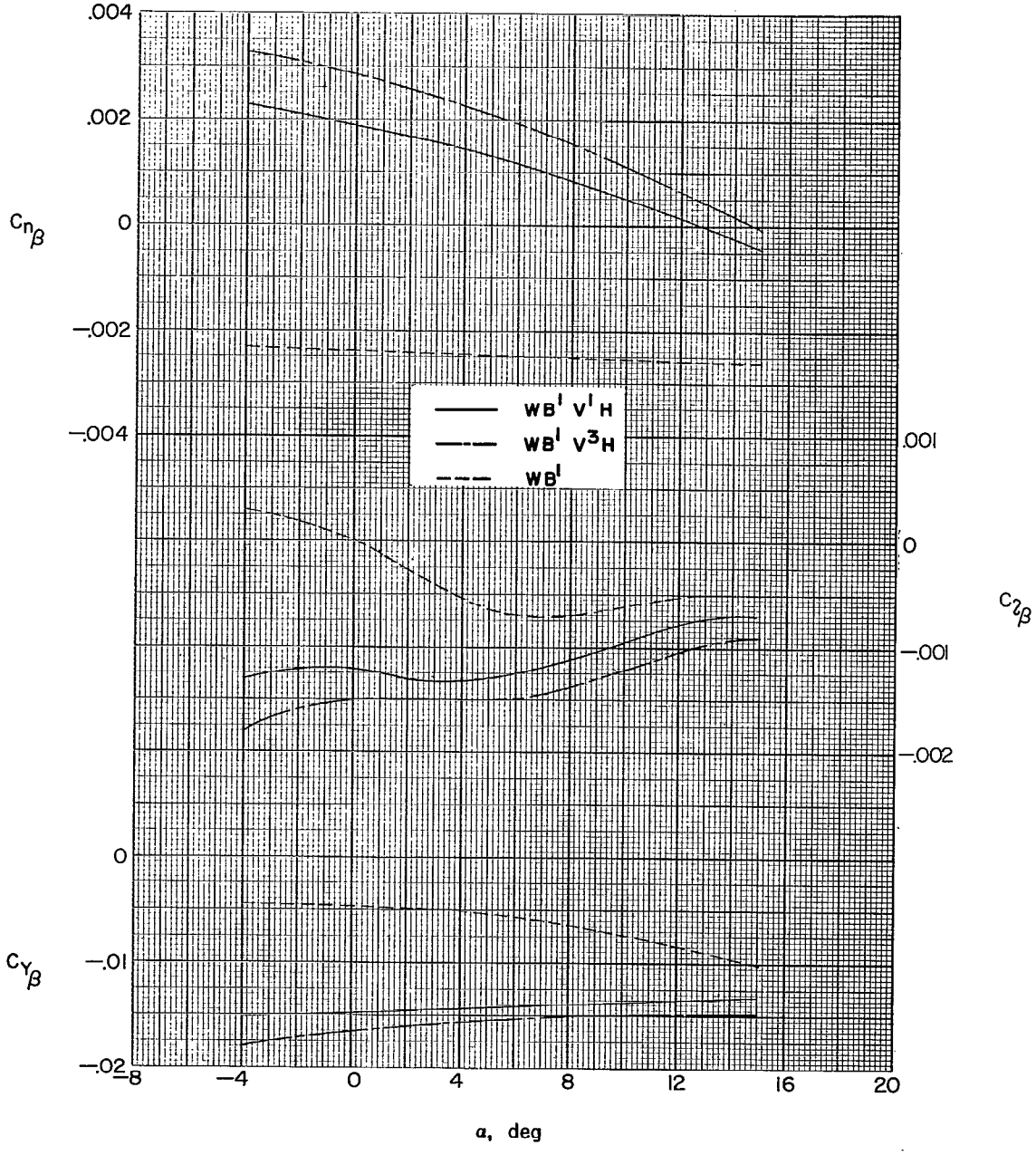


Figure 31.- Variation of sideslip derivatives with angle of attack for

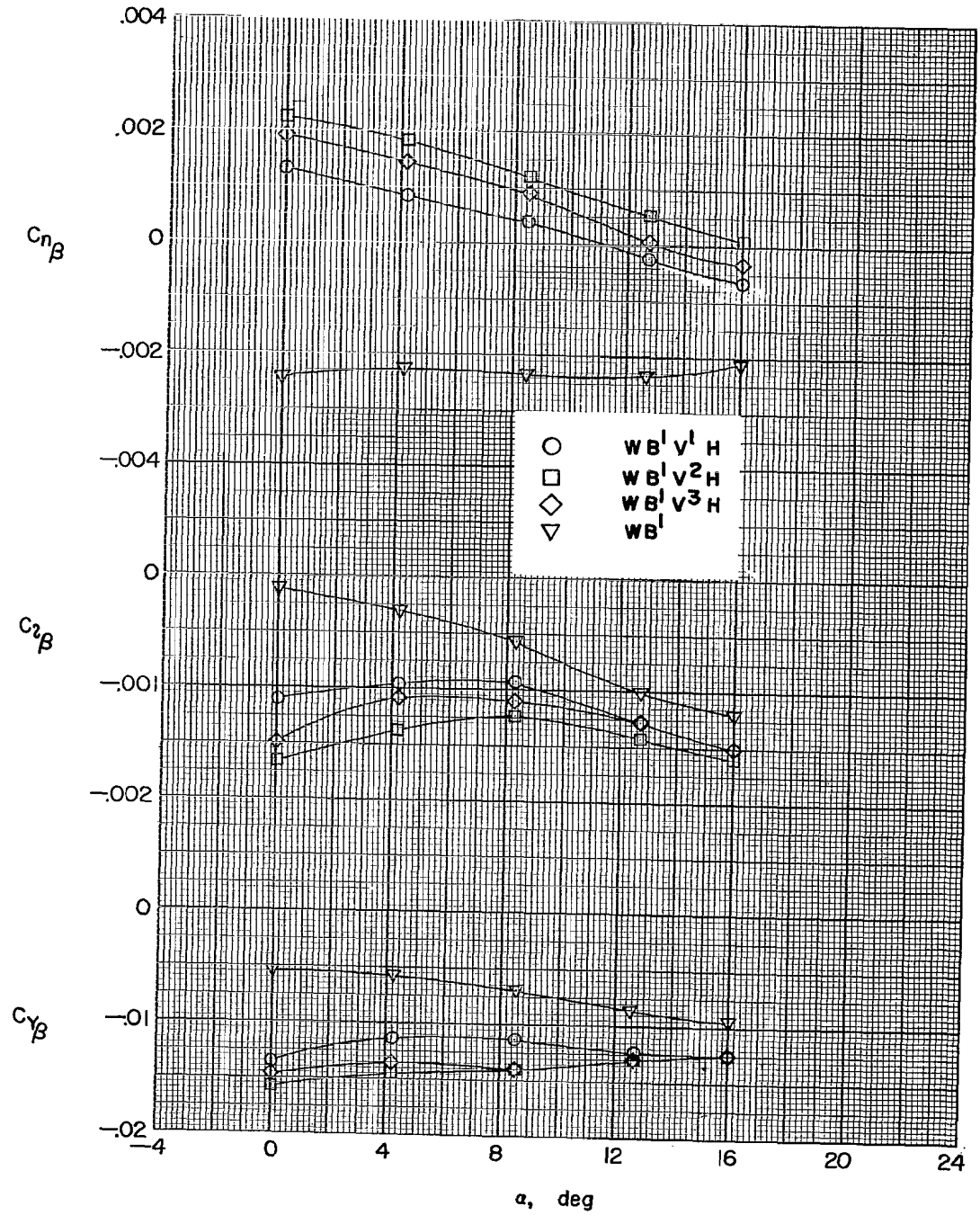


(b) M = 1.61.

Figure 31.- Continued.

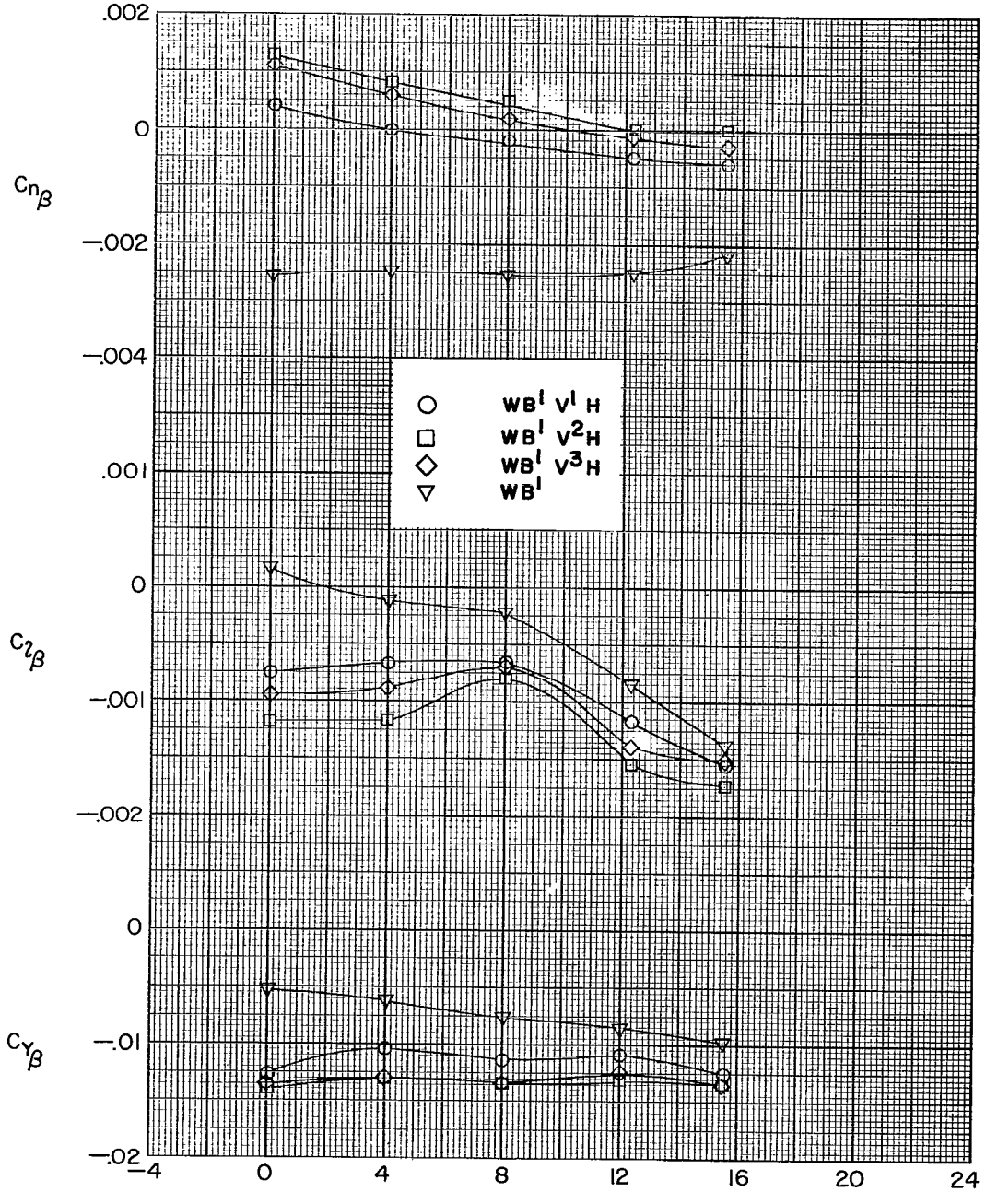
.002
0
−.002
−.004
.001
0
−.001
−.002
0
−.01
−.02
$C_{n_\beta}$
$C_{l_\beta}$
$C_{Y_\beta}$
−4
0
4
8
12
16
20
24
WB¹ V¹ H
WB¹ V²H
WB¹ V³H
WB¹

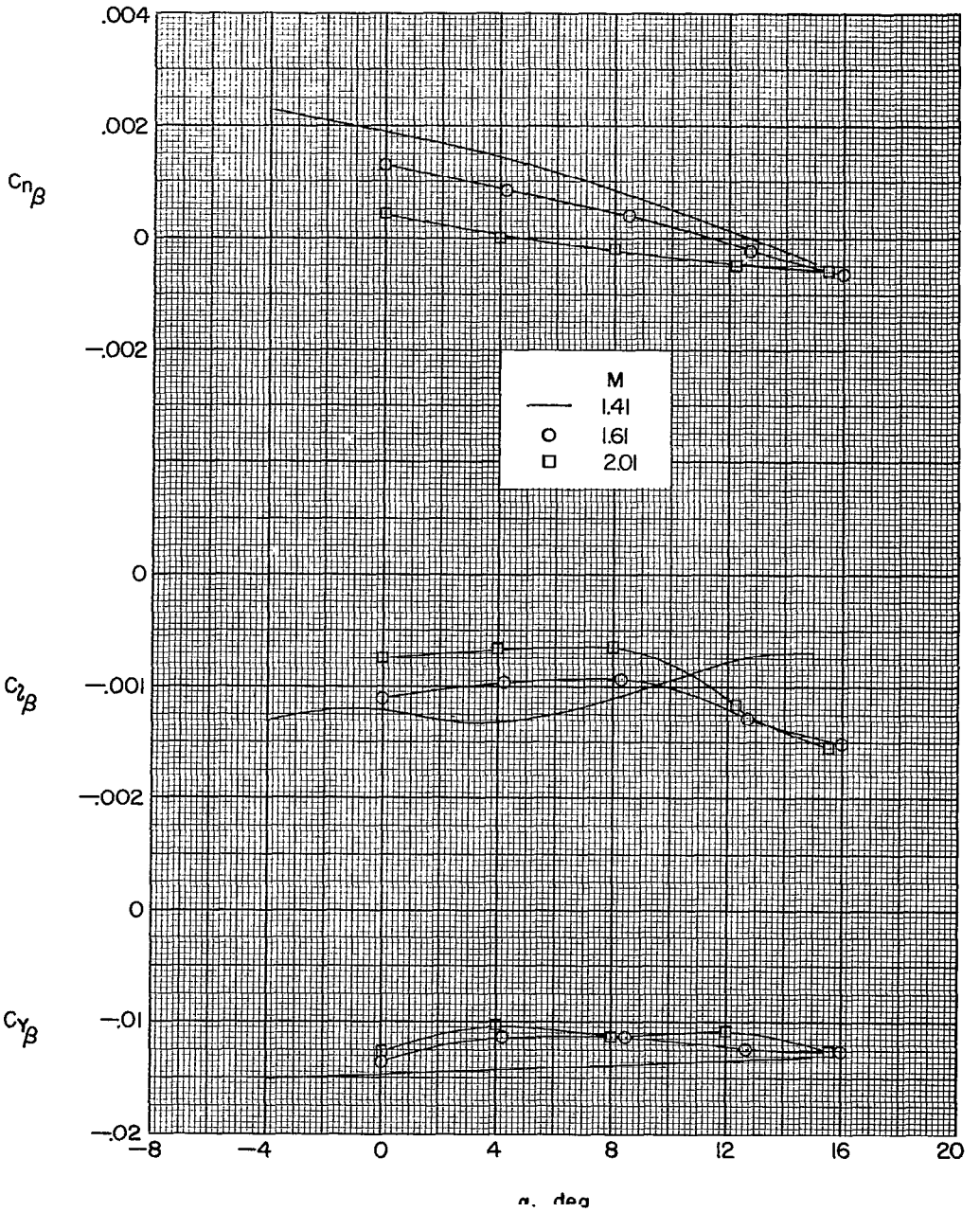
.004
.002
0
−.002
$C_{n_\beta}$
M
1.41
1.61
2.01
0
−.001
−.002
$C_{l_\beta}$
0
−.01
−.02
$C_{Y_\beta}$
−8
−4
0
4
8
12
16
20
α, deg

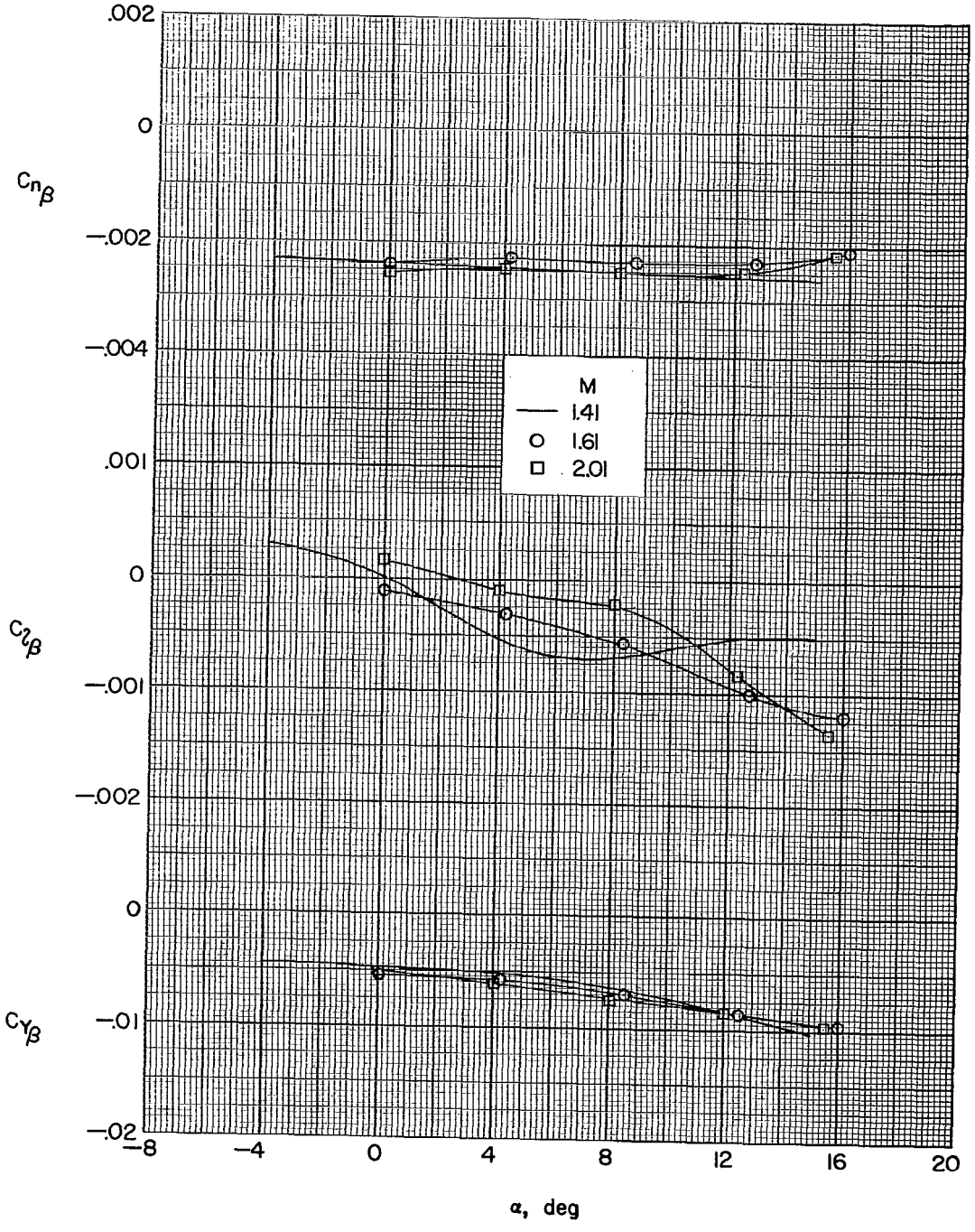
.002
0
−.002
−.004
.001
0
−.001
−.002
0
−.01
−.02
$C_{n_\beta}$
$C_{l_\beta}$
$C_{Y_\beta}$
M
1.41
1.61
2.01
−8
−4
0
4
8
12
16
20
α, deg

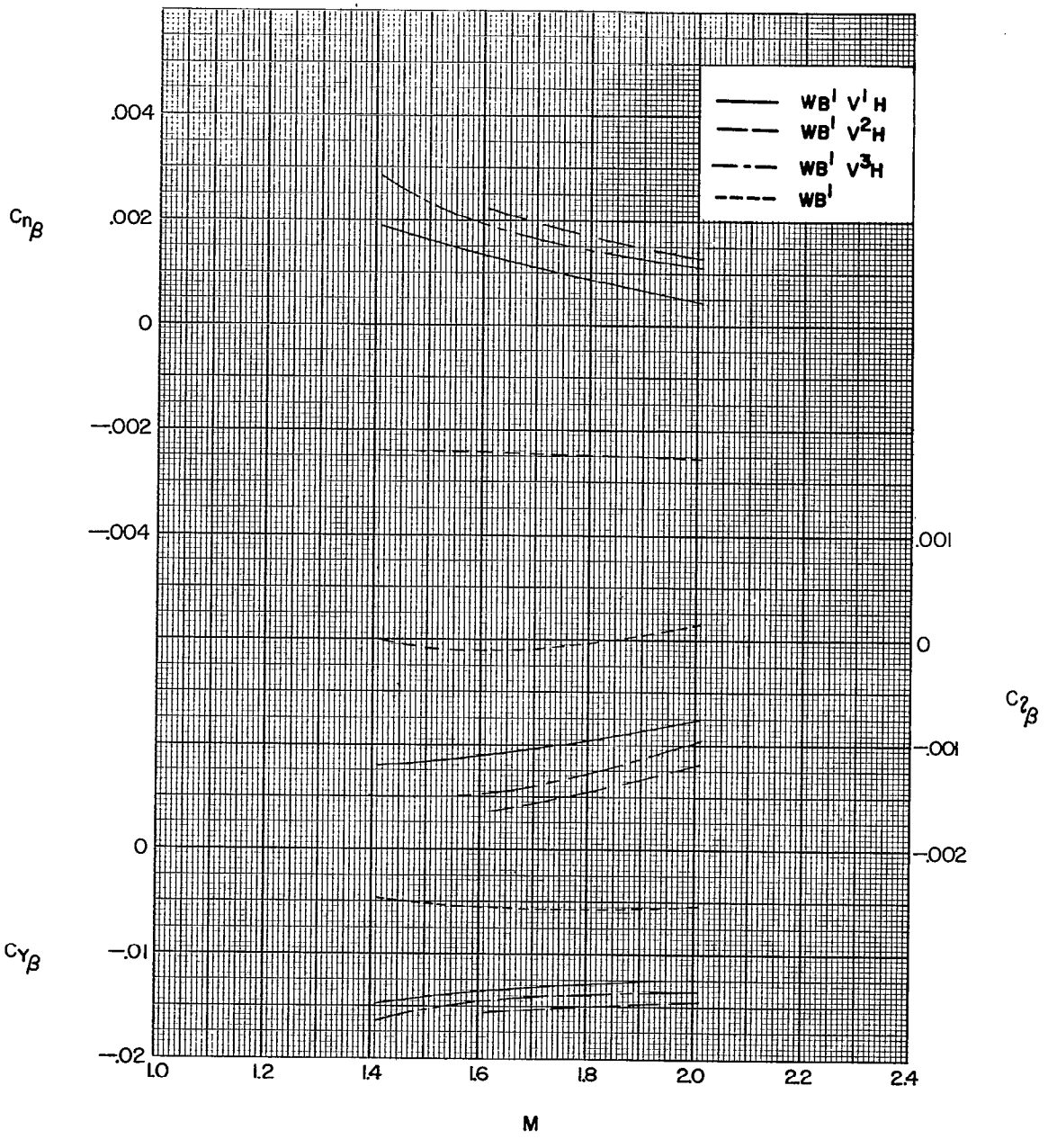


Figure 33.- Variation of sideslip derivatives with Mach number. R

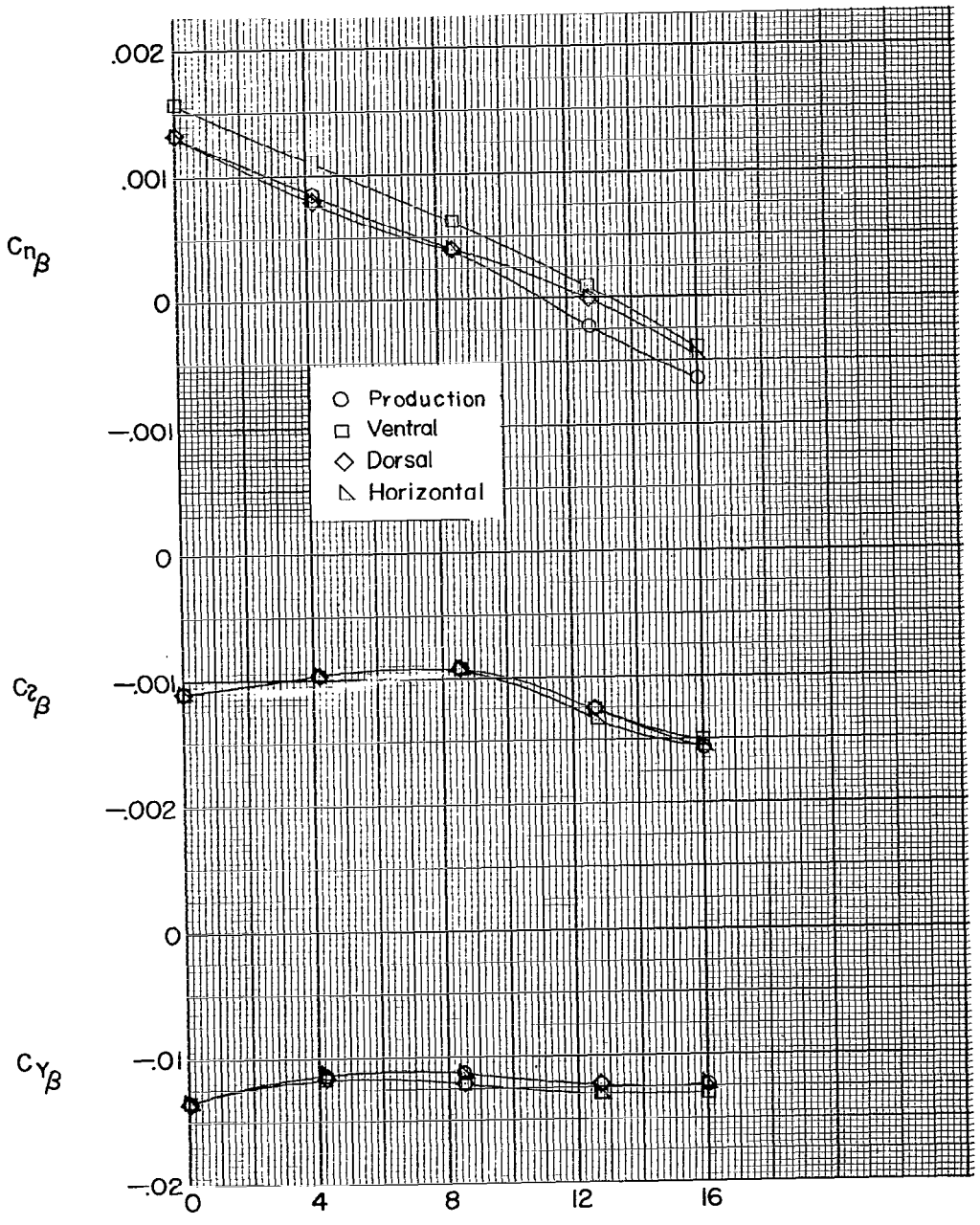
.002
.001
0
−.001
0
−.001
−.002
0
−.01
−.02
$C_{n_\beta}$
$C_{z_\beta}$
$C_{Y_\beta}$
Production
Ventral
Dorsal
Horizontal
0
4
8
12
16

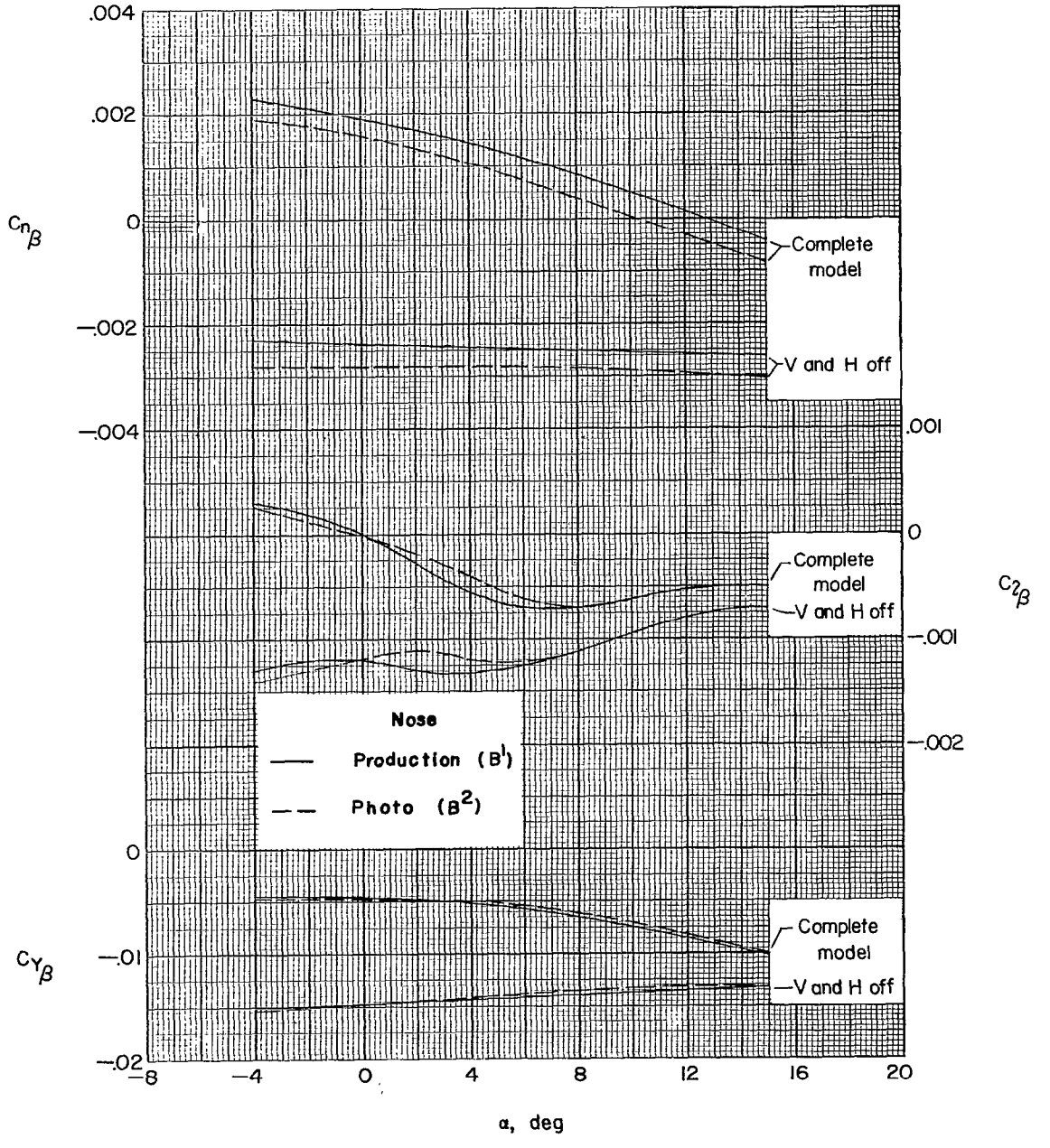
.004
.002
0
−.002
−.004
$C_{n_\beta}$
Complete model
V and H off
.001
0
−.001
−.002
$C_{l_\beta}$
Complete model
V and H off
Nose
Production (B¹)
Photo (B²)
0
−.01
−.02
$C_{Y_\beta}$
Complete model
V and H off
−8
−4
0
4
8
12
16
20
α, deg

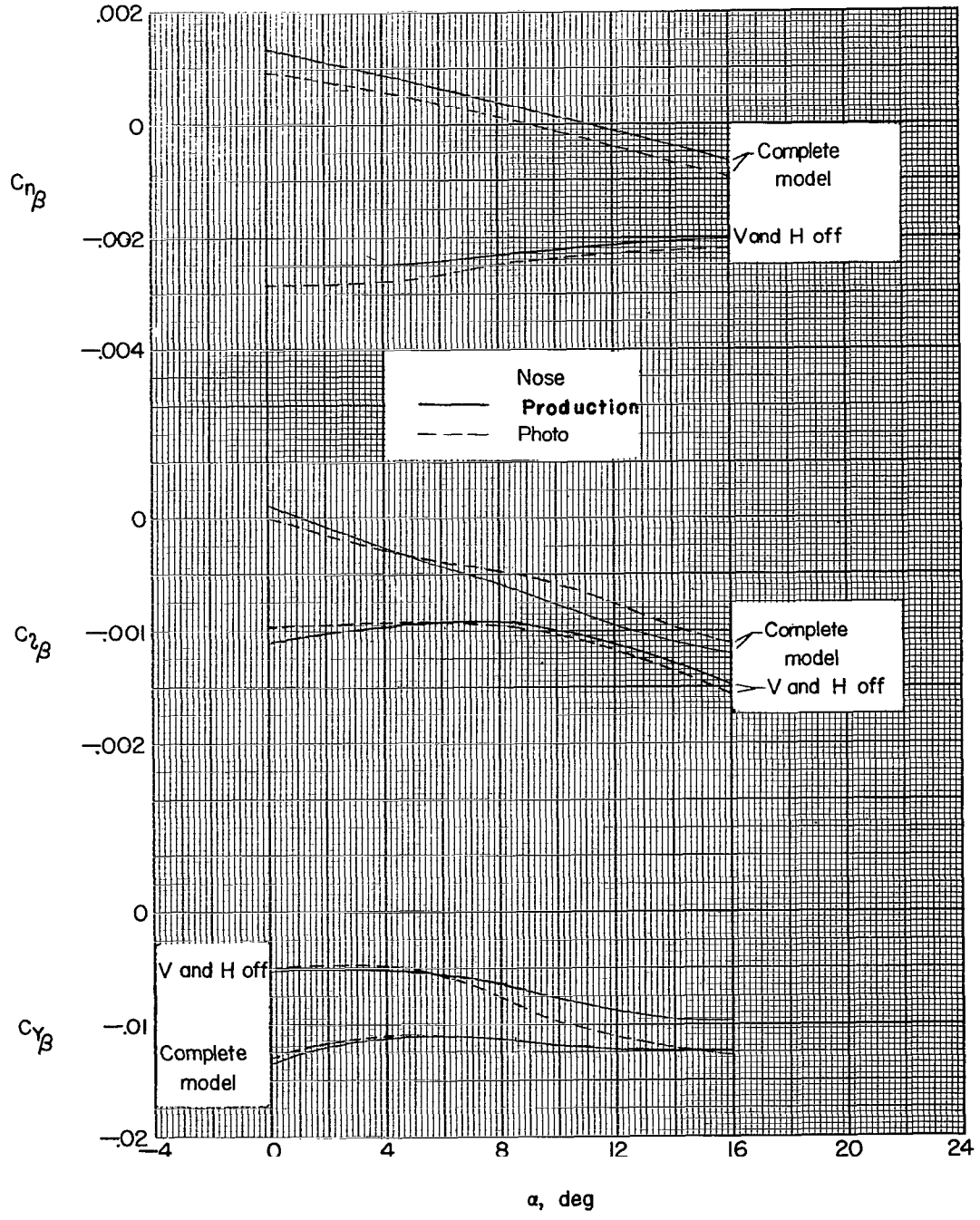
.002
0
−.002
−.004
$C_{n_\beta}$
Complete model
V and H off
Nose
Production
Photo
0
−.001
−.002
$C_{l_\beta}$
Complete model
V and H off
0
−.01
−.02
$C_{Y_\beta}$
V and H off
Complete model
−4
0
4
8
12
16
20
24
α, deg

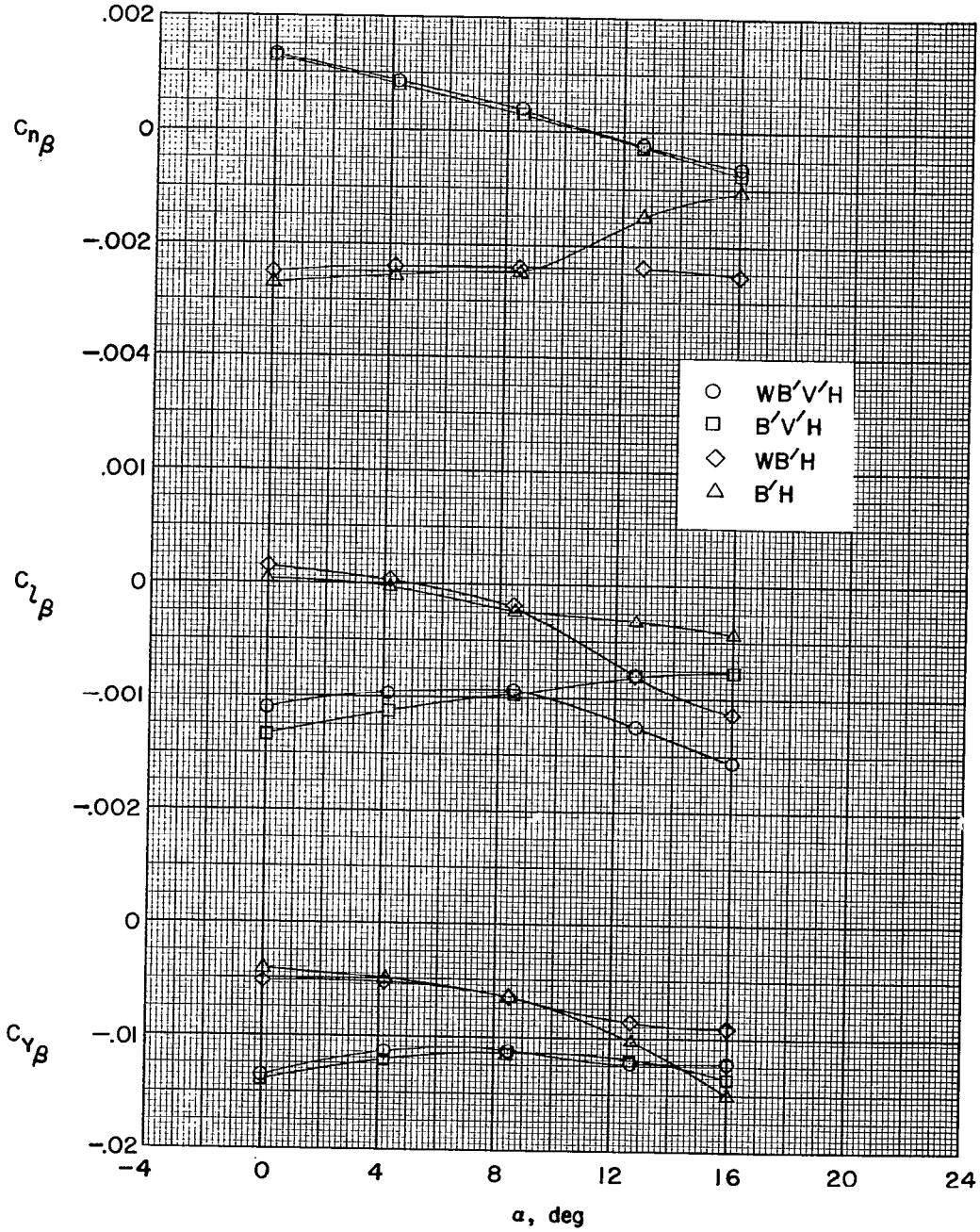
.002
0
−.002
−.004
.001
0
−.001
−.002
0
−.01
−.02
$C_{n_\beta}$
$C_{l_\beta}$
$C_{Y_\beta}$
WB′V′H
B′V′H
WB′H
B′H
−4
0
4
8
12
16
20
24
α, deg

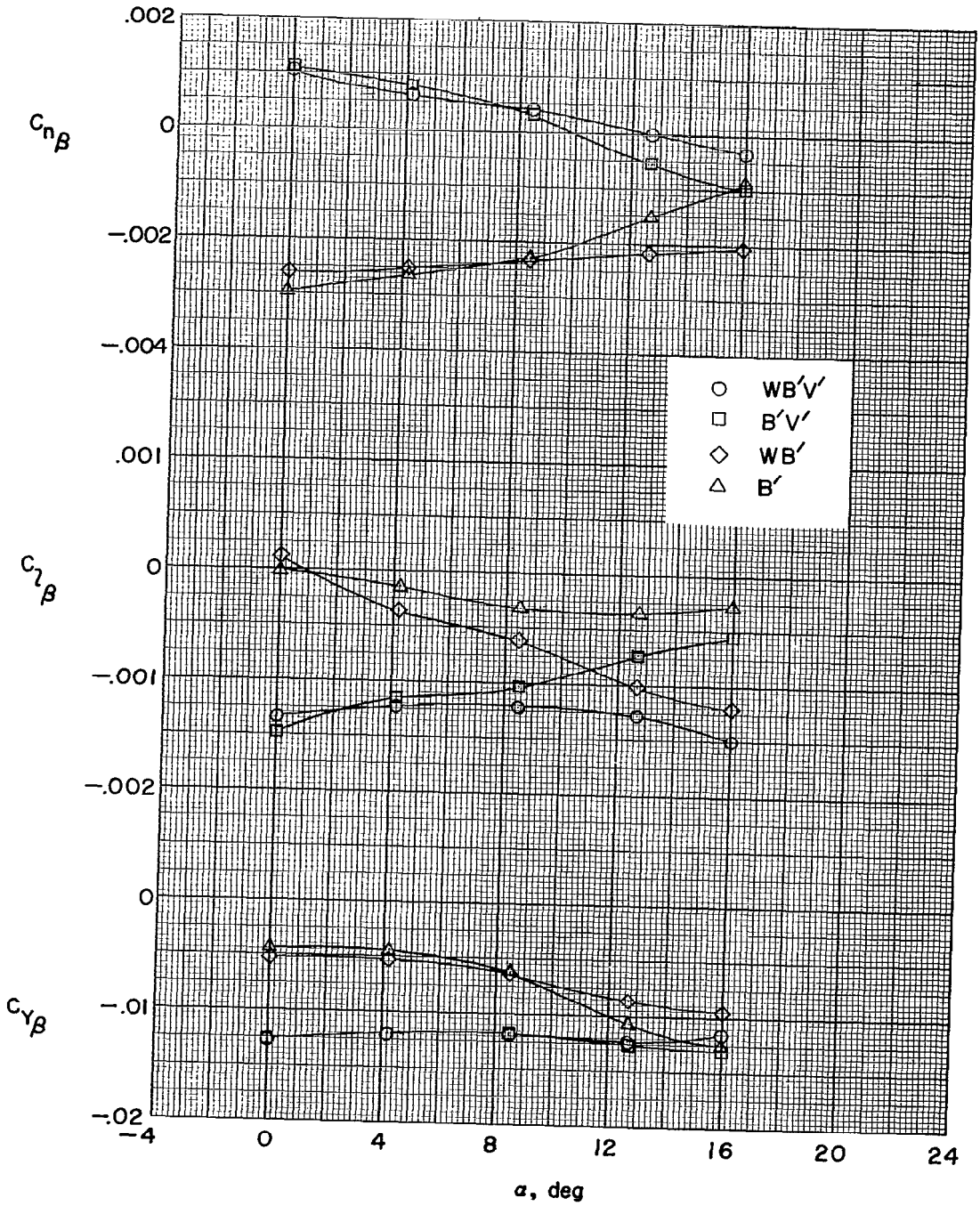
.002
0
−.002
−.004
.001
0
−.001
−.002
0
−.01
−.02
$C_{n_\beta}$
$C_{l_\beta}$
$C_{Y_\beta}$
WB′V′
B′V′
WB′
B′
−4
0
4
8
12
16
20
24
α, deg

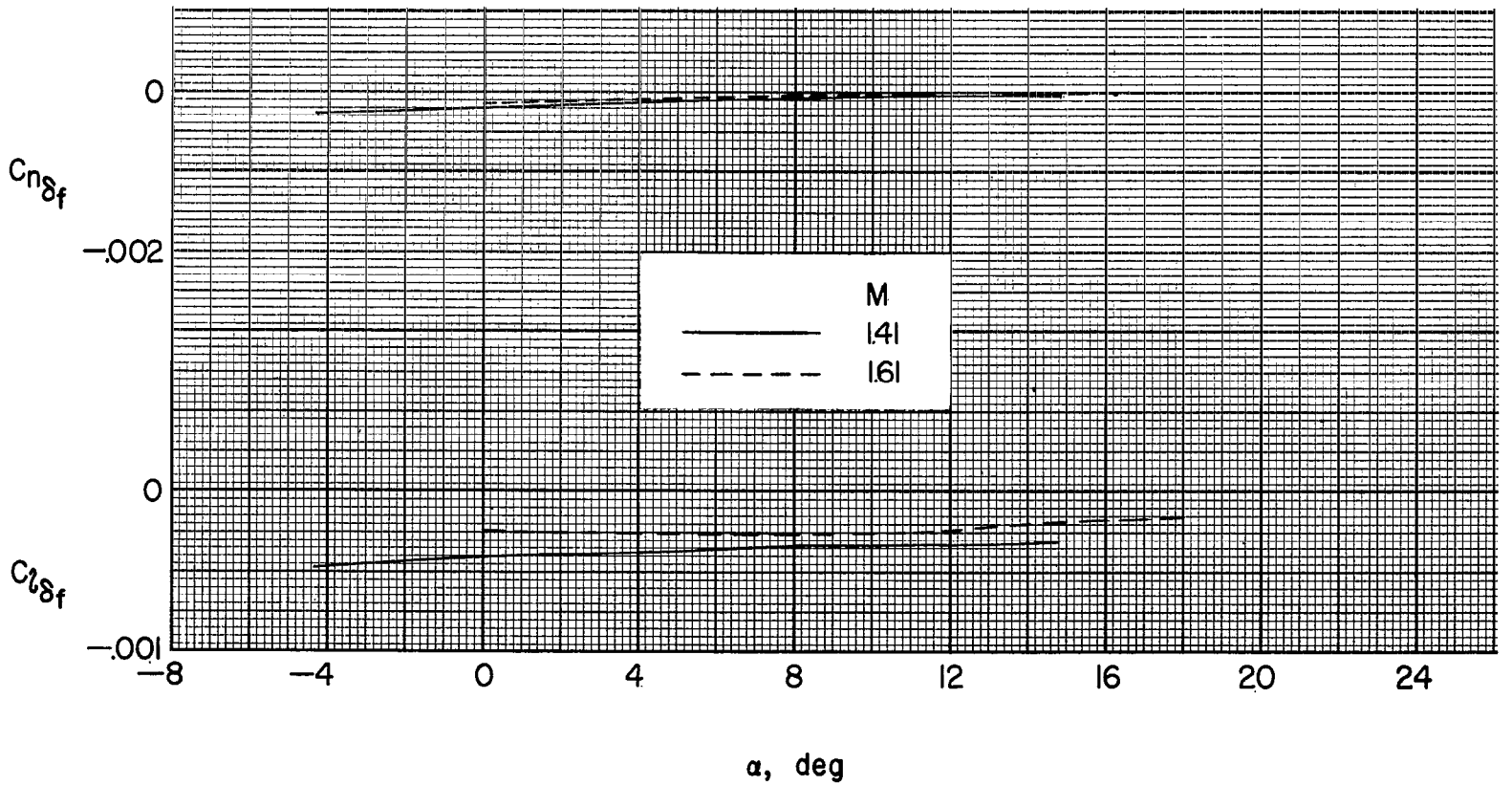


Figure 37.- Flaperon effectiveness. Production model.

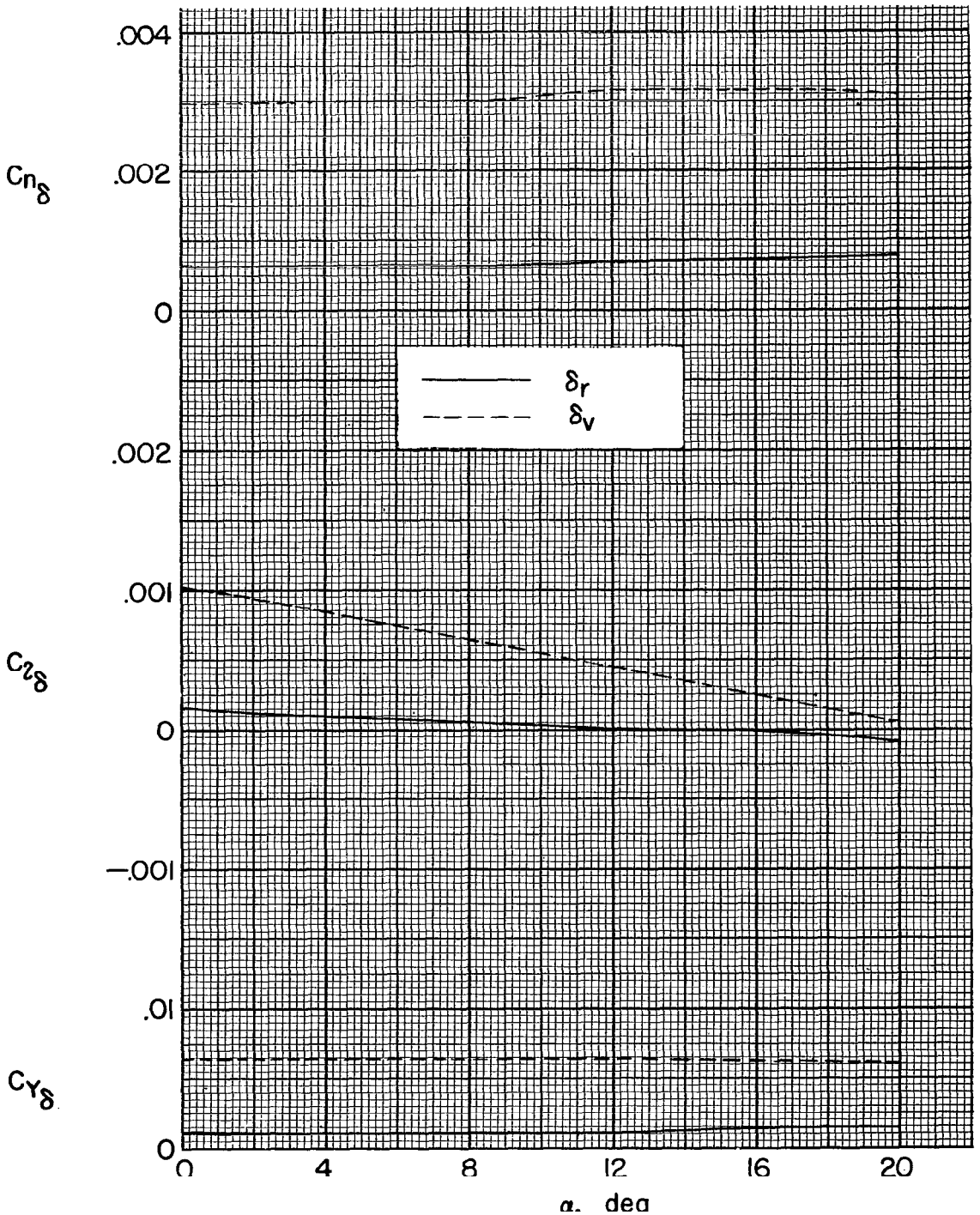
.004
.002
0
.002
.001
0
−.001
.01
0
$C_{n_\delta}$
$C_{l_\delta}$
$C_{Y_\delta}$
$\delta_r$
$\delta_v$
0
4
8
12
16
20
α, deg

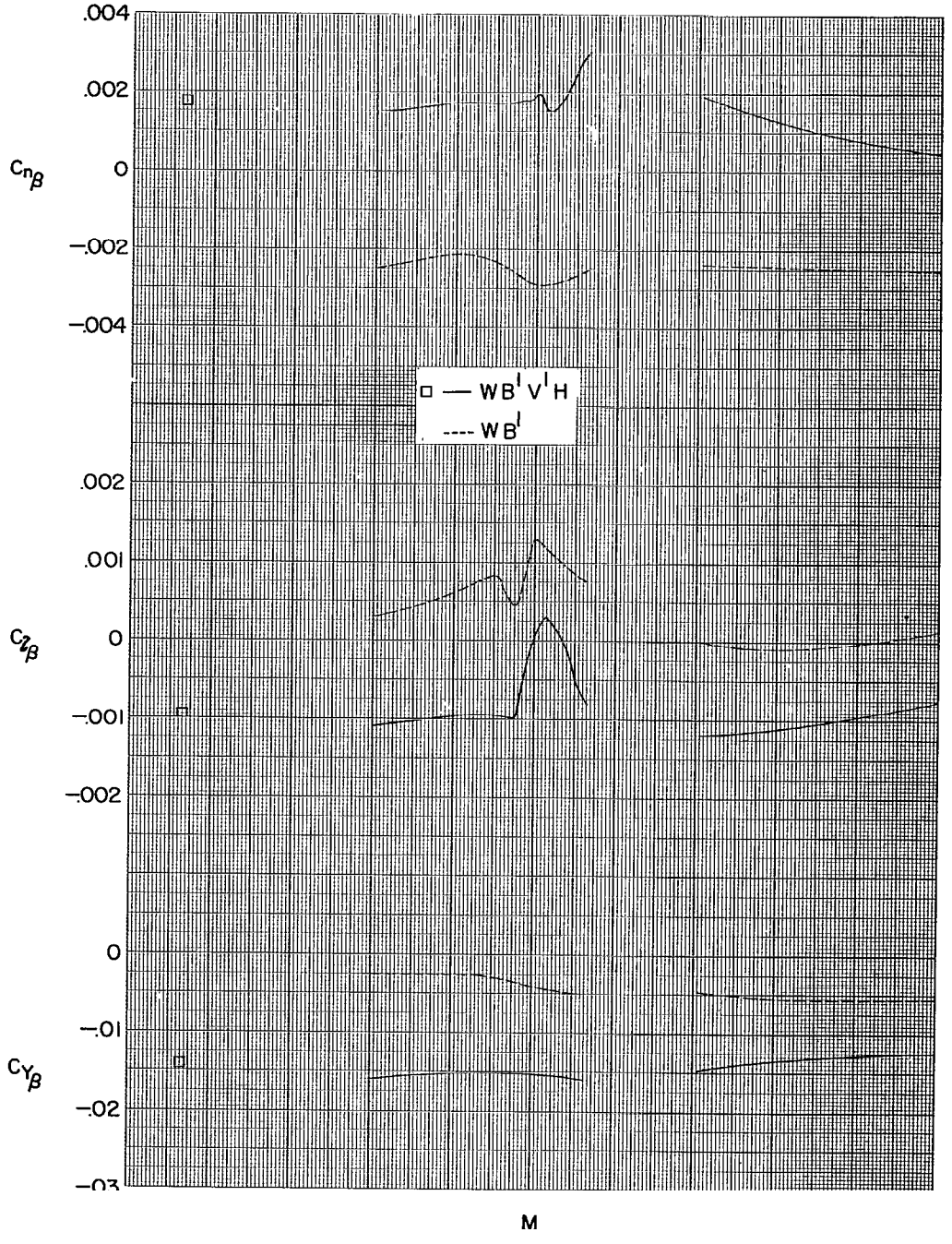
.004
.002
0
−.002
−.004
$C_{n_\beta}$
□ — WB'V'H
---- WB'
.002
.001
0
−.001
−.002
$C_{l_\beta}$
0
−.01
−.02
−.03
$C_{Y_\beta}$
M

INDEX


| Subject | Number |
|---|---|
| Tail-Wing-Fuselage Combination - Airplanes | 1.7.1.1.3 |
| Airplanes - Specific Types | 1.7.1.2 |
| Stability, Lateral - Static | 1.8.1.1.2 |
| Stability, Directional - Static | 1.8.1.1.3 |
| Control, Lateral | 1.8.2.2 |
| Control, Directional | 1.8.2.3 |


ABSTRACT

An investigation has been conducted in the Langley 4- by 4-foot supersonic pressure tunnel to determine the static lateral and directional stability and control characteristics of a 1/15-scale model of the Grumman F11F-1 airplane at Mach numbers of 1.41, 1.61, and 2.01. The effects of various body and vertical-tail modifications are included.

NASA Technical Library
3 1176 01438 5059